



## Contents

### **Einstein, Mach's principle, and the Unification of gravity and inertia**

J. F. Woodward

### **Voltage Power Law scaling of the Force for a Mach Effect Gravitational Assist Drive**

H. Fearn and J. F. Woodward

### **The Quantum Handshake Explored**

J. G. Cramer

### **The Relativistic Capacitor Model and the Mach-Lorentz theory**

J-P Montillet and C.Ziep

### **An Epitaxial Device for Dynamic Interaction with the Vacuum State**

D.C. Hyland

### **Dynamical Casimir Effect and the Possibility of Laser-like Generation of Gravitational Radiation**

R.Y. Chiao, J.S. Sharping, L.A. Martinez, B.S. Kang, A. Castelli, N. Inan and J.J. Thompson

### **Preparations for Thrust Measurement and Error Discussion of the IMPULSE Resonant Microwave Cavity**

M. S. McDonald, M. W. Nurnberger and L. T. Williams

**SPECIAL ISSUE: ADVANCED PROPULSION CONCEPTS**



## SUBMITTING PAPERS TO JBIS

JBIS welcomes the submission of technical papers for publication dealing with technical reviews, research, technology and engineering in astronautics and related fields.

### Text should be:

- As concise as the content allows – typically 5,000 to 6,000 words. Shorter papers (Technical Notes) will also be considered; longer papers will only be considered in exceptional circumstances – for example, in the case of a major subject review.
- Source references should be inserted in the text in square brackets – [1] – and then listed at the end of the paper.
- Illustration references should be cited in numerical order in the text; those not cited in the text risk omission.
- Captions must be labelled with their Fig. number and should be as short as possible.

### Illustrations should be:

- Colour or mono, but should be as close to print resolution (300 dpi) as possible. Poor-quality illustrations may compromise the acceptance of paper for publication. Images embedded in Word documents may be acceptable, but JBIS reserves the right to request separate higher-resolution image files from the author prior to publication.
- Responsibility for copyright clearance of images rests entirely with the author.

### Submission of papers

- Papers for consideration should be sent by email to [jbis@bis-space.com](mailto:jbis@bis-space.com) as **both** a Word document **and** as a Word PDF file (in order to check for font anomalies), together with any separate image files.
- If a paper is accepted for publication, the author will be asked to sign a License to Publish form. This can be downloaded at [www.bis-space.com/wp-content/uploads/2012/08/WebsiteLicense.pdf](http://www.bis-space.com/wp-content/uploads/2012/08/WebsiteLicense.pdf).
- Authors will receive a complimentary copy of the issue in which their paper appears.

We respectfully ask authors to adhere to these guidelines. Failure to do so will result in the delay of acceptable papers for publication.

Our full Guidelines for Authors can be downloaded from [www.bis-space.com](http://www.bis-space.com)

## International Advisory Board

**Rachel Armstrong**, Newcastle University, UK  
**Peter Bainum**, Howard University, USA  
**Stephen Baxter**, Science & Science Fiction Writer, UK  
**James Benford**, Microwave Sciences, California, USA  
**James Biggs**, The University of Strathclyde, UK  
**Anu Bowman**, Foundation for Enterprise Development, California, USA  
**Gerald Cleaver**, Baylor University, USA  
**Charles Cockell**, University of Edinburgh, UK  
**Ian A. Crawford**, Birkbeck College London, UK  
**Adam Crowl**, Icarus Interstellar, Australia  
**Eric W. Davis**, Institute for Advanced Studies at Austin, USA  
**Kathryn Denning**, York University, Toronto, Canada  
**Martyn Fogg**, Probability Research Group, UK  
**Raghavan Gopalaswami**, Aerospace Researcher, India  
**Lamartine Guimarães**, Institute for Advanced Studies, Brazil  
**Mark Hemsell**, Hemsell Astronautics Ltd, UK  
**Takuto Ishimatsu**, Massachusetts Institute of Technology, USA  
**Les Johnson**, Marshall Space Flight Center, USA  
**Terry Kammash**, University of Michigan, USA  
**Kelvin F. Long**, Initiative for Interstellar Studies  
**Inoue Makoto**, Institute of Astronomy & Astrophysics Academia Sinica, Taiwan  
**Gregory L. Matloff**, City University New York, USA  
**Koichi Mori**, Nagoya University, Japan  
**Richard Obousy**, Richard Obousy Consulting LLC, USA  
**Robert Parkinson**, BIS, Aylesbury, UK  
**George Schmidt**, NASA John H Glenn Research Center, Ohio, USA  
**Paul Schuch**, The SETI League Inc, USA  
**Tabitha Smith**, Bifrost, USA  
**Andreas Tziolas**, Variance Dynamical Corporation, USA  
**Chris Welch**, The International Space University, Strasbourg, France  
**Friedwardt Winterberg**, University of Nevada, Reno, USA

---

**Editor** Roger Longstaff **Deputy Editor** Duncan Law-Green **Associate Editors** Stephen Ashworth, Keith Cooper, Stephen Gamble, Paul Gilster, Rob Swinney, **Production** MP3 Media **Promotion** Gill Norman **JBIS Office** British Interplanetary Society, Arthur C. Clarke House, 27-29 South Lambeth Road, London, SW8 1SZ, United Kingdom tel +44 (0)20 7735 3160 fax +44 (0)20 7582 7167 email [jbis@bis-space.com](mailto:jbis@bis-space.com) [www.bis-space.com](http://www.bis-space.com)

### DISTRIBUTION

JBIS is distributed worldwide by mail and may be received by annual subscription or purchase of single copies. It is available through membership of the British Interplanetary Society at much reduced rates. Subscription details for members, non-members and libraries are available from the above address.

JBIS is a publication that promotes the mission of the British Interplanetary Society. Opinions expressed in signed articles are those of the contributors and do not necessarily reflect the views of the Editor or the Council of the British Interplanetary Society. Security clearance, where necessary, is the responsibility of the author.

**Published by the British Interplanetary Society.** Registered Company No: 402498. Registered Charity No: 250556.

Printed by Latimer Trend & Company Ltd, Estover Road, Plymouth, PL6 7PY, England.

© 2017 British Interplanetary Society. No part of this magazine may be reproduced or transmitted in any form or by any means, electronic or mechanical, including photocopying or recording by any information storage or retrieval system without prior permission from the Publishers.



## LIST OF CONTENTS

- 354 Einstein, Mach's Principle, and the Unification of Gravity and Inertia**  
James F. Woodward
- 365 Voltage Power Law scaling of the Force for a Mach Effect Gravitational Assist Drive**  
Heidi Fearn and James F. Woodward
- 372 The Quantum Handshake Explored**  
John G. Cramer
- 385 The Relativistic Capacitor Model and the Mach-Lorentz Theory**  
Jean-Phillipe Montillet and C. Ziep
- 394 An Epitaxial Device for Dynamic Interaction with the Vacuum State**  
David C. Hyland
- 405 Dynamical Casimir Effect and the Possibility of Laser-like Generation of Gravitational Radiation**  
R.Y. Chiao, J.S. Sharping, L.A. Martinez, B.S. Kang, A. Castelli, N. Inan and J.J. Thompson
- 415 Preparations for Thrust Measurement and Error Discussion of the IMPULSE Resonant Microwave Cavity**  
Michael S. McDonald, Michael W. Nurnberger and Logan T. Williams

### Note from the Editor

This special, double issue of JBIS, on the subject of advanced propulsion concepts, was suggested by Dr. Heidi Fearn, Professor of Physics at California State University Fullerton. The papers were selected from an invitation-only meeting at the Aerospace Corporation in El Segundo California, on 1-3 November, 2017. The purpose of the meeting was to bring together a group of researchers to exchange ideas on novel schemes of propulsion and to "push the boundaries of what is possible – a little." On behalf of the BIS, I would like to thank Heidi for her assistance in publishing this issue of selected papers in JBIS. *Roger Longstaff, Editor JBIS*

### MISSION

The British Interplanetary Society promotes the exploration and use of space for the benefit of humanity, by connecting people to create, educate and inspire, and advance knowledge in all aspects of astronautics.

## EINSTEIN, MACH'S PRINCIPLE, AND THE UNIFICATION OF GRAVITY AND INERTIA

JAMES F. WOODWARD, Department of Physics, California State University Fullerton, Fullerton, CA 92634 USA  
email: jwoodward@fullerton.edu

When my colleague Heidi Fearn organized the workshop on advanced propulsion at Aerospace Corporation at the beginning of November, 2017, I had no intention of presenting recent work, as she planned to do that for the two of us. I did not anticipate that any of the other presentations might merit formal comment from me. However, one of the presenters was at pains to explain that inertia is not accounted for in general relativity theory – that one must go to a scalar-tensor theory of the sort developed by Carl Brans and Robert Dicke in the 1960s to account for inertia. Alas, this is wrong. General relativity, notwithstanding that it is not widely appreciated, does correctly account for inertia as part of the gravitational interaction – not just phenomena involving rotation. Linear (translational) motion too. As it turns out, several years ago I was engaged in a lengthy email discussion of just this point with Paul Zielinski and Jack Sarfatti (supplemented by literature finds by Paul and Art Wagner). The earlier part of this then ongoing discussion had informed my treatment of general relativity in my book *Making Starships and Stargates: the Science of Interstellar Transport and Absurdly Benign Wormholes* (Springer, New York, 2012) and was acknowledged there. The conversation did not stop with the publication of *Starships*. Eventually, a couple of years later, it did stop, and I prepared an essay that I intended to be part of a second edition of *Starships*. Springer's price for doing a second edition, however, was my yielding to them some of the most lucrative royalties for the book. No second edition. But the 2015 essay was available for circulation to several of the workshop participants interested in the role of inertia in general relativity. Since getting gravity and inertia right is essential to figuring out how to get around spacetime quickly, I sent the 2015 version of the essay to those workshop participants. After all, scalar tensor theories were soundly discredited experimentally 40 and more years ago. Wishful thinking will not get anyone out of Earth's gravity well. Shortly after the essay on inertia in general relativity was finished, I circulated it to a number of friends and colleagues to get their critical comments. In this process, Bruce Camber brought a then recently published monograph by John Stachel<sup>1</sup> to my attention. In addition to calling Einstein's field equations the "inertio-gravitational" field equations, he employed several Einstein quotes on matters addressed here that I was not familiar with – now included below. This essay, edited from its 2015 form circulated at the workshop, recounts Einstein's evolving views on inertia and how they fit into general relativity, extending the material in chapters 1 and 2 of *Starships*. As elaborated below, we will see that Einstein's conviction that inertia and inertial forces are gravitational in origin never wavered after he identified the Equivalence Principle in 1907, notwithstanding that he was willing to abandon "Mach's principle" when he was challenged by Willem de Sitter shortly after the publication of general relativity theory in 1915. Some important episodes involving inertia after Einstein's death in 1955 are then considered.

**Keywords:** General Relativity, Origin of Inertia

1905, in the history of science, is known as Einstein's "miracle year".<sup>2</sup> In that year he published "On the Electrodynamics of Moving Bodies" wherein the "aether" of Maxwell's theory of electrodynamics was banished in his special relativity theory shortly after he gave the correct explanation of Phillip Lenard's photoelectric effect in terms of Planck's recently introduced quantum hypothesis. And then, seemingly almost as an afterthought, he wrote, "Does the Inertia of a Body depend on Its Energy Content?" Likely, most historians of science would say that the chronological order of publication correlates with the importance of these works. Special relativity and quantum mechanics being most important and energy and inertia being the least. But other considerations suggest that this ranking would be a mistake. For example, the formal content of special rela-

tivity theory – the Lorentz transformations – had already been published a year and more earlier. And Henri Poincaré already had a lengthy paper in the process of being published (in the *Rendiconti di Circolo Matematico di Palermo*) that would appear in 1906 where the physics of relativity was all disclosed. Poincaré and Lorentz, however, did not take the radical step that Einstein did in denying the presence of an aether in spacetime, and adopted the stance that the Lorentz transformations were applicable only to "local" spacetime. They persisted in the belief that there was an absolute background spacetime, although they understood that the background spacetime was unobservable in practice. Despite their belief in an absolute background spacetime, there can be no question but that they both understood the principle of relativity and the physics involved.

In the matter of the quantum explanation of the photoelectric effect, Einstein himself regarded this as a lesser contribution. But it eventually won him the Nobel prize for physics – and the undying hatred of Phillip Lenard, who regarded the effect as his personal property as he had discovered it. In the matter of energy and inertia, we are talking about the most famous equation in human experience:

<sup>1</sup> Stachel was the first editor of the Einstein papers and Director of the Center for Einstein Studies at Boston University for many years. His monograph, "The Hole Argument and Some Physical and Philosophical Implications" can be found online at Living Reviews in Relativity.

<sup>2</sup> Miracle years got their start with Newton, who allegedly figured out light, mechanics, and the law of gravity in 1666 while at home from school because of an outbreak of the plague.



$$E = mc^2 \quad (1)$$

Vast numbers of words have been written about this relationship. Einstein has been pilloried for allegedly never having given a correct accounting of how this relationship is obtained. But aside from literary invocations of the equation, almost all of the attention lavished on it has focused on the enormous magnitude of  $c^2$  and concomitantly, the enormous amount of energy locked up in even very modest amounts of mass.

Einstein, however, was after something else. He wanted to know what contributed to the resistance of bodies to changes in their state of motion. It's in the title of his paper. He wrote  $m = E/c^2$ . Already in 1905, he had identified inertia as a foundational concept wanting explanation. Since mass is both the manifestation of inertia and the source of the gravitational field (and the thing acted upon by the gravitational field), suspecting some sort of inter-relationship is hardly surprising. Doubtless, his interest had been piqued by reading Mach's critiques of classical mechanics. But speculative conjectures in the context of critiques are horses of very different colors from a fully elaborated theory that explicitly corrals the concept of inertia. If you suspect, as Einstein evidently did, that inertia is due to "some sort of interaction", as Mach had suggested, with other bodies in the universe, the obvious candidate interaction is gravity. Like inertia, gravity is a universal property of mass, and after 1905, energy too.

Einstein's first success in wedding gravity and inertia came in 1907 in the form of the Equivalence Principle. First identified by Galileo, and a central piece of Newtonian mechanics, the Equivalence Principle has been the subject of endless speculation since Einstein identified and named it – and made it a cornerstone of general relativity theory. Numerous different forms of the Principle have been and are articulated: the Weak Equivalence Principle (WEP), the Strong Equivalence Principle (SEP), and the Einstein Equivalence Principle (EEP) to name but a few. While it is widely acknowledged in the gravitational physics community that the EEP is part of the foundations of general relativity, there's a camp that denies that the Equivalence Principle in any form is a cornerstone of general relativity. They would have you believe that although the Equivalence principle served a heuristic purpose in the creation of general relativity theory, it is not a physically correct description of our experience. (See for example, Hans Ohanian's *Einstein's Mistakes*.) But as Einstein understood it, it is a cornerstone of general relativity. As John Norton, in a recent (2007) essay on Einstein's path to general relativity notes, Einstein always adhered to a particular formulation of the Equivalence Principle – one that avoids the confusion and contentions that often attend other formulations. Einstein's version consists of the assertion that in an accelerating frame of reference (in deep outer space, far from local concentrations of matter), a "gravity-like" field appears that acts on all objects attached to the accelerating frame of reference exactly as a real homogenous gravity field would.<sup>3</sup>

This formulation, Einstein's "happiest thought" as he later characterized it, leads immediately to the well-known exam-

ple of the indistinguishability of a chamber in a rocket sitting at rest on the Earth and a rocket accelerating at one "gee" in deep outer space. It also explains immediately why local inertial frames of reference in the vicinity of the Earth, free fall frames of reference, are those in which the Earth's gravity field is exactly cancelled by the "gravity-like" field that appears in accelerating frames of reference, since the free fall frames are accelerating with respect to the local cosmic rest frame.<sup>4</sup>

Since the cancelling "gravity-like" field behaves in all respects like a regular gravitational field, the obvious surmise is that it *is* a gravitational field. Why didn't Einstein make this claim? Well, there's a little problem. Fields have sources, and Einstein couldn't identify any plausible sources that would give rise to his "gravity-like" field – a field that would vanish (exert no forces) in all inertial frames of reference, but become manifest in frames of reference accelerating with respect to local inertial frames of reference. Note, by the way, that by definition a local inertial frame of reference is one in which the vector sum of all gravitational and "gravity-like" fields vanishes. But just because the vector sum of such fields is zero does not mean that no field – one that cannot be "gauged" away – is present.<sup>5</sup>

Einstein's earliest attempt to merge gravity and inertia appears in a short paper published in 1912, a year after his (incorrect by a factor of 2) prediction of the deflection of starlight passing close to the Sun. He had used a variable speed of light, dependent on the local gravitational field strength, to calculate the predicted deflection. Notwithstanding that he had made the speed of light (in vacuum) a constant in creating special relativity theory, he persisted in assuming that the speed of light was lower in strong gravity fields than it is in spacetime far from local concentrations of matter. At the time it appears that he did not see how these conflicting assumptions could be reconciled. But his physical intuition told him this was right. It was. The speed of light in vacuum in a region of strong gravity due to local matter concentrations is slower than that far from gravity producing bodies – as viewed by distant observers. Locally, it is always observed to have the same value – that is, it is a locally measured invariant. He must have understood this, at least at an intuitive level. Nowadays, in our age of black hole physics, the extreme illustrative example of this behavior is the fact that for distant observers, the speed of light measured at the event horizon of a black hole is zero (where time appears to stop, leading Russians to call such objects "frozen stars" in the days before black hole became the trendy appellation). But observers, regardless of their state of motion, at the horizon measure  $3 \times 10^{10}$  cm/s for light speed at their location.

<sup>4</sup> Some people object to the use of the "local cosmic rest frame", arguing that thus constitutes the selection of a preferred frame of reference, and thus constitutes a violation of the relativistic prohibition against preferred frames of reference. This is a mistake that proceeds from a faulty understanding of what a preferred frame of reference is. A preferred frame of reference is one that can be singled out by local observations alone. The mean cosmic rest frame clearly does not violate this stipulation, for it can only be identified by non-local observations. That is, by looking out into the universe to see what stuff that's far, far away is doing. In all other regards, the mean cosmic rest frame is just another inertial frame of reference (in the absence of local concentrations of matter of course).

<sup>5</sup> In particular, the scalar part of the gravitational field is present (and equal to the square of the vacuum speed of light). Unlike electrodynamics, where a scalar field can be "gauged" away at any point by a global rescaling of the electric potential, this is not possible in general relativity theory, for the theory is not invariant under global transformations of the Poincaré group. [General relativity is invariant under the group of arbitrary coordinate transformations; that is, physics is unaffected by your choice of coordinates. This property is called "general covariance".]

<sup>3</sup> This version of the Equivalence Principle was modified in the wake of the work of Carl Brans in the early 1960s to explicitly exclude the localization of gravitational potential energy, for as has already been noted in Starships, if gravitational potential energy can be localized, gravity fields and accelerating reference frames can always be distinguished from each other by local observations only. General relativity theory, specifically the relativity of inertia, and thus the principle of relativity, prohibits such distinguishability.

Einstein's chief aim in 1912 was to show that inertia was an "inductive" gravitational effect.<sup>6</sup> In Newtonian mechanics and special relativity theory, inertia is a property of mass-energy conferred on it by its presence in space – independent of the presence or absence of other material bodies in that space. Since space was thought to be a physical entity independent of its contents and their interactions, Einstein was proposing a radical, fundamental change in the understanding of physical reality by suggesting that the action of gravity was the origin of inertia and inertial effects. To do this he asks us to consider a mass point  $P$  at the center of a thin spherical shell of matter  $K$  – and what happens when the shell is accelerated. Drawing on his then recent exposition of his second law:<sup>7</sup>

$$m = E/c^2 \quad (2)$$

he notes that the masses of the point and shell are each modified by the presence of the other owing to the gravitational potential energy conferred on each by the other. These contributions are

$$\Delta m = m' - m = GmM/Rc^2 \quad (3)$$

where  $m$  is the mass of the point in the absence of the shell  $K$ ,  $m'$  its mass in the presence of the shell,  $M$  the mass of the shell, and  $R$  the distance from  $P$  to  $K$ . This relationship also obtains for  $M$  with the roles of  $m$  and  $M$  interchanged. Having written down the gravitational contribution to the mass of  $P$ , Einstein goes on to remark:

Th[is] result is of great interest in itself. It shows that the presence of the inertial shell  $K$  increases the inertial mass of the material point  $P$  inside the shell.<sup>1</sup> This suggests that the *entire* inertia of a mass point is an effect of the presence of all other masses, which is based on a kind of interaction with the latter. The degree to which this conception is justified will become known when we will be fortunate enough to have come into possession of a serviceable dynamics of gravitation.

Einstein's footnote:

<sup>1</sup> This is exactly the same point of view that E. Mach advanced in his astute investigation on this subject.

We see that already in 1912 Einstein had tentatively identified the origin of inertia: the gravitational interaction. Absent a "serviceable dynamics of gravitation" however, he could not simply show that the matter in the universe would produce a gravity field that would account for the third law reaction force experienced by an accelerating object accelerating when viewed in the "cosmic" rest frame (or one moving inertially with respect thereto). His way of dealing with this problem was to propose an *ansatz* relating the forces on  $K$  and  $P$ ; and then, using relationships of the sort above involving the masses of  $K$  and  $P$  in each other's presence, solve for the forces. He found that:

In the case where only  $K$  is accelerated, but  $P$  kept fixed, the second of equations (4) assumes the form, using the value of  $\alpha$  that was just found:

$$(-k) = \frac{3}{2} \frac{GmM}{Rc^2} \Gamma.$$

$k$  is here the force that must be exerted on the material point  $P$  in order for it to remain at rest; thus  $(-k)$  is the force exerted (induced) on  $P$  by the spherical shell  $K$  which possesses acceleration  $\Gamma$ . This force has the same sign as the acceleration, in contrast to the corresponding interaction between equivalent electrical masses.

Ignoring the factor of  $3/2$ , we see that were  $GmM/Rc^2 = 1$ , that is, if the condition for the entire inertia of the point mass  $m$  to be due to the gravitational interaction Einstein had identified obtains, then the gravitational force induced would just be the inertial reaction force involved. Did Einstein see this? Does the Sun rise in the east?

Being fortunate enough to have such an insight as a young man, alas, does not necessarily mean that you will remember it always. As John and Mary Gribbin relate in their biography of Feynman (pp. 266-7),

This curious fact – the balance between mass-energy and gravitational energy – had been known (as a mere curiosity) for about 20 years by the time Feynman gave his lectures on gravitation [in the '60s]. Back in the 1940s, on a visit to Einstein in Princeton, the pioneering cosmologist George Gamow casually mentioned, while they were out walking, that a colleague, Pasqual Jordan, had realized that a star might be made out of nothing, since at the point zero its negative gravitational energy is just numerically equal to its positive rest mass energy.

*Einstein stopped in his tracks, and, since we were crossing a street, several cars had to stop to avoid running us down.*

In spite of its impact on Einstein, Jordan's idea was regarded as no more than a curiosity, and probably Feynman had never heard of it. Certainly nobody had thought of applying it to the universe as a whole... All of this requires that the amount of matter in the universe should be just enough to match the so-called 'critical' density, for which spacetime is described as being [spatially] flat.

Actually, Einstein had applied it to the universe as a whole – in 1912. One wonders if Einstein stopped "in his tracks" because he remembered his conjecture of 1912?

After inventing general relativity theory, Einstein had "the serviceable dynamics of the gravitational field he needed to address the deficiencies of his arguments of 1912. But there were two problems with general relativity, at least from the point of view of the issue of inertia. The first was that the field equations of general relativity admitted solutions that were in conflict with any reasonable interpretation of inertia as a gravitational phenomenon. The second was that taking the Galaxy to be the extent of the universe,  $GM/R$  was less than a millionth of the value of  $c^2$ . Since astronomers at the time were just beginning to get a sense of what the universe was really like, the second problem could be dismissed on the grounds of ignorance. The first problem was a different matter. In a series of exchanges with Willem de Sitter, Einstein discovered just how much of a problem this turned out to be. Even the introduction of the

<sup>6</sup> As Pfister and King note in their *Inertia and Gravitation* (Springer, 2015), inductive effects of the sort encountered in electrodynamics (a vector field theory) are not possible in the scalar gravity theory of the sort that Einstein was using in 1912. But he was on the right track.

<sup>7</sup> I am using Frank Wilczek's enumeration of Einstein's laws here. The first law is  $E = mc^2$ .

cosmological constant term in his field equations was insufficient to suppress solutions clearly at variance with any reasonable version of “Mach's principle”.

It seems to be widely thought that in some sense Einstein “lost” the debate with de Sitter on the Machian nature of cosmological solutions of the field equations of general relativity. After all, some years later, near the end of his life, Einstein allowed as how it would be better not to talk about Mach's principle any more. But to believe that de Sitter had persuaded Einstein to abandon the gravitational origin of inertia and inertial forces would be a very serious mistake. De Sitter's argument forced Einstein to accept that his field equations of general relativity theory had solutions that were not consistent with the notion that the distribution and motion of matter in the universe determined the local inertial properties and behavior of matter. In a sense, it is perhaps unreasonable to expect a local field theory to do this without additional constraints. After all, Faraday had invented the field concept specifically to make it possible to treat interactions as local phenomena independent of the sources that produce the fields. Mach and Einstein were just asserting that the sources that produce the fields are important too, at least when it comes to inertia. More to the point is the question: did de Sitter's arguments cause Einstein to abandon his conviction that general relativity theory accounted for inertial phenomena? Simple answer: no. But Einstein complicated all this in the fall of 1920.

Paul Ehrenfest arranged an annual visiting professorship in 1920, a brief stay each fall, for Einstein at his home institution: the University of Leiden. Einstein took up this post in the fall of that year. In his traditional inaugural address upon taking up the post, Einstein complicated everything having to do with general relativity by making remarks about the “aether”. They have given those who would turn back the clock even on special relativity comfort. And those who would see gravity as a (quantum) phenomenon in spacetime, rather than as spacetime *per se* have likewise seized on them as precursory thinking on Einstein's part partial to their aspirations. Most, however, think Einstein was just sucking up to Ehrenfest's senior colleague, Hendrick Lorentz, whom he deeply admired, and who had never abandoned the aether of Maxwell.

Aside from the sucker-upper aspect of this, why would Einstein do this? Well, as the geometrical interpretation of general relativity, made possible by the fact that both gravity and inertia satisfy the Equivalence Principle, sank in after 1915, Einstein saw that space and time – spacetime in fact – would have to be conceptualized as a real physical substance independent of “matter” that resides in and distorts spacetime. Since general relativity theory is “background independent”, it follows inexorably that spacetime is the gravitational field. It is not something passive in which gravity fields exist.

Einstein seems to have been trying to kill two birds with one stone. First, making the point of the dynamical physicality of spacetime by calling it “aether”, thereby evoking the substantial nature of the aether of Maxwell; this notwithstanding that he had banished the aether of Maxwell with his special relativity theory. And, second, playing up to Lorentz's known prejudices. Whatever his motivation, it didn't work. Max Born, for example, was convinced that Lorentz never accepted relativity theory. And Einstein's critics were not bamboozled. They knew their enemy; and they gave him no quarter.

In May of 1921, Einstein gave a series of lectures at Prince-

ton University on general relativity theory. In those lectures he gave his then present thinking on Mach's ideas on inertia, as mentioned in chapter 2 of *Starships*. Armed with the dynamical theory of the gravitational field that he lacked in 1912, he could be more explicit about the behavior of matter due to the action of gravity. To do this he calculated the gravitational action on a (unit mass) test particle due to the presence of surrounding “spectator” matter. [Einstein's introductory remarks are quoted near the beginning of chapter 2 (p. 31) of *Starships* and his results are discussed by Carl Brans in the excerpt of his 1962 article at the end of chapter 2 (pp. 58-59).] The equation of motion he found, at linear order in small quantities using the weak field approximation, is:

$$\frac{d}{dt}[(1 + \bar{\sigma})\mathbf{v}] = \nabla \bar{\sigma} + \frac{\partial \mathbf{A}}{\partial t} + (\nabla \times \mathbf{A}) \times \mathbf{v} \quad (4)$$

The left hand side of this equation is just the derivative with respect to local [proper] time of the [unit] mass of the test particle with the scalar gravitational potential contribution written explicitly as  $\bar{\sigma}$  since the scalar potential is:

$$\bar{\sigma} = \frac{\kappa}{8\pi} \int \frac{\sigma dV}{r} \quad (5)$$

where  $\kappa$  is the Newtonian gravitational constant and the integration is to extend over the spectator matter. The vector potential is:

$$\mathbf{A} = \frac{\kappa}{2\pi} \int \frac{\sigma \mathbf{v}}{r} dV \quad (6)$$

where  $\mathbf{v}$  is the velocity of a spectator matter element  $\sigma$  with respect to the test particle. Since he was formally only considering spectator matter, he went on to say:

Although all of these effects [mass increase of the test particle and the forces induced by the vector potential terms in equation 5] are inaccessible to experiment, because of  $\kappa$  being so small, nevertheless they certainly exist according to the general theory of relativity. We must see in them a strong support for Mach's ideas as to the relativity of all inertial actions. If we think these ideas consistently through to the end, we must expect the *whole* inertia, that is the whole  $g_{\mu\nu}$ -field, to be determined by the matter of the universe, and not mainly by the boundary conditions at infinity.

What Einstein lacked in 1921 was the knowledge that in FRW cosmologies, when spacetime is spatially flat, the integration for the scalar potential, over matter of “critical” density out the past lightcone to the past particle horizon, leads to the scalar potential being equal to  $c^2$ . And he didn't see that he could employ Dennis Sciama's “trick” to remove the velocity from the integration in Equation (6).<sup>8</sup> Had he been armed with these things, it is difficult to believe that he would have failed

<sup>8</sup> This “trick” consists of noting that if an object is moving with velocity  $\mathbf{v}$  with respect to the local cosmic frame of rest, one can take the object at rest and assume the universe is moving relative to the object with velocity  $-\mathbf{v}$ . Since this appears to be the case looking out the past lightcone, such an assumption automatically takes into account retardation effects in the calculation. So  $\mathbf{v}$  can be removed from the integration over the matter currents to get the three-vector potential  $\mathbf{A}$ . The integration, with  $\mathbf{v}$  removed, is just that for the scalar potential.



to make a formal argument for his belief that inertia is due to the distant matter in the universe mediated by the gravitational field. But in 1921 there was the problem of the sources of such a gravitational field, for  $GM/R$  for the universe – then thought to be the Galaxy – didn't look to be anything like  $c^2$ .

Having reintroduced the aether into discourse about space-time in 1920, Einstein found himself writing about it again in 1924 – likely an attempt to clean up the mess he had created several years earlier. In his paper, “On the Aether”, he wasted no time getting to this, for he opened his essay with:

When we speak of the aether, we are, of course, not referring to the corporeal aether of mechanical wave theory that underlies Newtonian mechanics, whose individual points each have a velocity assigned to them... Instead of ‘aether’, one could equally well speak of ‘the physical qualities of space’. Now, it might be claimed that this concept covers all objects of physics, for according to consistent field theory, even ponderable matter, or its constituent elementary particles, are to be understood as fields of some kind or particular ‘states of space’. But it must be admitted that such a view would be premature, since, thus far, all efforts directed toward this goal have foundered. [and still have]

He then went on to talk about “absolute” aether – aether [space] that is not acted upon by its material contents. For example, the absolute space/aether of Newtonian mechanics. To make his point, he remarked that, “The occurrence of centrifugal effect with a (rotating) body whose material points do not change their distances from one another, shows that this aether is not to be understood as a mere hallucination of the Newtonian theory, but rather it corresponds to something real that exists in nature.” Einstein continues:

We see that for Newton, ‘space’ was something physically real, in spite of the curiously indirect way this real thing reaches our awareness. Ernst Mach, the first after Newton to subject the foundations of mechanics to a deep analysis, perceived this clearly. He sought to escape this hypothesis of the ‘mechanical aether’ by reducing inertia to immediate interaction between the perceived mass and all other masses in the universe. This view was certainly a logical possibility but, as a theory involving action at a distance, cannot be taken seriously today. The mechanical aether – which Newton called absolute space – must remain for us a physical reality...

When Newton referred to the space of physics as ‘absolute’, he was thinking of yet another property of what we call here aether. Every physical thing influences others and is, in its turn, generally influenced by other things. This does not however apply to the aether of Newtonian mechanics. For the inertia-giving property of this aether is, according to classical mechanics, not susceptible to any influence, either from the configuration of matter or anything else. Hence the term ‘absolute’.

This passage is where Einstein identifies ‘Mach’s principle’ as an action at a distance proposition, and rejects it as unphysical because of its instantaneous propagation of physical effects over finite distances. By spelling out in detail how inertia fits into Newtonian mechanics, he was preparing the way for his introduction to how inertia fits into general relativity. In his words:

...It was recognized that the equations of electromagnetism did not, in fact, single out one particular state of motion, but rather that, in accordance with these equations, just as with those of classical mechanics, there exists an infinite multitude of coordinate systems in mutually equivalent states of motion, providing the appropriate transformation formulas are used for the spatial and temporal coordinates... No longer was a special state of motion to be ascribed to the electromagnetic aether. Now, like the aether of classical mechanics, it resulted not in favoring a particular state of motion, only favoring a particular state of acceleration... According to special relativity too, the aether was absolute, since its influence on inertia and the propagation of light was thought of as being itself independent of physical influence...

Having prepared the way:

The general theory of relativity rectified a mischief of classical dynamics. According to the latter, inertia and gravity appear as quite different, mutually independent phenomena, even though they both depend on the same quantity, mass. The theory of relativity resolved this problem by establishing the behavior of the electrically neutral point-mass by the law of the geodetic line, according to which inertial and gravitational effects are no longer considered as separate. In doing so, it attached characteristics to the aether which vary from point to point, determining the metric and dynamical behavior of material points, and determined, in their turn, by physical factors, namely the distribution of mass/energy.

The aether of general relativity differs from those of classical mechanics and special relativity in that it is not ‘absolute’ but determined, in its locally variable characteristics, by ponderable matter. This determination is a complete one if the universe is finite and closed. That there are, in general relativity, no preferred spacetime coordinates uniquely associated with the metric is more a characteristic of its mathematical form than its physical framework.

Einstein’s last remark is worth noting. It’s his way of saying the “general covariance” is more a matter of mathematical formalism, and less one of physics. By implication, the physics of general relativity is its treatment of gravity and inertia.

The remainder of Einstein’s 1924 article on the aether was devoted to remarks about the unification of gravity and electromagnetism. In this connection he mentioned Arthur Schuster’s speculations on planetary and stellar magnetic fields (without attribution), later pursued by Patrick M.S. Blackett in the ‘40s and ‘50s.<sup>9</sup> Also mentioned are the Compton effect and the work of Bose on the statistics of what are now named bosons. His conclusion, however, bluntly addresses his core belief about gravity and inertia at the time:

...we will not be able to do without the ether in theoretic-

<sup>9</sup>This conjecture proposes that a rotating electrically neutral massive body generates an electromagnetic magnetic field and implies that the gyromagnetic (or magnetogyro) ratio for such a body should remain fixed as the object spins down. When pulsars were discovered in the late ‘60s and understood to be highly magnetized neutron stars, a new way of testing this conjecture became available. See: J.F. Woodward, articles on pulsar evolution in the *Astrophysical Journal*, 225, 574 (1978); 256, 617(1982); 279, 802 (1984); 316, 743 (1987).



cal physics – that is, a continuum endowed with physical properties; for general relativity, to whose fundamental viewpoints physicists will always hold fast, rules out direct action at a distance. But every theory of local action assumes continuous fields, and thus also the existence of an ‘aether’.

\*\*\*\*\*

In Newtonian mechanics, space, and in special relativity spacetime, is absolute. It confers inertia on its material content, but is not acted upon by them in any way. In general relativity spacetime, as the local agent of the action of other matter in the universe via the gravitational field, also confers inertia on the local matter present. But unlike all other fields, both the distant and local matter act on the spacetime, since spacetime is not a field *in* something else and it *is* the gravitational field. As his article of 1924 makes plain, Einstein had come to this arguably odd, counterintuitive view by the mid ‘20s, notwithstanding de Sitter’s demonstration that empty universes were consistent with his field equations. As John Stachel, in a recent article relates, in 1921 (after the exchange with de Sitter), when asked by a reporter what would happen to space and time if matter were “destroyed”, he replied: “Then there would be no time and space.” And in 1931, when asked to sum up his theory in one sentence, he replied, “Before my theory, people thought if you removed all the matter from the universe, you would be left with empty space. My theory says that if you remove all the matter, space disappears too!” Yes, two sentences. But his meaning is clear. Spacetime is the gravitational field, and the gravitational field must have matter sources. No matter, no gravitational field. No gravitational field, no spacetime. And since spacetime confers inertia on its material contents, that means that gravity and inertia are inextricable.

Did Einstein abandon Mach’s principle, defined as an action at a distance proposition, by the mid ‘20s as the above suggest? Well, no, not really. How do we know? Because in 1940, when John Wheeler and Richard Feynman (at Princeton) went to see Einstein (at the Institute for Advanced Study in Princeton) to get his take on their action at a distance theory of electrodynamics, Einstein immediately told them of the work of Hugo Tetrode (in 1921) and Adriaan Fokker (in 1929) on action at a distance theory. A skeptic might argue that this is only evidence for Einstein’s familiarity with the literature. The action at a distance theories of Tetrode, Fokker, and Wheeler and Feynman, however, were not the instantaneous propagation type. They invoked the time-reversed, “advanced” solutions of equations to make interactions with the future appear to be instantaneous. Not long after their meeting with Einstein, Feynman gave a talk (his first) on the theory at a Physics Department colloquium. At the end of the talk, Feynman relates that:

Wolfgang Pauli, who was sitting next to Einstein, said: ‘I do not think this theory can be right because of this, that and the other thing.’ ... At the end of this criticism, Pauli said to Einstein, ‘Don’t you agree, Professor Einstein?’ I don’t believe this I right, don’t you agree, Professor Einstein? Einstein said, ‘No,’ in a soft German voice that sounded very pleasant to me, very polite. ‘I find only that it would be very difficult to make a corresponding theory [i.e., an action at a distance theory] for gravitational interactions.’

Einstein didn’t need to develop an action at a distance version of general relativity theory, for he was certain that the

weaker version of Mach’s principle – the origin and relativity of inertia – was already built into the very foundations of his theory. And that was good enough. But general relativity theory had acquired a life of its own. And others that appropriated it did not necessarily understand its physical content on the same terms as Einstein. By the early ‘50s there was already a budding “modernist” interpretation of general relativity – where “fictitious” forces are never “real” and the full physical content of the theory is nothing more than the metric and the geodesics derivable therefrom; that in the absence of curvature, no gravitational field is present; and later, the Equivalence Principle is excess baggage of historical interest only. Some, who fancied themselves true general relativists, even suggested that Einstein didn’t understand his own theory – at any rate, not as well as they.

One may ask, had Einstein’s understanding of general relativity changed in any significant way since the 1920s? And how did the “modernist” interpretation of general relativity come about? The answer to the first question is simple. No. Einstein’s understanding of his theory had not changed. This is evidenced in his understanding of the content and significance of the Equivalence Principle (which, as John Norton has noted, did not change from its inception in 1907 to his death in 1955). We know because his friend and colleague Max von Laue queried him on precisely this point in 1950.<sup>10</sup> Laue, who had written books on relativity theory, sought Einstein’s views on claims then circulating that curvature was the key to gravitation; that in the absence of any curvature, no gravity field was present in spacetime. Perhaps he smelled a rat, because Einstein had said for years that spacetime is the gravitational field; and were that true, spacetime without gravity wouldn’t make much sense. Einstein’s answer:

It is true that in the case of the  $R^i_{klm}$  [the Riemann curvature tensor components] vanish, so that one could say: “There is no gravitational field present.” However, what characterizes the existence of a gravitational field from the empirical standpoint is the non-vanishing of the  $\Gamma^l_{ik}$  [the connection components], not the vanishing of the  $R^i_{klm}$ . If one does not think intuitively in such a way, one cannot grasp why something like curvature should have anything at all to do with gravitation. In any case, no reasonable person would have hit upon such a thing. The key for understanding the equality of inertial and gravitational mass [the Equivalence Principle] is missing.

It’s worth remarking that Laue later allowed as how he didn’t really understand general relativity theory until 1950.

Einstein’s view on spacetime and its relation to the gravitational field toward the end of his life is also found in his published writings of that time, as John Stachel has recently pointed out. One finds in Appendix II of *The Meaning of Relativity*, written and published in the 1950s, as quoted by Stachel:

It is the essential achievement of the general theory of relativity that it freed physics from the necessity of introducing the “inertial system” (or inertial systems)... The

<sup>10</sup> Laue won the 1914 Nobel Prize for physics for the theory of X-ray diffraction. He and Einstein had been esteemed friends and colleagues for decades. Indeed, when Einstein refused to return from travels to Germany in the early ‘30s, after the ascension of the Nazis, he allowed as how the only two colleagues he would really miss were Laue and Planck.

development... of the mathematical theories essential for the setting up of general relativity had the result that at first the Riemann metric was considered the fundamental concept on which the general theory of relativity and thus the avoidance of the inertial system were based. Later, however, [Tullio] Levi-Civita rightly pointed out that the element of the theory that makes it possible to avoid the inertial system is rather the infinitesimal displacement field  $\Gamma$ .

Stachel goes on to comment that:

Einstein's vision can be summed up in the sentence: 'Spacetime does not claim existence on its own, but only as a structural quality of the field.' The two main elements of this vision are:

1. If there is no field, there can be no spacetime manifold.
2. The spatio-temporal 'structural qualities' of the field include the affine connection, which is actually of primary significance compared to the metric tensor field.

Up until quite recently [2014], the standard formulations of general relativity did not incorporate this vision.<sup>11</sup>

The reason why "standard formulations of general relativity didn't incorporate this vision" is a consequence of how general relativity came of age in the '50s and '60s. As Herman Bondi relates in his textbook, *Cosmology* (esp. chapter 4), written at the time, Mach's principle had become a matter of serious interest in the relativity community. Especially after Dennis Sciama published his paper, "On the Origin of Inertia", in the *Monthly Notices of the Royal Astronomical Society* in 1953.<sup>12</sup> Sciama sought to simplify the problem of inertia by ignoring general relativity and writing out a simple vector theory of gravity analogous to the theory of electrodynamics. He assumed that the scalar potential of the field is:

$$\Phi = -\int_V \frac{\rho}{r} dV \quad (7)$$

And the vector potential is:

$$\mathbf{A} = -\int_V \frac{\mathbf{v}\rho}{cr} dV \quad (8)$$

where  $\rho$  is the matter density,  $r$  is the distance from a test particle at the origin of coordinates to the matter density element, and  $V$  is the volume to be integrated over – in principle all space out the past light cone to the past particle horizon. Sciama notes that if we take  $\mathbf{v}$  to be the velocity of the test particle relative to the universe, since in the rest frame of an observer moving with

the test particle the universe appears to be moving rigidly with velocity  $-\mathbf{v}$ ,  $\mathbf{v}$  can be removed from the integration, leaving the integration for  $\Phi$ , so,

$$\mathbf{A} = \frac{\Phi}{c} \mathbf{v}(t) \quad (9)$$

Taking the "gravelectric" field equation to be:

$$\mathbf{E} = -\nabla\Phi - \frac{1}{c} \frac{\partial \mathbf{A}}{\partial t} \quad (10)$$

Far from any local concentrations of matter the gradient of the scalar potential can be taken to be 0, so the gravelectric field in such regions becomes:

$$\mathbf{E} = -\frac{\Phi}{c^2} \frac{\partial \mathbf{v}}{\partial t} \quad (11)$$

And if  $\Phi/c^2 = 1$ , then the gravelectric field provides the inertial reaction force experienced by objects subjected to [proper] accelerations. Sciama considered the effects of local concentrations of matter that give rise to scalar potentials  $\phi$ . Generally, these are much, much smaller than the potential that follows from cosmic matter. If Sciama's vector theory is an approximation to general relativity, then his theory makes plain that inertia and inertial forces are gravitational actions that depend chiefly on the most distant matter in the universe.

Sciama assumed that his theory was different from general relativity. This assumption was challenged a few years later by W. Davidson.<sup>13</sup> In particular, Davidson recovered from general relativity the equation of motion that Einstein had in 1921 with a few minor corrections:

$$\frac{d}{dt}[(1-3\phi)\mathbf{v}] = -\nabla\phi - \frac{\partial \mathbf{A}}{\partial t} + \mathbf{v} \times (\nabla \times \mathbf{A}) \quad (12)$$

As in Einstein's case, this equation is supposed to apply to the effects of "spectator" matter, so the integrations for the potentials only extend over fairly nearby matter, resulting in exceedingly small effects as noted by Einstein. Davidson, in extending the calculation to the entire universe, notes that the potentials are not calculated as deviations from flat Minkowski spacetime (which he calls Galilean spacetime). With the slow motion approximation, he gets:

$$(\mathbf{A}, \Phi) = \left( -g_{4i}, \frac{1}{2} g_{44} \right) \quad (13,15)$$

And

$$\frac{d\mathbf{v}}{dt} = -\nabla\Phi - \frac{\partial \mathbf{A}}{\partial t} + \mathbf{v} \times (\nabla \times \mathbf{A}) \quad (14,16)$$

Davidson's equation enumeration is indicated by the numbers after the commas. He uses indexes 1 through 4, 4 being the time index. The switch from the local calculation of Einstein to the global calculation of a Machian nature is encoded, following Sciama's notation, in the use of capital *phi* for the scalar potential, rather than the small *phi*. Davidson notes that for this to work,  $\Phi$  must be equal to  $c^2/2$  [his equation (19)]. All this he

<sup>11</sup> Stachel goes on to put this in modern terminology, "...the concepts of fiber bundles and sheaves enable a mathematical formulation of general relativity consistent with Einstein's vision...":

1. If there is no total space for the fields, then there is no base manifold.
2. The conceptual distinction between the roles of metric and connection becomes evident: The metric lives on the vertical fibers of the total space; while the connection lives on the horizontal directions of the total space, connecting the fibers with each other."

<sup>12</sup> This was part of his doctoral work for Paul Dirac.

<sup>13</sup> M.N.R.A.S. **117**, 212-224 (1957).

embedded in steady state cosmology, fashionable in Britain in the '50s and '60s.

\*\*\*\*\*

One might think that since Sciamma had shown what had to be the case for inertial forces to be gravitational in his simple vector theory of gravity and Davidson had shown general relativity theory properly accounted for inertial effects and forces (providing that  $\Phi \sim$  equal to  $c^2$ ), the gravitational origin of inertia should have been a settled issue. But that didn't happen. Davidson's work seems to have been pretty much ignored, perhaps because of his support for steady state cosmology. But other things than inertia bore on debates in gravitational physics in the '50s and '60s. A few eminent physicists worked in the field at the time; but as Richard Feynman wrote home to his wife from a gravity conference in Warsaw in 1961, the field of gravity was dominated by "second raters". And by the '40s and '50s, Einstein had been relegated to the sidelines of the physics community because of his refusal to go along with the mainstream regarding quantum mechanics and his insistence on pursuing a unified theory of the gravitational and electromagnetic fields. While, after about 1920, due to the success of his prediction of the deflection of starlight by the Sun's gravity field, measured the year before by Arthur Eddington, Einstein appeared to be a heroic genius to the general public, those who knew him saw him differently. This is captured by David Hilbert's well-known remark that, "Every boy in the streets of Göttingen understands more about four-dimensional geometry than Einstein. Yet, in spite of that, Einstein did the work and not the mathematicians."<sup>14</sup> Not exactly familiarity breeds contempt – after all, we are talking about Einstein. But something along those lines.<sup>15</sup>

When asked by his former assistant (in the 1930s), Leopold Infeld, how he was getting along at the Institute for Advanced Studies in the early '50s, Einstein responded, "*Sie denken das ich bin einer alter trottel.*" [They think I'm an old fool.] His close friends from earlier years, Laue for example, knew better. And others were laying the foundations for the eventual ascendancy of gravitational physics into the mainstream. But in the 1960s, Jeremy Bernstein, an excellent physicist who occasionally wrote popular articles for the *New Yorker* magazine,<sup>16</sup> remarked in a piece on John Wheeler and gravitational physics at Princeton University, that many of Wheeler's colleagues were displeased with Wheeler for snagging some of their best grad students and seducing them into working on general relativity, which they regarded as a stagnant backwater.<sup>17</sup>

From the inception of general relativity in 1915 through the early part of the 1950s, general relativity was the preserve of a handful of physicists – likely no more than a dozen or two world-wide at any given time. While it was widely hailed as the

profound and elegant theory that it in fact is, the experimental confirmations of the theory were few in number, and less than compellingly accurate. The mathematics was (is) difficult, and courses in general relativity graced the curricula of almost no universities, at any level. In very broad brush strokes, the '50s saw the formation of what amounted to "schools" of general relativity around charismatic teachers, notably John Wheeler at Princeton and Dennis Sciama at Cambridge. Major research universities started hiring a general relativist or two as the importance of the field became increasingly apparent – especially after the discovery of quasars in the mid- '60s and the advent of "relativistic astrophysics". Advances in radio astronomy in the '50s and '60s also played a role in the surge of interest in general relativity. Irwin Shapiro at MIT put the radar facilities built at MIT during the war and after to use to do a "fourth test of general relativity" – a time-delay observed in the radar ranging of the inferior planets (Mercury and Venus). Strong radio sources were observed as they were occulted by the Sun to look for relativistic effects. At Princeton, Robert Dicke did an exquisite test of the Equivalence Principle and geared up his group to look for cosmic background radiation expected on the basis of general relativistic cosmology. Penzias and Wilson beat them to the observational discovery (and subsequent Nobel Prizes). Joseph Weber at the University of Maryland started looking for gravitational waves with a donated aluminum bar of prodigious proportions. Eventually, Eric Adelberger instituted a first-rate experimental program at the University of Washington focused on Eötvös-type (Equivalence Principle) experiments.

Mach's principle was a topic of high visibility and attention, especially after Sciama published his first, 1953, paper on it and then wrote popular books and more technical articles on the subject in subsequent years. Discussion around the topic became heated and at times polemical. Indeed, Abraham Pais recounts<sup>18</sup> that the *Zeitschrift für Physik* stopped taking papers on general relativity because those that mentioned Mach's principle evoked such hostile replies. When Carl Brans published part of his doctoral work, excerpted *in extenso* at the end of chapter 2 in *Starships*, it pretty much put an end to arguments about the localizability of gravitational potential energy in general relativity. Since Einstein had argued that Mach's ideas (but not explicitly "Mach's principle", which demanded action at a distance) on the origin and relativity of inertia predicted that spectator matter should change the rest masses of local objects, Brans' correction of this mistake on Einstein's part was taken to mean that Mach's principle, however defined, was not built into general relativity theory (notwithstanding Davidson's work). Neither Sciama nor Wheeler, though they accepted Brans' argument (in Wheeler's case, see the excerpt from Misner, Thorne, and Wheeler on gravitational energy localization at the end of chapter 1 in *Starships* and below), ever accepted that general relativity had nothing to say about the origin and nature of inertia.

Arguments about Mach's principle continued. But Robert Dicke and Carl Brans inferred, as did many others, that Mach's principle was not to be found in general relativity, and went off and reinvented scalar-tensor gravity as a way of trying to bring Mach's principle back into gravity theory. They did this by noting that Mach's principle requires that  $GM/Rc^2 = 1$ , or,  $1/G = M/Rc^2$ . Since  $R$  is a function of time, it would seem to follow that  $G$  should also be a function of time. Brans and Dicke, already aware that Paul Dirac had proposed that  $G$  might be a func-

<sup>14</sup> Ohanian, *Einstein's Mistakes* p. 221.

<sup>15</sup> Einstein's self-image, as one might expect, was not affected by the public hype. As he remarked to Levi-Civita, complimenting him on an elegant calculation, "It must be nice to ride through these fields on the horse of true mathematics while the like of us make our way laboriously on foot."

<sup>16</sup> My favorite opening for an article is one of Bernstein's where he recounts the story of a medieval scribe being interrogated by the abbot of his monastery regarding a manuscript he had recently produced. The abbot suspected the scribe of making up, rather than simply copying, some of the material relating to miracles. The scribe defended himself by pointing out that he wasn't smart enough to make up the material being challenged.

<sup>17</sup> Some of those students have been among the most eminent of the physics community, one having recently won the Nobel Prize for physics.

<sup>18</sup> In *Subtle is the Lord*, p. 288.



tion of time, took this as the basis for proposing a universally coupled, time-dependent scalar field that would supplement general relativity, but not replace it. As they noted, they were merely reviving a theory already explored by Pasqual Jordan more than a decade earlier.<sup>19</sup> A series of exacting experiments to test scalar-tensor gravity by Dicke and others over the next decade and a half followed. They showed that the proposed scalar field is either inconsequential or non-existent.<sup>20</sup>

The irony in all this is that Brans' critique of Einstein's 1921 work on Mach's principle was dead-on correct. Allowing the gravitational influence of spectator matter to affect the value of the total scalar gravitational potential, changing the rest masses of nearby objects, is a violation of the Equivalence Principle, and if there is no Equivalence Principle, there is no general relativity. And there is no "relativity of inertia", the weaker form of Mach's ideas that Einstein insisted was built into general relativity. But the inference that he and Dicke, and most everyone else took away from this – that Machian inertia was not to be found in general relativity – was, to be blunt, wrong. This notwithstanding that they had clearly understood that Machian inertia demands that  $GM/Rc^2 = 1$ , or,  $\Phi = c^2$  so that the coefficient of  $\partial \mathbf{v} / \partial t$  in  $[\partial \mathbf{A} / \partial t = ] (\Phi / c^2) \partial \mathbf{v} / \partial t$  is one. For this condition to be true everywhere and everywhen,  $\Phi$  must be a locally measured invariant like  $c$ . Brans' argument, contrary to what was widely thought, locks Machian inertia into general relativity – unless you are willing to abandon the Equivalence Principle. And critical cosmic matter density – evidenced by spatial flatness at cosmic scale – ensures that  $\Phi = c^2$  is invariant in time since critical cosmic matter density universes evolve preserving this condition.

Since  $\Phi$ , the total scalar gravitational potential, is a locally measured invariant so that spectator masses cannot change the rest masses of local objects, one might think that spectator matter cannot have any effects on local objects in general relativity. This is a mistake. Spectator matter in the vicinity of a shielded lab cannot change the rest masses of things in the lab, but if the spectator matter is in accelerating motion with respect to the lab, it will exert forces on the lab's contents via the vector potential. Since those forces obey the Equivalence Principle, they can be treated as "accelerative linear frame dragging" if one chooses. Such effects due to local concentrations of matter (other than black holes and neutron stars) are utterly minute, even now beyond the level of detectability in laboratory circumstances.

\*\*\*\*\*

Brans' argument on spectator matter was/is the keystone that locks Machian relativity and origin of inertia into general relativity theory, despite the fact that this was not how his argument was understood at the time – it was taken to be a "coordinate condition" that was required to do calculations correctly. Sciama and Wheeler did not abandon the hope that inertia really was accounted for in general relativity. But by the early '70s, the nature and role of inertia in general relativity had faded into memories of battles of yesteryear. In Stachel's turn of phrase, Einstein's vision disappeared from the community, then expanding, of general relativists. To the extent that Einstein's vi-

sion ever really informed the community of general relativists, as it receded it was replaced by the view that gravity is only present when spacetime curvature is present – a point of view, as we have seen, as old as general relativity.

If one's goal is to eliminate even the possibility of accounting for inertia in general relativity, the best way to do that is to gin up some argument for suppressing the  $\partial \mathbf{A} / \partial t$  term in the equations of motion we've considered above. This was done in 1991 by Edward Harris in an *American Journal of Physics* article comparing the weak field approximation of general relativity with Maxwell's equations. Invoking the deDonder coordinate condition (also called the harmonic gauge) Harris claimed that the time derivative of  $\mathbf{A}$  vanished. Of course, in the weak field approximation it may be small, and can be ignored when considering only the action of nearby local concentrations of matter. This seems to be the actual basis of Harris's suppression of the  $\partial \mathbf{A} / \partial t$  term, for he said,

Of course, if the sources of the fields are changing with time,  $\mathbf{A}$  and  $\partial \phi / \partial t$  cannot be rigorously constant. We arrive at  $[\partial \mathbf{A} / \partial t = 0]$  and  $[\partial^2 \phi / \partial t^2 = 0]$  because we neglected terms that were quadratic in [the velocity in the source tensor]  $S_{\mu\nu}$ .

That is, Harris was *not* actually claiming that  $\partial \mathbf{A} / \partial t$  is rigorously 0 as the result of a gauge condition, only that for local matter concentrations that produce weak fields it can be taken to be approximately zero as it is a term with coefficient of  $\sim (\mathbf{v}/c)^2$ . Now, if  $\partial \mathbf{A} / \partial t$  is calculated as in the Sciama treatment considering only the local perturbation field, then you will get approximately

$$\frac{\phi}{c^2} \frac{d\mathbf{v}}{dt}$$

And the fact that  $\phi / c^2 \ll 1$  can be used to set  $\partial \mathbf{A} / \partial t = 0$ . This seems to be what Harris did. To attribute this to a gauge condition is misleading at best. It is set to zero because it is a higher order term in  $(\mathbf{v}/c)$ , where the local value of the potential is a stand-in for  $\mathbf{v}$ .

The problem with doing this is that if you take  $\partial \mathbf{A} / \partial t = 0$  to be generally true, you suppress the term in the equation of motion that produces linear (translational) inertial forces. In addition to taking  $\partial \mathbf{A} / \partial t = 0$  for weak fields, the weak field approximation is embedded in a Minkowskian (flat) background spacetime. If you take Minkowski spacetime as it is widely understood – namely a Riemann flat spacetime with inertial structure and no gravitational field present – then you will likely follow the path of those who took Harris's assertion that  $\partial \mathbf{A} / \partial t = 0$  seriously and find themselves unable to explain translational inertial effects because they have cancelled the term in the equation of motion that produces those effects. Minkowski spacetime, of course, is an unobservable fiction that exists nowhere in our universe, a pre-general relativistic artefact. The closest thing to flat spacetime in our reality is the spatially flat spacetime of FRW cosmology. And that spacetime is a gravitational field with  $\Phi = c^2$  where  $\partial \mathbf{A} / \partial t$  cannot be ignored (and doesn't vanish by any choice of an applicable gauge). Only a few moments of reflection should be needed to ascertain that any gauge condition that might suppress  $\partial \mathbf{A} / \partial t$  must allow the rescaling of  $\Phi$  to zero (since  $d\mathbf{v}/dt$  is not in general equal to zero). This is obviously wrong, as gauge invariance of the "first kind" (global rescaling of the scalar potential) clearly does *not* apply to gravitation.

Harris's mistake, or misdirection if you prefer, was picked up

<sup>19</sup> Brans has recounted these developments in a 2010 article found on Einstein .online>.

<sup>20</sup> All this is recounted in Clifford Will's excellent book, *Was Einstein Right? Putting General Relativity to the Test*, Basic Books, New York, 1986.



by Hans Ohanian and Remo Ruffini in their textbook *Gravitation and Spacetime* in 1994.<sup>21</sup> Jose' Pasqual Sanchez tried to correct this mistake in 2000. He was unsuccessful in convincing everyone that the mistake is a mistake. Others adopted Harris's claim that  $\partial \mathbf{A} / \partial t = 0$  and some even generated elaborate arguments for its general validity, leading to claims that "Faraday induction effects" are absent in general relativity. If such effects are not expected in general relativity, then you are faced with accounting for translational inertial effects without recourse to the action of the cosmological scale matter currents that are the basis of the calculations Sciama and Davidson, and others uncorrupted by claims that  $\partial \mathbf{A} / \partial t = 0$ . As it turns out, not long after Harris introduced the  $\partial \mathbf{A} / \partial t = 0$  claim and it was picked up by Ohanian and Ruffini, Ignazio Ciufolini and John Wheeler, and independently Donald Lynden-Bell, provided a way to explain inertial effects generally without recourse to integration over matter currents out the past light cone to the past particle horizon. They proposed that systems be characterized by the specification of initial conditions on some suitable spacelike hypersurface and then analyze the dynamical evolution of the system by considering the constraint equations on the initial conditions. The constraint equations, since the initial conditions are time-independent, are elliptic, not hyperbolic, equations. So the propagation velocity of their effects is infinite, yielding instantaneous non-local interactions. Those who have adopted the Harris/Ohanian line seem to have bought into this "explanation" of non-rotational inertial effects.

Did Wheeler appreciate that the hypersurface/constraint equations approach was just a stand-in for a retarded integration out the past light cone? Does the Sun set in the west? In his book with Ciufolini, *Gravitation and Inertia*, published in 1995, we find in chapter 5:

**5.6.3 [An Integral Equation to Give Spacetime Geometry, and Therefore Inertia, in Terms of the Density and Flow of Material Mass There and Then?]**

After appealing to the Coulomb gauge in electrodynamics [wherein the electric field propagates instantaneously] and asserting that the wild and chaotic local motions of matter out there in the cosmos that presumably beset any attempt at an integration out the past light cone with insuperable difficulties, Wheeler said:

However, no one will choose that route to knowledge who has in initial value data and dynamic equations a simpler way to follow what is going on – simpler because the initial-value equations operate on a space-like hypersurface rather than on the past light "cone." We forego here any integral over the past light "cone" in favor of **initial-value data on a spacelike hypersurface plus evolution by dynamic equation.**

Does this mean that Wheeler thought that an integration out the past light cone over the matter currents, done correctly, would return incorrect results (because  $\partial \mathbf{A} / \partial t = 0$ )? Of course not. As he says in section 6.2,

*Gravitomagnetism* may be thought of as a manifestation of the way inertia originates in Einstein geometrodynamics

[that is, general relativity theory]; "*mass-energy there rules inertia here*" (chap 5). The measurement of the gravitomagnetic field will be the experimental evidence of this interpretation of the origin of the local inertial forces, that might be called a weak general relativistic interpretation of the Mach principle.

The emphasis is Wheeler's. This comment is followed immediately by a reprinting of Einstein's 1921 comments on Mach's principle, already quoted in chapter 2 of *Starships*. Worthy of note is the footnote that Wheeler attached to Einstein's comment on the influence of spectator matter: "However, regarding this point it has to be stressed that in general relativity, because of the very strong equivalence principle, the inertial mass and the gravitational mass, or  $G$ , do not change in the field of other masses... Indeed, in 1962, Brans had shown that in general relativity this change is a mere coordinate effect." It's more than a mere coordinate effect. It's a consequence of the total scalar gravitational potential being a locally measured invariant – as it must be for inertia to be correctly accounted for in our reality.

The Harris/Ohanian "interpretation" of general relativity – with its rejection of Faraday-like induction effects allegedly because of the "fact" that  $\partial \mathbf{A} / \partial t = 0$  – has attracted more than a few followers. For example, although they do not seem to reject the correctness of the Equivalence Principle (as does Ohanian), Pfister and King, in their recent book, *Inertia and Gravitation*, accept that Faraday induction-like effects (that follow if  $\partial \mathbf{A} / \partial t$  is not always and everywhere equal to 0) are everywhere and everywhere identically zero. Indeed, they allow they want to, "in a way amend Ciufolini and Wheeler's view on gravitation and inertia." [Page 124. Pun on the title of Ciufolini and Wheeler's book intended.] In particular, the view they want to amend is Ciufolini and Wheeler's assumption that the initial data-hypersurface/constraint equation approach is merely equivalent to a (possibly messy) retarded integration over the matter currents out the past light cone to the past particle horizon. Ciufolini and Wheeler clearly prefer the hypersurface/constraint equation approach. But that's not good enough for Pfister and King, for Ciufolini and Wheeler do not deny the validity of the retarded integration approach. Is this really right? Well, on page 134 they say, "Below we will document quite generally, and also in a real cosmological setting, Mach's principle is connected with the time-independent constraint equations of general relativity." Is it really mandatory to adopt the constraint equation interpretation of general relativity to get Machian inertia?

It's probably a good idea to keep in mind here that the hypersurface/constraint equation only approach has its origin in Harris's claim that a gauge condition justifies setting  $\partial \mathbf{A} / \partial t = 0$ , whereas this actually follows from the fact that

$$\partial \mathbf{A} / \partial t \approx \frac{\phi}{c^2} \frac{d \mathbf{v}}{dt}$$

where  $\mathbf{v}$  is the velocity of an object relative to some local sources and  $\phi$  is the integral of  $Gm/r$  for the local sources with  $m$  and  $r$  the mass and distance of local sources integrated over. We further assume that  $\phi$  is modest (not near a black hole for example, so that  $\phi / c^2$  is much, much less than one). This is a "higher order term" argument, not a gauge invariance argument. Moreover, the FRW cosmology that characterizes our reality is the critical cosmic matter density ( $k = 0$ ) model where  $\Phi = c^2$  everywhere/when. Ciufolini and Wheeler got it right. As simple common sense suggests.

Consider yourself to be driving down a long straight road at

<sup>21</sup> Ohanian is a supporter of the view that the Equivalence Principle has only historical heuristic value; that it is in fact wrong, and thus not a proper foundation for general relativity. See his *Einstein's Mistakes*.

constant velocity with respect to the stars and distant matter in the universe, which in your frame of reference, looking out your past lightcone, appears to be moving rigidly past you with velocity  $-v$ . You slam on the brakes to avoid hitting a deer crossing the road. Your girl or boy friend sitting in the passenger's seat without a seatbelt on declaims, "damn those distant galaxies" as s/he lurches toward the windshield. Why? S/he knows that it's the gravitational action of those galaxies, acting when s/he sees them out the past lightcone, that creates the gigantic gravitational field we all live in. It creates the inertial effects of his/her situation and can be calculated by an integration out the past lightcone of the matter currents s/he can literally see (s/he has eyes with the light gathering power of our largest telescopes) while traveling inertially toward the windshield where it will produce the reaction force to the force of the windshield on his/her head.

To be fair, Pfister and King have a point. While general relativity, contrary to their belief, suffices to deal with routine inertial effects – where the local sources of the field do not produce strong fields themselves – using retarded integrations out the past lightcone, when the local sources produce strong fields that react on the distant sources, this approximation may fail. Recourse to the constraint equation approach, however, is not then demanded. But the Hoyle-Narlikar action at a distance version of general relativity (with the accelerating expansion cutoff) is required to provide the seemingly time-independent interaction of the local and distant sources using retarded and advanced interactions.

\*\*\*\*\*

## A NOTE ON ADVANCED PROPULSION

What does all of the above have to do with advanced propulsion? Well, if inertial forces are the gravitational action of chiefly distant matter in the universe, as they are in general relativity theory, then locally we can produce gigantic gravitational effects by simply accelerating local objects. And it is reasonable to assume that at least large transient gravitational effects can be generated. If, however, local effects can only be generated by interactions with local sources of gravity, as argued by the workshop participant who triggered the circulation of the 2015 version of this essay, then all laboratory scale gravitational effects are hopelessly too small to be of any practical use. But Einstein got inertia right in general relativity theory. Inertia is a gravitational phenomenon.

As a coda of sorts to this essay, I note that interest in action at a distance, or "absorber" theory of the Wheeler-Feynman type, is again in evidence. From my perspective, the chief problem with absorber theory was the absorber part. In electrodynamics, envisioning an absorber that eventually perfectly absorbs electromagnetic radiation, creating the needed conditions for the theory to work, is not difficult. The problem is that gravity and electromagnetism are not exactly analogous. Where electromagnetic signals are attenuated by electrically net-charge neutral matter, gravity is not so attenuated. This is a consequence

of there being no naturally occurring negative masses to act as "sinks" for the fields produced by positive masses. This means that as gravitational disturbances propagate out the future lightcone and interact with matter they encounter, the underlying gravity field and changes therein continue unabated. That is, in electrodynamics there is no invariant  $\Phi = c^2$  field as there are both positive and negative charges as sources and sinks. In positive mass gravity there are only sources, but no sinks – just other positive masses to act on. The result of this peculiar situation is that gravity disturbances continue to propagate indefinitely, unless they are cut off by some physical process other than simple recessional velocity as in most standard FRW cosmologies. In these cosmologies, light signals and gravity disturbances can propagate infinitely far into the future, and wherever they can get, the advanced signals from anything they encounter can get back to the source, seemingly instantaneously. This bothered me so much that I wrote a paper, "Killing Time", with it as the central theme back in 1996 [see the technical articles section of the bibliography of *Starships*].

Years later, I discovered that Stephen Hawking had seen the same problem which he characterized as the "divergence of the advanced solution" in Hoyle and Narlikar's action at distance version of general relativity theory.<sup>22</sup> Hawking suggested that negative mass might help with this problem (just as negative electric charge solves the problem that would otherwise arise in electrodynamics) – a suggestion not then taken seriously in that age of the positive energy theorem. But there is another way to solve this problem: accelerating expansion of the universe. This didn't dawn on me until I read Brian Greene's *The Fabric of the Cosmos*, in particular, footnote 10 for chapter 8, where he mentions that accelerating expansion produces a "cosmic horizon" that renders the spacetime beyond the horizon forever inaccessible to light signals emitted at the origin of coordinates, no matter how long they propagate into the future. This is the "cut-off" that keeps the action at a distance interaction finite. Were I a clever theoretician, I could have predicted accelerating cosmic expansion before it was discovered. Instead, I kept plugging away at the experimental stuff.

But in the fall of 2014, I convinced my colleague, Heidi Fearn, who had joined me on the Mach effects project a few years earlier, to fill in the formalism and write this up. She sent it to the "gr-qc" section of the arXiv operation. Her first submission there. They told her she needed to get endorsers. She asked two world-famous general relativists, who immediately begged off, and Jayant Narlikar, who allowed that he had never used the arXiv and so could not be an endorser. But the next day the paper was up on the server. She had submitted the paper to the *Journal of Modern Physics* for a special issue on gravitation and cosmology. It was accepted in less than a week. Perhaps there is more to Einstein's outrageous legacy than hitherto has been widely thought. And perhaps there is a way to manipulate the spatiotemporal continuum that is the inertia-gravitational field to get around spacetime quickly.

## ACKNOWLEDGEMENTS

In addition to those mentioned above, I am indebted to Raymond Chiao, John Cramer, Marshall Eubanks, and José Rodal for helpful conversations. This work was supported by NASA Innovative Advanced Concepts (NIAC) grant NNX17AJ78G "Mach Effects for In Space Propulsion: Interstellar Mission."

<sup>22</sup> Hawking detected this problem while reading Hoyle and Narlikar's manuscript overnight before Hoyle presented the work at the Royal Society meeting the following day. It took me a lot longer to zero in on this problem. But hey, I'm just a bumbling experimentalist.

# VOLTAGE POWER LAW SCALING OF THE FORCE FOR A MACH EFFECT GRAVITATIONAL ASSIST DRIVE

HEIDI FEARN and JAMES F. WOODWARD, Physics department, California State University Fullerton, 800 N State College Blvd., Fullerton CA 92834, USA  
Email: (hfearn@fullerton.edu)

We report on new experimental data taken at Fullerton to show a scaling law of force with voltage to the fourth power,  $V^4$  for the Mach effect drive. Rather than just 4 averaged points (each point represented 24 averaged forward minus 24 averaged reversed data points to cancel none reversing thrust) as reported previously [1] we have several week's worth of data with over a hundred data points covering a larger voltage range and an excel regression showing a scaling of  $V^{3.97}$  which is very close to the theoretical  $V^4$  scaling law.

**Keywords:** Mach effect, Propellant-less propulsion

## 1 INTRODUCTION

A stack of lead zirconate titanate (PZT) disks is clamped between a brass reaction mass and aluminum end mass, and excited with a periodic voltage, causing the stack to expand and contract. The induced acceleration of the end of the stack near the aluminum cap produces mass fluctuations. A second induced acceleration transforms the mass fluctuation into a force. Fig. 1 below shows a current realization of such a Mach effect gravity assist (MEGA) drive mounted in the half-shell of a (mu metal lined aluminum) Faraday cage.

The mass change is predicted from general relativity by JFW [2] and papers in reference [3], we give the result here for convenience. The mass change occurs when an extended object is undergoing internal energy changes and is also undergoing acceleration. The mass change is defined in terms of the second derivative with respect to time of the energy density within the device, this can be written as the rate of change of power as

$$\delta m = \frac{1}{4\pi G} \left( \frac{1}{\rho c^2} \frac{\partial P}{\partial t} \right), \quad (1)$$

where  $m$  is mass,  $\rho$  is energy density of the device,  $c$  is the speed of light and  $P$  is the power in the device. The device is undergoing deformation via the piezoelectric effect. The power goes as the square of the voltage. To generate a thrust, there must be a second force acting in sync with the piezoelectric force to create acceleration. The phase here is very important if the forces are out of sync there would be no resultant thrust. The piezoelectric force causes the energy changes within the device and enables the mass fluctuation. The second force is the electrostriction. Electrostriction goes with the square of the electric field. The electric field goes as  $V/d$  where  $V$  is the voltage and  $d$  is the thickness of each PZT disc. Hence the acceleration of the device would go as the voltage squared if we consider it to be mainly due to electrostriction. Therefore, we expect the force, going like the mass change times acceleration, goes with voltage to the fourth power,  $V^4$ .

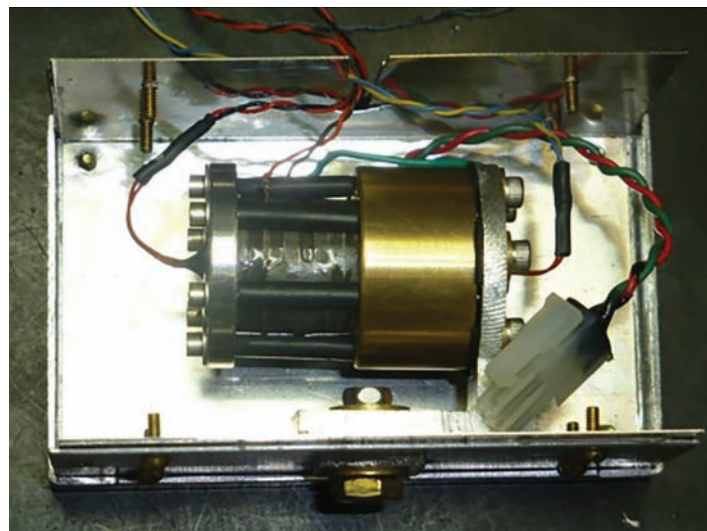


Fig. 1: The MEGA device consists of a stack of 2mm thick lead zirconate titanate (PZT) discs clamped between a thin aluminum mass and a heavy brass mass. The photograph shows the device mounted in a Faraday half cage with mu metal lining.



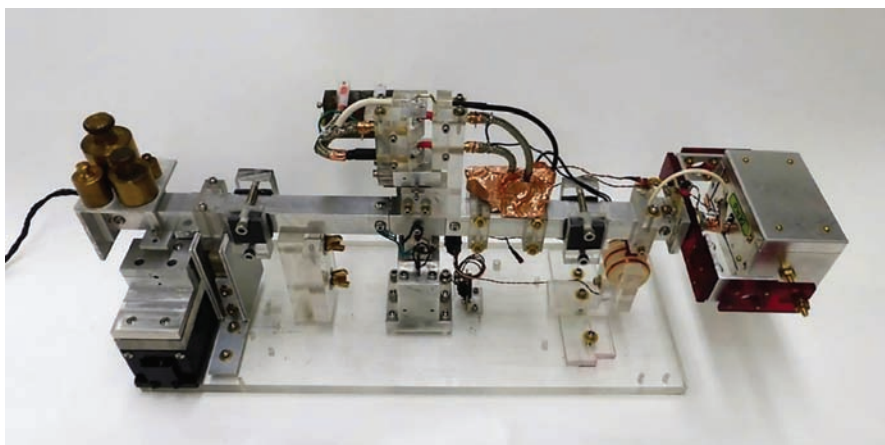


Fig. 2: The balance pendulum capable of measuring sub-micro Newton forces.

## 2 EXPERIMENTAL SETUP

The balance pendulum capable of measuring sub-micro Newton forces is shown in Fig. 2. It features Galinstan liquid metal contacts. The torsional stiffness is given by 2 c-flex flexural bearings mounted inside the central column. The Faraday cage is seen to the right and the brass weights on the left act as a counterpoise for the Faraday cage. Under the brass weights on the left is a stepper motor holding a Philtec optical sensor. A shiny aluminum plate is attached to the balance arm. The laser light from the fiber optic sensor on the Philtec reflects from the shiny plate and gives a distance measurement output in voltage, which is converted to a thrust measurement. The coils just below the Faraday cage can be used to inject a calibrated force to the system when the device inside the Faraday cage is not powered. This is a second way of calibrating the thrust from the deflection voltage measured by the optical sensor.

The device operates on 36.3 kHz at approximately 180 volts.

A second harmonic frequency at 72.6 kHz is also present due to electrostriction in the PZT stack. Typically the device is allowed to sit to get ambient noise data. Then an 8 second on resonant pulse is applied to the device, followed by more ambient background for 8 seconds, then another 8 second pulse on resonance. The run finishes with more ambient, no voltage, data. Typically several forward runs are averaged and then the device is reversed in direction and several reverse runs taken and averaged. We also subtract the reverse runs from the forward runs so that any non reversing thrust is eliminated. Typical data is shown below.

## 3 RESULTS

Fig. 3 suggests that it might be advantageous to produce thrust as a succession of periodic switching transients. The obvious problem with this is that the off and on transients appear to be roughly equal, and thus cancel each other. This may be dealt with by “chirping” the frequency to suppress either the off or on

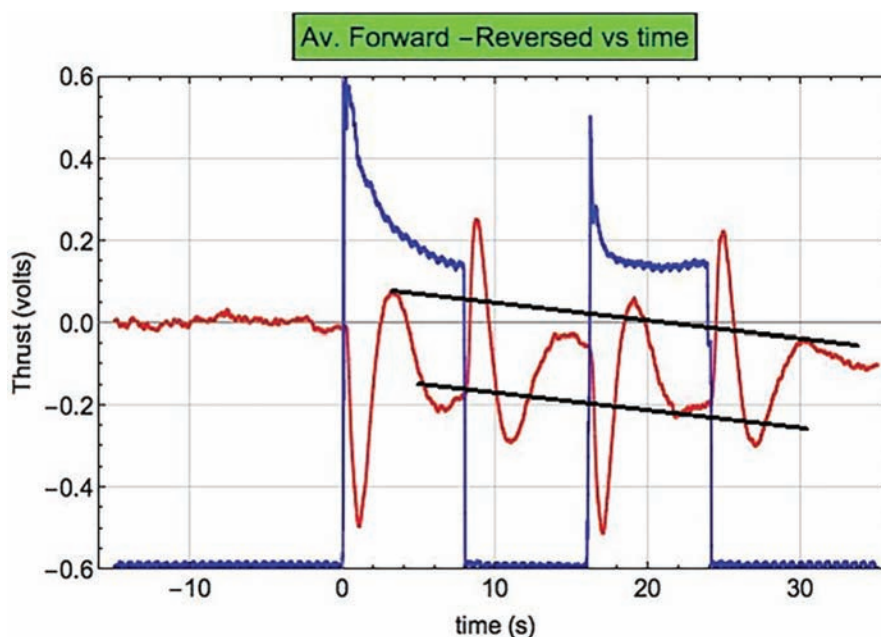
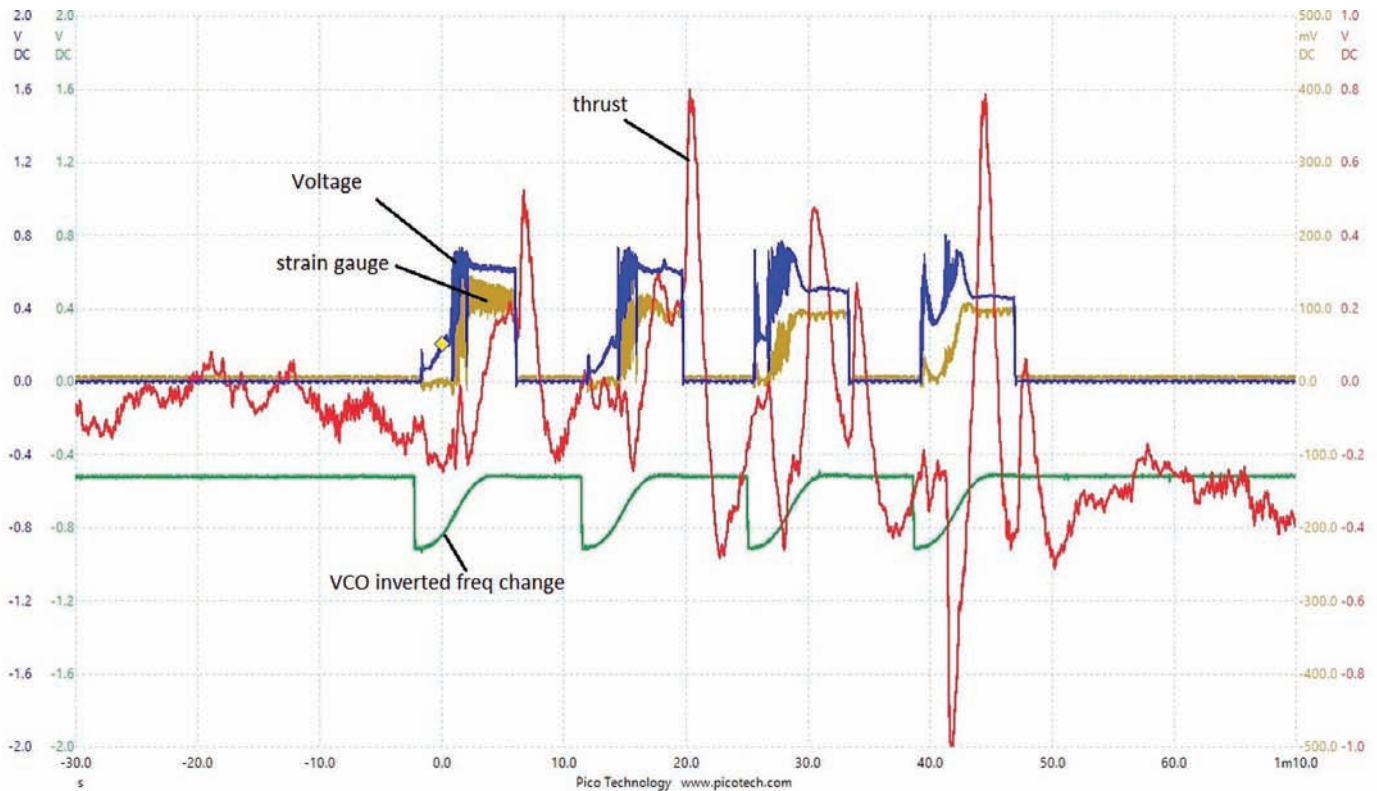


Fig. 3: The blue trace tracks the applied voltage to the device with two 8-second long on intervals. The thrust (red trace) switching transients at on and off are obvious. Less obvious are the intervals of “steady” thrust toward the ends of the on intervals. These are brought out by the black lines. The upper line is the “zero” thrust line. Notice that it passes through the thrust trace at the end of the off interval between the voltage pulses. The lower black line, however, passes through the corresponding power on parts of the thrust traces, with non-zero values. The thrust scale is 1 microNewton to 0.162 volts.





**Fig. 4:** First two chirps are with 37.0 kHz as the chirped to frequency (the steady value of the VCO control frequency [green trace]). Realizing the error, the frequency was changed to 35.8 kHz between the second and third chirps. Note the behavior in the third and fourth chirps where the resonant frequency is swept in the chirp. Most noticeable in the last chirp the thrust changes sign as we sweep through the resonance. The thrust scale is 1 microNewton to 0.162 volts. The voltage scale is 0.69 volts measured translates to 240 actual volts applied.

transient. The voltage signal is produced by a voltage controlled oscillator (VCO).

The VCO control voltage is set to produce some desired frequency on or near a resonance of the device being tested. The chirp event consists of changing the control voltage to produce some desired frequency above the nominal voltage that produces the resonance frequency of the device – usually to produce a frequency 3.5 kHz higher than the nominal voltage – turning the power on, and then ramping the control voltage to the nominal voltage in some programmed way (duration, inflections, etc.). This suppresses switching transients in the ramped part of the event, leaving only the off (or on) switching transient. The operating conditions for the vacuum are typically between 10 to 20 mTorr. The start temperature is always less than 30 deg C and the voltage resonance frequency is between 36.3 to 36.5 kHz.

In the spring of 2015, a curious property of the MEGA devices then in use was brought to our attention [4]. The devices were (and are) operated with the application of a single frequency voltage signal. Normally, two frequencies are required to produce thrust: the first harmonic to induce mass fluctuations at the second harmonic frequency; and a second harmonic signal (with appropriate phase) to render the mass fluctuations as a thrust [1-3]. The feature of the Steiner Martins SM-111 devices made with material acquired in 2011 is that they display anomalously large electrostrictive behavior that makes supplying a second harmonic signal unnecessary as electrostriction goes as the square of the applied electric field ( $V/d$ ) where  $V$  is the voltage and  $d$  is the thickness of the discs.

The thrust goes as the product of the mass fluctuation and the mechanical electrostrictive force. The mass fluctuation goes as the power, which scales with the square of the applied voltage. So, the thrust should scale with the 4<sup>th</sup> power of the applied voltage. This voltage scaling is not replicated by other natural processes that might be expected in these devices.

Chirped runs were used to supply the data for the following scatter plots. Recorded are applied voltage (blue), thrust (red), temperature (green), and accelerometer (brown). Each run has 4 or 5 chirps, and they show evolution from chirp to chirp, as well as run to run.

Each chirp starts with the frequency of the driving signal 3.5 kHz above the resonant frequency [36.3 kHz]. After a couple of seconds, the frequency is smoothly ramped down to the resonant frequency. (The VCO control voltage follows a patched parabolic path to avoid any large changes in frequency that might induce a switching transient.) After a second or so at the resonant frequency, the voltage signal is switched off, producing a switching transient (that is, a predicted Mach effect).

Several features of the chirped thrust pulses can be singled out for measurement. The one chosen for this test was the “off” switching transient amplitude (as described below). This choice was made because the transient event, after the power is switched off, is unpowered and thus not influenced by effects that might complicate the analysis.

Before turning to the measurements of runs, a word on high power behavior is advisable. As the frequency sweeps the res-

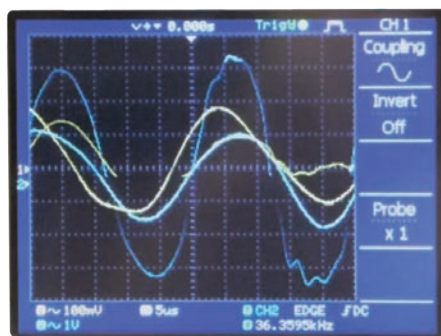


Fig. 5: The blue traces in these slides are those for the voltage across the device. The scale factor is 1 volt = 100 volts. The yellow traces are those for the strain gauge. The strain gauge consists of two 0.3 mm thick disks embedded in the PZT stack near the aluminum cap. It passively monitors mechanical activity in the stack. It is not calibrated to an absolute standard.

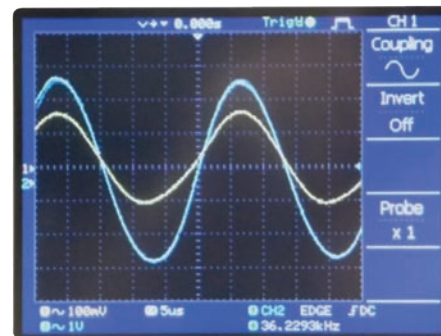
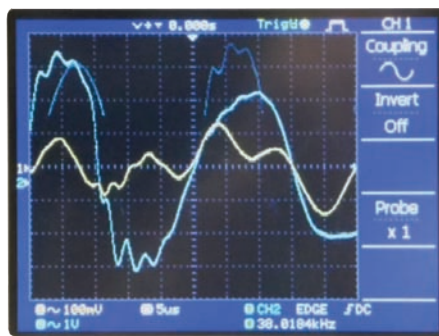


Fig. 6: Stable operation of the device, shows the applied voltage (blue) and strain gauge (yellow) in phase with respect to each other.

onance that leads to the observed thrusts, the thrust first goes smoothly negative, and then, as the resonance is swept, positive. When the device is not in the “sweet” temperature range, sweeping the resonance induces chaotic behavior that persists for the rest of the chirp. Examples of this chaotic behavior are shown in Fig. 5.

After an interval that varies with the operating conditions, especially the temperature, the device may settle from chaotic into stable operation. This is evidenced by the waveforms transitioning into ones like those in Fig. 6.

Note that the waveforms are in phase. Waveforms as large, or larger, are seen in some devices. But they are not in phase. Such behavior does not result in serious thrust. Phase matters. If the waveforms become out of phase, then the thrust is lost. This completely negates the idea of a Dean drive, or slip-stick effect, as the cause of the thrust. A ratchetting effect would not be governed by this phase relationship. Transition to stable be-

havior can be detected in the voltage and accelerometer traces for the runs. At high power, the voltage trace increases slightly, and the accelerometer trace decreases. At intermediate power, this changes. At low power, chaotic behavior is rarely seen.

The run shown in Fig.7 below was done at a higher initial temperature [by a few degrees C; check the green trace, which in this case tracks temperature, not the VCO control voltage].

As a result, the behavior of the last chirp in the first run now appears in the 3<sup>rd</sup> chirp, and both the 4<sup>th</sup> and 5<sup>th</sup> chirps display stable behavior shortly after the resonance is swept. This means that the thrust produced during the chirps 4 and 5 is suitable for measurement for the voltage scaling test. Note that this measurement is fundamentally different from the measurement of the switching transient thrust [which is unpowered, and merely a ballistic reaction to a thrust impulse at power off].

Runs for amplifier level 10 were similar to those at amplifier

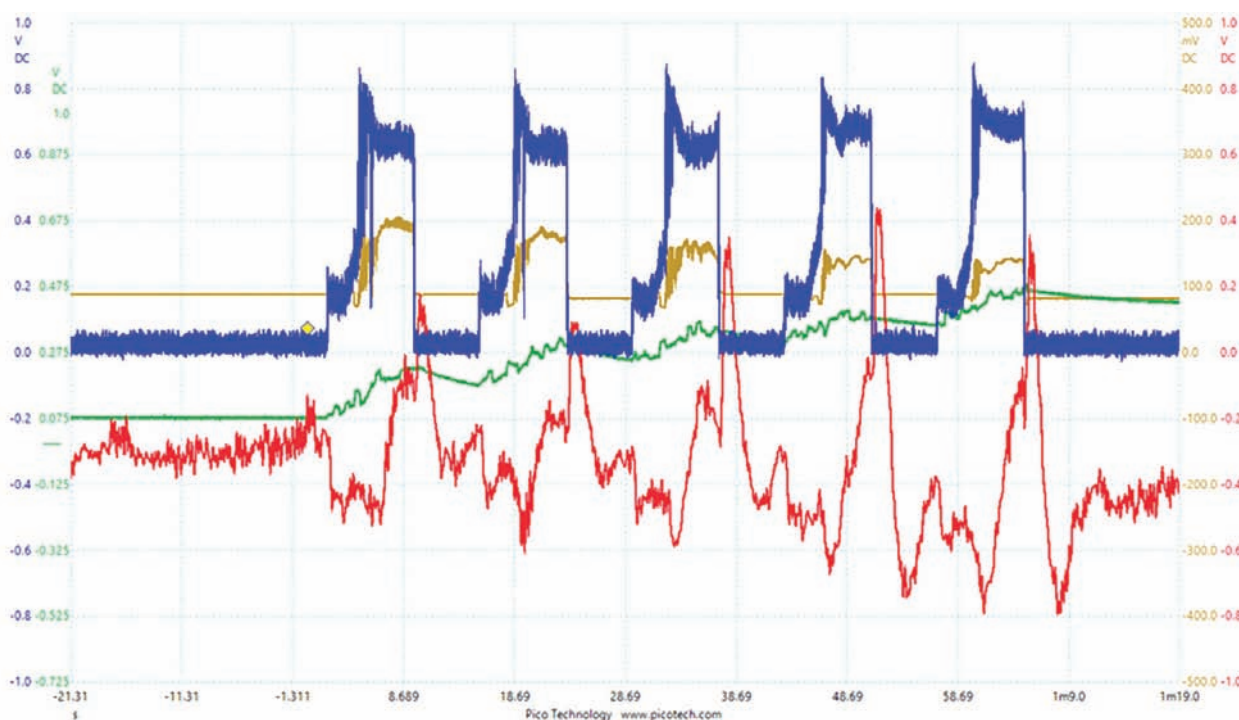


Fig. 7: Chirped runs taken at amplifier level 6. Chirps 3,4 and 5 are usable here. The green trace here is temperature measured by a thermistor embedded in the aluminum end mass.

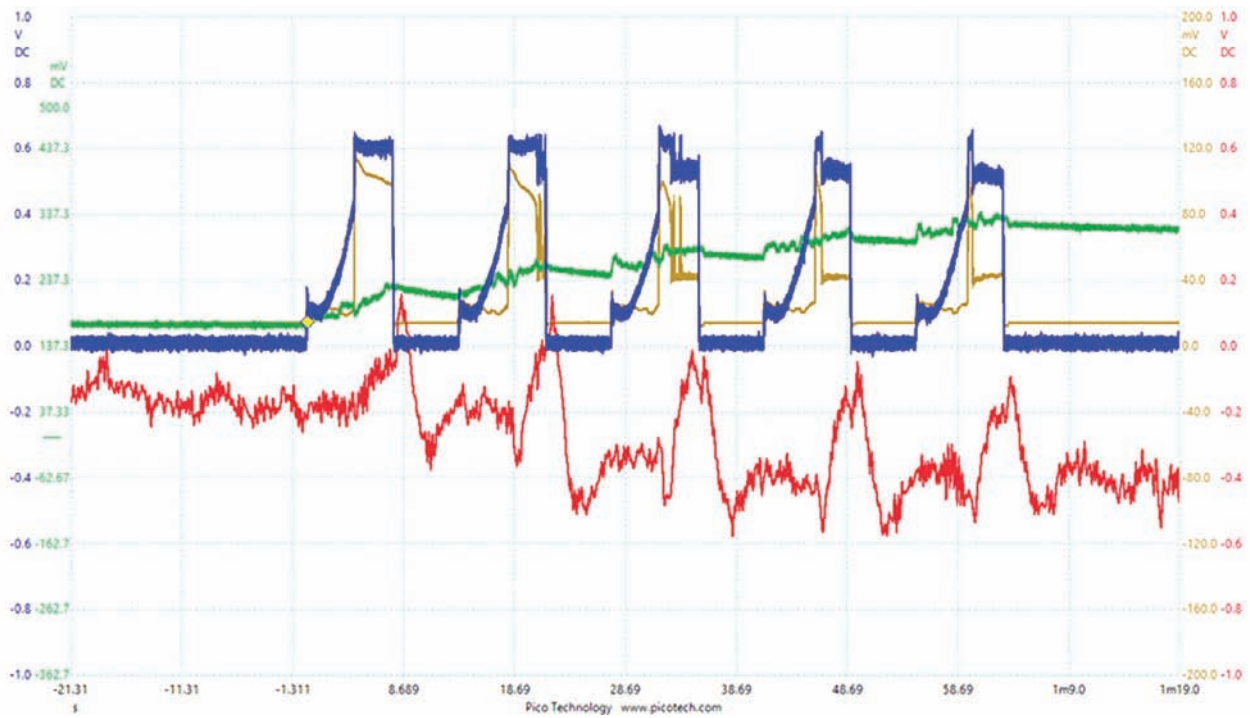


Fig. 8: Chirped runs taken at amplifier level 10. Chirps 2-5 used. Green trace is temperature.

level 12 – that is, stable running was only achieved for operation at optimum thermal conditions. So chirps displaying stable operation had to be identified to get data consistent with that for amplifier level 6. The noteworthy difference in operation at this level was the pronounced drop in both the voltage and strain gauge responses at the transition to stable operation – easily seen in Fig. 8. Runs done at amplifier level 12 were not beset with chaotic behavior like those done at higher power. The only signs of chaotic-like behavior were brief flashes of such behavior as the sweep progressed across the true resonance, which

itself is very narrow. This is displayed in the runs shown in Figs. 9 and 10 (overleaf) as the voltage and accelerometer spikes that occur just at the end of the sweep. Those spikes require “just so” conditions and are usually not seen, as shown in the third run where no spikes at all are present. Stable running being the normal mode of operation at level 12, essentially all of the data was usable for the voltage scaling test.

Runs were done for both the “forward” and “reversed” orientations of the device on the beam. The actual measurements

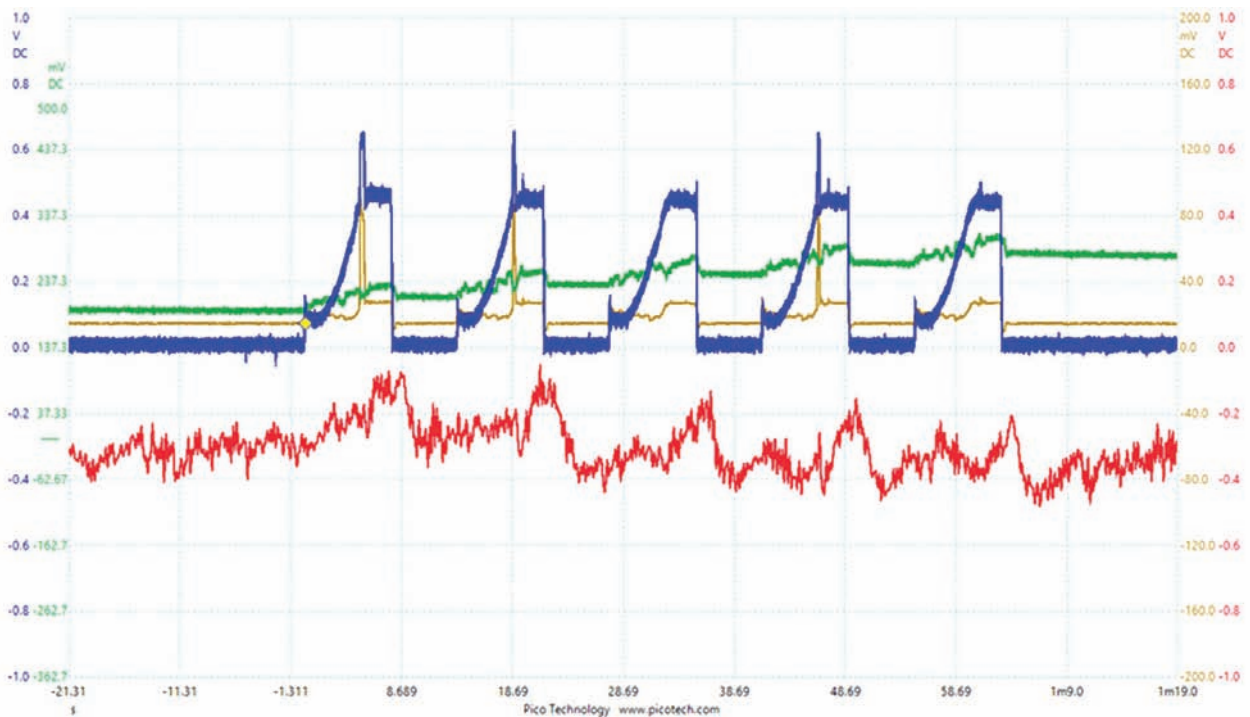


Fig. 9: Chirped runs taken at amplifier level 12.



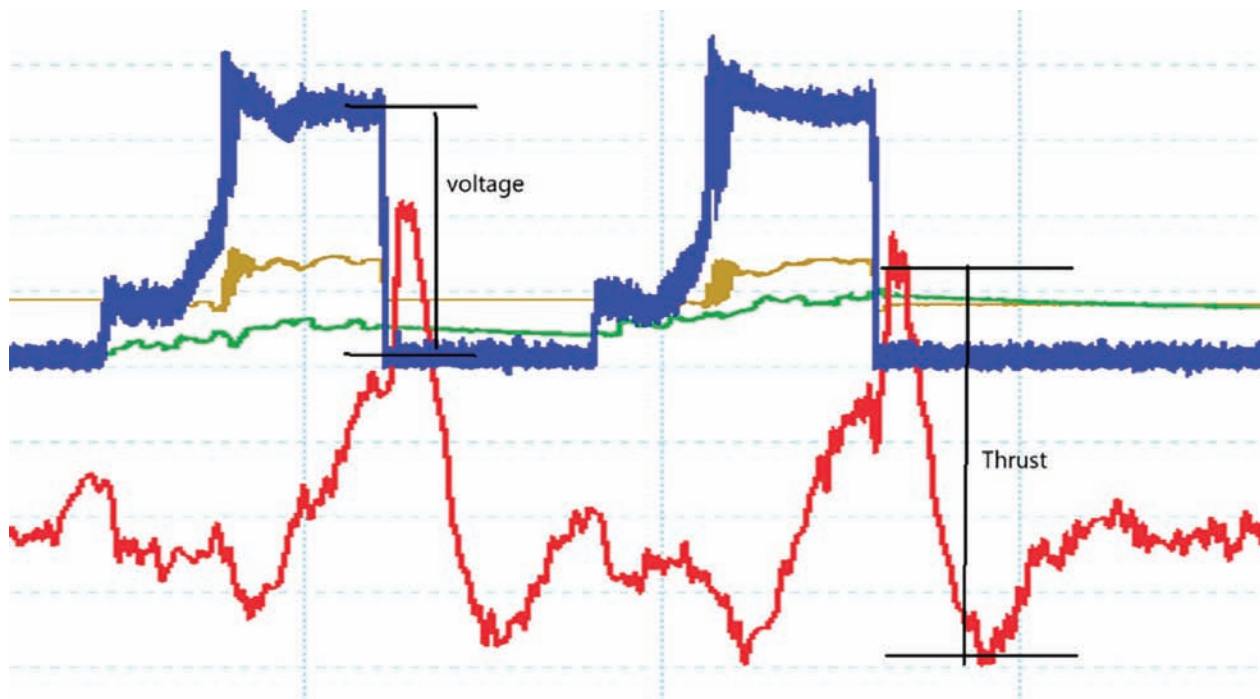


Fig.10: The measurements taken from the chirped runs. (1 microNewton corresponds to 0.162 volts. Also 0.69 measured volts corresponds to 240 applied volts.)

taken are shown in Fig.10.

Thrust versus applied voltage data were recorded and plotted as Excel “series” for each day. The daily “series” for the reversed direction are displayed in the Fig.11. Some clustering is present in the data due to particular power amplifier settings having been used. The reversed data was taken over a period of a week and a half. During this short time the device did not undergo much change, (damage, cracking, moisture absorption etc.)

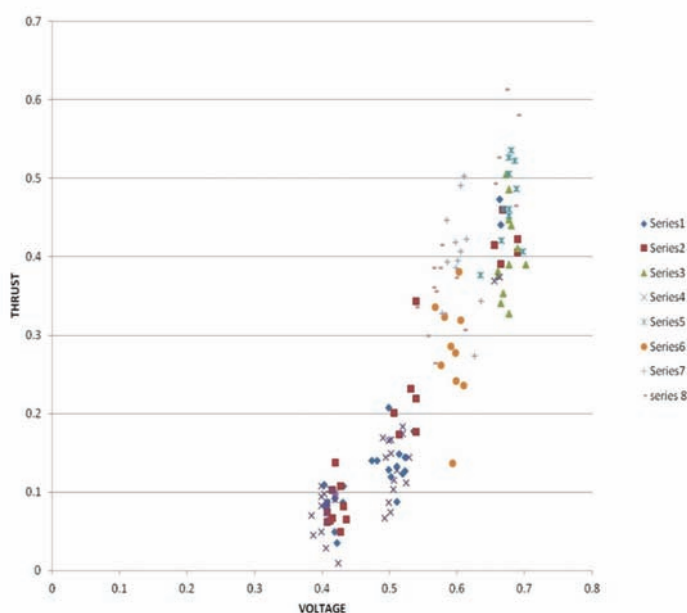


Fig. 11: Reversed data showing voltage versus thrust as measured in Figure 10. Each series represents a dataset for one day. The scales show the voltages actually measured by the apparatus. These must be scaled to obtain the correct voltages and thrust in microNewtons. (1 micro Newton corresponds to 0.162 volts. Also 0.69 measured volts corresponds to 240 applied volts.)

The data appears to be fairly closely bunched.

To get the thrust dependence on applied voltage, a simple power law regression was performed on the complete data set. This is displayed in Fig.12.

Note that the power exponent, 3.97, is very nearly the predicted value of 4. (Scale factors have been applied to render the thrusts and voltages in conventional units. A single microNewton corresponds to 0.162 measured volts on the thrust scale and 0.69 measured volts corresponds to 240 applied volts on the voltage scale.)

The plots shown are for the forward orientation. The forward data are both larger and less well bunched than the reversed data. In part, this is a consequence of a non-reversing “thrust” that does not share quartic voltage scaling with the reversing

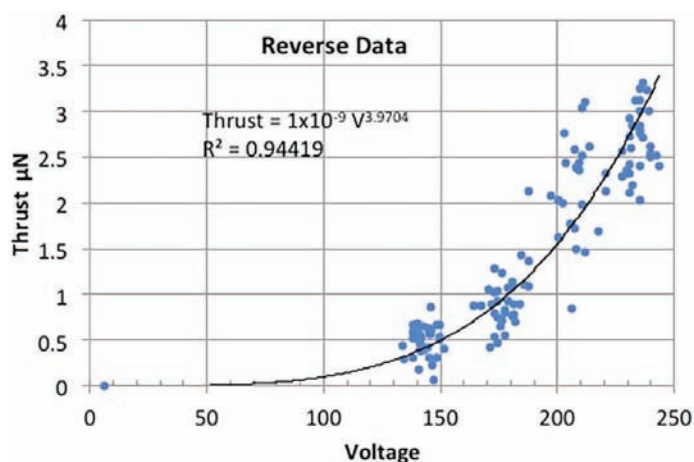


Fig. 12: Voltage versus force in micro Newtons for the reversed direction of the device. The plot shows a  $V^{3.97}$  dependence. The point near zero is not a true data point and is there to force the curve through zero and to increase the  $R^2$  value to a maximum.



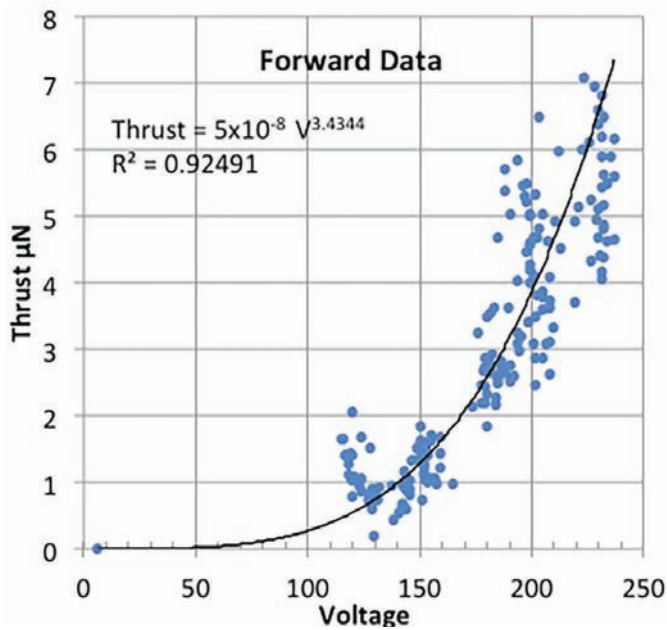


Fig. 13: The voltage versus thrust for the forward direction. This yields a power law scale of  $V^{3.4}$  – slightly lower than for the reversed direction. There are 184 data points on this plot, each data point corresponding to one chirp. The point near zero is not a true data point and is there to force the curve through zero and increase the  $R^2$  value to a maximum. It is the same point as taken for the reversed runs. This data includes some non-reversing thrust, which is causing a problem with the fit.

part of the total thrust. The forward data was taken over a much longer time frame of more than a month. During this time the device had time to change its characteristics, which is seen from the lesser grouping of the data points. In particular

the device could have suffered damage from over running it, cracking, retorquing of the bolts and moisture absorption.

The power law regression in this case returns 3.4, markedly less than that for the reversed orientation case. Nonetheless, the exponent is greater than 3.

#### 4 CONCLUSIONS

We have shown “chirp” data (a decreasing sweep of frequency from 3.5kHz above resonance down to resonance at 36.3 kHz) for 184 data points in the forward and 125 data points in the reversed orientation of the device. The forward and reversed data was plotted, using applied voltage, versus thrust in micro Newtons. The thrust scales were shown to be  $V^{3.97}$  in the reversed direction and  $V^{3.4}$  in the forward direction where a voltage  $V$  was applied. Since theoretically we expect no difference in the forward and reversed direction voltage scale law, we account for the lower scale power for the forward direction because the runs were taken (after the reverse runs) and over a longer time period and the device had time to change its characteristics. Also these runs do not subtract off any non-reversing thrust, so there is some error introduced there. More runs were taken, but the data points are more widely spaced.

The theory suggests that the voltage scale law for the thrust should scale as  $V^4$ . We take our presented data to verify the theoretical prediction within the bounds of error of the measurements.

#### ACKNOWLEDGEMENT

This work was supported by NASA Innovative Advanced Concepts (NIAC) grant NNX17AJ78G “Mach Effects for In Space Propulsion: Interstellar Mission.”

#### REFERENCES

1. H. Fearn et al. “Theory of a Mach effect thruster II”, *Jour. of Mod. Phys.* 6, pp1868-1880 (2015).
2. J. F. Woodward, *Making Starships and Stargates*, Springer Press, Dec 2013.
3. See papers in the proceedings of the “Estes Park Advanced Propulsion workshop” (2016) edited by H. Fearn and L. L. Williams, available for free download on the website <http://ssi.org>
4. Private communication with Nick Herbert 2015.

Received 18 December, 2017 Accepted 22 February 2017

# THE QUANTUM HANDSHAKE EXPLORED

JOHN G CRAMER, Department of Physics, University of Washington  
email: jcramer@uw.edu

---

We discuss the transactional interpretation of quantum mechanics, apply it to several counter-intuitive quantum optics experiments (two-slit, quantum eraser, trapped atom, ...), and describe a mathematical model that shows in detail how transactions form.

**Keywords:** Quantum mechanics, Quantum interpretation, Transactional interpretation, Quantum paradoxes, Advanced waves, Nonlocality, Entanglement

---

## 1 QUANTUM ENTANGLEMENT AND NONLOCALITY

Quantum mechanics, our standard theoretical model of the physical world at the smallest scales of energy and size, differs from the classical mechanics of Newton that preceded it in one very important way. Newtonian systems are always local. If a Newtonian system breaks up, each of its parts has a definite and well-defined energy, momentum, and angular momentum, parceled out at breakup by the system while respecting conservation laws. After the component subsystems are separated, the properties of any subsystem are completely independent and do not depend on those of the other subsystems.

On the other hand, quantum mechanics is nonlocal, meaning that the component parts of a quantum system may continue to influence each other, even when they are well separated in space and out of speed-of-light contact. This characteristic of standard quantum theory was first pointed out by Albert Einstein and his colleagues Boris Podolsky and Nathan Rosen (EPR) in 1935, in a critical paper[1] in which they held up the discovered nonlocality as a devastating flaw that, it was claimed, demonstrated that the standard quantum formalism must be incomplete or wrong. Einstein called nonlocality “spooky actions at a distance”. Schrödinger followed on the discovery of quantum nonlocality by showing in detail how the components of a multi-part quantum system must depend on each other, even when they are well separated [2].

Beginning in 1972 with the pioneering experimental work of Stuart Freedman and John Clauser[3], a series of quantum-optics EPR experiments testing Bell inequality violations [4] and other aspects of entangled quantum systems were performed. This body of experimental results can be taken as a demonstration that, like it or not, both quantum mechanics and the underlying reality it describes are intrinsically nonlocal. Einstein’s spooky actions-at-a-distance are really out there in the physical world, whether we understand and accept them or not.

How and why is quantum mechanics nonlocal? Nonlocality comes from two seemingly conflicting aspects of the quantum formalism: (1) energy, momentum, and angular momentum, important properties of light and matter, are conserved in all

quantum systems, in the sense that, in the absence of external forces and torques, their net values must remain unchanged as the system evolves, while (2) in the wave functions describing quantum systems, as required by Heisenberg’s uncertainty principle[5], the conserved quantities may be indefinite and unspecified and typically can span a large range of possible values. This non-specificity persists until a measurement is made that “collapses” the wave function and fixes the measured quantities with specific values. These seemingly inconsistent requirements of (1) and (2) raise an important question: how can the wave functions describing the separated members of a system of particles, which may be light-years apart, have arbitrary and unspecified values for the conserved quantities and yet respect the conservation laws when the wave functions are collapsed?

This paradox is accommodated in the formalism of quantum mechanics because the quantum wave functions of particles are entangled – the term coined by Schrödinger [2] to mean that even when the wave functions describe system parts that are spatially separated and out of light-speed contact, the separate wave functions continue to depend on each other and cannot be separately specified. In particular, the conserved quantities in the system’s parts (even though individually indefinite) must always add up to the values possessed by the overall quantum system before it separated into parts.

How could this entanglement and preservation of conservation laws possibly be arranged by Nature? The mathematics of quantum mechanics gives us no answers to this question: it only insists that the wave functions of separated parts of a quantum system do depend on each other. Theorists prone to abstraction have found it convenient to abandon the three-dimensional universe and describe such quantum systems as residing in a many-dimensional Hilbert hyperspace in which the conserved variables form extra dimensions and in which the interconnections between particle wave functions are represented as allowed sub-regions of the overall hyperspace. That has led to elegant mathematics, but it provides little assistance in visualizing what is really going on in the physical world.

Then, how is this behavior possible? The transactional interpretation of quantum mechanics provides the answer.

## 2 THE TRANSACTIONAL INTERPRETATION OF QUANTUM MECHANICS

The Transactional Interpretation of quantum mechanics [6–11], inspired by the structure of the quantum wave mechanics formalism itself, views each quantum event as a Wheeler-Feynman[12] “handshake” or “transaction” process extending across spacetime that involves the exchange of advanced and retarded quantum wave functions to enforce the conservation of certain quantities (energy, momentum, angular momentum, etc.). It asserts that each quantum transition forms in four stages: (1) emission, (2) response, (3) stochastic choice, and (4) repetition to completion.

The first stage of a quantum event is the emission of an “offer wave” by the “source”, which is the object supplying the quantities transferred. The offer wave is the time-dependent retarded quantum wave function  $\psi$ , as used in standard quantum mechanics. It spreads through spacetime until it encounters the “absorber”, the object receiving the conserved quantities.

The second stage of a quantum event is the response to the offer wave by any potential absorber (there may be many in a given event). Such an absorber produces an advanced “confirmation wave”  $\psi^*$ , the complex conjugate of the quantum offer wave function  $\psi$ . The confirmation wave travels in the reverse time direction and arrives back to the source at precisely the instant of emission with an amplitude given by  $\psi\psi^*$ .

The third stage of a quantum event is the stochastic choice that the source exercises in selecting one of the many received confirmations. The strengths  $\psi\psi^*$  of the advanced-wave “echoes” determine which transaction forms in a linear probabilistic way.

The final stage of a quantum event is the repetition to completion of this process by the source and selected absorber, each perturbed by the other in an unstable configuration that avalanches to completion, reinforcing the selected transaction with multiple wave exchanges until the conserved quantities are transferred, the states stabilize, and the potential quantum event becomes a real event.

Here we summarize the principal elements of the Transactional Interpretation, structured in order to contrast it with the Copenhagen Interpretation:

- The fundamental quantum mechanical interaction is taken to be the transaction. The state vector  $\psi$  of the quantum mechanical formalism is a physical wave with spatial extent and is identical to the initial “offer wave” of the transaction. The complex conjugate of the state vector  $\psi^*$  is also a physical wave and is identical to the subsequent “confirmation wave” of the transaction. The particle (photon, electron, etc.) and the collapsed state vector are identical to the completed transaction. The transaction may involve a single emitter and absorber and two vertices or multiple emitters and absorbers and many vertices, but is only complete when appropriate quantum boundary conditions are satisfied at all vertices, i.e., loci of emission and absorption. Particles transferred have no separate identity independent from the satisfaction of the boundary conditions at the vertices.
- The correspondence of “knowledge of the system” with

the state vector  $y$  is a fortuitous but deceptive consequence of the transaction, in that such knowledge must necessarily follow and describe the transaction.

- Heisenberg’s Uncertainty Principle [5] is a consequence of the fact that a transaction in going to completion is able to project out and localize only one of a pair of conjugate variables (e.g., position or momentum) from the offer wave, and in the process it delocalizes the other member of the pair, as required by the mathematics of Fourier analysis. Thus, the Uncertainty Principle is a consequence of the transactional model and is not a separate assumption.
- Born’s Probability Rule [13] is a consequence of the fact that the magnitude of the “echo” received by the emitter, which initiates a transaction in a linear probabilistic way, has strength  $P = \psi\psi^*$ . Thus, Born’s Probability Rule is a consequence of the transactional model and is not a separate assumption of the interpretation.
- All physical processes have equal status, with the observer, intelligent or otherwise, given no special status. Measurement and measuring apparatus have no special status, except that they happen to be processes that connect and provide information to observers.
- Bohr’s “wholeness” of measurement and measured system exists, but is not related to any special character of measurements but rather to the connection between emitter and absorber through the transaction.
- Bohr’s “complementarity” between conjugate variables exists, but like the Uncertainty Principle is just a manifestation of the requirement that a given transaction going to completion can project out only one of a pair of conjugate variables, as required by the mathematics of Fourier analysis.
- Resort to the positivism of “don’t-ask-don’t-tell” is unnecessary and undesirable. A distinction is made between observable and inferred quantities. The former are firm predictions of the overall theory and may be subjected to experimental verification. The latter, particularly those that are complex quantities, are not verifiable and are useful only for visualization, interpretational, and pedagogical purposes. It is assumed that both kinds of quantities must obey conservation laws, macroscopic causality conditions, relativistic invariance, etc.

In summary, the Transactional Interpretation explains the origin of the major elements of the Copenhagen Interpretation while avoiding their paradoxical implications. It drops the positivism of the Copenhagen Interpretation as unnecessary, because the positivist curtain is no longer needed to hide the nonlocal backstage machinery.

It should also be pointed out that giving some level of objective reality to the state vector colors all of the other elements of the interpretation. Although in the Transactional Interpretation, the Uncertainty Principle and the statistical interpretation are formally the same as in the Copenhagen Interpretation, their philosophical implications, about which so much has been written from the Copenhagen viewpoint, may be rather different.

The Transactional Interpretation offers the possibility of resolving all of the many interpretational paradoxes that quantum mechanics has accumulated over the years. Many of these are analyzed in reference [6], the publication in which the Transactional Interpretation was introduced. Here we will not attempt to deal with all of the paradoxes. We will instead focus on the interpretational problems associated with quantum nonlocality and entanglement.

### 3 APPLYING THE TRANSACTIONAL INTERPRETATION TO QUANTUM PARADOXES

#### 3.1 Einstein's Bubble *Gedankenexperiment* (1927)

Quantum nonlocality is one of the principal counterintuitive aspects of quantum mechanics. Einstein's "spooky action-at-a-distance" is a real feature of quantum mechanics, but the quantum formalism and the orthodox Copenhagen Interpretation provide little assistance in understanding nonlocality or in visualizing what is going on in a nonlocal process. The Transactional Interpretation provides the tools for doing this. Perhaps the first example of a nonlocality paradox is the Einstein's bubble paradox was proposed by Albert Einstein at the 5<sup>th</sup> Solvay Conference in 1927 [14,15].

A source emits a single photon isotropically, so that there is no preferred emission direction. According to the Copenhagen view of the quantum formalism, this should produce a spherical wave function  $\psi$  that expands like an inflating bubble centered on the source. At some later time, the photon is detected, and, since the photon does not propagate further, its wave function bubble should "pop", disappearing instantaneously from all locations except the position of the detector. Einstein asked how the parts of the wave function away from the detector could "know" that they should disappear, and how it could be arranged that only a single photon was always detected when only one was emitted?

At the 5<sup>th</sup> Solvay Conference, Werner Heisenberg [15] dismissed Einstein's bubble paradox by asserting that the wave function cannot be depicted as a real object moving through space, as Einstein had implicitly assumed, but instead is a mathematical representation of the knowledge of some observer who is watching the process. Until detection, the observer knows nothing about the location of the emitted photon, so the wave function must be spherical, distributed over the  $4\pi$  solid angle to represent his ignorance. However, after detection the location of the photon is known to the observer, so the wave function "collapses" and is localized at the detector. One photon is detected because only one photon was emitted.

The Transactional Interpretation provides an alternative explanation, one that permits the wave function to be, in some sense, a real object moving through space rather than an esoteric representation of knowledge. This is illustrated in Fig. 1. The offer wave  $\psi$  from the source indeed spreads out as a spherical wave front and eventually encounters the detector on the right. The detector responds by returning to the source a confirmation wave  $\psi^*$ . Other detectors (i.e., potential absorbers) also return confirmation waves, but the source, randomly weighted by the  $\psi\psi^*$  echoes from the potential absorbers, selects the detector on the right to form a transaction. The transaction forms between source and detector, and one  $\hbar\omega$  photon's worth of energy is transferred from the source to the detector. The formation of this particular transaction, satisfying the source boundary condition that only one photon is emitted,

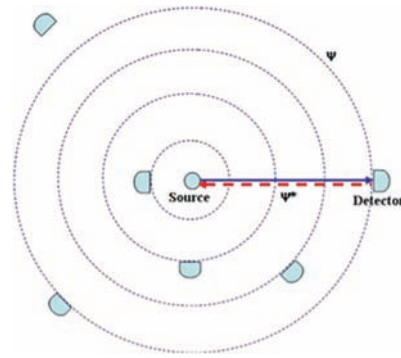


**Fig. 1: Schematic of the transaction involved in the Einstein's bubble paradox. The offer wave  $\psi$  (blue/solid) forms a spherical wave front, reaching the detector on the right and causing it to return a confirmation wave  $\psi^*$  (red/dashed), so that a transaction forms and one photon's worth of energy  $\hbar\omega$  is transferred. Other detectors also return confirmation waves, but the source has randomly selected the detector on the right for the transaction.**

prevents the formation of any other transaction to another possible photon absorber, so only one photon is detected. This is an illustration of a simple two-vertex transaction in which the transfer of a single photon is implemented nonlocally. It avoids Heisenberg's assertion that the mathematical solution to a simple second-order differential equation involving momentum, energy, time, and space has somehow become a map of the mind, deductions, and knowledge of a hypothetical observer.

In this context, we note that there is a significant (but untestable) difference between Heisenberg's knowledge interpretation and the Transactional Interpretation as to whether the outgoing state vector or offer wave changes, collapses, or disappears at the instant when knowledge from a measurement is obtained. The knowledge interpretation would lead us to expect, without any observational evidence and with some conflict with special relativity, that Einstein's bubble "pops" when the detector registers the arrival of a photon and that other parts of the outgoing wave disappear at that instant. The bubble needs to pop in the knowledge interpretation because the state of knowledge changes, and also because this prevent multiple photon detections from a single photon emission.

In the analogous description by the Transactional Interpretation, the parts of the offer wave away from the detection site, because they represent only the *possibility* of a quantum event, do not disappear, but instead continue to propagate to more distant potential detection sites. These sites return confirmation echoes that compete with the echo from the detector of interest for transaction formation. The consequence of this difference is that the TI does not have to explain how wave functions can change in mid-flight, how the absence of a detection can change a propagating wave function, or what "instantaneous disappearance" means in the context of special relativity.

#### 3.2 Young's Two-Slit Experiment (1893)

Thomas Young (1773–1829) presented the results of his two-slit experiment to the Royal Society of London on November 24, 1803. A century and a half later, Richard Feynman [16] described Young's experiment as "a phenomenon that is impossible... to explain in any classical way, and that has in it the heart of quantum mechanics. In reality, it contains the only (quantum) mystery."

The experimental arrangement of Young's two-slit experi-



ment is shown in Fig. 2. Plane waves of light diffract from a small aperture in screen A, pass through two slits in screen B, and produce an interference pattern in their overlap region on screen C. The interference pattern is caused by the arrival of light waves at screen C from the two slits, with a variable relative phase because the relative path lengths of the two waves depends on the location on screen C. When the path lengths are equal or differ by an integer number of light wavelengths  $\lambda$ , the waves add coherently (constructive interference) to produce an intensity maximum. When the path lengths differ by an odd number of half-wavelengths  $\lambda/2$ , the waves subtract coherently to zero (destructive interference) and produce an intensity minimum.

One can “turn off” this interference pattern by making the two paths through slits distinguishable. In this case, the “comb” interference pattern is replaced by a broad diffraction “bump” distribution, as shown by the green/dashed line at C in Fig. 2. This might be accomplished by arranging for the waves on the two paths to be in different polarization states, thereby “labeling” the wave paths with polarization. For example, one could use a light source that produces vertically polarized light, and one could place behind one slit a small optical half-wave plate, shown in Fig. 2 behind the upper slit at B, set to rotate vertical to horizontal polarization. This would eliminate the previously observed two-slit interference pattern, because the light waves arriving at screen C from the two slits are now in distinguishable polarization states, with the waves from the lower slit vertically polarized and waves from the upper slit horizontally polarized. The intensities of the waves will now add instead of their amplitudes, and there can be no destructive cancellation. This interference suppression occurs even if no polarization is actually measured at C.

In the 19th century Young’s experiment was taken as conclusive proof that light was a wave and that Newton’s earlier depiction of light as a particle was incorrect. Einstein’s 1905 explanation of the photoelectric effect as caused by the emission of photon particles of light cast doubt on this view. In 1909, a low-intensity double slit experiment performed by Sir Geoffrey Taylor [17] demonstrated that the same interference pattern is obtained, even when the light intensity is so low that the interference pattern must be accumulated one photon at a time. The emergence of the interference pattern from individual photon events is illustrated in Fig. 3, in which we see the build-up of the two-slit interference pattern as single photon events (green points) are accumulated, one at a time. Based on Taylor’s experimental results, in 1926 G. N. Lewis [18] reasoned, in a remarkable precursor to the Transactional Interpretation, that “an atom never emits light except to another atom ... I propose to eliminate the idea of mere emission of light and substitute the idea of transmission, or a process of exchange of energy between two definite atoms or molecules.”

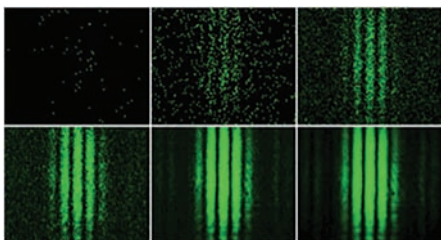


Fig. 3: Build-up of a two-slit interference pattern in a Young’s two-slit experiment at low illumination intensity as more and more single-photon events (green points) are accumulated [19].

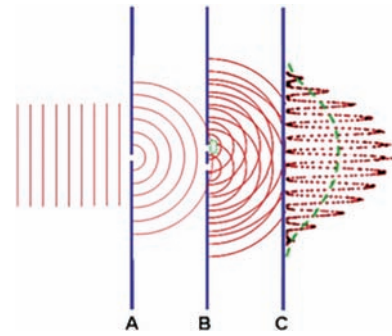


Fig. 2: Young’s two-slit experiment. Light waves diffract from the aperture in screen A, pass through two slits in screen B, and produce a “comb” interference pattern in their overlap region on screen C. The green/dashed line at C shows the diffraction pattern that would be observed if the two paths through the slits were made distinguishable, e.g., put in different states of polarization by a half-wave plate, shown behind the upper slit at B.

The emergence of the interference pattern from individual photon events is the “quantum mystery” to which Richard Feynman referred: How is it possible that an ensemble of single photons, arriving at the screen one at a time, can produce such a wave-like interference pattern? It would appear that each individual photon particle must pass through both slits and must interfere with itself at the screen..

The Transactional Interpretation explains the puzzling build-up of a wave interference pattern from photon events as follows: in Fig. 2 the source emits plane offer waves moving to the right that are diffracted at screen A, pass through both slits at screen B, and arrive at any point on screen C from two directions. At locations along screen C where the two components of the offer wave interfere constructively there is a high probability of transaction formation, and at locations where the two components of the offer wave interfere destructively and cancel there is zero probability of a transaction.

Confirmation waves propagate to the left, moving back through the slits at B and the aperture at A to the light source. There the source, which is seeking to emit one photon, selects among the confirmation offers, and a transaction delivers a photon to screen C. The position at which the photon arrives is likely to be where the offer waves were constructive and unlikely to be where the waves were destructive. Therefore, an interference pattern that is made of many single photon transactions that build up on screen C, as shown in Fig. 3, is a natural consequence of the Transactional Interpretation.

The interference suppression from labeling can also be explained by the TI. Screen C receives offer waves that have passed through both slits and returns corresponding confirmation waves to the source. However, the vertically polarized offer wave will cause the return of a vertically polarized confirmation, and likewise for the horizontally polarized offer wave. The confirmation wave echo arriving at the source will only match the vertical polarization of the source if it returned through the same slit that the corresponding offer had passed through, so the transaction that forms will pass through only one of the two slits. Therefore, there will be no two-slit interference pattern for this case.

### 3.3 Wheeler’s Delayed Choice Experiment (1978)

In 1978, John A. Wheeler raised another interpretational issue

[20] that is now known as Wheeler's Delayed-Choice Experiment (Fig. 4). Suppose that we have a Young's two slit interference apparatus as discussed above, with photons produced by a light source that illuminates two slits. The source emits one and only one photon in the general direction of the slits during the time interval chosen by the observer who is operating the apparatus. Downstream of the slits are two different measuring devices. One of these is a photographic emulsion  $\sigma_1$  that, when placed in the path of the photons, will record photons' positions as they strike the emulsion, so that after many photon events, the emulsion will show a collection of spots that form a two-slit interference pattern characteristic of the photons' wavelength, momentum, and the slit separation. The other measuring device consists of a lens focusing the slit-images on photographic emulsion  $\sigma_2$  at image points  $1'$  and  $2'$ . A photon striking either image point tells us that the photon had passed through the slit that is imaged at that position. Therefore, detection at  $\sigma_2$  constitutes a determination of the slit (1 or 2) through which the photon passed.

Such an apparatus is often used to illustrate the wave-particle duality of light. The light waves that form the interference pattern on the emulsion must have passed through both slits of the apparatus in order to interfere at the emulsion, while the photon particles that strike the photographic emulsion  $\sigma_2$  can have passed through only one slit – the one imaged by the lens  $L$  at image point  $1'$  or  $2'$ . The photographic emulsion  $\sigma_1$  measures momentum (and wavelength) and the photographic emulsion  $\sigma_2$  measures position, i.e., conjugate variables are measured. Thus, the two experimental measurements are “complimentary” in Bohr's sense. The Uncertainty Principle is not violated, however, because only one of the two experiments can be performed with a given photon. But Wheeler is not done yet.

The emulsion  $\sigma_1$  is mounted on a fast acting pivot mechanism, so that on command it can almost instantaneously either be raised into position to intercept the photon from the source or rapidly dropped out of the way so that the photon can proceed to  $\sigma_2$ . Thus when the emulsion  $\sigma_1$  is up, we make an interference measurement requiring the photon to pass through both slits, and when the emulsion  $\sigma_1$  is down, we make a position measurement requiring that the photon pass through only one slit.

Wheeler's innovative modification of this old *gedankenexperiment* is this: We wait until a time at which the photon has safely passed the slits but has not yet reached the emulsion apparatus  $\sigma_1$ . Only at that time do we decide whether to place the  $\sigma_1$  emulsion up or down. The decision is made after the photon must have passed through the slit system. Therefore, the photon has already emerged from the slit system when the experimenter decides whether it should be caused to pass through one slit (emulsion down) or both slits (emulsion up). Wheeler concluded that the delayed-choice experiment illustrated his paradigm about quantum mechanics: “No phenomenon is a real phenomenon until it is an observed phenomenon.”

It might be argued that there would not really be time enough for a conscious observer to make the measurement decision. However, Wheeler has pointed out that the light source might be a quasar, and the “slit system” might be a foreground galaxy that bends the light waves around both sides by gravitational lensing. Thus, there would be a time interval of millions of years for the decision to be made, during which time the light waves from the quasar were in transit from the foreground galaxy to the observer. The delayed choice experiment, since it

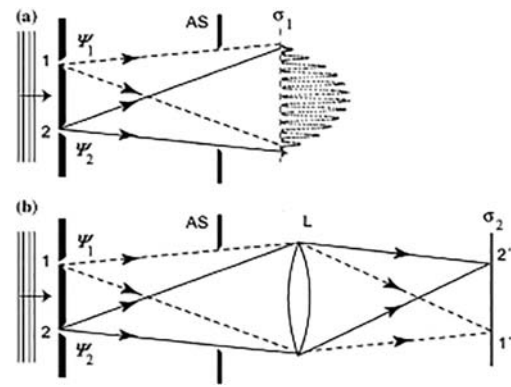


**Fig. 4: Wheeler's delayed choice experiment: Light from a single-photon source can either (a) produce an interference pattern on photographic emulsion  $\sigma_1$  or (b) be imaged by lens  $L$  to produce images of the two slits on photographic emulsion  $\sigma_2$  at points  $1'$  and  $2'$ . The experimenter waits until after the photon has passed through the slits to decide whether to lower photographic emulsion  $\sigma_1$  so that photographic emulsion  $\sigma_2$  provides which-slit information, or to leave it place so that the two-slit interference pattern characteristic of passage through both slits is observed at  $\sigma_1$ .**

seems to determine the path of the photon after it has passed through the slit system, has been used as an illustration of retrocausal effects in quantum processes.

The *gedankenexperiment* does not lead to any explicit contradictions, but it demonstrates some of the retrocausal implications of the standard quantum formalism. In particular, the cause (emulsion  $\sigma_1$  down or up) of the change in the photon's path has come after the effect (passage through one or two slits). There have been several experimental implementations of this experiment, the most recent (2007) performed by the Aspect Group in France [21]. All have shown the expected results, i.e., the predictions of standard quantum mechanics.

The Transactional Interpretation is able to give an account of the delayed choice experiment without resort to observers as collapse triggers. In the TI description, the source emits a retarded OW that propagates through slits 1 and 2, producing offer waves  $\psi_1$  and  $\psi_2$ . These reach the region of screen  $\sigma_1$ , where either (a) they find the screen  $\sigma_1$  up and form a two-path transaction with it as illustrated in Fig. 4(a) or; (b) they find the screen  $\sigma_1$  down and proceed through lens  $L$  on separate paths to screen  $\sigma_2$  where they strike the screen at image points  $1'$  and  $2'$  and create confirmation waves that return through the lens and slits to the source. In case (b), the source receives confirmation wave echoes from two separate sites on screen  $\sigma_2$  and must decide which of them to use in a one-slit competed transaction, as shown by the solid and dashed lines in Fig. 4(b).

For case (a) in which the photon is absorbed by  $\sigma_1$ , the advanced confirmation wave retraces the path of the OW, traveling in the negative time direction back through both slits and back to the source. Therefore the final transaction, as shown in Fig. 4(a), forms along the paths that pass through both slits in connecting the source with the screen  $\sigma_1$ . The transaction is therefore a “two-slit” quantum event. The photon can be said to have passed through both slits to reach the emulsion.

For case (b) the offer wave also passes through both slits on its way to  $\sigma_2$ . However, when the absorption takes place at one of the images (not both, because of the single quantum bound-

ary condition), the lens focuses the confirmation wave so that it passes through only the slit imaged at the detection point. Thus the confirmation wave passes through only one slit in passing back from image to source, and the transaction which forms is characteristic of a “one-slit” quantum event. The source, receiving confirmation waves from two mutually exclusive one-slit possibilities, must choose only one of these for the formation of a transaction. The photon can be said to have passed through only one slit to reach  $\sigma_2$ .

Since in the TI description the transaction forms atemporal-ly, the issue of when the observer decides which experiment to perform is not significant. The observer determined the experimental configuration and boundary conditions and the transaction formed accordingly. Further, the fact that the detection event involves a measurement (as opposed to any other interaction) is not significant and so the observer has no special role in the process. To paraphrase Wheeler’s paradigm, we might say: “No offer wave is a real transaction until it is a confirmed transaction”.

### 3.4 The Afshar Experiment (2002)

The Afshar experiment [22] shows that, contrary to some of Niels Bohr’s pronouncements about complementarity and wave particle duality, it is possible to see the effects of wave-like behavior and interference, even when particle-like behavior is being directly observed. In Bohr’s words [23]: “...we are presented with a choice of either tracing the path of the particle, or observing interference effects,... we have to do with a typical example of how the complementary phenomena appear under mutually exclusive experimental arrangements.” In the context of a two-slit experiment, Bohr asserted [24] that complementarity in the Copenhagen Interpretation dictates that “the observation of an interference pattern and the acquisition of which-way information are mutually exclusive.”

The Afshar experiment, shown in Fig. 5, was first performed in 2003 by Shariar S. Afshar and was later repeated while he was a Visiting Scientist at Harvard. It used two pinholes in an opaque sheet illuminated by a laser. The light passing through the pinholes formed an interference pattern, a zebra-stripe set of maxima and zeroes of light intensity that were recorded by a digital camera. The precise locations of the interference minimum positions, the places where the light intensity went to zero, were carefully measured and recorded.

Behind the plane where the interference pattern formed, Afshar placed a lens that formed an image of each pinhole at a second plane. A light flash observed at image 1’ on this plane indicated unambiguously that a photon of light had passed through pinhole 1, and a flash at image 2’ similarly indicated that the photon had passed through pinhole 2. Observation of the photon flashes therefore provided particle path which-way information, as described by Bohr. According to the Copenhagen Interpretation, in this situation all wave-mode interference effects must be excluded. However, at this point Afshar introduced a new element to the experiment. He placed one or more vertical wires at the previously measured positions of the interference minima. In such a setup, if the wire plane was uniformly illuminated the wires absorbed about 6% of the light. Then Afshar measured the difference in the light intensity received at the pinhole image detectors with and without the wires in place.

We are led by the Copenhagen Interpretation to expect that

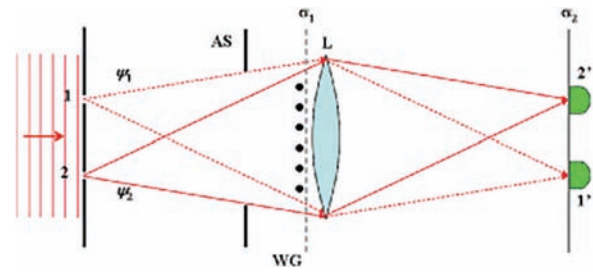


**Fig. 5:** In the Afshar experiment, a version of Wheeler’s delayed-choice experiment is modified by placing vertical wires (WG) at the locations at which the interference pattern has interference minima on screen  $\sigma_1$ . High transmission of light through the system when the wires are present and  $\sigma_1$  is absent implies that the interference pattern is *still* present, even when which-way information is available from the downstream detectors 1’ and 2’.

when which-way information is obtained the positions of the interference minima should have no particular significance, and that the wires should intercept 6% of the light, as they do for uniform illumination. However, what Afshar observed was that the amount of light intercepted by the wires is very small, consistent with 0% interception. This implies that the interference minima are still locations of zero intensity and that the wave interference pattern is still present, even when which-way measurements are being made. Wires that are placed at the zero-intensity locations of the interference minima intercept no light. This observation would seem to create problems for the complementarity assertions of the Copenhagen Interpretation. Thus, the Afshar experiment is a significant quantum paradox.

The Transactional Interpretation explains Afshar’s results as follows: The initial offer waves pass through both slits on their way to possible absorbers. At the wires, the offer waves cancel in first order, so that no transactions to wires can form, and no photons can be intercepted by the wires. Therefore, the absorption by the wires should be very small ( $\ll 6\%$ ) and consistent with what is observed. This is also what is predicted by the QM formalism. The implication is that the Afshar experiment has revealed a situation in which the Copenhagen Interpretation has failed to properly map the standard formalism of quantum mechanics.

We note that the many-worlds interpretation of quantum mechanics [25, 26] asserts that interference between its “worlds” (e.g., paths taken by particles) should not occur when the worlds are quantum-distinguishable. Therefore, the “many-worlds” interpretation would also predict that there should be no interference effects in the Afshar experiment. Thus, the “many-worlds” interpretation has also failed to properly map the standard formalism of quantum mechanics.

### 3.5 The Freedman-Clauser EPR Experiment (1972)

Another quantum puzzle is the Freedman-Clauser experiment [27]. An atomic 2-photon cascade source produces a pair of polarization-entangled photons. If we select only entangled photons emitted back-to-back, then because of angular momentum conservation, both photons must be in the same state of circular or linear polarization. Measurements on the photons with linear polarimeters in each arm of the experiment show that when the planes of the polarimeters are aligned, independent of the direction of alignment, the two polarimeters always measure HH or VV for the two linear polarization states, i.e.,



both photons are always in the same linear polarization state.

When the polarization plane of one polarimeter is rotated by an angle  $\theta$  with respect to the other polarization plane, some opposite-correlation **HV** and **VH** events creep in. If  $\theta$  is increased, the fraction of these events grows proportional to  $1-\cos 2(\theta)$ , which for small values of  $\theta$  is proportional to  $2\theta$ . This polarization correlation behavior produces a dramatic violation of the Bell inequalities [28], which for local hidden variable alternatives to standard quantum mechanics require a growth in **HV** and **VH** events that is linear with  $\theta$ . The implication of the Bell-inequality violations is that quantum nonlocality is required to explain the observed quadratic polarization correlations.

How are the nonlocality-based polarization correlations of the Freedman–Clauser experiment possible? The Transactional Interpretation provides a clear answer, which is illustrated in Fig. 6. The source of the polarization-entangled photons seeks to emit the photon pair by sending out offer waves  $\psi_L$  and  $\psi_R$  to the left and right detectors.

The detectors respond by returning confirmation waves  $\psi_L^*$  and  $\psi_R^*$  back to the source. A completed three-vertex transaction can form from these echoes, however, only if the two potential detections are compatible with the conservation of angular momentum at the source. This requirement produces the observed polarization correlations. The transaction does not depend on the separation distance of the polarimeters or on which of the polarization detection events occurs first, since the transaction formation is atemporal, and it even-handedly treats any sequence of detection events.

### 3.6 Interaction-Free Measurements (1993)

In 1993, Elitzur and Vaidmann [29] (EV) showed a surprised physics community that quantum mechanics permits the non-classical use of light to examine an object without a single photon of the light actually interacting with the object. The EV experiment requires only the possibility of an interaction.

In their paper [29] Elitzur and Vaidmann discuss their scenario in terms of the standard Copenhagen Interpretation of quantum mechanics, in which the interaction-free result is rather mysterious, particularly since the measurement produces “knowledge” that is not available classically. They also considered their scenario in terms of the Everett–Wheeler or “many-worlds” interpretation of quantum mechanics [25, 26].

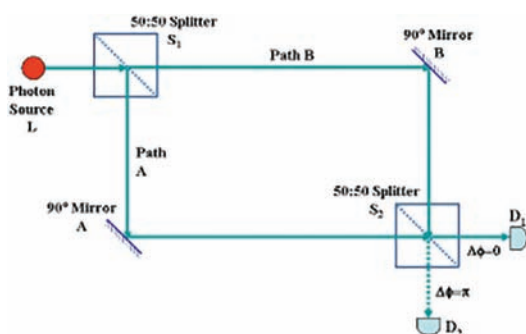


Fig. 7: Mach Zehnder interferometer with both beam paths open. All photons go to  $D_1$  because of destructive interference at  $D_2$ .

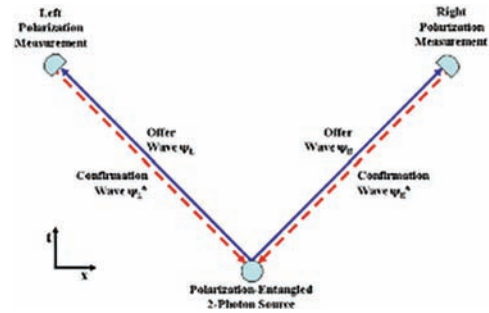


Fig. 6: Spacetime schematic of a nonlocal “V” transaction for visualizing the polarization-entangled Freedman–Clauser EPR experiment. Offer waves  $\psi_L$  and  $\psi_R$  (blue/solid) move from source to linear polarization detectors, and in response, confirmation waves  $\psi_L^*$  and  $\psi_R^*$  (red/dashed) move from detectors to source. The three-vertex transaction can form only if angular momentum is conserved by having correlated and consistent measured linear polarizations for both detected photons.

Considering the latter, they suggest that the information indicating the presence of the opaque object can be considered to have come from an interaction that had occurred in a separate Everett–Wheeler universe and was transferred to our universe through the absence of interference. Here we will examine the same scenario in terms of the Transactional Interpretation and will provide a more plausible account of the physical processes that underlie interaction-free measurements.

The basic apparatus used by EV is a Mach–Zehnder interferometer, as shown in Fig. 7. Light from a light source  $L$  goes to a 50:50% beam splitter  $S_1$  that divides incoming light into two possible paths or beams. These beams are deflected by  $90^\circ$  by mirrors  $A$  and  $B$ , so that they meet at a second beam splitter  $S_2$ , which recombines them by another reflection or transmission. The combined beams from  $S_2$  then go to the photon detectors  $D_1$  and  $D_2$ .

The Mach–Zehnder interferometer has the characteristic that, if the paths  $A$  and  $B$  have precisely the same path lengths, the superimposed waves from the two paths are in phase at  $D_1$  ( $\Delta\phi = 0$ ) and out of phase at  $D_2$  ( $\Delta\phi = \pi$ ). This is because with beam splitters, an emerging wave reflected at  $90^\circ$  is always  $90^\circ$  out of phase with the incident and transmitted waves [30]. The result is that all photons from light source  $L$  will go to detector  $D_1$  and none will go to detector  $D_2$ .

Now, as shown in Fig. 8, we place an opaque object (Obj) on path  $A$ . It will block light waves along the lower path after reflection from mirror  $A$ , ensuring that all of the light arriving at

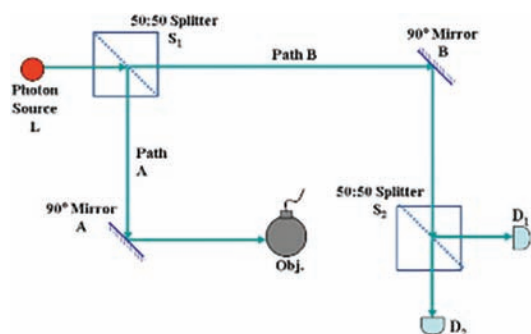


Fig. 8: Mach Zehnder interferometer with one beam path blocked. Half of the photons are absorbed by the blocking object, 25% go to  $D_1$ , and 25% go to  $D_2$ .

beam splitter  $S_2$  has traveled there via path B. In this case there is no interference, and beam splitter  $S_2$  sends equal components of the incident wave to the two detectors.

Now suppose that we arrange for the light source  $L$  to emit only one photon within a given time period. Then, if we do the measurement with no opaque object on path A, we should detect the photon at  $D_1$  100% of the time. If we perform the same measurement with the opaque object  $Obj$  blocking path A, we should detect a photon at  $D_1$  25% of the time, a photon at  $D_2$  25% of the time, and should detect no photon at all 50% of the time (because it was removed by  $Obj$  in path A). In other words, the detection of a photon at  $D_2$  guarantees that an opaque object is blocking path A, although no photon had actually interacted with object  $Obj$ . This is the essence of the Elitzur and Vaidmann interaction-free measurement.

Note that if a photon is detected at detector  $D_1$ , the issue of whether an object blocks path A is unresolved. However, in that case another photon can be sent into the system, and this can be repeated until either a photon is detected at  $D_2$  or absorbed by  $Obj$ . The net result of such a recursive procedure is that 66% of the time a photon will strike the object, resulting in no detection signal, while 33% of the time a photon will be detected at  $D_2$ , indicating without interaction that an object blocks the A path. Thus, the EV procedure has an efficiency of 33% for non-interactive detection.

As before, in analyzing interaction-free measurements with the Transactional Interpretation, we will explicitly indicate offer waves  $\psi$  by a specification of the path in a Dirac ket state vector  $\psi = |\text{path}\rangle$ , and we will underline the symbols for optical elements at which a reflection has occurred. Confirmation waves  $\psi^*$  will similarly be indicated by a Dirac Bra state vector  $\psi^* = \langle \text{path} |$ , and will indicate the path considered by listing the elements in the time-reversed path with reflections underlined.

Consider first the situation in which no object is present in path A as shown in Fig. 8. The offer waves from  $L$  to detector  $D_1$  are  $|L-S_1-A-S_2-D_1\rangle$  and  $|L-S_1-B-S_2-D_1\rangle$ . They arrive at detector  $D_1$  in phase because the offer waves on both paths have been transmitted once and reflected twice. The offer wave from  $L$  initially has unit amplitude, but the splits at  $1/\sqrt{2}$  each reduce the wave amplitude by  $1/\sqrt{2}$  so that each wave, having been split twice, has an amplitude of  $1/2$  as it reaches detector  $D_1$ . Therefore, the two offer waves of equal amplitude and phase interfere constructively, reinforce, and produce a confirmation wave that is initially of unit amplitude.

Similarly, the offer waves from  $L$  to detector  $D_2$  are  $|L-S_1-A-S_2-D_2\rangle$  and  $|L-S_1-B-S_2-D_2\rangle$ . They arrive at detector  $D_2$  180° out of phase, because the offer wave on path A has been reflected three times while the offer wave on path B has been trans-

mitted twice and reflected once. Therefore, the two waves with amplitudes  $\pm i/2$  interfere destructively, cancel at detector  $D_2$ , and produce no confirmation wave. The confirmation waves from detector  $D_1$  to  $L$  are  $\langle D_1-S_2-A-S_1-L |$  and  $\langle D_1-S_2-B-S_1-L |$ . They arrive back at the source  $L$  in phase because, as in the previous case, the confirmation waves on both paths have been transmitted once and reflected twice.

As before the splits at  $S_1$  and  $S_2$  each reduce the wave amplitude by  $1/\sqrt{2}$ , so that each confirmation wave has an amplitude of  $1/2$  as it reaches source  $L$ . Therefore, the two offer waves interfere constructively, reinforce and have unit amplitude. Since the source  $L$  receives a unit amplitude confirmation wave from detector  $D_1$  and no confirmation wave from detector  $D_2$ , the transaction forms along the path from  $L$  to  $D_1$  via A and B. The result of the transaction is that a photon is always transferred from the source  $L$  to detector  $D_1$  and that no photons can be transferred to  $D_2$ . Note that the transaction forms along both paths from  $L$  to  $D_1$ . This is a transactional account of the operation of the Mach-Zender interferometer.

Now let us consider the situation when the object blocks path A as shown in Fig. 9. The offer wave on path A is  $|L-S_1-A-Obj\rangle$ . As before an offer wave on path B is  $|L-S_1-B-S_2-D_1\rangle$ , and it travels from  $L$  to detector  $D_1$ . The wave on path B also splits at  $S_2$  to form offer wave  $|L-S_1-B-S_2-D_2\rangle$ , which arrives at detector  $D_2$ . The splits at  $S_1$  and  $S_2$  each reduce the wave amplitude by  $1/\sqrt{2}$ , so that the offer wave at each detector, having been split twice, has an amplitude of  $1/2$ . However, the offer wave  $|L-S_1-A-Obj\rangle$  to the object in path A, having been split only once, is stronger and has amplitude of  $1/\sqrt{2}$ .

In this situation, the source  $L$  will receive confirmation waves from both detectors and also from the object. These, respectively, will be confirmation waves  $\langle D_1-S_2-B-S_1-L |$ ,  $\langle D_2-S_2-B-S_1-L |$  and  $\langle Obj-A-S_1-L |$ . The first two confirmation waves started from their detectors with amplitudes of  $1/2$  (the final amplitude of their respective offer waves) and have subsequently been split twice. Therefore, they arrive at source  $L$  with amplitudes of  $1/4$ . On the other hand, the confirmation wave from the object initially has amplitude  $1/\sqrt{2}$ , and it has been split only once, so it arrives at the source with amplitude  $1/2$ .

The source  $L$  has one photon to emit and three confirmations to choose from, with round-trip amplitudes ( $\psi\psi^*$ ) of  $1/4$ , to  $D_1$   $1/4$  to  $D_2$ , and  $1/2$  to object  $Obj$ . In keeping with the probability assumption of the Transactional Interpretation and Born's probability law, it will choose with a probability proportional to these amplitudes. Therefore, the emitted photon goes to  $D_1$  25% of the time, to  $D_2$  25% of the time, and to object  $Obj$  in path A 50% of the time. As we have seen above, the presence of the object in path A modifies the detection probabilities so that detector  $D_2$  will receive  $1/4$  of the emitted photons, rather than

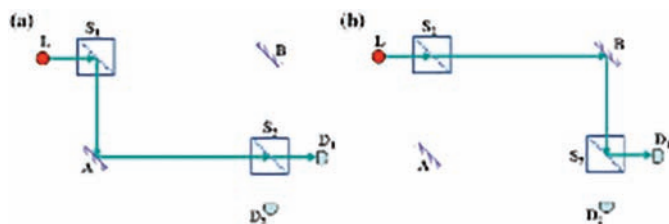


Fig. 9: Offer waves (a)  $|L-S_1-A-S_2-D_1\rangle$  and (b)  $|L-S_1-B-S_2-D_1\rangle$ .

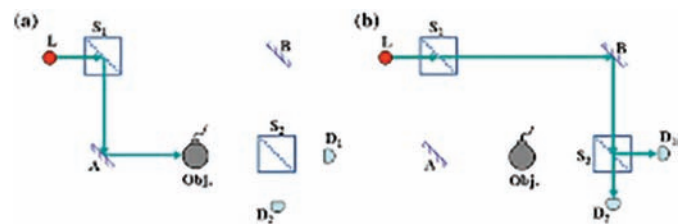


Fig. 10: Offer waves (a)  $|L-S_1-A-Obj\rangle$  and (b)  $|L-S_1-B-S_2-D_1\rangle + |L-S_1-B-S_2-D_2\rangle$ .

none of them, as it would do if the object were absent.

How can the transfer of non-classical knowledge be understood in terms of the transactional account of the process? In the case where there is an object in the A path, it is probed both by the offer wave from L and by the aborted confirmation waves from D<sub>1</sub> and D<sub>2</sub>. The latter are 180° out of phase and cancel. When we detect a photon at D<sub>2</sub>, (i.e., when a transaction forms between L and D<sub>2</sub>), the object has not interacted with a photon (i.e., a transaction has not formed between L and the object Obj). However, it has been probed by an offer wave from the source, which “feels” its presence and modifies the interference balance at the detectors, providing non-classical information. Thus, the Transactional Interpretation gives a simple explanation of the mystery of interaction-free measurements.

### 3.8 The Hardy One-Atom *Gedankenexperiment* (1992)

In 1992 Lucien Hardy [31, 32] proposed the *gedankenexperiment* shown in Fig. 11, which is a modified version of the interaction-free measurement scenario of Elitzur and Vaidmann [29] (see Sect. 6.13) in which their blocking object (or bomb) is replaced by a single spin- $\frac{1}{2}$  atom, initially prepared in an X-axis  $+\frac{1}{2}$  spin-projection, then Stern–Gerlach separated [33] into one of two spatially separated boxes that momentarily contain the atom in its Z-axis  $+\frac{1}{2}$  and  $-\frac{1}{2}$  spin projections, then transmit their contents to be recombined by an inverse Stern–Gerlach process, so that the X-axis projection of the atom can be measured.

The Z-spin  $+\frac{1}{2}$  box (Z+) is placed directly in one path of a Mach–Zehnder interferometer, so that if the atom is present in that box during photon transit, it has a 100% probability of absorbing a photon traveling along that arm of the interferometer. After a single photon from light source L traverses the interferometer, the final X-axis spin projection of the atom is measured. The non-classical outcome of the *gedankenexperiment* is that, for events in which a photon is detected by dark detector D, the spin measurement of the atom has a 50% probability of having an X-axis spin projection of  $-\frac{1}{2}$ , even though the atom had previously been prepared in the  $+\frac{1}{2}$  X-axis spin state, and the atom had never directly interacted with the photon.

Hardy analyzes the measurement in terms of the Bohm–de Broglie interpretation/revision of quantum mechanics [34] and concludes that the non-classical outcome of the measurement can be attributed to “empty waves”, by which he means de Broglie guide waves that have traversed the interferometer along paths not subsequently followed by the single emitted photon. At least four other papers [35–38] have analyzed the Hardy *gedankenexperiment* using alternative QM interpretations that focus on wave function collapse, notably the “collapse” and the “consistent histories” interpretations.

The Transactional Interpretation explains the transfer of non-classical knowledge in terms of the transactional account of the process. In particular, in the case where there is an atom in the v path, it is probed by the offer wave from L. When we detect a photon at D, (i.e., when a transaction forms between L and D), the object has not interacted with a photon (i.e., a transaction has not formed between L and the atom in box Z+). However, the atom has been probed by offer waves from L, which “feel” its presence and modify the interference balance at the detectors and the spin statistics of the atom. Thus, the Transactional Interpretation gives a simple explanation of the Hardy *gedankenexperiment*.

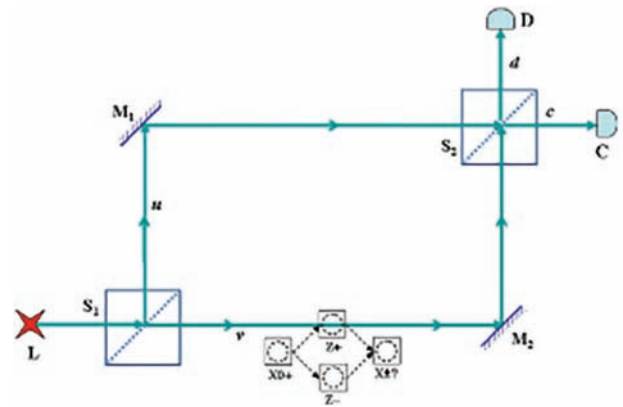


Fig. 11: The Hardy single-atom interaction-free measurement.

### 3.9 The Quantum Eraser (1995)

A more elaborate delayed-choice variation is the quantum eraser experiment, a high-tech descendant of Wheeler’s delayed choice concept. The experiment used a new (in 1995) trick for making “entangled” quantum states. If ultraviolet light from a 351 nanometer (nm) argon-ion laser passes through a LiIO<sub>3</sub> crystal, non-linear effects in the crystal can “split” the laser photon into two longer wavelength photons at 633 nm and 789 nm in a process called “down-conversion”. The energies of these two “daughter” photons add up to the energy of their pump-photon parent, as do their vector momenta, and they are connected non-locally because they constitute a single “entangled” quantum state. They are required to be in correlated states of polarization, and under the conditions of this down-conversion they will be vertically polarized. As in other EPR experiments, a measurement performed on one of these photons affects the outcome of measurements performed on the other.

In a version of the experiment performed by Anton Zeilinger’s group in Innsbruck, Austria, [39] the laser beam is reflected so that it makes two passes through the nonlinear crystal, so that an entangled photon pair may be produced in either the first or the second pass through the non-linear crystal. As shown in Fig. 12, the experiment has the configuration of a six-pointed star formed of three beam paths intersecting at a point inside the crystal. The laser beam first passes through the crystal moving horizontally downstream, is reflected by a

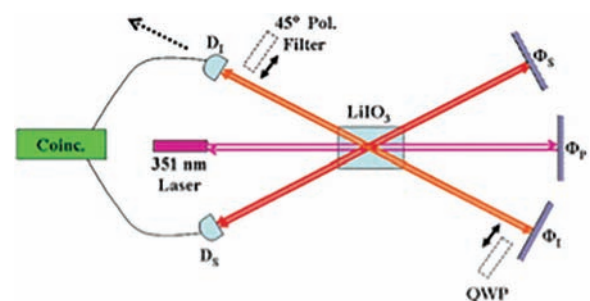


Fig. 12: Schematic diagram of the quantum eraser experiment. A LiIO<sub>3</sub> nonlinear crystal is pumped by a 351nm laser beam (violet) and produces by down-conversion vertically polarized 633 nm (orange) and 789 nm (red) photons that can be made in either pump-photon pass through the crystal. A quarter-wave plate (QWP) and 45° polarizing filter may be inserted in the I path and the path to D<sub>1</sub> may be lengthened to produce a time delay (see text).



downstream mirror  $\Phi_P$ , and then passes through the crystal again moving horizontally upstream. Along the two diagonal branches downstream of the laser the two down-converted photons made in the first laser-pass travel to mirrors  $\Phi_S$  and  $\Phi_I$  (S for signal and I for idler), where they are reflected back to their production point and travel past it to upstream detectors  $D_S$  and  $D_I$ . The laser beam, in making its second pass through the crystal has a second chance to make a pair of down-converted photons. If these are produced, they travel directly to the upstream detectors along the two upstream diagonal branches.

The net result is that a photon arriving in coincidence at the two upstream detectors may have been produced in either the first laser pass through the crystal and then reflected to the detector, or in the second pass and traveled directly to the detector. There is no way of determining which “history” (direct vs. reflected) happened, so the states are superimposed. Therefore, the quantum wave functions describing these two possible production histories must interfere. The interference may be constructive or destructive, depending on the interference phase determined by the downstream path lengths (all about 13 cm) to the three mirrors of the system. Changing the path length to one of the mirrors (for example, by moving the laser-beam reflector  $\Phi_P$ ) is observed to produce a succession of interference maxima and minima in the two detectors.

This experimental setup is governed by the same physics as the delayed-choice experiment of Sect. 3.3, but, because there are two coincident photons and well separated paths for the two possible histories, it is easier to play quantum tricks with the system. Initially, all polarizations are vertical. Now the experiment is modified to remove the quantum interference by placing distinguishing polarization labels on the two possible photon histories (direct vs. reflected). A transparent optical element called a “quarter-wave plate” (QWP) is placed in front of the photon reflection mirror  $\Phi_I$ . The QWP is set to rotate the polarization state of the reflected photons from vertical to horizontal polarization as they pass twice through it. This polarization modification allows the reflected and direct “histories” to be quantum-distinguishable, because one of the reflected photons is horizontally polarized while the direct photons are vertically polarized. The two superimposed quantum states are now distinguishable (even if no polarization measurement is actually made), and the interference pattern is eliminated, both in the I arm of the experiment in which the QWP is placed and also in the other S arm, where no modification was made.

Finally, the “quantum eraser” is brought into use. Any vertically or horizontally polarized light beam can be separated into a light component polarized  $45^\circ$  to the left of vertical and a light component polarized  $45^\circ$  to the right of vertical. Therefore, for the photons with the QWP in front of their mirror, placing just in front of their detector a filter that passes only light polarized  $45^\circ$  to the left of vertical “erases” the label that had distinguished the two histories by making the polarizations of the two waves reaching detector  $D_I$  the same. When this is done, it is found that interference is restored.

Further, the paths to the two detectors can have different lengths, with the path through the  $45^\circ$  filter to  $D_I$  made much longer than the path to detector  $D_S$ . This has the effect of erasing the path-distinguishing label on the I photon after the S photon had already been detected. This modification is observed to have no effect on the interference. The *post-facto* erasure still restores interference. The path label can be erased retroactively and has the same effect (retroactive or not) on the quantum

interference of the waves. Effectively, the quantum eraser has erased the past!

The Transactional Interpretation can easily explain the curious retroactive erasure of “which-way” information. When which-way information is present, separate transactions must form for each of the paths, and no interference can be observed. When the which-way information is erased, the overall transaction that forms involves both paths, and interference is observed. Modifying the polarizations causes a different type of transaction formation, resulting in different observations. The retroactive erasure of the which-way information is irrelevant, because the transaction forms atemporally, connecting the source and detectors in single or double advanced-retarded TI handshakes across spacetime.

### 3.10 The Black Hole Information Paradox (1975-2015)

Stephen Hawking’s 1975 calculations [40] predicting black hole evaporation by Hawking radiation described a process that apparently does not preserve information. This created the Black Hole Information Paradox, which has been an outstanding problem at the boundary between general relativity and quantum mechanics ever since. Lately, gravitational theorists have focused on pairs of quantum-entangled particles, in part because the particle pair involved in Hawking radiation should be entangled. They have considered ways in which the quantum entanglement might be broken or preserved when one photon of the entangled photon pair crosses the event horizon and enters a black hole.

One recent suggestion is that the quantum entanglement breaks (whatever that means) when the infalling member of the entangled particle pair crosses the event horizon, with each breaking link creating a little burst of gravitational energy that cumulatively create a firewall just inside the event horizon. This firewall then destroys any infalling object in transit [41]. The firewall hypothesis, however, remains very controversial, and there is no apparent way of testing it.

More recently Maldacena and Susskind [42] have suggested an alternative. When two entangled black holes separate, they hypothesize that a wormhole connection forms between them to implement their entanglement. It has even been suggested that such quantum wormholes may link all entangled particle pairs. There are, however, problems with this interesting scenario, not the least of which is that such wormholes should have significant mass that is not observed.

The Transactional Interpretation offers a milder, if less dramatic solution to this problem, providing an interesting insight into the Black Hole Information Paradox. One normally thinks that absolutely nothing can break out of the event horizon of a black hole from the inside and escape. However, as illustrated in Fig. 13, there is one exception: advanced waves can emerge from a black hole interior, because they are just the time-reverse of a particle-wave falling in. An advanced wave “sees” the black hole in the reverse time direction, in which it looks like a white hole that emits particles. The strong gravitational force facilitates rather than preventing the escape of an advanced wave. Thus, an entangled particle pair, linked by an advanced-retarded wave handshake, has no problem in maintaining the entanglement, participating in transactions, and preserving conservation laws, even when one member of the pair has fallen into a black hole. There is no need for entanglement-breaking firewalls or entanglement-preserving wormholes, just a trans-

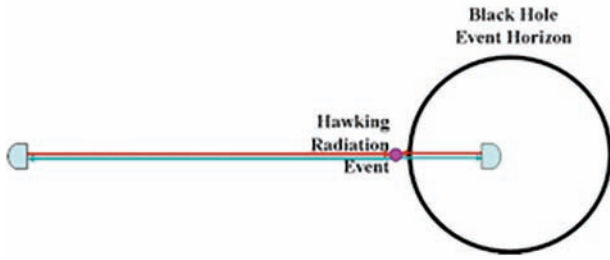


Fig. 13: Transaction through Black Hole event horizon using escaping advanced waves.

actional handshake. Thus, it would seem that the Transactional Interpretation goes some considerable distance toward solving the Black Hole Information Paradox and resolving an issue that divides quantum mechanics and gravitation and providing a mechanism for preserving information across event horizons.

#### 4 THE PROCESS OF FORMING TRANSACTIONS

Some critics of the Transactional Interpretation have asked why it does not provide a detailed mathematical description of transaction formation. This question betrays a fundamental misunderstanding of what an interpretation of quantum mechanics actually is. In our view, the mathematics is (and should be) exclusively contained in the standard quantum formalism itself. The function of the interpretation is to interpret that mathematics, not to introduce any new additional mathematics. We note, however, that this principle is violated by the Bohm-de Broglie “interpretation”, in the Ghirardi-Rimini-Weber “interpretation”, and in many other so-called interpretations. In that sense, these are not interpretations of standard quantum mechanics at all, but rather are alternative theories.

It is true that while the Transactional Interpretation leans heavily on the quantum formalism, the standard formalism of quantum mechanics does not contain mathematics that explicitly describes wave function collapse (which the TI interprets as transaction formation). However, there has been an application of the standard QM formalism in the literature that provides a detailed mathematical description of the “quantum-jump” exponential build-up of a transaction involving the transfer of a photon from one atom to another. In particular, Carver Mead does this in Sect. 5.4 of his book *Collective Electrodynamics* [43].

Briefly, Mead considers an emitter atom in an excited state with excitation energy  $E_1$  and a space-antisymmetric wave function of  $\psi_E = A_E(\mathbf{r}) \exp(-i E_1 t/\hbar)$  and a structurally identical absorber atom in its ground state with excitation energy  $E_0$  and a space-symmetric wave function of  $\psi_A = S_A(\mathbf{r}) \exp(-i E_0 t/\hbar)$ , where  $A$  is an antisymmetric function and  $S$  is a symmetric function. Both of these are stable states with no initial

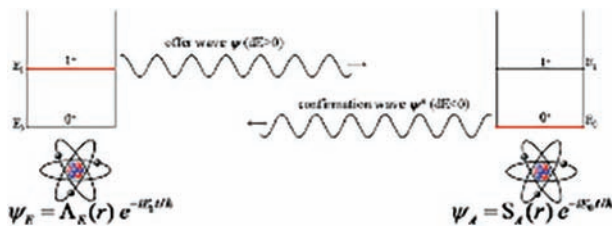


Fig. 14: Mead model of transaction formation: Emitter in antisymmetric excited state of energy  $E_1$  perturbs absorber in symmetric ground state of energy  $E_0$  with offer wave.

dipole moments. He assumes that the initial positive-energy offer wave from the excited emitter atom  $E$  interacting with the absorber atom  $A$  perturbs it into a mixed state that adds a very small component of excited-state wave function to its ground-state wave function. Similarly, the negative-energy confirmation wave echo from the absorber atom interacting with the emitter atom perturbs it into a mixed state that adds a very small component of ground-state wave function to its excited-state wave function, as shown schematically in Fig. 14.

Because of these perturbations, both atoms develop small time-dependent dipole moments that, because of the mixed-energy states, oscillate with the same beat frequency  $\omega = (E_1 - E_0)/\hbar$  and act as coupled dipole resonators. The phasing of their resulting waves is such that energy is transferred from emitter to absorber at a rate that initially rises exponentially.

To quote from Mead’s discussion:

*The energy transferred from one atom to another causes an increase in the minority state of the superposition, thus increasing the dipole moment of both states and increasing the coupling and, hence, the rate of energy transfer. This self-reinforcing behavior gives the transition its initial exponential character.*

In other words, Mead shows mathematically that the perturbations induced by the initial offer/confirmation exchange trigger the formation of a full-blown transaction in which a photon-worth of energy  $E_1 - E_0$  is transferred from emitter to absorber, resulting in a confirmation wave from absorber similarly perturbing the emitter. The result is a pair of dipole resonators oscillating at the same beat frequency  $\omega = (E_1 - E_0)/\hbar$ , to produce an exponentially rising coupling and transaction formation. Thus, mutual offer/confirmation perturbations of the emitter and absorber acting on each other create a frequency-matched pair of dipole resonators as mixed states, and this dynamically unstable system must either exponentially avalanche to the formation of a completed transaction or disappear when a competing transaction forms.

In a universe full of particles, this process does not occur in isolation, and both emitter and absorber are also randomly perturbed by waves from other systems that can randomly drive the exponential instability in either direction. This is the source of the intrinsic randomness in quantum processes – the missing random element that changes quantum mechanics from the determinism of classical mechanics. Ruth Kastner [44] likes to describe this intrinsic randomness as “spontaneous symmetry breaking”, which perhaps clarifies the process by analogy with quantum field theory.

Because the waves carrying positive energy from emitter to absorber are retarded waves with positive transit time, and the waves carrying negative energy from absorber to emitter are advanced waves with negative transit time, there is no net time delay – aside from time-of-flight propagation time of the transferred energy, in the quantum-jump process – and it is effectively instantaneous. Thus, the Transactional Interpretation explains Niels Bohr’s “instantaneous” quantum jumps – a concept that Schrödinger found impossible to accept [45].

In Figs. 15 to 19 we have used Mead’s formalism with standard hydrogen-atom wave functions to calculate example transactions and to make plots of various aspects of the transaction formation in progress.

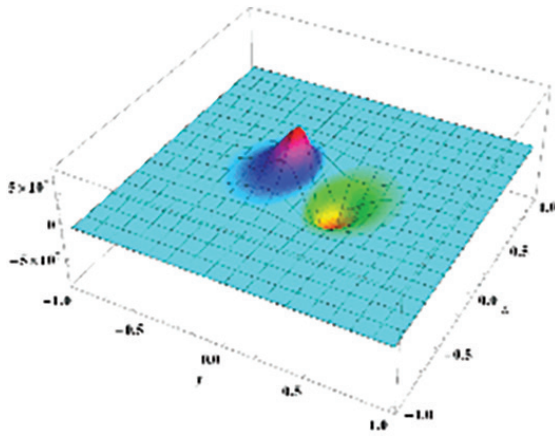


Fig. 15: Electric dipole oscillating at beat frequency  $\omega=(E_1-E_0)/\hbar$  created by mixture of states with excitation energies  $E_0$  and  $E_1$ .

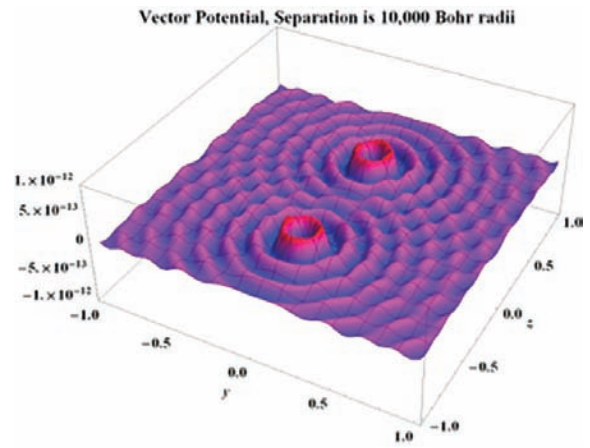


Fig. 16: Waves of electric potential created by coupled dipole oscillations in atoms undergoing energy exchange transaction.

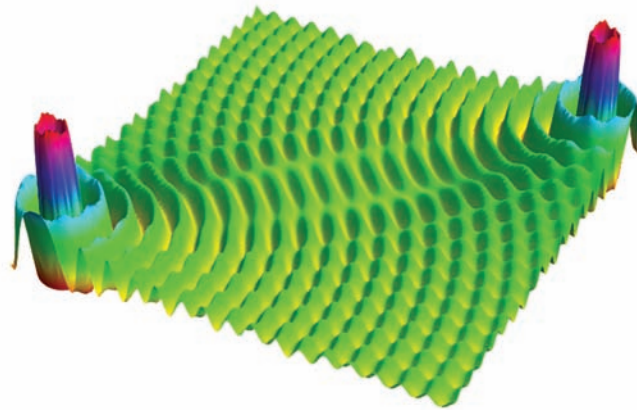


Fig. 17: Waves of electric potential created by coupled dipole oscillations in atoms undergoing energy exchange transaction.

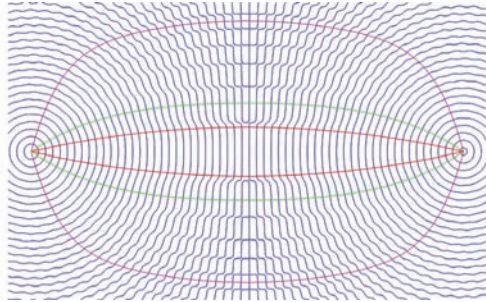


Fig. 18: Paths of equal phase from emitter atom, arriving at absorber atom to coherently reinforce the developing transaction.

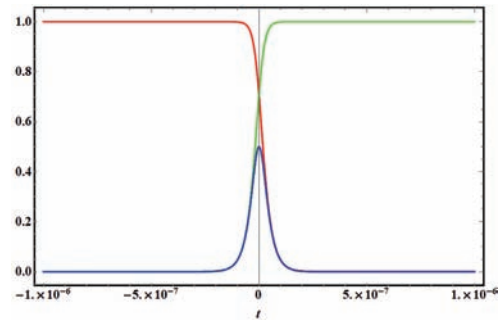


Fig. 19: Amplitudes of the excited state and ground state wave functions that are present in the emitter atom as it is undergoing a transaction.

This is, of course, not a general proof that the offer/confirmation exchange always triggers the formation of a transaction, but it represents a demonstration of that behavior in a tractable case, and it represents a prototype of the general transaction behavior. It further demonstrates that the transaction model is implicit in and consistent with the standard quantum formalism, and it demonstrates how the transaction, as a spacetime standing wave connecting emitter to absorber, can form.

## 5 CONCLUSIONS

- The Transactional Interpretation provides a rational way of visualizing and understanding the mechanisms behind entanglement, nonlocality, and wave function collapse.

- The plethora of interpretational paradoxes and non-classical quantum-optics experimental results can all be understood by applying the Transactional Interpretation.
- The process of transaction formation, at least in simple cases, emerges directly from the application of standard quantum mechanics to the advanced-retarded-wave handshake process as it builds and avalanches to completion.
- As the mattress commercial asks: *Why buy your Quantum Interpretation anywhere else?*



## REFERENCES

1. A. Einstein, B. Podolsky, N. Rosen, *Phys. Rev.* 47, 777–785 (1935)
2. E. Schrödinger, *Proc. Camb. Philos. Soc.* 31, 555–563 (1935); *Proc. Camb. Philos. Soc.* 32, 446–451 (1936)
3. S.J. Freedman, J.F. Clauser, *Phys. Rev. Lett.* 28, 938 (1972)
4. J.S. Bell, *Physics* 1, 195 (1964)
5. W. Heisenberg, *Z. für Phys.* 43, 172 (1927) (translated in [20], pp. 62–84)
6. J.G. Cramer, “The transactional interpretation of quantum mechanics”, *Rev. Mod. Phys.* 58, 647–687 (1986)
7. J.G. Cramer, “An overview of the transactional interpretation of quantum mechanics”, *Int. J. Theor. Phys.* 27, 227–236 (1988)
8. J.G. Cramer, “The plane of the present and the new transactional paradigm of time”. Chapter 9, in *Time and the Instant*, ed. by R. Drurie (Clinamen Press, Manchester, 2001), arXiv:quant-ph/0507089
9. J.G. Cramer, *Found. Phys. Lett.* 19, 63–73 (2006)
10. J.G. Cramer, “The Transactional Interpretation of Quantum Mechanics and Quantum Nonlocality” (to be published as a book chapter), arXiv:1503.00039 [quant-ph]
11. J.G. Cramer, *The Quantum Handshake – Entanglement, Nonlocality and Transactions* (Springer, Heidelberg, 2016)
12. J.A. Wheeler, R.P. Feynman, *Rev. Mod. Phys.* 17, 157 (1945); *Rev. Mod. Phys.* 21, 425 (1949)
13. M. Born, *Z. für Phys.* 37, 863 (1926), pp. 52–55. Translated in [40]
14. A. Einstein, in “Electrons et Photons – Rapports et Discussions du Cinquième Conseil de Physique tenu, Bruxelles du 24 au 29 Octobre 1927 sous les Auspices de l’Institut International de Physique Solvay” (Gauthier-Villars, Paris 1928)
15. M. Jammer, *The Conceptual Development of Quantum Mechanics* (McGraw-Hill, New York, 1966)
16. R.P. Feynman, R.B. Leighton, M. Sands, *The Feynman Lectures*, vol. 3 (Addison-Wesley, Reading, 1965). ISBN: 0201021188
17. Sir G.I. Taylor, Interference fringes with feeble light. *Proc. Camb. Philos. Soc.* 15, 114 (1909)
18. G.N. Lewis, The nature of light. *Proc. Natl. Acad. Sci.* 12, 22–29 (1926)
19. T.L. Dimitrova, A. Weis, “The wave-particle duality of light: a demonstration experiment”. *Am. J. Phys.* 76, 137–142 (2008)
20. J.A. Wheeler, in *The Mathematical Foundations of Quantum Mechanics*, ed. by A.R. Marlow (Academic Press, New York, 1978)
21. V. Jacques, E. Wu, F. Grosshans, F. Treussart, P. Grangier, A. Aspect (LCFIO), J.-F. Roch, “Experimental realization of Wheeler’s delayed-choice gedankenexperiment”. *Science* 315, 966 (2007), arXiv:0610241 [quant-ph]
22. S.S. Afshar, “Violation of the principle of complementarity, and its implications”. *Proc. SPIE* 5866, 229–244 (2005), arXiv:0701027 [quant-ph]
23. N. Bohr, “Discussions with Einstein on epistemological problems in atomic physics”, in *Albert Einstein: Philosopher-Scientist*, ed. by P. Schilpp (Open Court, Peru, 1949)
24. N. Bohr, *Atti del Congresso Internazionale dei Fisici Como*, 11–20 Settembre 1927, vol. 2 (Zanchelli, Bologna, 1928), pp. 565–588
25. H. Everett III, *Rev. Mod. Phys.* 29, 454 (1957), see also [26]
26. J.A. Wheeler, *Rev. Mod. Phys.* 29, 463 (1957), see also [25]
27. S.J. Freedman, J.F. Clauser, *Phys. Rev. Lett.* 28, 938 (1972)
28. J.S. Bell, *Physics* 1, 195 (1964)
29. A.C. Elitzur, L. Vaidman, *Found. Phys.* 23, 987–997 (1993)
30. L. Mandel, E. Wolf, *Optical Coherence and Quantum Optics* (Cambridge University Press, Cambridge, 1995)
31. L. Hardy, *Phys. Lett. A* 167, 11–19 (1992)
32. L. Hardy, *Phys. Lett. A* 175, 259–260 (1993)
33. W. Gerlach, O. Stern, “Das magnetische Moment des Silberatoms”. *Zeitschrift für Physik* 9, 353–355 (1922)
34. D. Bohm, B.J. Hiley, *The Undivided Universe: An Ontological Interpretation of Quantum Theory* (Routledge, London, 1993). ISBN: 0-415-06588-7
35. R. Clifton, P. Neimann, *Phys. Lett. A* 166, 177–184 (1992)
36. C. Pagonis, *Phys. Lett. A* 169, 219–221 (1992)
37. R.B. Griffith, *Phys. Lett. A* 178, 17 (1993)
38. C. Dewdney, L. Hardy, E.J. Squires, *Phys. Lett. A* 184, 6–11 (1993)
39. T.J. Herzog et al., *Phys. Rev. Lett.* 75, 3034–3037 (1995)
40. S.W. Hawking, “Particle creation by black holes”. *Commun. Math. Phys.* 43, 199–220 (1975)
41. A. Almheiri, D. Marolf, J. Polchinski, J. Sully, “Black holes: complementarity or firewalls?”. *J. High Energy Phys.* 2013(2), 062 (2013)
42. J. Maldacena, L. Susskind, “Cool horizons for entangled black holes”. *Fortsch. Phys.* 61, 781–811 (2013)
43. C. Mead, *Collective Electrodynamics* (The MIT Press, Cambridge, 2000); ISBN: 0-262-13378-4
44. R.E. Kastner, *Understanding Our Unseen Reality: Solving Quantum Riddles* (Imperial College Press, London, 2015)
45. W. Heisenberg, *Reminiscences from 1926 and 1927*, in A.P. French, P.J. Kennedy (eds.), *Niels Bohr, A Centenary Volume* (Harvard University Press, Cambridge, 1985)

Received 18 December 2017 Accepted 22 February 2018

# THE RELATIVISTIC CAPACITOR MODEL AND THE MACH-LORENTZ THEORY

JEAN-PHILLIPE MONTILLET, Independent Researcher, Neuchatel, Switzerland, and C. ZIEP, Independent Researcher, Magdeburg, Germany

Email: Jeanfi\_montillet@yahoo.fr

---

Various theories have recently emerged to explain the anomalous thrust generated by the controversial EM Drive [1, 2]. This work follows previous works on the Mach-Lorentz thruster [3, 4, 5] to explain the anomalous thrust, based on a capacitor model in the particular case of the TM010 mode. Here, we expand this model with further assumptions, such as the asymmetry due to the geometry of the Electromagnetic cavity, in order to explain the thrust generated in the TE012 mode. This general model is called the “relativistic” capacitor to explain the triggering of the Woodward effect in those various experiments. We show that for the TM010 mode the “relativistic” capacitor models the cavity as a sum of capacitors in series with various capacitances, whereas the TE012 mode is best described as a sum of capacitors in parallel with various capacitances. However, the anomalous thrust results from the Electromagnetic and Gravitational coupling.

**Keywords:** Relativistic, Capacitor, Woodward effect, TE mode, Electromagnetism, Mach-Lorentz theory

---

## INTRODUCTION

Since the first experiment at the beginning of this new millennium, the EM Drive has been the focus of many critics from scientists and engineers. In addition, public debates have also contributed in casting doubts on this possible technology. However, the latest tests and measurements by government agencies [2, 6] and academics [7], which should have dismissed this technology once and for all, have confirmed the anomalous thrust generated by this device. This latest development has sparked new interests for this device, which could play a critical role in space exploration of our solar system [8]. Nevertheless, the ultimate goal remains the creation of a model of the EM Drive supporting the experiments.

In the last two decades, various theories have emerged to understand the thrust generated by the EM Drive. The author in [1] or [9] developed a theory based on the difference of radiation pressure forces on the end plates of the cavity. More recently, an explanation of the anomalous thrust has been supported by the introduction of the Unruh radiation [10]. Another theory [11] attempts to model this exotic propulsion engine based on the emission of paired photons expelled through the cavity end plates and to generate the recorded thrust. In [12], the thrust is the result of a man-made gravitational field gradient taking place in the cavity walls. Other emerging theories can be found online. Among all those theories, we are here only interested in the application of the Mach-Lorentz thruster (MLT) [3, 4] to the EM Drive. This theory is based on the Lorentz force coupled to the Woodward effect [13] in order to explain the anomalous thrust. The Woodward effect is derived from Mach's principle. This theory defines inertia within general relativity theory [14], and demonstrates the possible interaction of gravitational forces resulting from massive bodies in the universe. Experiments with capacitors and piezoelectric materials have reproduced the Woodward effect in a laboratory environment [15].

The Mach Lorentz Thruster (MLT) model was first formulated by J. Woodward in [15] in the early 2000s to mitigate issues with sonic interference in his original 50 kHz PZT stacks (i.e. lead-zirconium-titanate actuator). This original MLT design used a cap-ring with their electrodes set up to provide a circular set of radial AC electric fields, combined with a toroidal B-field coil wrapped around the cap-ring so the AC B-field was at right angles to the AC E-fields. This geometry automatically set up and controlled the EM field configuration so that its resulting Lorentz force was always at right angles to both the AC E and B fields aligned at right-angles to each other along the thruster's longitudinal axis. This configuration gave optimal force output with good control on how the MLT's electric and magnetic fields are set up and controlled. Further developments and tests were carried out from this initial design to understand the Woodward effect and the resulting thrust in [3, 4, 15, 16].

Recently, in [5], we use the same MLT model for the application of the Mach effect to a conical frustum resonant cavity. Our model is an attempt to explain how the Woodward effect is triggered in the EM Drive concept, knowing that internal E-fields and B-fields can be in any relative orientation to each other dependent on the driven resonant mode and shape of the frustum. Beyond the explanation of the anomalous thrust, we want also to explain the possible direction of the thrust force. One important assumption is that the Woodward effect cannot be triggered by classical mechanics (i.e. some outside forces are applied to the considered system and trigger this effect somehow).

Previous works [3, 5, 15, 16] assumed that the model of a capacitor is the key to introduce the Woodward effect within the explanation of the anomalous thrust force. Indeed, both the EM Drive and the Woodward's PZT stack experiments can be modelled from an Electromagnetic (EM) point of view (i.e. EM cavity properties, piezoelectric properties) such as a capacitor in parallel with a resistance, inductance and a capacitor

with smaller capacitance [5, 15]. In this work, we introduce the concept of a “relativistic” capacitor. “Relativistic” stands for a capacitor with a variable electrical charge, hence inducing a variable voltage at the capacitor terminals. In other words, the EM cavity can be modelled as several capacitors (in parallel or in series) with a capacitance varying due to the local density of the electrical charges on the cavity’s wall. We also underline that this “relativistic” capacitor model involves the geometry of the EM cavity and especially the asymmetry between the top and bottom of it.

The next section focuses on the “relativistic” capacitor model. Section III is the study of the TE012 mode in a similar approach used to study the TM010 mode in [5]. The last section is an open discussion on how to improve the thrust considering the limitations intrinsic to the properties of the EM cavity (i.e. Q factor, resonant frequency). A conclusion ends this work. In Appendix I, we first develop further the estimation of the Woodward effect using the EM energy density. Secondly, we draw an analogy between the “relativistic” capacitor model and a particle (with a mass) evolving within a varying EM field along a world line. We define its evolution with a Lagrangian. The idea is to look at the action principle considering an off-shell variation (time dependent Lagrangian) in order to show a similar expression of the Woodward effect as established in [15]. Appendix II is the theoretical derivation of the mass variation and Lorentz forces around the EM cavity using our assumptions. Those formulas are then used in the calculus of the thrust in Section III.

## II ASSUMPTIONS ON THE RELATIVISTIC CAPACITOR MODEL

The author in [5] modelled the EM drive in TM modes as a capacitor where the two end plates are charged (and discharged) continuously due to the EM field generated inside the cavity. Thus, the model of the “relativistic” capacitor is due to the asymmetry between the large end plate and small end plate. An overview is to consider that there are  $N$  capacitors in series between the two end plates, increasing the size of the capacitor’s plates starting with the small end plate and finishing with a capacitor with the size of the large end plate. The distance between two plates of the  $i$ -th capacitor is  $\delta z_i$ , with capacitance

$$C_i = (S_i \cdot \epsilon) / \delta z_i \quad \text{and charge } q_i(t)$$

$S_i$  is the surface of the plates for the  $i$ -th capacitor, and  $\epsilon$  the permittivity (most likely the permittivity of the vacuum). Because the amplitude of the voltage at the terminals of the  $i$ -th capacitor is assumed to fluctuate with time, the charge is also a function of time. Note that the capacitance of our “relativistic” capacitor, in TM mode, is:

$$C = \prod_{i=1}^N C_i / \sum_{i=1}^N C_i \quad [17]$$

The “relativistic” capacitor models the variable electrical charges.

The TE mode is less intuitive, because we postulate that the EM field inside the cavity creates charges on the conical wall of the frustum (i.e. EM cavity). Simulations and experiments [2, 6, 18] show that the EM field varies inside the cavity. Let us assume that the charge density on the conical wall varies with the height ( $\delta z_i$ ).  $\rho_i(t)$  is the charge density distributed inside an infinitesimally (pseudo) circular strip of conical wall of length  $\delta z_i$ . An overview is when opening the frustum, the conical wall

is a (pseudo) trapezoid with non-homogeneous distribution of the charges on the Z-axis due to the varying E field perpendicular to the Z-axis. For each infinitesimally strip of conical wall (with width  $\delta z_i$ ), we associate a capacitor  $C_i$  with a specific capacitance. Each capacitor  $C_i$  is associated with the charge density  $\rho_i(t)$  and a voltage at the terminals:

$$V_i(t) = \int_{\delta z_i} \frac{\rho_i(t)}{\epsilon_0 \epsilon_{Cu}} dz$$

with  $\epsilon_0$  the permittivity of the vacuum, and  $\epsilon_{Cu}$  the permittivity of the copper (e.g., [2, 6]).

This mode is not intuitive, because the size of the plates varies with the density of charges  $\rho_i(t)$  and not directly with the geometry of the problem as postulated for the TM010 mode [5]. Thus, the general model of the TE modes is  $N$  capacitors in parallel.

The second assumption is that the variation of electric charge density on the EM cavity’s wall induces a variation of mass of the cavity via the Woodward effect. This assumption is the same as in the explanation of thrust for the piezoelectric stack [3, 4] and the TM010 mode [5]. Further simplifications to estimate this mass variation using the EM energy density described in [19] also called Electromagnetic and Gravitational coupling, are summarized in the next section. Finally, we follow the hypothesis in [15] where it is assumed in an MLT model that as soon as the Woodward effect takes place, the system becomes open and Newton’s third law can then be applied. In the MLT model, the Lorentz forces take place when the system is open due to the surface currents around the cavity’s walls. Those forces play a crucial role, because their amplitude is varying locally in the cavity with the amplitude of the surface currents. The thrust force is assumed to be the reaction of the sum of those forces in order to nullify the acceleration. In other words, if we assume a mass between two springs being pulled in opposite directions due to the different stiffness of the springs, the thrust is the additional force to pull the mass back to its original place. In this simplistic view, the difference of the springs’ stiffness models the asymmetry of the amplitude of the surface currents within the EM cavity, which is a consequence of the geometry of the EM Drive.

## III THE RELATIVISTIC CAPACITOR MODEL AND THE ELECTROMAGNETIC AND GRAVITATIONAL COUPLING APPLIED TO THE TE012

In Section II, we describe how the relativistic capacitor model can be applied to the TE modes in order to produce the anomalous thrust with the Woodward effect. One needs to take into account the Electromagnetic and Gravitational coupling (EMG) as discussed in [5, 19]. In order to parallel the theory developed for the TM modes, we follow the same three steps as in [5]. The following section refers to Fig. 1 of the frustum aligned on the Z-axis.

### A Step 1: Charge-Discharge of the Relativistic Capacitor

Let us first assume that there is no force or no thrust acting on the cavity. The electric field is exciting the conical wall, and the B field follows the longitudinal axis inside the cavity (i.e. perpendicular to the end plates – e.g., [20]). Following the explanation in Section II, the relativistic capacitor model is applied to the TE modes, with  $N$  capacitors in parallel. The capacitor charges and discharges instantaneously due to the creation



and dissipation of the charges by EM excitation on the surface of the conical wall. Now, taking into account the dissipation intrinsic to the conductor properties, the EM cavity can be modelled such as an RC circuit [21], with  $C$  the total capacitance of the  $N$  capacitors with:

$$C = \sum_{i=1}^N C_i.$$

The equations read:

$$\begin{aligned} R \cdot i + \frac{q}{C} &= 0 \\ R \cdot \frac{dq}{dt} + \frac{q}{C} &= 0 \\ q(t) &\approx q_0(t) \cdot e^{-\frac{t}{RC}} \end{aligned} \quad (III.1)$$

$q_0$  is the charge at the initial time. The equation of the charge  $q(t)$  shows that the dissipation of the initial charge  $q_0$  during the discharge time  $\tau = RC$ . This model is similar to a switch on-off capacitor. In order to estimate the discharge time  $\tau$ , one needs to look at the distribution of the charge along the conical wall. Now, we assume that the charge distribution on the wall follows the Eddy currents around the EM cavity's walls.

Let us consider the density of the charge  $\rho_i(t)$  associated with the section of the conical wall (or the  $i$ -th capacitor with capacitance  $C_i$ ), the conductivity of the copper  $\sigma$  and  $\epsilon_{Cu}$  its permittivity, then [22]

$$\begin{aligned} \partial_t \rho_i(t) + \nabla \cdot \vec{J}_i &= 0 \\ \epsilon_0 \epsilon_{Cu} \partial_t (\nabla \cdot \vec{E}) + \sigma \nabla \cdot \vec{E} &= 0 \\ \epsilon_0 \epsilon_{Cu} \partial_t (\Delta V_i(t)) + \sigma \Delta V_i(t) &= 0 \\ \Delta V_i(t) &\approx V_0 \cdot e^{-\frac{\sigma}{\epsilon_0 \epsilon_{Cu}} t} \end{aligned} \quad (III.2)$$

$\Delta$  is the scalar Laplacian. The discharge time, associated with the capacitance  $C_i$ , equals

$$\frac{\epsilon_0 \epsilon_{Cu}}{\sigma} \sim 1 \text{e-18 s} \quad (\text{values from [23]}).$$

Note that we assume at the surface of the plate (no magnetic potential)

$$\vec{E} = \vec{\nabla} V_i$$

where  $V_i$  is the electrical potential.  $V_0$  is the potential at the initial time before the discharge. With the description in Section II, the conical wall is similar to  $N$  capacitors in parallel, divided in strips with a density of charge  $\rho_i(t)$  and width  $\delta z_i$ . Thus, the equation (III.2) is the general equation if we consider one capacitor with capacitance

$$C = \sum_{i=1}^N C_i$$

Because of the variation of  $\rho_i(t)$  (due to the variation of the EM field inside the cavity), the charge/discharge time varies for each  $C_i$ .

In the first step, **the main assumption is the creation of electric charges at the surface of the cavity's walls.**

### B The acceleration of the cavity due to the Lorentz force

The second step is the forces acting on the cavity. The current propagates inside the electromagnetic field, and thus triggers a

Lorentz force  $F_{Lo}$ . In the TM mode, the author in [5] assumed that the Lorentz forces take place on the conical wall only for simplification of our model. Here, we assume that the Lorentz forces are not localized and can also be on the conical wall as the spherical ends. However, momentum is conserved if no mass variation (or open system) takes place. Thus, this section should be combined with the last step in order to produce a thrust.

Using the same circuit analogy as in the TM mode [5], the cavity is now an RLC circuit with an induced electromotive force  $\mathcal{G}$ :

$$R \cdot i + \frac{q}{C} + L \cdot \frac{di}{dt} - \mathcal{G} = 0 \quad (III.3)$$

$L \cdot \frac{di}{dt}$  is equivalent to the mechanical action of the cavity getting accelerated (or

$m \frac{dv}{dt}$  in classical mechanics – Newton's second law – with  $m$  the mass of the cavity and  $v$  the speed).

$\mathcal{G}$  can be expressed such as  $\mathcal{G} = -\partial_t \Phi_B(t)$

with  $\partial_t$  the partial derivative in time and  $\Phi_B(t)$  the magnetic flux through the surface of the cavity's walls [22]. Using the mechanical analogy, when projecting the forces on the Z-axis, the equation (III.3) becomes:

$$m \cdot \frac{d^2 Z}{dt^2} = \alpha \frac{dZ}{dt} - K \cdot Z + F_{Lo} \quad (III.4)$$

Where  $\alpha \frac{dZ}{dt}$

is the dissipative force due to the resistivity of the copper during the propagation of the surface currents. The term  $K \cdot Z$  is the mechanical analogy of the capacitor properties  $\frac{q}{C}$  of the EM cavity.

Let us estimate the Lorentz force applied to one electron (with charge  $q_e$  and speed  $v_e$ ) moving through the magnetic field  $\vec{B}$  at the surface of one of the end plates.

$$\vec{F}_{Lo} = q_e \vec{v}_e \times \vec{B} \quad (III.5)$$

Here ( $\times$ ) is the vectorial product. One can estimate the Lorentz force per unit of surface ( $dS_i$ ), and define the surface current:

$$J_S = N_e q_e v_e, N_e$$

is the number of charges per unit of surface. The Lorentz force per unit of surface now reads:

$$\vec{F}_{Lo} = N_e q_e \vec{v}_e dS_i \times \vec{B} = \vec{J}_S dS_i \times \vec{B} \quad (III.6)$$

$\vec{F}_{Lo}$  is estimated for the whole interior surface of the EM cavity. Further assumptions are required to estimate  $F_{Lo}$  around the EM cavity. Such an estimation is made in Appendix II. Now, to recall the first paragraph of this section, the conservation of momentum states that the cavity cannot be accelerated by the creation of Lorentz forces. In fact, equation (III.4) is only stated from a pedagogical point of view.

In the second step, the main assumption is that **the current propagating at the surface of the conical wall inside the cavity generates the Lorentz Forces around the EM cavity.**

### C Triggering the Woodward effect and the anomalous thrust

The last step is the triggering of the Woodward effect generating the thrust. It is the introduction of

$$\frac{dZ}{dt} \frac{dm}{dt}$$

into equation (III.4). As previously mentioned, the variation of the mass of the cavity is due to the Woodward effect applied to the EM energy density stored in the skin layer of the copper cavity's walls. Before recalling the Woodward effect, we can think about the capacitance properties of the cavity and the mechanical analogy in (III.3) such as

$$\frac{q}{c} \sim \frac{q}{c} + \frac{1}{c} \frac{dq}{dt} \cdot \frac{q}{c}$$

is intrinsic to the properties of the cavity with the direct mechanical analogy

$$K \cdot Z \cdot \frac{1}{c} \frac{dq}{dt}$$

which is the relativistic part in our relativistic capacitor model. The mechanical analogy is given by the Woodward effect. Thus, the Woodward effect is mostly associated with the capacitor model and not the inductor for each element of the cavity, so introducing a dielectric should reduce it. In the TE012, the asymmetry of the charges on the conical wall creates the capacitor (i.e.  $N$  capacitors in parallel) as discussed in Section II.

Recalling that the Woodward effect takes place while the energy inside the cavity (i.e. rest energy) is fluctuating, the variation of mass is translated into the equation [5, 15]

$$\delta\rho_0(t) = \frac{1}{4 \cdot \pi \cdot G} \left[ \frac{1}{\rho_0 c^2} \partial_t^2 \Xi - \left( \frac{1}{\rho_0 c^2} \partial_t \Xi \right)^2 \right] \quad (\text{III.7})$$

where  $\rho_0$  is the transient mass source and  $c$  the speed of light. Considering a rest energy  $\Xi$ , the energy of the frustum at rest, including all the particles within the frustum with no EM excitation, one can state the famous Einstein's relationship in special relativity between  $\Xi$  and the rest mass

$$m, \Xi = mc^2$$

In [5] (in Appendix III) and [19], the author justifies (via the energy space theory) the assumption that the variation with time of  $\Xi$  equals the variation of EM energy density with the capacitor model, replacing the transient mass source  $\rho_0$  with the mass density

$$\delta\rho(t) = \delta m/V$$

The variation of EM energy in the copper material (skin layer) is expressed with  $d U_{EM}$ . The Woodward effect in (III.7) can then be rewritten:

$$\delta\rho_0(t) = \frac{1}{4 \cdot \pi \cdot G} \left[ \frac{1}{\rho \cdot c^2} \partial_t^2 U_{EM} - \left( \frac{1}{\rho \cdot c^2} \partial_t U_{EM} \right)^2 \right] \quad (\text{III.8})$$

The author in [15] calls  $\partial_t^2 \Xi$  the impulse engine, and  $(\partial_t \Xi)^2$  is the wormhole term. He also warns that the wormhole term is many orders of magnitude smaller than the impulse engine. In [5] and [19], the author discusses the first and second order derivatives of  $U_{EM}$  in terms of EM theory and the relationship with the Energy Space theory. The so-called Electromagnetic and Gravitational coupling follows Equation (III.7) in [19].

Now for the TM010 mode, the Woodward effect assumes to create a variation of mass (mass density) at the small end and large end plate independently. For the TE012, the Woodward effect takes place mostly on the conical wall. Equation (III.4) becomes

$$m \cdot \frac{d^2 Z}{dt^2} + \frac{dZ}{dt} \cdot \frac{dm}{dt} = \alpha \frac{dZ}{dt} - K \cdot Z + F_{Lo} \quad (\text{III.7})$$

One needs to underline that the terms

$$\alpha \frac{dZ}{dt} \text{ and } K \cdot Z$$

are intrinsic to the cavity parameters (i.e. resistivity, dimension), whereas the thrust or acceleration of the cavity

$$\left( m \cdot \frac{d^2 Z}{dt^2} \right)$$

depends on the Lorentz force  $F_{Lo}$  and the relativistic terms coming from the Woodward effect

$$\frac{dZ}{dt} \cdot \frac{dm}{dt}$$

Similar to the TM010 mode [5], the measurable thrust in the MLT comes from equation (III.9) which results from the coupling between the Lorentz force and the Woodward effect – a Mach-Lorentz Thruster.

In the last step, we assume that **the anomalous thrust is a combination of Lorentz forces around the cavity and the Woodward effect**.

### IV SIMULATIONS OF THE TE012 MODE

This section reports the simulations done using the FEKO software. The following description is referenced using Fig.1.

The frustum is modelled in 3D via the software graphical interface, using a mesh resolution of  $\sim \lambda/12$ . This leads to a resolution of more than 5000 triangles at the conductive wall, which builds the basis for the simulations. Note that FEKO software uses a solver to estimate the EM fields based on the Methods of Moments (or MoM). The dimensions of the frustum are the same as described in the testbed reported by NASA in [6], 279.4mm diameter of the large end plate, 158.8 mm diameter of the small end plate and 228.6 mm for the height of the cavity. The properties of the copper material (i.e. conductivity, permittivity, permeability, ...) are already predefined within the software library, which facilitates the setup for the simulations.

Now, in order to select the reflection properties intrinsic to the TE012 mode (or others), one needs to configure a high frequency source. An "equivalent magnetic dipole" is used to excite the specific modes in the cavity resonator. Note that the dipole is modelled as a matched loop antenna source. For each mode, the input power is equal to 1 W. The data are extracted by measuring the field strength along predefined strait lines across the interior surfaces of the EM cavity. This configuration allows us to make an estimate of the EM excitation inside the cavity on all the planes (i.e. conical wall, small and big end plates). It is equivalent to the coupling between a (matched) EM source and the cavity at the resonant frequency. Here, the source is placed 40 mm above the big end plate, at the axis of symmetry. One can get an estimate of the surface currents, the EM field inside the cavity, at the walls and near the walls. The resonant frequency is also an output, estimated from the simulations (i.e. from a power vs. frequency plot).

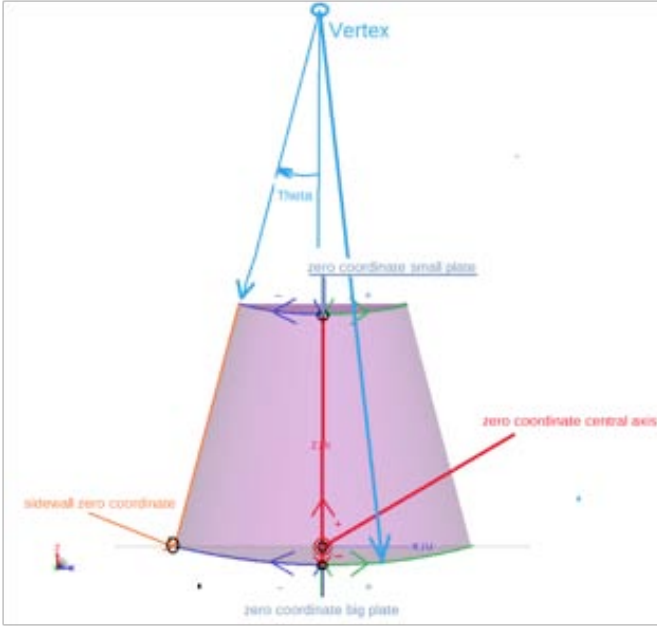


Fig. 1: Parameters - EM Drive Frustum

Now, the Woodward effect and the Lorentz forces are estimated for each end plate and the conical wall independently. The Lorentz forces are an integral over the considered surface. According to Section III, the Woodward effect is estimated via the EM energy density stored inside the skin layer of the copper material for each element of the EM cavity. The approximations of the EM energy density, the mass variation ( $\delta m$ ) the amplitude of the Lorentz Forces ( $F_{Lo}$ ) and the resulting thrust ( $F_{Thrust}$ ) are given in Appendix II. Fig. 2 displays the surface currents and magnetic field for the simulations described in the previous paragraph for the TE012 mode. One can see the high amplitude surface currents on the conical wall.

Now, Table 1 shows the results.

TE012	Without HDPE	
$F_{Thrust}$ (Estimated Thrust) [microN]	-40 +/- 30 **	(-77*)
$\delta m$ (conical wall) [Kg/s <sup>2</sup> ] (av.)	3e-3 +/- 2.8e-3	
$\delta m$ (small end) [Kg/s <sup>2</sup> ] (av.)	1.6e-6 +/- 1.1e-6	
$\delta m$ (large end) [Kg/s <sup>2</sup> ] (av.)	1.3e-5 +/- 1e-6	
$F_{Lo}$ (conical wall) (av.) [N/m]	-1.4926e-04 +/- 5.7e-3	
$F_{Lo}$ (small end) (av.) [N/m]	-1.99e-6 +/- 9.1e-4	
$F_{Lo}$ (large end) (av.) [N/m]	4e-20 +/- 1.4e-3	

TABLE 1: Estimation of Woodward effect and Thrust in the TE012 mode. (\*) is the NASA estimates from [6, 18]. (\*\*) mean value and associated standard deviation due to the various assumptions in our model.

The results in the Table 1 are averaged over 1 cycle. The direction of the Lorentz forces averaged for each element independently (i.e. conical wall, large end, small end) is given by the sign in front of the amplitude. Thus, the (total) Lorentz forces for the conical wall and the small end plate point towards the direction of the large end, whereas the (total) Lorentz force for the large end plate is in the opposite direction. Note that the estimation is dependent of the various assumptions given in the previous section (i.e. Woodward effect varying with EM energy

density, current on the cavity's wall, to estimate amplitude and direction of Lorentz forces). That is why we do not disclose one estimate for each element, but a mean value and the standard deviation. Overall, we can see that our estimated anomalous thrust (first row) is -40 microN +/- 30 microN. In [6], the authors recorded a thrust force of ~77 microN. Our estimate is slightly less using our current simulations, but within the right order of magnitude of the thrust force. Another important result is that in terms of mass variation and Lorentz forces, the conical wall contributes most to the estimate of thrust. This result is interesting for the TE012 mode and it could confirm the relativistic capacitor model.

## DISCUSSIONS ON INCREASING THE ANOMALOUS THRUST

This section relates a discussion between the authors, Dr. José Rodal and Mr. Paul March around the present model and the discussions during the workshop at Estes Park in the fall of 2016 (see proceedings [5]). The purpose is to understand the relationship between the Q-factor (quality factor), the power loss due to heating radiation from the cavity, and the energy stored within the skin depth from the EM waves propagating inside the cavity and the results published in [6] and [24]. In [24], the author has already discussed the efficiency of the EM Drive in terms of maximizing the ratio "thrust" force ( $F$ ) per input power ( $P_m$ ). Indeed, he shows that for the EM Drive, the ratio is equal ( $F/P_m = Q.g/c$ ), where  $Q$  is the quality factor,  $g$  a dimensionless factor, and  $c$  the speed of light.

By definition [25], the Q-factor can be defined such as  $Q = w_o / (2.Dw)$  with  $w_o$  the resonant pulsation and  $Dw$  the frequency bandwidth. Now, we have modelled the TM and TE modes as a relativistic capacitor (with variable capacitance  $C$ ). Thus, the Q-factor can also be defined as  $Q = w_o.R.C$  [25]. The first parameter to estimate is the resistance of the cavity walls ( $R$ ). It should be the integral over the whole interior surface of the cavity's walls of

$$R_i = 1/[d(x_i, y_i, z_i). \sigma] . d(x_i, y_i, z_i)$$

the skin depth on the cavity's walls at the coordinates  $[x_i, y_i, z_i]$  (i.e. end plates and conical wall,  $\sigma$  the conductivity of the material – copper). However, software for EM simulations such as FEKO can approximate the cavity resistance. It is also possible to estimate the Q-factor for a given TM or TE mode. Assuming small variations of the cavity's resistance  $R$ , one can estimate, with the model of the relativistic capacitor, the variance of the capacitance. Then, one can check the formula  $Dw = 1/(R.C)$ .

Moreover, we use the formula

$$Q = w_o . \{Energy\ Stored\} / \{Power\ Loss\}$$

and make the assumption that most of the energy stored is the EM energy density ( $U_{EM}$ ), hence

$$Q = w_o . U_{EM} / \{Power\ Loss\} . = R . C$$

showing that increasing  $U_{EM}$  in order to increase the Woodward effect will also increase the heat radiated. In other words, the higher the field strength in a specific volume of the cavity's wall, the higher the induced current in the wall (i.e. surface charges, Eddy currents) and the greater the heating due to the ohmic losses. Note that this competition between the Woodward effect and the ohmic losses is shown in equation (III.9)



with the mechanical analogy. To recall that the resistivity of the EM cavity (or ohmic losses) is the term

$$= \alpha \frac{dZ}{dt}$$

and the Woodward effect is translated with

$$\frac{dZ}{dt} \cdot \frac{dm}{dt}$$

Both terms are in  $\frac{dZ}{dt}$

and thus compete against each other, which means that at low variations of the electric charge, the Woodward effect may not be measurable due to the ohmic losses. Note that in [12], one fundamental assumption is that the thrust is generated by the ohmic losses and the variation in time of power dissipation without any Woodward effect. Thus, one idea has been to increase the skin depth in order to increase the EM energy density variation. In line with the previous paragraph, this increase will also increase the ohmic losses when using a copper frustum. In fact, it is most likely that we will not record a higher thrust (or even no thrust at all). The NASA group have postulated that the use of superconductive materials such as YBCo (Yttrium Barium Copper Oxide) or MGB2 (Magnesium diboride) to replace the copper, or lowering the outside temperature of the EM cavity (i.e. using liquid nitrogen), could improve the thrust by limiting the power losses. A thermal camera inside and outside the cavity should be used to estimate the ohmic losses and thus see the effect of lowering the outside temperature. Note that in [6], the authors have been using a thermal camera to estimate the outside temperature of the cavity while recording the anomalous thrust.

Another way to understand the formula:

$$Q = w_o \cdot U_{EM} / \{Power Loss\} = R \cdot C$$

is to assume for an infinitesimal volume of the copper cavity, the skin depth  $d(x, y, z)$  is approximated with the general formula (e.g., [22])

$$\sqrt{2 \cdot (\omega \cdot \mu_0 \cdot \sigma)}$$

where  $\mu_0$  is the permeability in the vacuum,  $\sigma$  the conductivity of copper, and considering that  $\omega$  is equal to the resonant frequency  $w_o$ . Thus, we can write:

$$\frac{U_{EM}}{\{Power Loss\}} \sim C \cdot \sqrt{(\omega \cdot \mu_0) / (2 \cdot \sigma)}$$

If Power loss is an averaged quantity, the above formula shows the fluctuation of the capacitance  $C$  as a linear relationship with the fluctuation of the EM energy density ( $U_{EM}$ ). Note that in [5], we have already assumed that the variation of mass required to trigger the Woodward effect was due to the EM excitation on the end plates creating electric charges (i.e. electrons) in the TM010 mode. This assumption echoes some previous work such as [26].

Moreover, the model of the TE modes (i.e. TE012) seems more promising to increase the thrust, because of its capability to trigger a large amplitude of mass variation (via the Woodward effect) due to the model of capacitors in parallel. However,

the EM excitation on the conical wall should also produce an important heat radiation. In addition, the dimensions of the cavity (i.e.  $L$ , the length of the conical wall measured perpendicular to the end plates) is also an important factor in producing this thrust. According to [24], the analytical expression of  $Q$  is a function of  $L$ .

## VI CONCLUSIONS

This work is based on a few experiments released by NASA and published in [6]. Our model shows that the relativistic capacitor approach could explain how the Woodward effect is triggered from an asymmetrical distribution of the charges on the EM cavity's walls. However, in the Mach Lorentz Thruster model, we also postulate that the Lorentz forces take place on the cavity's wall. Further discussions, together with the recent model exposed in [27], led us to think that those Lorentz forces are modelling the stress of the copper material or more generally the whole cavity when there is a rapid variation of mass. If we recall our discussion in the first section about the PZT stacks, we can make a bold comparison by associating the piezo electric effect with the relativistic capacitor in our model, justified by the postulate of asymmetry of charges. Further comparison would take into account the electrostriction in a piezoelectric material, but copper does not experience any electrostrictive properties. Instead, we could postulate that those Lorentz forces modelling the stress of the copper material are the substitute phenomenon for the EM Drive.

Due to the number of assumptions made to formulate this model, a large amount of work is still required to make a definite claim. One weakness is the use of an averaged profile of the EM cavity over 1 cycle. Thus, a more dynamic approach should be used. In addition, some recent simulations have shown the existence of eigen frequencies of the EM cavity, which means higher modes could produce a thrust force with different amplitudes – hence some kind of gearbox could be developed.

Finally, one assumption is that the EM field inside the cavity is responsible for the thrust and is used for the estimation of the Lorentz forces. It means that the Earth's magnetic field or the magnetic fields of nearby devices (e.g. the magnetic damper mounted on the experimental testbed) could potentially change the amplitude and direction of the thrust.

## ACKNOWLEDGEMENTS

The authors would like to acknowledge the people who have been involved in developing the presented model during the past two years via discussions or various feedbacks including Mr. Paul March (NASA, Eagleworks), Dr. José Rodal and Prof. Heidi Fearn (California State Fullerton University).

## APPENDIX I Theoretical Model of the Relativistic Capacitor: The point Mass Particle with a Varying Charge

The idea is to use the Lagrangian for a particle inside an EM field subject to a Lorentz force, but with a varying charge in time  $q(t)$  and a varying mass in time and space  $m(x,t)$ . Let us state the Lagrangian for such a system with simply the electric field (see [28] for a full statement):

$$L = \frac{1}{2} m(x,t) V(t)^2 - q(t) \phi(x,t) \quad A(I.1)$$

where  $\phi(x, t)$  is the electric potential such as  $\vec{E} = -\vec{\nabla}\phi$ . The system is not conservative (off-shell variation) and thus at the first order variation of the Lagrangian we can apply (i.e. [27])

$$\begin{aligned} \sum_i \varepsilon_i \left( \frac{\partial L}{\partial \phi^i} - \frac{d}{dt} \frac{\partial L}{\partial \dot{\phi}^i} \right) + \delta t \frac{\partial L}{\partial t} &= 0 \\ \sum_{i=1}^3 \delta x_i \left( \frac{\partial L}{\partial x^i} - \frac{d}{dt} \frac{\partial L}{\partial \dot{x}^i} \right) + \delta t \frac{\partial L}{\partial t} &= 0 \end{aligned} \quad \text{A(I.2)}$$

Knowing that  $V = (\partial x_i / \partial t)_{i=1,2,3}$  one can develop further

$$\begin{aligned} \frac{\partial L}{\partial t} &= mV \frac{\partial V}{\partial t} + \frac{V^2}{2} \frac{\partial m}{\partial t} - \phi \frac{\partial q}{\partial t} - q \frac{\partial \phi}{\partial t} \\ \frac{\partial L}{\partial x_i} &= \frac{V^2}{2} \frac{\partial m}{\partial x_i} - q \frac{\partial \phi}{\partial x_i} \\ \frac{d}{dt} \frac{\partial L}{\partial \dot{x}_i} &= m \frac{dV}{dt} + V \frac{dm}{dt} \end{aligned} \quad \text{A(I.3)}$$

with the assumptions that

$$\frac{\partial V}{\partial x_i} = 0, \quad \frac{\partial V}{\partial \dot{x}_i} = 1, \quad \frac{d}{dt} \frac{\partial V}{\partial \dot{x}_i} = 0, \quad \frac{d}{dt} \frac{\partial V^2}{\partial \dot{x}_i} = 2 \frac{dV}{dt}, \quad \frac{d}{dt} \frac{\partial(q\phi)}{\partial \dot{x}_i} = 0.$$

and also with the approximation

$$\frac{\partial V}{\partial t} = \frac{dV}{dt}, \quad \frac{\partial q}{\partial t} = \frac{dq}{dt}$$

Now, if we separate the variables as internal and external parameters, such as  $(\phi, V)$  are external (or parameters in on-shell transformation); and  $(m, q)$  are the parameters due to the “relativistic” capacitor model. We can then rewrite Eq. (3) such as:

$$\begin{aligned} \delta t \left( mV \frac{dV}{dt} - q \frac{\partial \phi}{\partial t} \right) + \delta x_i \left( -q \frac{\partial \phi}{\partial x_i} - m \frac{dV}{dt} - V \frac{dm}{dt} \right) \\ + \delta t \left( -\phi \frac{dq}{dt} + \frac{V^2}{2} \frac{\partial m}{\partial t} \right) + \delta x_i \left( \frac{V^2}{2} \frac{\partial m}{\partial x_i} \right) &= 0 \end{aligned} \quad \text{A(I.4)}$$

Thus, from this equation, we can see that the first group of terms in  $\partial t$  and the second group of terms in  $\partial x_i$  are with derivatives of the external variables (e.g.,  $\phi, V$ ), whereas the two last groups of variables are with derivatives of the internal variables (e.g.,  $m, q$ ). Now, if we assume that  $\delta t \approx 0$

$$-q \frac{\partial \phi}{\partial x_i} - m \frac{dV}{dt} - V \frac{dm}{dt} + \frac{V^2}{2} \frac{\partial m}{\partial x_i} = 0 \quad \text{A(I.5)}$$

and by definition  $\partial/\partial x_i = \vec{\nabla}$ . One can set  $\partial m/\partial x_i = 0$ , and see the variation of mass only dependent on the variation of charge  $q(t)$  in our “relativistic” capacitor model. Furthermore, we can get the equation without variation of the internal variables if

$$dm/dt = 0 : \quad q \vec{\nabla} \phi + m dV/dt = 0$$

As the “relativistic” capacitor model is a particle moving along a world line, one can follow the same method that Prof. Woodward used to establish the Woodward effect (See Appendix A of [15]). Let us write the equation of the momentum when the particle is stimulated by external force:  $d\vec{p}/dt = -\vec{f}$

With equation A(I.5), one can write:

$$-m \frac{dV}{dt} - V \frac{dm}{dt} = q \frac{\partial \phi}{\partial x_i} \quad \text{A(I.6)}$$

which ends up in

$$-\frac{d\vec{p}}{dt} = q \vec{\nabla} \phi \quad \text{A(I.7)}$$

This equation is the particle accelerated by a Lorentz force with only the electric field. We can qualify it as the macroscopic view of the system. One can then define a force  $\vec{F} = -(V dm/dt, -q \vec{\nabla} \phi)$ . Making the same assumption as in [15], one can apply the four divergence to the normalized force

$$\begin{aligned} \frac{\vec{F}}{m} &:= -\left( \frac{V}{m} \frac{dm}{dt}, -\frac{q}{m} \vec{\nabla} \phi \right), \\ -\frac{\partial}{\partial t} \left( \frac{V}{m} \frac{dm}{dt} \right) + \frac{\partial}{\partial t} \left( \frac{q}{m} \vec{\nabla} \phi \right) + \frac{q}{m} \nabla^2 \phi &= 4\pi G \rho_0 \end{aligned} \quad \text{A(I.8)}$$

with  $\rho_0$  the first term of the stress energy tensor (or  $T_{00}$ ), which is the EM energy density. Let us make the assumption that the particle is accelerated to the speed of light  $V \approx c$ , and if the fluctuation of the total energy is equal to the fluctuation of the EM energy density ( $\partial_i u_{EM} \equiv \partial_i \rho_0$ ), thus we have also ( $\partial_i \rho_0 \equiv \partial_i mc^2$ ). The above equation is then:

$$-\frac{\partial}{\partial t} \left( \frac{1}{E} \frac{\partial \rho_0}{\partial t} \right) + c \frac{\partial}{\partial t} \left( \frac{q}{E} \vec{\nabla} \phi \right) + \frac{qc^2}{E} \nabla^2 \phi = 4\pi G \rho_0 \quad \text{A(I.9)}$$

Let us define the potential  $\psi = q\phi/E$  and rewrite the previous equation:

$$-\frac{\partial}{\partial t} \left( \frac{1}{E} \frac{\partial \rho_0}{\partial t} \right) + c \frac{\partial}{\partial t} (\vec{\nabla} \psi) + c^2 \nabla^2 \psi = 4\pi G \rho_0 \quad \text{A(I.10)}$$

The infinitesimally variation  $\delta \rho_0$  is only due to the variation in time in the LHS term, then

$$-\frac{\partial}{\partial t} \left( \frac{1}{E} \frac{\partial \rho_0}{\partial t} \right) = 4\pi G \delta \rho_0 \quad \text{A(I.11)}$$

This equation is what is described as the Woodward effect in [15].

## APPENDIX II Simplifications to Estimate the thrust with the Woodward effect

This section shows the approximations to estimate the Lorentz force and the mass variation around the EM cavity. We use the boundary conditions for the electric and magnetic fields stated in [20]. Thus, the electric field is null at both spherical ends (large and small end plates) and at the conical wall. The magnetic field is in the polar direction at the spherical ends and radial direction at the conical wall following Fig.1.

Now, the surface integral on the end plate or conical wall of the Lorentz force  $\vec{F}_{Lo} = \iint q_e \cdot \vec{v}_e \times \vec{B} dS = \vec{j}_s \times \vec{B}$  ( $q_e$  and  $\vec{v}_e$  are the charge and velocity of one electron,  $\vec{j}_s$  the surface current density) can then be estimated on the Z-axis of the frustum,

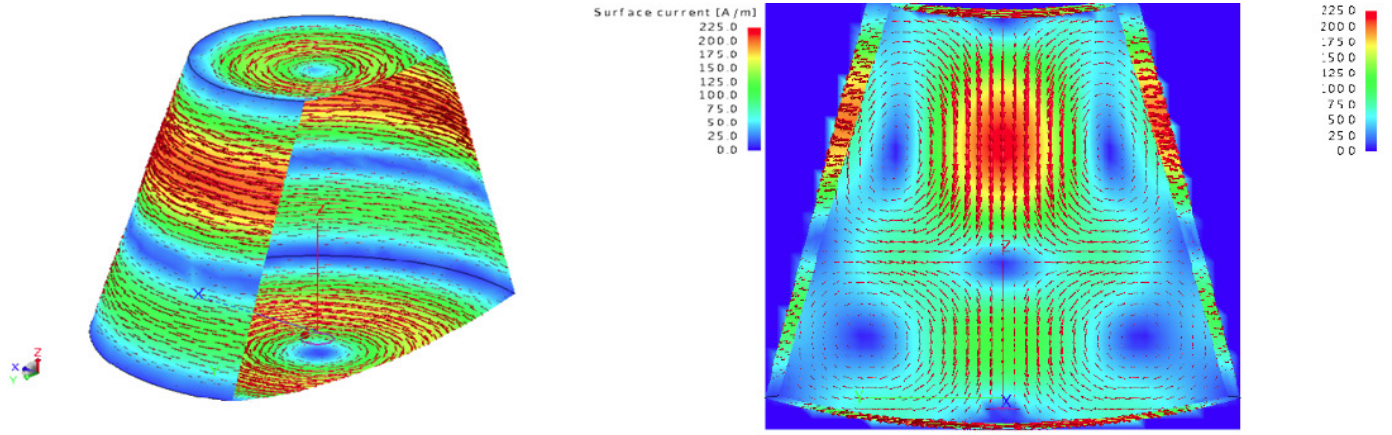


Fig. 2: Surface Current (left) and magnetic field (right) in Amp./m inside and around the EM cavity for the TE012 mode. The input power is equal to 1W.

and using the averaged profile in Fig. 2a such as :

$$\vec{F}_{Lo}(\theta, \varphi) = -J_s \cdot B \cdot r^2 \cdot \sin(\theta) \cos(\theta) d\theta \cdot d\varphi \vec{u}_z \quad \text{A(II.1)}$$

(at the spherical ends)

$$\vec{F}_{Lo}(z, \varphi) = -J_s \cdot B \cdot \tan(\theta_w)^2 \cdot \sin(\theta) z \cdot dz \cdot d\varphi \vec{u}_z \quad \text{A(II.2)}$$

(at the conical wall)

In addition, we justify in Section III that the mass variation estimated using the Woodward effect in (i.e. equation III.8) depends on the second order variation of the EM energy density within the skin layer of the EM cavity. Here, we estimate the second order variation of EM energy density using the EM energy conservation [22].

$$\partial_t^2 U_{EM} = -\partial_t(\vec{\nabla} \cdot \vec{S} + \vec{J}_s \cdot \vec{E}) \quad \text{A(II.3)}$$

Knowing that  $\vec{J}_s = \sigma \vec{E}$

with  $\sigma$  the conductivity of the copper at the surface of the walls and the Poynting vector

$$\vec{S} = \frac{\vec{E} \times \vec{B}}{\mu_0} = \frac{\vec{J}_s \times \vec{B}}{\sigma \mu_0}$$

( $\mu_0$  the permeability of the vacuum). The magnetic field  $\vec{B}$  is parametrized as an evanescent wave using the magnetic field propagating inside the cavity and resulting from the Maxwell equations

$$\nabla^2 B = -j \cdot \sigma \mu_0 \cdot \omega \cdot B, \text{ with } \omega = 2\pi \cdot f_0$$

( $f_0$  the central frequency). Note that here  $j = \sqrt{-1}$ . The evanescent wave has the wave number

$$k = (1 + j) \cdot \frac{1}{\delta}$$

With the skin depth

$$\delta = \sqrt{\frac{2}{\sigma \mu_0 \cdot \omega}}$$

With a numerical approximation of the surface of each element (i.e. spherical ends, conical wall), one can find the following expression:

$$\partial_t^2 U_{EM} \sim \frac{10 \cdot \omega}{\sigma} \cdot J_s^2 \cdot S \quad \text{A(II.4)}$$

where  $S$  is the surface of the spherical ends or conical walls. Now, we can approximate the anomalous thrust using a similar development to that in [3, 4]. Thus, by combining equation (III.4) with  $Z(t) = Z_0 \cdot e^{j \cdot \omega t}$ , we find

$$|F_{thrust}| \sim \delta m_0 \cdot \partial_t^2 Z \sim \delta m_0 \cdot FL_0 / m \quad \text{A(II.5)}$$

where  $\delta m_0$  is the mass variation resulting from the Woodward effect. Thus, using A(II.2) to A(II.5), we can approximate the amplitude of the anomalous thrust for each element:

$$F_{Thrust} \sim \frac{V}{4\pi G m^2} \cdot \frac{1}{c^2} \partial_t^2 U_{EM} \int_r 2 \cdot \pi \cdot Df(R) \cdot dR$$

$$F_{Thrust} \sim \frac{V}{4\pi G m^2} \cdot \frac{1}{c^2} \partial_t^2 U_{EM} \cdot \pi r^2$$

Finally, the total thrust (in Table 1) is the sum of the different thrust forces from each element. Each thrust force has a sign depending on the force direction (from the Lorentz force direction projected onto the Z-axis).



# REFERENCES

1. R. Shawyer, "The EM Drive – a New Satellite Propulsion Technology", in Proc. of the 2nd Conference on Disruptive Technology in Space Activities, 2010.
2. D.A. Brady, H.G. White, P. March, J.T. Lawrence, and F.J. Davies, "Anomalous Thrust Production from an RF Test Device Measured on a Low-Thrust Torsion Pendulum", AIAA Joint Propulsion Conference, doi: 10.2514/6.2014-4029, 2014.
3. H. Fearn, A. Zachar, J. F. Woodward and K. Wanser, "Theory of a Mach Effect Thruster", in Proc. of the AIAA Joint Propulsion Conference, Tech. Session: Nuclear and Future Flight Propulsion, doi: 10.2514/6.2014-3821.
4. H. Fearn and K. Wanser, "Experimental tests of the Mach effect thruster", J. of Space Exploration, 3 (3), pp. 197-205, 2014.
5. J.P. Montillet, "Theory of the EM Drive in TM mode Based on Mach-Lorentz Theory", Estes Park 2016 Advanced Propulsion Workshop, 19-22 September, 2016.
6. H. White, P. March, J. Lawrence, J. Vera, A. Sylvester, D. Brady, P. Bailey, "Measurement of Impulsive Thrust from Closed Radio Frequency Cavity in Vacuum", AIAA Journal of Propulsion and Power, 33 (4), 2017, doi: 10.2514/1.B36120.
7. M. Tajmar, and G. Fiedler, "Direct Thrust Measurements of an EM Drive and Evaluation of Possible Side-Effects", in Proc. of the 51st AIAA/SAE/ASEE Joint Propulsion Conference, AIAA 2015-4083, doi: 10.2514/6.2015-4083
8. J.F. Woodward, *Making Starships and Stargates*, Springer-Verlag, New York, 2013, doi: 10.1007/978-1-4614-5623-0
9. R. Shawyer, "Second generation EmDrive propulsion applied to SSTO launcher and interstellar probe", *Acta Astronautica*, p. 166-174, doi: 10.1016/j.actaastro.2015.07.002.
10. M. E. McCulloch, "Can the EmDrive Be Explained by Quantised Inertia?", *Progress in Physics*, 11 (1), 2015.
11. P. Grah, A. Annala, E. Kolehmainen, "On the Exhaust of Electromagnetic Drive", *AIP Advances*, 6 (6), 2016, doi: 10.1063/1.4953807
12. T. J. Desiato, "An Engineering Model of Quantum Gravity", Estes Park 2016 Advanced Propulsion Workshop, 19-22 September 2016.
13. J.F. Woodward, "Gravity, Inertia, and Quantum Vacuum Zero Point Fields", *Foundations of Physics*, 31 (5), p. 819–835, 2001, doi: 10.1023/A:1017500513005
14. D. W. Sciama, "On the Origin of Inertia", *Monthly Notices of the Royal Astronomical Society*, 113 (1), p. 34-42, 1953, doi: 10.1093/mnras/113.1.34
15. J. F. Woodward, "Life Imitating Art: Flux Capacitors, Mach Effects, and Our Future in Spacetime", *AIP Conference Proceedings. Space Technology Applications International Forum (STAIF 2004)*, Albuquerque, New Mexico, p. 1127–1137, 2004, doi: 10.1063/1.1649682.
16. P. March, A. Palfreyman, "The Woodward effect: Math Modeling and Continued Experimental Verifications at 2 to 4 MHz", *AIP Conference Proceedings. Space Technology Applications International Forum (STAIF 2006)*, 2006.
17. J. Bird, *Electrical and Electronic Principles and Technology*, 4th Ed., Elsevier, USA. ISBN: 978-0-08-089056-2.
18. P. March, "Experiments with RF Cavity Thrusters, Estes Park 2016 Advanced Propulsion Workshop, 19-22 September, 2016.
19. J.P. Montillet, "Sobolev Spaces, Schwartz Spaces, and a definition of the Electromagnetic and Gravitational coupling", *J. of Modern Physics*, 2017, doi: 10.4236/jmp.2017.810100.
20. G. Egan, "Resonant Modes of a Conical Cavity". <http://greggan.customer.netspace.net.au/SCIENCE/Cavity/Cavity.html>
21. D. Pozar, *Microwave Engineering*, 2nd edition, Wiley, New York, NY, 1998.
22. R. Petit, *Ondes Electromagnetiques en radioelectricite et en optique*, 2nd Edition, Masson, 1993.
23. David R. Lide, *CRC Handbook of Chemistry and Physics*, CRC Press Inc, 2009. ISBN 978-1-420-09084-0.
24. J. Rodal, "Proof that EM Drive Thrust/Power and Q scale as  $\sqrt{L}$ ", Estes Park 2016 Advanced Propulsion Workshop, 19-22 September, 2016.
25. R. Paschotta, *Encyclopedia of Laser Physics and Technology*, John Wiley & Sons, 2008. ISBN: 3527408282.
26. E. B. Porcelli, V. S. Filho, "On the Anomalous Weight Losses of High Voltage Symmetrical Capacitors", 2015. doi: 10.4006/0836-1398-29.1.002
27. M. Tajmar, "Mach-Effect thruster model", *Acta Astronautica*, 141, December, 2017. doi: 10.1016/j.actaastro.2017.09.021
28. B. Hornberger, "Electric and Magnetic Forces in Lagrangian and Hamiltonian Formalism", Lecture notes, available at <http://insti.physics.sunysb.edu/itp/lectures/01-Fall/PHY505/09c/notes09c.pdf>

Received 18 December, 2017 Accepted 22 February, 2018

# AN EPITAXIAL DEVICE FOR DYNAMIC INTERACTION WITH THE VACUUM STATE

DAVID C. HYLAND, Professor Emeritus, Texas A&M University, 4904 Augusta Circle, College Station, Texas 77845 USA  
email: dhiland@tamu.edu

This paper re-examines the dynamic Casimir effect as a possible mechanism for propulsion. Previous investigations assumed mechanical motion of a mirror to generate thrust. In this case, because of the finite strength of materials and the high frequencies necessary, the amplitudes of motion must be restricted to the nanometer range. To permit larger amplitudes, an epitaxial stack of transparent semiconductor laminae is proposed. Voltage is rapidly switched to successive lamina, creating continuous, large amplitude motion of a reflective surface without mechanical contrivances. The paper provides relativistic results for large amplitude motion. With centimeter-level magnitudes, propulsive forces are raised to significant levels.

**Keywords:** Dynamic Casimir, Vacuum radiation pressure, Quantum propulsion, transparent semiconductors, Transflecting liquid crystals

## INTRODUCTION

More than 60 years ago, H. B. G. Casimir [1], and Casimir and D. Polder [2] explained the retarded van der Waals force in terms of the zero-point energy of a quantized field. Both the static and dynamic Casimir effects are discussed in several reviews [3-7]. This work is concerned with the dynamic Casimir effect, which involves the interaction between moving mirrors and the ground state ("vacuum state") of the electromagnetic field. In particular, following Maclay and Forward, [8], the present analysis is motivated by the possibility of a propulsive mechanism.

When estimating the magnitude of the force that could be generated, Maclay and Forward assumed that the amplitude of high frequency motion of an actual mirror need be in the nanometer range due to the finite strength of materials. This restriction limits the possible propulsive force to very small values. However, this author observes that motion of a single reflective surface is not essential: that the Casimir effect is due to the motion of the boundary conditions constraining the free field in its ground state. The advent of amorphous oxide, transparent semiconductors used for thin film applications [9-14] suggests the possibility of achieving large motions of reflective surfaces without mechanically moving parts. The proposed epitaxial assembly of semiconductor laminae, is illustrated in Fig. 1. Without the application of voltage, each lamina is a partially transparent dielectric; but when supplied by voltage it becomes a reflecting conductor serving as a mirror. Voltage inputs can

be switched among the laminae at high speed, effectively moving the mirror at high velocities and accelerations without the use of moving parts. Thus motions of the reflective surface that have both high frequencies and large amplitudes can be produced. In a treatment of the pressure on moving mirrors due to the Casimir effect, Neto and his colleagues [7], took a perturbative approach consistent with the assumption that the mirror motion be constrained to very small amplitudes. The objectives of this paper are to extend the analysis to large motions and the epitaxial approach described above; to obtain explicit expressions for the forces produced by a particular trajectory of motion; and to estimate the numerical values of these forces.

It is assumed that within certain wavelength bands, the reflectivity of each lamina can be set within a continuous range from completely reflective to completely transparent. The laminae are also characterized by a finite response time. These features can be combined so that when the laminae are sufficiently closely spaced, and their energizing processes are properly phased, multi-laminae propagating wave of reflectivity can be created that sustains the properties of a continuously moving mirror (see Appendix A). In the following, the multi-laminae phasing wave is treated as a single, perfectly reflecting surface.

## FUNDAMENTAL DEVELOPMENT

Define a coordinate system,  $(x, y, z)$ , with unit orthogonal basis vectors  $(\hat{x}, \hat{y}, \hat{z})$ . Consider the case in which surface  $\wp(\tau)$  is a section of a plane having area  $A$  and parallel to the  $x$ - $y$  axis, as illustrated in Fig. 2. Its motion is along the  $z$  axis with  $z$ -coordinate  $q(t)$ , where  $q(t) \in [0, \bar{Z}]$ . Before the reflectivity is "turned on" at  $t = 0$ , the field is in the vacuum state. Also, the surface starts a cycle of motion coinciding with the  $x$ - $y$  plane, so that  $q(t = 0) = 0$ . It is assumed that  $\bar{Z} \ll \sqrt{\lambda}$ , so that one may treat the conductive surface and the field it produces without accounting for edge effects. In the following the  $x$ -axis is defined to be perpendicular to  $z$  and in the plane formed by  $z$  and the direction of propagation of the plane wave associated with a particular vacuum state mode.

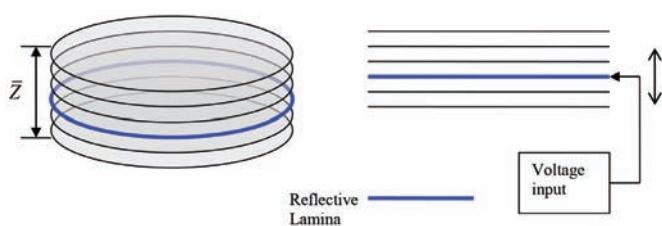


Fig. 1: Epitaxial stack of semiconductor lamina.

For simplicity in this initial development, the surface is presumed to be either perfectly reflecting or perfectly transparent, depending only upon the wave number. This is modelled as a scalar function,  $R(k) = 1$  (reflective),  $R(k) = 0$  (transparent).

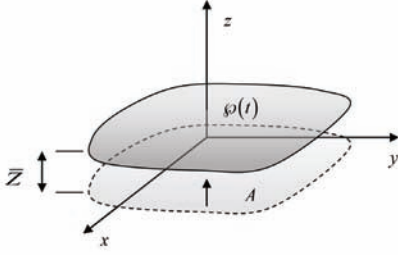


Fig. 2: Geometry of the motion of the conductive surface.

As a minimum, a model of  $R(k)$  should capture the fact that any conductive material is transparent to radiation that has frequencies above the plasma frequency,  $\omega_p$ . Following the Drude-Sommerfeld model [15-17], the upper limit of the wave number might be some fraction of:

$$\bar{k} = \omega_p / c$$

$$\omega_p = \sqrt{\frac{4\pi n_e e^2}{m^*}} \quad (= 8980 \sqrt{n_e} \text{ Hz}) \quad (1 \text{ a,b})$$

where  $m^*$  is the effective mass of the charge carriers,  $e$  is the elementary charge, and  $n_e$  is the volumetric number density of the charge carriers.  $\omega_p$  may be typically  $\approx 10^{14}$  Hz, and the value for metals can be a hundred or even a thousand-fold larger. The simplest model has the form:

$$R(k) = \begin{cases} 1, & k < \bar{k} \\ 0, & \text{otherwise} \end{cases} \quad (2)$$

(2) is essentially a formal regularization since the details of the dielectric function of the materials, the effects of absorption, and the semiconductor design and parameters are ignored. The reflective properties are conceived to be homogeneous and isotropic.

To begin the analysis, the notational conventions of [18] are followed. Also, the continuous Fock space approach to quantizing the electromagnetic field [19] is adopted. The electric field operator in empty space and in the absence of boundaries is given by:

$$\hat{\mathbf{E}}(\mathbf{r}, t) = \frac{i}{(2\pi)^2} \sum_{s=1}^2 \int \sqrt{\frac{\hbar c k}{2\epsilon_0}} [\hat{a}(\mathbf{k}, s) \boldsymbol{\epsilon}(\mathbf{k}, s) e^{i(\mathbf{k} \cdot \mathbf{r} - \omega t)} - h.c.] d^3 k \quad (3)$$

where  $\epsilon_0$  is the vacuum dielectric constant. Quantities in bold type are 3-vectors, and a carrot over the symbol indicates a quantum operator. “h.c.” stands for “Hermitian conjugate”.  $\mathbf{k}$  is the continuous wave number vector and  $\omega$  is the angular frequency, where  $\omega(\mathbf{k}) = ck$ ,  $k = \|\mathbf{k}\|$ .  $\boldsymbol{\epsilon}(\mathbf{k}, s)$ ,  $s=1, 2$  are the polarization vectors obeying the orthonormality requirements:

$$\begin{aligned} \mathbf{k} \cdot \boldsymbol{\epsilon}(\mathbf{k}, s) &= 0, \quad (s=1, 2) \\ \boldsymbol{\epsilon}^*(\mathbf{k}, s) \cdot \boldsymbol{\epsilon}(\mathbf{k}, s') &= \delta_{ss'} \quad (s, s'=1, 2) \\ \boldsymbol{\epsilon}(\mathbf{k}, 1) \times \boldsymbol{\epsilon}(\mathbf{k}, 2) &= \mathbf{k}/k \triangleq \boldsymbol{\kappa} \end{aligned} \quad (4 \text{ a,b,c})$$

The terms  $\hat{a}(\mathbf{k}, s)$ , and  $\hat{a}^\dagger(\mathbf{k}, s)$  are the annihilation and creation operators for field modes of wave vector  $\mathbf{k}$ , and polarization  $s$ . These obey the commutation relations:

$$\begin{aligned} [\hat{a}(\mathbf{k}, s), \hat{a}^\dagger(\mathbf{k}', s')] &= \delta^3(\mathbf{k} - \mathbf{k}') \delta_{ss'} \\ [\hat{a}(\mathbf{k}, s), \hat{a}(\mathbf{k}', s')] &= 0 \\ [\hat{a}^\dagger(\mathbf{k}, s), \hat{a}^\dagger(\mathbf{k}', s')] &= 0 \end{aligned} \quad (5 \text{ a,b,c})$$

Equation (3) describes the free electromagnetic field, which is taken to be the condition of the field at the initial instant,  $t = 0$ . Note that the quantized fields are coupled by the same Maxwell Equations as the classical fields from which they came, i.e.:

$$\begin{aligned} \nabla \times \hat{\mathbf{E}}(\mathbf{r}, t) &= -\frac{\partial}{\partial t} \hat{\mathbf{B}}(\mathbf{r}, t), \quad \nabla \times \hat{\mathbf{B}}(\mathbf{r}, t) = \frac{1}{c^2} \frac{\partial}{\partial t} \hat{\mathbf{E}}(\mathbf{r}, t) \\ \nabla \cdot \hat{\mathbf{E}}(\mathbf{r}, t) &= 0, \quad \nabla \cdot \hat{\mathbf{B}}(\mathbf{r}, t) = 0 \end{aligned} \quad (6 \text{ a,b,c,d})$$

Since the time dependence of all terms in (1) is  $e^{-i\omega t}$ , one can substitute (1) into (4.a) and integrate with respect to time to obtain:

$$\hat{\mathbf{B}}(\mathbf{r}, t) = \frac{1}{(2\pi)^2} \sum_{s=1}^2 \int \sqrt{\frac{\hbar}{2ck\epsilon_0}} [\hat{a}(\mathbf{k}, s) (\nabla \times \boldsymbol{\epsilon}(\mathbf{k}, s) e^{i(\mathbf{k} \cdot \mathbf{r} - \omega t)}) + h.c.] d^3 k \quad (7)$$

Because the only spatial dependence in the free field is  $e^{i\mathbf{k} \cdot \mathbf{r}}$ , the  $\nabla \times \boldsymbol{\epsilon}(\mathbf{k}, s) e^{i(\mathbf{k} \cdot \mathbf{r} - \omega t)}$  term can be replaced by  $i\mathbf{k} \times \boldsymbol{\epsilon}(\mathbf{k}, s) e^{i(\mathbf{k} \cdot \mathbf{r} - \omega t)}$ . Thus, in the free field, the magnetic field operator is:

$$\hat{\mathbf{B}}(\mathbf{r}, t) = \frac{i}{(2\pi)^2} \sum_{s=1}^2 \int \sqrt{\frac{\hbar}{2ck\epsilon_0}} [\hat{a}(\mathbf{k}, s) (\mathbf{k} \times \boldsymbol{\epsilon}(\mathbf{k}, s)) e^{i(\mathbf{k} \cdot \mathbf{r} - \omega t)} - h.c.] d^3 k \quad (8)$$

The Heisenberg picture, in which the initial state is fixed and it is the operators that evolve in time, is chosen for the present analysis. It is assumed that the field is initially (at time  $t = 0$ ) in the free-field state; thus (3) and (8) give the initial values of the electric and magnetic field operators. The operators then evolve according to the Heisenberg equations of motion. However, these are equivalent to the Maxwell operator equations, (6), (see [18], Art. 10.4.5).

As (3) and (8) indicate, to determine the electric field operator beyond  $t = 0$ , we need only consider the time evolution of the operator  $\hat{a}(\mathbf{k}, s) \boldsymbol{\epsilon}(\mathbf{k}, s) e^{i(\mathbf{k} \cdot \mathbf{r} - \omega t)}$ . Hence beyond  $t = 0$ , (3) and (8) become:

$$\begin{aligned} \hat{\mathbf{E}}(\mathbf{r}, t) &= \frac{i}{(2\pi)^2} \sum_{s=1}^2 \int \sqrt{\frac{\hbar \hat{\omega}}{2\epsilon_0}} [\boldsymbol{\Phi}_{\mathbf{k},s}(\mathbf{r}, t) \hat{a}(\mathbf{k}, s) - h.c.] d^3 k \\ \hat{\mathbf{B}}(\mathbf{r}, t) &= \frac{1}{(2\pi)^2} \sum_{s=1}^2 \int \sqrt{\frac{\hbar}{2\hat{\omega}\epsilon_0}} [(\nabla \times \boldsymbol{\Phi}_{\mathbf{k},s}(\mathbf{r}, t) \hat{a}(\mathbf{k}, s) + h.c.)] d^3 k \end{aligned} \quad (9)$$

$\boldsymbol{\Phi}_{\mathbf{k},s}(\mathbf{r}, t)$  is a vector-valued function satisfying the wave equation derived from (6), all boundary conditions for  $t = 0$ , and the initial condition  $\boldsymbol{\Phi}_{\mathbf{k},s}(\mathbf{r}, t=0) = \boldsymbol{\epsilon}(\mathbf{k}, s) e^{i(\mathbf{k} \cdot \mathbf{r})}$ .  $\hat{\omega}(\mathbf{r}, t)$  represents the evolution of the initial wave vector to its value at the space-time point  $(\mathbf{r}, t)$ .

The Lorentz force operator per unit volume on the field,  $\hat{\mathbf{f}}$ , is the primary object of attention:

$$\begin{aligned} \hat{\mathbf{f}} &= \epsilon_0 [(\nabla \cdot \hat{\mathbf{E}}) \hat{\mathbf{E}} + (\hat{\mathbf{E}} \cdot \nabla) \hat{\mathbf{E}}] + \frac{1}{\mu_0} [(\nabla \cdot \hat{\mathbf{B}}) \hat{\mathbf{B}} + (\hat{\mathbf{B}} \cdot \nabla) \hat{\mathbf{B}}] \\ &\quad - \frac{1}{2} \nabla \left( \epsilon_0 \hat{E}^2 + \frac{1}{\mu_0} \hat{B}^2 \right) - \epsilon_0 \mu_0 \frac{\partial \hat{\mathbf{S}}}{\partial t} \end{aligned} \quad (10)$$



where  $\hat{\mathbf{S}}$  is the symmetrized Poynting vector operator:

$$\hat{\mathbf{S}} = \frac{1}{2\mu_0} [\hat{\mathbf{E}}(\mathbf{r}, t) \times \hat{\mathbf{B}}(\mathbf{r}, t) - \hat{\mathbf{B}}(\mathbf{r}, t) \times \hat{\mathbf{E}}(\mathbf{r}, t)] \quad (11)$$

Define volume  $V_{R,\delta}$  enclosed by surface  $S_{R,\delta}$  as in Fig. 3. Integration of (11) over this volume and use of the divergence theorem, produces:

$$\hat{\mathbf{F}}_F(t) = \int_{V_{R,\delta}} \hat{\mathbf{f}} d\tau^3 = \frac{\varepsilon_0}{c} \frac{d}{dt} \int_0^t d\tau \int_{V_{R,\delta}} \hat{\mathbf{g}} \cdot \mathbf{n}_{V_{R,\delta}} dS_{R,\delta} - \varepsilon_0 \mu_0 \frac{d}{dt} \int_{V_{R,\delta}} \hat{\mathbf{S}} d\tau^3 \quad (12)$$

where  $\hat{\mathbf{g}}$  is the Maxwell tensor operator:

$$(\hat{\mathbf{g}})_{ij} = \varepsilon_0 \left[ \left( \hat{E}_i \hat{E}_j - \frac{1}{2} \delta_{ij} \hat{E}^2 \right) + c^2 \left( \hat{B}_i \hat{B}_j - \frac{1}{2} \delta_{ij} \hat{B}^2 \right) \right] \quad (13)$$

and where  $\int_0^t d\tau \int_{V_{R,\delta}} \hat{\mathbf{g}} \cdot \mathbf{n}_{V_{R,\delta}} dS_{R,\delta}$  is the total momentum produced by the stress operator up to time  $t$ .

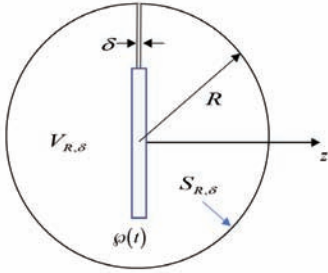


Fig. 3: Geometry of the volume of integration.

Letting  $R \rightarrow \infty$  and  $\delta \rightarrow 0$ , one can appreciate that the volume integral extends over the entire space, excluding only the energized lamina (parallel to the x-y plane), and the surface integral is to be taken over the reflective lamina surface, which is treated as of infinitesimal thickness. Therefore:

$$\hat{\mathbf{F}}_F(t) = \frac{\varepsilon_0}{c} \frac{d}{dt} \int_0^t d\tau \int_{\varphi(t)} \hat{\mathbf{g}} \cdot \mathbf{n}_{\varphi(t)} dS_{\varphi} - \varepsilon_0 \mu_0 \frac{d}{dt} \int_{-\infty}^{\infty} \hat{\mathbf{S}} d^3r \quad (14)$$

where  $\mathbf{n}_{\varphi(t)}$  is the unit normal vector to each surface of the reflective lamina, pointing inward.

A considerable simplification is achieved by recognizing the consequences of the planar surface maintained parallel to the x-y plane, motion solely in the z direction and the homogeneity and isotropy of the reflection coefficient. Further, the free field comprises field modes of all possible wave vectors and polarization states. These characteristics ensure that the force acting on the field must have only a z-component. Thus:

$$\hat{F}_{Fz} = \hat{\mathbf{z}} \cdot \hat{\mathbf{F}}_F = \frac{\varepsilon_0}{c} \frac{d}{dt} \int_0^t d\tau \int_{\varphi(t)} \hat{\mathbf{z}} \cdot \hat{\mathbf{g}} \cdot \mathbf{n}_{\varphi(t)} dS_{\varphi} - \varepsilon_0 \mu_0 \frac{d}{dt} \int \hat{\mathbf{z}} \cdot \hat{\mathbf{S}} d^3r \quad (15)$$

Finally, the average force on the reflective surface, denoted by  $\langle F_z \rangle$ , is:

$$\begin{aligned} \langle F_z \rangle = & -\varepsilon_0 \frac{\varepsilon_0}{c} \frac{d}{dt} \int_0^t d\tau \int_{\varphi(t)} \langle \text{vac} | \hat{\mathbf{z}} \cdot \hat{\mathbf{g}} \cdot \mathbf{n}_{\varphi(t)} | \text{vac} \rangle dS_{\varphi} \\ & + \varepsilon_0 \mu_0 \frac{d}{dt} \int \langle \text{vac} | \hat{\mathbf{z}} \cdot \hat{\mathbf{S}} | \text{vac} \rangle d^3r \end{aligned} \quad (16)$$

## EVALUATION OF THE AVERAGE FORCE IN TERMS OF $\Phi_{\mathbf{k},s}(\mathbf{r},t)$

First, consider the second term in (16). Substituting (11), and (9):

$$\begin{aligned} \varepsilon_0 \mu_0 \frac{d}{dt} \int \langle \text{vac} | \hat{\mathbf{z}} \cdot \hat{\mathbf{S}} | \text{vac} \rangle d^3r = & -\hat{\mathbf{z}} \cdot \frac{d}{dt} \frac{ih}{4(2\pi)^3} \int \sum_{s=1}^2 \sum_{s'=1}^2 \int d^3k \int d^3k' \sqrt{\frac{\omega}{\omega'}} \langle \text{vac} | \\ & \left[ \begin{aligned} & \Phi_{\mathbf{k},s}(\mathbf{r},t) \times (\nabla \times \Phi_{\mathbf{k}',s'}^*(\mathbf{r},t)) \hat{a}(\mathbf{k},s) \hat{a}^\dagger(\mathbf{k}',s') \\ & + \Phi_{\mathbf{k},s}(\mathbf{r},t) \times (\nabla \times \Phi_{\mathbf{k}',s'}^*(\mathbf{r},t)) \hat{a}(\mathbf{k},s) \hat{a}^\dagger(\mathbf{k}',s') \\ & - \Phi_{\mathbf{k},s}^*(\mathbf{r},t) \times \nabla \times \Phi_{\mathbf{k}',s'}(\mathbf{r},t) \hat{a}^\dagger(\mathbf{k},s) \hat{a}(\mathbf{k}',s') \\ & - \Phi_{\mathbf{k},s}^*(\mathbf{r},t) \times \nabla \times \Phi_{\mathbf{k}',s'}(\mathbf{r},t) \hat{a}^\dagger(\mathbf{k},s) \hat{a}^\dagger(\mathbf{k}',s') \\ & - \Phi_{\mathbf{k},s}(\mathbf{r},t) \times (\nabla \times \Phi_{\mathbf{k}',s'}(\mathbf{r},t)) \hat{a}^\dagger(\mathbf{k},s) \hat{a}(\mathbf{k}',s') \\ & + \Phi_{\mathbf{k},s}^*(\mathbf{r},t) \times (\nabla \times \Phi_{\mathbf{k}',s'}(\mathbf{r},t)) \hat{a}^\dagger(\mathbf{k},s) \hat{a}^\dagger(\mathbf{k}',s') \\ & - \Phi_{\mathbf{k},s}(\mathbf{r},t) \times (\nabla \times \Phi_{\mathbf{k}',s'}^*(\mathbf{r},t)) \hat{a}^\dagger(\mathbf{k}',s') \hat{a}(\mathbf{k},s) \\ & + \Phi_{\mathbf{k},s}^*(\mathbf{r},t) \times (\nabla \times \Phi_{\mathbf{k}',s'}^*(\mathbf{r},t)) \hat{a}^\dagger(\mathbf{k}',s') \hat{a}^\dagger(\mathbf{k},s) \end{aligned} \right] | \text{vac} \rangle d^3r \end{aligned} \quad (17)$$

Since  $\hat{a}(\mathbf{k})|\text{vac}\rangle = \langle \text{vac} | \hat{a}^\dagger(\mathbf{k}) = 0$ , the only non-vanishing portion is shown in Equation (18) at the foot of the page.

Using the commutation relations, one obtains the result in Equation (19) at the foot of the page.

Or, more concisely:

$$\begin{aligned} \varepsilon_0 \mu_0 \frac{d}{dt} \int \langle \text{vac} | \hat{\mathbf{z}} \cdot \hat{\mathbf{S}} | \text{vac} \rangle d^3r & \\ = \hat{\mathbf{z}} \cdot \frac{d}{dt} \frac{h}{2(2\pi)^3} \sum_{s=1}^2 \int d^3r \int d^3k \text{Im} \left[ \Phi_{\mathbf{k},s}(\mathbf{r},t) \times (\nabla \times \Phi_{\mathbf{k},s}^*(\mathbf{r},t)) \right] & \end{aligned} \quad (20)$$

Next, the stress tensor term is considered. In the first term in (16),  $\mathbf{n}_{\varphi(t)}$  is  $-\hat{\mathbf{z}}$  for  $z = q(t) + \zeta$ , and  $+\hat{\mathbf{z}}$  for  $z = q(t) - \zeta$ .

Hence this term can be written:

$$\begin{aligned} & -\frac{\varepsilon_0}{c} \frac{d}{dt} \int_0^t d\tau \int_{\varphi(t)} \langle \text{vac} | \hat{\mathbf{z}} \cdot \hat{\mathbf{g}} \cdot \mathbf{n}_{\varphi(t)} | \text{vac} \rangle dS_{\varphi} \\ & = \frac{\varepsilon_0}{c} \frac{d}{dt} \int_0^t d\tau \left[ A \langle \text{vac} | \hat{\mathbf{g}}_{zz} | \text{vac} \rangle_{z=q+\zeta} - \varepsilon_0 A \langle \text{vac} | \hat{\mathbf{g}}_{zz} | \text{vac} \rangle_{z=q-\zeta} \right] \\ & = \frac{1}{2} A \frac{\varepsilon_0}{c} \frac{d}{dt} \int_0^t d\tau \sum_{s=1,-1} S \langle \text{vac} | -(\hat{E}_x^2 + \hat{E}_y^2 - \hat{E}_z^2) - c^2 (\hat{B}_x^2 + \hat{B}_y^2 - \hat{B}_z^2) | \text{vac} \rangle_{z=q+S\zeta} \end{aligned} \quad (21)$$

where in the last line, (13) has been used to evaluate  $(\hat{\mathbf{g}})_{zz}$  and the thickness,  $\zeta$ , has been assumed several wavelengths beyond the skin layer. Hence  $(\hat{E}_x)_{z=q+S\zeta}$  and  $(\hat{E}_y)_{z=q+S\zeta}$  are not zero. Each portion of the integrand is evaluated separately as follows:

$$\begin{aligned} \langle \text{vac} | \hat{E}_z^2 | \text{vac} \rangle &= \frac{hc}{2(2\pi)^4 \varepsilon_0} \sum_{s=1}^2 \int \hat{k} |\hat{\mathbf{z}} \cdot \Phi_{\mathbf{k},s}(\mathbf{r},t)|^2 d^3k \\ \langle \text{vac} | \hat{E}_x^2 + \hat{E}_y^2 | \text{vac} \rangle &= \frac{hc}{2(2\pi)^4 \varepsilon_0} \sum_{s=1}^2 \int \hat{k} |\Phi_{\mathbf{k},s}(\mathbf{r},t)|^2 d^3k - \langle \text{vac} | \hat{E}_z^2 | \text{vac} \rangle \\ c^2 \langle \text{vac} | \hat{B}_z^2 | \text{vac} \rangle &= -\frac{hc}{2(2\pi)^4 \varepsilon_0} \sum_{s=1}^2 \int \frac{1}{\hat{k}} |\hat{\mathbf{z}} \cdot (\nabla \times \Phi_{\mathbf{k},s}(\mathbf{r},t))|^2 d^3k \\ c^2 \langle \text{vac} | \hat{B}_x^2 + \hat{B}_y^2 | \text{vac} \rangle &= -\frac{hc}{2(2\pi)^4 \varepsilon_0} \sum_{s=1}^2 \int \frac{1}{\hat{k}} |\nabla \times \Phi_{\mathbf{k},s}(\mathbf{r},t)|^2 d^3k - c^2 \langle \text{vac} | \hat{B}_z^2 | \text{vac} \rangle \end{aligned} \quad (22 \text{ a,b,c,d})$$

$$\begin{aligned} \varepsilon_0 \mu_0 \frac{d}{dt} \int \langle \text{vac} | \hat{\mathbf{z}} \cdot \hat{\mathbf{S}} | \text{vac} \rangle d^3r & \\ = \hat{\mathbf{z}} \cdot \frac{d}{dt} \frac{ih}{4(2\pi)^3} \int \sum_{s=1}^2 \sum_{s'=1}^2 \int d^3k \int d^3k' \sqrt{\frac{\omega}{\omega'}} \left[ \Phi_{\mathbf{k},s}(\mathbf{r},t) \times (\nabla \times \Phi_{\mathbf{k}',s'}^*(\mathbf{r},t)) - \Phi_{\mathbf{k}',s'}^*(\mathbf{r},t) \times (\nabla \times \Phi_{\mathbf{k},s}(\mathbf{r},t)) \right] \langle \text{vac} | \hat{a}(\mathbf{k},s) \hat{a}^\dagger(\mathbf{k}',s') | \text{vac} \rangle d^3r & \end{aligned} \quad (18)$$

$$\varepsilon_0 \mu_0 \frac{d}{dt} \int \langle \text{vac} | \hat{\mathbf{z}} \cdot \hat{\mathbf{S}} | \text{vac} \rangle d^3r = -\hat{\mathbf{z}} \cdot \frac{d}{dt} \frac{ih}{4(2\pi)^3} \sum_{s=1}^2 \int d^3r \int d^3k \left[ \Phi_{\mathbf{k},s}(\mathbf{r},t) \times (\nabla \times \Phi_{\mathbf{k},s}^*(\mathbf{r},t)) - \Phi_{\mathbf{k},s}^*(\mathbf{r},t) \times (\nabla \times \Phi_{\mathbf{k},s}(\mathbf{r},t)) \right] \quad (19)$$

where  $\hat{k} = \hat{\omega}(\mathbf{r}, t)/c$  represents the evolution of the initial wave vector to its value at the space-time point  $(\mathbf{r}, t)$ .

Collecting results, the following expression is constructed:

$$\begin{aligned} \langle F_z \rangle = & \hat{\mathbf{z}} \cdot \frac{d}{dt} \frac{h}{2(2\pi)^3} \sum_{s=1, -1} \int d^3 r \int d^3 k R(k) \text{Im} [\Phi_{\mathbf{k}, s}(\mathbf{r}, t) \times (\nabla \times \Phi_{\mathbf{k}, s}^*(\mathbf{r}, t))] \\ & - \frac{1}{2} A \frac{h}{2(2\pi)^3} \frac{d}{dt} \int_0^{\pi/2} d\tau \sum_{s=1, -1} S \\ & \times \sum_{s=1}^2 \left[ \int \hat{k} \left\{ |\hat{\mathbf{x}} \cdot \Phi_{\mathbf{k}, s}(\mathbf{r}, t)|^2 + |\hat{\mathbf{y}} \cdot \Phi_{\mathbf{k}, s}(\mathbf{r}, t)|^2 - |\hat{\mathbf{z}} \cdot \Phi_{\mathbf{k}, s}(\mathbf{r}, t)|^2 \right\} R(k) d^3 k \right. \\ & \left. + \int \frac{1}{k} \left\{ |\hat{\mathbf{x}} \cdot (\nabla \times \Phi_{\mathbf{k}, s}(\mathbf{r}, t))|^2 + |\hat{\mathbf{y}} \cdot (\nabla \times \Phi_{\mathbf{k}, s}(\mathbf{r}, t))|^2 - |\hat{\mathbf{z}} \cdot (\nabla \times \Phi_{\mathbf{k}, s}(\mathbf{r}, t))|^2 \right\} R(k) d^3 k \right] \end{aligned} \quad (23)$$

## DECOUPLING DIRECTIVITY AND PROPAGATION – THE 1-D CASE

Recall that  $\Phi_{\mathbf{k}, s}(\mathbf{r}, t)$  represents the evolution of the electric field operator from the initial plane wave configuration in the vacuum state having wave vector  $\mathbf{k}$ . For each half space,  $z > q + \zeta$  and  $z < q - \zeta$  there is an incident wave with wave vector  $\mathbf{k}$  and a reflected wave, also planar. Since the objective is to determine such forces as are produced by a reflective surface motion that is much larger than the wavelengths involved, this paper assumes that (1) the total amplitude of motion is much larger than a wavelength, (2) during the time required for the passage of one wavelength, the relative change in the surface velocity is very small. That assumption (2) is compatible with (1) is discussed below in connection with a particular class of motions.

With the above assumptions, consider the angular distribution of the integrands in the above expression for  $\langle F_z \rangle$  with a view toward simplifying the calculation.

To accomplish this, define spherical coordinates for the  $\mathbf{k}$  space. In each half of position space, the polar axis is taken parallel to the  $z$ -axis, pointing toward the reflective surface for the incident wave and the opposite for the reflected wave. Denote the azimuth angle by  $\phi$  and the co-latitude angle by  $\theta$ . First consider the  $\mathbf{k}$  space integral in the first term of  $\langle F_z \rangle$ :

$$\begin{aligned} & \hat{\mathbf{z}} \cdot \int d^3 k R(k) \text{Im} [\Phi_{\mathbf{k}, s}(\mathbf{r}, t) \times (\nabla \times \Phi_{\mathbf{k}, s}^*(\mathbf{r}, t))] \\ & = \int_0^{2\pi} d\phi \int_0^{\pi/2} \sin \theta d\theta \int_0^{\bar{k}} dk R(k) k^2 \text{Im} [\hat{\mathbf{z}} \cdot (\Phi_{\mathbf{k}, s}(\mathbf{r}, t) \times (\nabla \times \Phi_{\mathbf{k}, s}^*(\mathbf{r}, t)))] \end{aligned} \quad (24)$$

Because of assumption (1), cross-products of the incident and reflected waves contribute very little to the spatial integral, hence the quantity  $\Phi_{\mathbf{k}, s}(\mathbf{r}, t) \times (\nabla \times \Phi_{\mathbf{k}, s}^*(\mathbf{r}, t))$  is parallel to the wave vector of either incident or reflected wave, independently of polarization. At least in the non-relativistic approximation, the wave vectors of both incident and reflected waves are inclined by angle  $\theta$  to the  $z$ -axis. Hence:

$$\begin{aligned} & \hat{\mathbf{z}} \cdot \int d^3 k R(k) \text{Im} [\Phi_{\mathbf{k}, s}(\mathbf{r}, t) \times (\nabla \times \Phi_{\mathbf{k}, s}^*(\mathbf{r}, t))] \\ & \approx 2\pi \int_0^{\pi/2} \sin \theta \cos \theta d\theta \int_0^{\bar{k}} dk R(k) k^2 \text{Im} [\hat{\mathbf{z}} \cdot (\Phi_{\mathbf{k}, s}(\mathbf{r}, t) \times (\nabla \times \Phi_{\mathbf{k}, s}^*(\mathbf{r}, t)))]_{\mathbf{k}=\pm k\hat{\mathbf{z}}} \\ & = \pi \int_0^{\bar{k}} dk R(k) k^2 \text{Im} [\hat{\mathbf{z}} \cdot (\Phi_{\mathbf{k}, s}(\mathbf{r}, t) \times (\nabla \times \Phi_{\mathbf{k}, s}^*(\mathbf{r}, t)))]_{\mathbf{k}=\pm k\hat{\mathbf{z}}} \end{aligned} \quad (25)$$

Similarly, in the relativistic case, the integral is distinctly weighted near  $\theta = 0$ .

Regarding the remaining integrals, if one averages over the uniformly distributed polarization vectors, the quantity

$$\sum_{s=1}^2 \int k |\hat{\mathbf{z}} \cdot \Phi_{\mathbf{k}, s}(\mathbf{r}, t)|^2_{z=q+S_\zeta} R(k) d^3 k$$

has the angular dependence  $\frac{1}{2} \sin^2 \theta$ , thus:

$$\begin{aligned} & \sum_{s=1}^2 \int k |\hat{\mathbf{z}} \cdot \Phi_{\mathbf{k}, s}(\mathbf{r}, t)|^2_{z=q+S_\zeta} R(k) d^3 k \\ & = \int_0^{2\pi} d\phi \int_0^{\pi/2} \sin^3 \theta d\theta \int_0^{\bar{k}} dk R(k) k^3 \max_{z=q+S_\zeta} |\hat{\mathbf{z}} \cdot \Phi_{\mathbf{k}, s}(\mathbf{r}, t)|^2 \end{aligned} \quad (26)$$

In this case, the integrand is weighted toward the wave vectors with large inclinations to the  $z$ -axis. But by symmetry, these contributions to the force are negligible. Similarly, the integrals involving  $|\hat{\mathbf{z}} \cdot (\nabla \times \Phi_{\mathbf{k}, s}(\mathbf{r}, t))|^2$  and  $|\hat{\mathbf{z}} \cdot \Phi_{\mathbf{k}, s}(\mathbf{r}, t)|^2$  can be neglected. Finally, treating the remaining terms in the same fashion as the first term:

$$\begin{aligned} & \int \frac{1}{k} \left\{ |\hat{\mathbf{x}} \cdot (\nabla \times \Phi_{\mathbf{k}, s}(\mathbf{r}, t))|^2 + |\hat{\mathbf{y}} \cdot (\nabla \times \Phi_{\mathbf{k}, s}(\mathbf{r}, t))|^2 \right\}_{z=q+S_\zeta} R(k) d^3 k \\ & = \int_0^{2\pi} d\phi \int_0^{\pi/2} \sin \theta d\theta \int_0^{\bar{k}} dk R(k) k \left\{ |\hat{\mathbf{x}} \cdot (\nabla \times \Phi_{\mathbf{k}, s}(\mathbf{r}, t))|^2 + |\hat{\mathbf{y}} \cdot (\nabla \times \Phi_{\mathbf{k}, s}(\mathbf{r}, t))|^2 \right\}_{z=q+S_\zeta} \\ & = 2\pi \int_0^{\pi/2} \sin \theta \cos^2 \theta d\theta \int_0^{\bar{k}} dk R(k) k \max_{\mathbf{k}} \left\{ |\hat{\mathbf{x}} \cdot (\nabla \times \Phi_{\mathbf{k}, s}(\mathbf{r}, t))|^2 + |\hat{\mathbf{y}} \cdot (\nabla \times \Phi_{\mathbf{k}, s}(\mathbf{r}, t))|^2 \right\}_{z=q+S_\zeta} \\ & \approx \pi \int_0^{\bar{k}} dk R(k) k \left\{ |\hat{\mathbf{x}} \cdot (\nabla \times \Phi_{\mathbf{k}, s}(\mathbf{r}, t))|^2 + |\hat{\mathbf{y}} \cdot (\nabla \times \Phi_{\mathbf{k}, s}(\mathbf{r}, t))|^2 \right\}_{\mathbf{k}=\pm k\hat{\mathbf{z}}} \end{aligned} \quad (27)$$

In view of the above results, it is reasonable to approximate the electromagnetic field involved as one propagating along the  $z$  axis. Consequently, one can set:

$$\Phi_{\mathbf{k}, s}(\mathbf{r}, t) = \Phi_k(\mathbf{r}, t) \mathbf{e}(\mathbf{k}, s) \quad (28)$$

where  $\Phi_k(\mathbf{r}, t)$  is a scalar function and  $\mathbf{e}(\mathbf{k}, s)$  is in the  $x$ - $y$  plane. Then we have the identities:

$$\begin{aligned} & \Phi_{\mathbf{k}, s}(\mathbf{r}, t) \times (\nabla \times \Phi_{\mathbf{k}, s}^*(\mathbf{r}, t)) = \Phi_k(\mathbf{r}, t) \nabla \Phi_k^*(\mathbf{r}, t) \\ & |\hat{\mathbf{x}} \cdot (\nabla \times \Phi_{\mathbf{k}, s}(\mathbf{r}, t))|^2 + |\hat{\mathbf{y}} \cdot (\nabla \times \Phi_{\mathbf{k}, s}(\mathbf{r}, t))|^2 = \left| \frac{\partial}{\partial z} \Phi_k(\mathbf{r}, t) \right|^2 \end{aligned} \quad (29)$$

Then, collecting results produces:

$$\begin{aligned} \langle F_z \rangle \approx & A \frac{\hbar c}{2\pi} \frac{d}{dct} \int_0^\infty dk R(k) k^2 \int dz \text{Im} [\Phi_k(\mathbf{r}, t) \nabla \Phi_k^*(\mathbf{r}, t)] \\ & - A \frac{\hbar c}{16(\pi)^2} \frac{d}{dct} \int_0^{\pi/2} d\tau \sum_{s=1, -1} S \int_0^\infty dk R(k) k^2 \left\{ \hat{k} |\Phi_k(\mathbf{r}, t)|^2 + \frac{1}{k} \left| \frac{\partial}{\partial z} \Phi_k(\mathbf{r}, t) \right|^2 \right\}_{z=q+S_\zeta} \end{aligned} \quad (30)$$

## EVOLUTION OF THE FIELD MODES, $\Phi_k(z, t)$

From the foregoing simplifications, it is clear that field amplitudes must be computed in two distinct half-spaces in the setting of a one-dimensional propagation problem. To adopt more precise notation, let:

$$\Phi_{\alpha k}(z, \tau) = \begin{cases} \Phi_{k=+k\hat{\mathbf{z}}}(z, \tau), & \alpha = +1, z < q(\tau) - \zeta \\ \Phi_{k=-k\hat{\mathbf{z}}}(z, \tau), & \alpha = -1, z > q(\tau) + \zeta \end{cases} \quad (31)$$

where in this and what follows,  $\tau = ct$ . The  $\Phi_k(\mathbf{r}, t)$  must satisfy:

$$\begin{aligned} & \frac{\partial^2}{\partial z^2} \Phi_{\alpha k}(z, \tau) = \frac{\partial^2}{\partial \tau^2} \Phi_{\alpha k}(z, \tau) \\ & \Phi_{\alpha k}(z, \tau = 0) = e^{i\alpha k z} \end{aligned} \quad (32)$$

The boundary conditions are:

$$\Phi_{\alpha k}(z = q(\tau), \tau) = 0, \alpha = \pm 1 \quad (33)$$

Suppose that the surface  $\wp = (x, y)$  is created (turned on) at location  $z = 0$  at time  $\tau = 0$ , then travels in the positive  $z$  direction with displacement  $q(\tau)$  until it reaches  $z = \bar{z}$  at time  $T$  at which point it is annihilated (turned off). For further reference, let  $V(\tau)$  denote the continuous portion of  $dq/d\tau$ .

Obviously, for  $|z| > \tau$ , the field is undisturbed and thus, by (33), must have the form:

$$\Phi_{\alpha k}(z, \tau) = \exp(ik(\alpha z - \tau)), \alpha = -1, +1 \quad (34)$$

which contributes nothing to the average force.

Consider first the solution to the wave equation for  $\Phi_{+1,k}(z, \tau)$ . This quantity is the evolution of the field when it is initially in the single mode  $\Phi_{+1,k}(z, \tau = 0) = \exp(ikz)$ .

It therefore has both rightward and leftward traveling waves. Since there is a discontinuity at  $z = q(t)$ ,  $\Phi_{+1,k}(z, \tau)$ , and  $\Phi_{-1,k}(z, \tau)$  have the form:

$$\Phi_{+1,k}(z, \tau) = \begin{cases} \exp(ik(z - \tau)) - \exp(ikS_+(-z - \tau)), & z \leq q(\tau) \\ 0, & \tau \geq z > q(\tau) \end{cases}$$

$$\Phi_{-1,k}(z, \tau) = \begin{cases} \exp(ik(-z - \tau)) - \exp(ikS_-(z - \tau)), & z \geq q(\tau) \\ 0, & -\tau \leq z < q(\tau) \end{cases} \quad (35)$$

where the quantities  $S_+$ , and  $S_-$  are determined by:

$$S_+(-q(\tau) - \tau) = q(\tau) - \tau, \quad S_-(q(\tau) - \tau) = -q(\tau) - \tau \quad (36)$$

Since  $|q(t)| < ct$ ,  $S_{\pm}$  can be evaluated by the following sequence (convergent for all  $\xi$ ):

$$S_{\pm}(\xi) = \xi \pm 2 \lim_{k \rightarrow \infty} q(\xi_{k,\pm}) \quad (37)$$

$$\xi_{k,\pm} = -\xi \mp q(\xi_{k-1}), \quad k \geq 1$$

$$\xi_0 = -\xi$$

One should also note the identities:

$$S_+(0) = 0 \quad \lim_{\xi \rightarrow -2\tau} \{S_+(\xi)\} = 0 \quad (38)$$

$$S_-(0) = 0 \quad \lim_{\xi \rightarrow 0-} \{S_-(\xi)\} = -2\tau$$

## DETERMINATION OF THE AVERAGE FORCE

### Evaluation of the Poynting Vector Term

In the notation of (31), introduced above, the first term given for the average force takes the form:

$$A \frac{\hbar}{2\pi} \frac{d}{dt} \int_0^\infty dk R(k) k^2 \int dz \operatorname{Im} [\Phi_k(\mathbf{r}, t) \nabla \Phi_k^*(\mathbf{r}, t)] \quad (39)$$

$$= A \frac{\hbar}{2\pi} \frac{d}{dt} \int_0^\infty dk R(k) k^2 \left\{ \sum_{\alpha=-1}^{+1} \int_{-\infty}^\infty \operatorname{Im} \left[ \Phi_{\alpha k}(z, \tau) \frac{\partial}{\partial z} \Phi_{\alpha k}^*(z, \tau) \right] dz \right\}$$

It can be shown (see Appendix B) that the spatial integral in braces is:

$$\sum_{\alpha=-1}^{+1} \int_{-\infty}^\infty \operatorname{Im} \left[ \Phi_{\alpha k}(z, \tau) \frac{\partial}{\partial z} \Phi_{\alpha k}^*(z, \tau) \right] dz \quad (40)$$

$$= -k \int_0^{q(\tau)-\tau} d\chi_+ \left[ 1 - \cos(k(\chi_+ - 2\tau - S_+(\chi_+))) \right] \left[ \frac{\partial S_+(\chi_+)}{\partial \chi_+} - 1 \right]$$

$$+ k \int_{q(\tau)-\tau}^0 d\chi_- \left[ 1 - \cos(k(\chi_- + 2\tau - S_-(\chi_-))) \right] \left[ \frac{\partial S_-(\chi_-)}{\partial \chi_-} - 1 \right]$$

By assumption (1), after a brief initial transient  $\tau \pm q(\tau) \gg 2\pi/k$ , so that the cosine terms (with twice the spatial frequency of the incident waves) contribute very little to the integral. This serves to illustrate the eikonal approximation

motivated by assumption (1).

In any case, letting  $\Gamma_{\pm} = S_{\pm} - \chi_{\pm}$  and using the relations  $S_{\pm}(\mp q(\tau) - \tau) = \pm q(\tau) - \tau$ , one can show that the above integral is identically zero. Thus, the Poynting term vanishes.

### Evaluation of the Radiation Term

The second term in the average force has the form:

$$A \frac{\hbar c}{16(\pi)^2} \frac{d}{d\tau} \int_0^{ct} d\tau \sum_{s=1,-1} S \int_0^\infty dk R(k) k^2 \left[ \hat{k} |\Phi_k(\mathbf{r}, t)|^2 - \frac{1}{k} \left| \frac{\partial}{\partial z} \Phi_k(\mathbf{r}, t) \right|^2 \right]_{z=q+S\zeta} \quad (41)$$

$$\cong A \frac{\hbar c}{16(\pi)^2} \int_0^\infty dk R(k) k^3 \frac{d}{d\tau} \left\{ \int_{-\tau}^q d\tilde{\tau} [1 + S_+'(-q - \tilde{\tau})] - \int_q^\tau d\tilde{\tau} [1 + S_-'(q - \tilde{\tau})] \right\}$$

Differentiating the relations

$$S_+(-q(\tau) - \tau) = q(\tau) - \tau, \quad S_-(q(\tau) - \tau) = -q(\tau)$$

one may determine that:

$$S_+'(-q(\tau) - \tau) = \frac{1 - V(\tau)}{1 + V(\tau)}, \quad S_-'(q(\tau) - \tau) = \frac{1 + V(\tau)}{1 - V(\tau)} \quad (42)$$

where  $V(\tau) = dq(\tau)/d\tau$ .

Inserting these into (41):

$$-A \frac{\hbar c}{16(\pi)^2} \frac{d}{d\tau} \int_0^{ct} d\tau \sum_{s=1,-1} S \int_0^\infty dk R(k) k \left| \frac{\partial}{\partial z} \Phi_k(\mathbf{r}, t) \right|^2_{z=q+S\zeta}$$

$$= A \frac{\hbar c}{16(\pi)^2} \int_0^\infty dk R(k) k^3 \frac{d}{d\tau} \left\{ \int_{-\tau}^q d\tilde{\tau} [1 + S_+'(-q - \tilde{\tau})] - \int_q^\tau d\tilde{\tau} [1 + S_-'(q - \tilde{\tau})] \right\}$$

$$= A \frac{\hbar c}{8(\pi)^2} \int_0^\infty dk R(k) k^3 \frac{d}{d\tau} \left\{ \int_{-\tau}^q d\tilde{\tau} \frac{1}{1 + V(\tau + \tilde{\tau})} - \int_q^\tau d\tilde{\tau} \frac{1}{1 - V(\tau - \tilde{\tau})} \right\} \quad (43)$$

As this is the only remaining non-zero term, it follows that the average force per unit area is:

$$\langle F_z \rangle / A = \frac{\hbar c}{8\pi^2} \int_0^\infty dk R(k) k^3 \frac{d}{d\tau} (q(\tau) \Lambda(\tau)) \quad (44)$$

$$\Lambda(\tau) = \frac{1}{q(\tau)} \left\{ \int_{-\tau}^{q(\tau)} d\tilde{\tau} \frac{1}{1 + V(\tau + \tilde{\tau})} - \int_{q(\tau)}^\tau d\tilde{\tau} \frac{1}{1 - V(\tau - \tilde{\tau})} \right\}$$

Obviously, when the velocity is constant, the force vanishes.

## EXAMPLES OF VARIOUS MOTION CASES

Note that if the velocity is constant, then as expected, the force is identically zero. Thus, some acceleration of the reflective surface is needed. To study a family of simple examples, consider surface motions that are powers of time:

$$q(\tau) = \bar{Z}(\tau/T)^N, \quad \tau \in [0, T] \quad (45)$$

The reflective surface is turned "on" at time zero, accelerates according to an integral power,  $N$ , of time, until time  $T$  at which it reaches its maximum displacement,  $\bar{Z}$ , and is turned off. Note that both  $\bar{Z}$  and  $T$  have the dimension of length. The velocity may be written:

$$V(\tau) = \bar{V}(T)^{N-1}, \quad \bar{V} = N\bar{Z}/T \quad (46)$$

It is seen that  $\bar{V}$  is the maximum attainable velocity during the maneuver, and is expressed as a fraction of the speed of light.

The first object for computation is the quantity  $\Lambda(\tau = T)$ , which



$$\begin{aligned} \langle F_z \rangle = & \frac{d}{dt} \frac{h}{2(2\pi)^3} \sum_{s=1}^2 \int d^3k R(k) \text{Im} \left[ \Phi_{k,s}(\mathbf{r}, t) \times (\nabla \times \Phi_{k,s}^*(\mathbf{r}, t)) \right] \\ & - \frac{1}{2} A \frac{h}{2(2\pi)^4} \frac{d}{dt} \int_0^t d\tau \sum_{s=1,-1}^2 S \sum_{s=1}^2 \left[ \int_{z=q+S_z}^z \left\{ \hat{\mathbf{x}} \cdot \Phi_{k,s}(\mathbf{r}, t) \right\}^2 + \left\{ \hat{\mathbf{y}} \cdot \Phi_{k,s}(\mathbf{r}, t) \right\}^2 - \left\{ \hat{\mathbf{z}} \cdot \Phi_{k,s}(\mathbf{r}, t) \right\}^2 \right] R(k) d^3k \\ & + \int_{z=q+S_z}^z \left\{ \hat{\mathbf{x}} \cdot (\nabla \times \Phi_{k,s}(\mathbf{r}, t)) \right\}^2 + \left\{ \hat{\mathbf{y}} \cdot (\nabla \times \Phi_{k,s}(\mathbf{r}, t)) \right\}^2 - \left\{ \hat{\mathbf{z}} \cdot (\nabla \times \Phi_{k,s}(\mathbf{r}, t)) \right\}^2 \right] R(k) d^3k \end{aligned} \quad (50)$$

epitomizes the asymmetry in the field due to the reflective surface motion. Substituting the above expressions:

$$\Lambda(\tau = T) = \frac{1}{\bar{Z}} \left\{ \int_{-\bar{Z}}^{\bar{Z}} d\bar{\tau} \frac{1}{1 + \bar{V} \left( \frac{T + \bar{\tau}}{T + \bar{Z}} \right)^{N-1}} - \int_{\bar{Z}}^T d\bar{\tau} \frac{1}{1 - \bar{V} \left( \frac{T - \bar{\tau}}{T - \bar{Z}} \right)^{N-1}} \right\} \quad (47)$$

Clearly for  $N = 1$  the above quantity vanishes. To evaluate it explicitly for  $N > 1$ , the two integrands are expanded as geometric series, then the integration performed term-by-term, with the following result:

$$\Lambda(\tau = T) = \sum_{m=0}^{\infty} \frac{\bar{V}^m}{m(N-1)+1} \left[ (-1)^m \left( \frac{N}{\bar{V}} + 1 \right) - \left( \frac{N}{\bar{V}} - 1 \right) \right] \quad (48)$$

Thus  $\Lambda(\tau = T)$  is solely a function of  $\bar{V}$  and independent of  $\bar{Z}$ . Fig. 4 shows the behavior of  $\Lambda(\tau = T)$  as  $\bar{V}$  increases for various values of  $N$ . For  $\bar{V}$  close to unity,  $\Lambda$  begins to diverge. For large  $N$ ,  $\Lambda(\tau = T)$  approaches an asymptotic limit (approximated here by  $N = 20$ ).

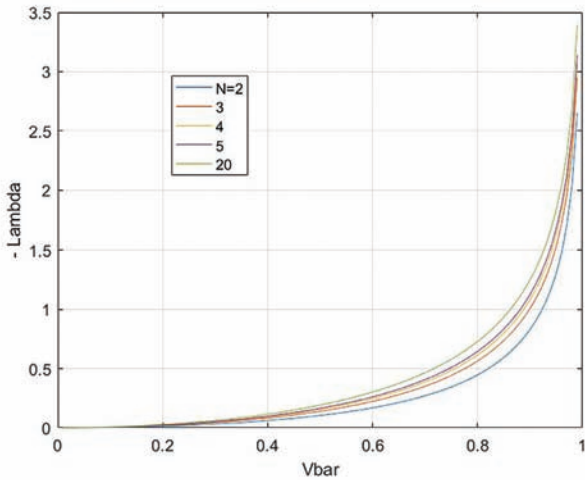


Fig. 4: The Lambda integral versus maximum speed.

At this point, one might pause to consider the validity of assumption (2) given the condition  $\tau \pm q(\tau) \gg 2\pi/k$  implied by assumption (1). The time required for a wave with initial wave number  $k$ , to travel one wavelength is  $2\pi/kc$ . Under the current motion model, the change in the normalized velocity in that time interval, denoted by  $\Delta V$  is given by:

$$\frac{\Delta V}{\bar{V}} = (N-1) \frac{\lambda}{T} \left( \frac{\tau}{T} \right)^{N-2} \quad (49)$$

In other words, the change of velocity over one cycle relative to the maximum speed is of the order of the ratio of the wavelength to the distance light travels over the entire duration of the motion. Since this analysis considers wavelengths of the order of microns, and motion sequences covering centimeters, both assumptions (1) and (2) are well justified.

### CONSIDERATION OF THE THREE-DIMENSIONAL PROBLEM

Now consider the more general formulation, Equation (23), as expressed above in Equation 50:

One consequence of assumption (2) is that the above quantities may be approximated by their running time averages over periods that include many oscillations, yet are still so short that there is little variation in the reflector surface velocity. Henceforth, it is understood that such averaging is to be applied. In each half space, and for a given incident wave vector, each of the two terms above has three contributions: One involving the incident wave alone, a second involving the reflected wave alone and the third composed of products of the incident and reflected waves. As in the one-dimensional formulation, and assuming the range of motion is much larger than the wavelengths involved, the third has a higher spatial frequency and averages out to a negligible contribution. Since only pairs of waves passing in the same direction survive the time averaging process, and because all waves are planar (but not monochromatic), the field appearing in the force expression is described by the eikonal approximation (for propagation in a homogeneous medium):

$$\Phi_{k,s}(\mathbf{r}, t) = \exp(i(\mathbf{k}(\tau) \cdot \mathbf{r} - k\tau)) \mathbf{e}(\mathbf{k}(\tau), s) \quad (51)$$

Then one obtains:

$$\text{Im} \left[ \Phi_{k,s}(\mathbf{r}, t) \times (\nabla \times \Phi_{k,s}^*(\mathbf{r}, t)) \right] = k\kappa(\mathbf{r}, \theta, \tau) \quad (52)$$

$$\begin{aligned} \hat{k} \left\{ \left| \mathbf{u} \cdot \Phi_{k,s}(\mathbf{r}, t) \right|^2 \right\} &= \frac{1}{k} \left| \mathbf{u} \cdot (\nabla \times \Phi_{k,s}(\mathbf{r}, t)) \right|^2 = k \left| (\mathbf{u} - (\hat{\mathbf{x}} \cdot \mathbf{u}) \hat{\mathbf{x}}) \cdot \kappa(\mathbf{r}, \theta, \tau) \right|^2 \\ \kappa(\mathbf{r}, \theta, \tau) &= \mathbf{k}(\mathbf{r}, \theta, \tau) / k \end{aligned}$$

where  $\mathbf{u}$  is any constant unit vector, and recall that  $\hat{\mathbf{x}}$  is orthogonal to the  $z$  axis and in the plane of  $z$  and the direction of propagation of the vacuum mode under consideration. Substituting the above results into the force expression (50), noting that the integrands are independent of the polarization vector, and replacing  $d^3k$  with  $2\pi \sin\theta d\theta k^2 dk$ , the force becomes:

$$\begin{aligned} \langle F_z \rangle = & A \frac{hc}{(2\pi)^2} \int d^3k R(k) k^3 \int_0^{\pi/2} d\theta \sin\theta \frac{d}{d\tau} \int d\bar{\tau} \hat{\mathbf{z}} \cdot \kappa(\mathbf{r}, \theta, \tau) \\ & - A \frac{hc}{(2\pi)^2} \int d^3k R(k) k^3 \int_0^{\pi/2} d\theta \sin\theta \frac{d}{d\tau} \int_0^{\tau} d\bar{\tau} \sum_{s=1,-1}^2 S \left[ \int_{z=q+S_z}^z \left\{ \left| \kappa(\mathbf{r}, \theta, \bar{\tau}) \right|^2 - 2 \left| \hat{\mathbf{x}} \cdot \kappa(\mathbf{r}, \theta, \bar{\tau}) \right|^2 \right\} \right] \end{aligned} \quad (53)$$

In consequence of the assumptions, one can show that the first term vanishes. First, for each inclination angle of the incident waves, no tangential component of force can be produced by specular reflection without violating the idea of relativity. If this were possible, one could measure the force in its rest frame and deduce the reflective surface velocity relative to a nonexistent "ether". Thus, on both sides of the surface, the net momentum change is along the direction of motion. The direction is positive for the left side and negative for the right.

Next consider the change in the spatial integral of the momentum density over a period of many oscillations but dur-

ing which the velocity change is negligible. Then, in the rest frame, the approximations for uniform motion apply. In this frame, the space-time factor of the vacuum state remains the same, and one can define the inclination angle of the incident waves as having the same amplitude, but opposite directions. Since the rest frame presents negligible asymmetry, the reflected waves must be very nearly symmetric with respect to the surface and have equal and opposite components along the  $z$  axis. Therefore, within the approximate formulation, the rate of change of the spatial integral of the Poynting vector is negligible (and, rigorously, identically zero). Likewise, the average energy of the field can be shown to be unchanging.

If  $\beta$  is the angle of reflection corresponding to the angle of incidence,  $\theta$ , then the absence of a tangential component of force implies that  $\kappa(\mathbf{r}, \theta, \tau) \sin \beta = k \sin \theta$ . This, in turn, permits the conclusion that  $\{\kappa(\mathbf{r}, \theta, \tau) - 2\hat{\mathbf{x}} \cdot \kappa(\mathbf{r}, \theta, \tau)\} = \{\hat{\mathbf{z}} \cdot \kappa(\mathbf{r}, \theta, \tau)\}$ . As a result of the foregoing simplifications, the expression for the force becomes:

$$\langle F_z \rangle = -A \frac{\hbar c}{(2\pi)^3} \int d^3k R(k) k^3 \int_0^{\pi/2} d\theta \sin \theta \times \int_0^\tau d\tilde{\tau} \times \frac{d}{d\tau} \sum_{S=1,-1} S \left[ \int \{\hat{\mathbf{z}} \cdot \kappa(\mathbf{r}, \theta, \tilde{\tau})\}_{z=q+S\zeta} \right] \quad (54)$$

Let the incident wave vectors both form angle  $\theta$  with the  $z$  axis, and let  $\beta_1$  and  $\beta_2$  be the inclination angles of the reflected wave vectors in the regions  $z < q$  and  $z \geq q$ , respectively. Then, considering only the  $\tau$  integrals for the moment:

$$\begin{aligned} & \int_0^\tau d\tilde{\tau} \left\{ \{\hat{\mathbf{z}} \cdot \kappa(\mathbf{r}, \theta, \tilde{\tau})\}_{z=q-\zeta} - \{\hat{\mathbf{z}} \cdot \kappa(\mathbf{r}, \theta, \tilde{\tau})\}_{z=q+\zeta} \right\} \\ &= \int_0^\tau d\tilde{\tau} (\cos \theta + |\kappa_1(\mathbf{r}, \theta, \tilde{\tau})| \cos \beta_1) \\ &- \int_0^\tau d\tilde{\tau} (\cos \theta + |\kappa_2(\mathbf{r}, \theta, \tilde{\tau})| \cos \beta_2) \end{aligned} \quad (55)$$

where  $\kappa_1(\mathbf{r}, \theta, \tilde{\tau})$  and  $\kappa_2(\mathbf{r}, \theta, \tilde{\tau})$  are the wave vectors of the reflected waves. Next, as above, it is assumed that the variations of the reflected wave amplitudes over several wavelengths are very small. Then the formulae related to the uniform motion of a mirror [20, 21] may be used:

$$\begin{aligned} |\kappa_1(\mathbf{r}, \theta, \tilde{\tau})| &= \frac{1 - 2V \cos \theta + V^2}{1 - V^2}, \quad \cos \beta_1 = \frac{-2V + (1 + V^2) \cos \theta}{1 - 2V \cos \theta + V^2} \\ |\kappa_2(\mathbf{r}, \theta, \tilde{\tau})| &= \frac{1 + 2V \cos \theta + V^2}{1 - V^2}, \quad \cos \beta_2 = \frac{2V + (1 + V^2) \cos \theta}{1 + 2V \cos \theta + V^2} \end{aligned} \quad (56)$$

Then making substitutions into (55), one concludes:

$$\begin{aligned} & \int_0^\tau d\tilde{\tau} \left\{ \{\hat{\mathbf{z}} \cdot \kappa(\mathbf{r}, \theta, \tilde{\tau})\}_{z=q-\zeta} - \{\hat{\mathbf{z}} \cdot \kappa(\mathbf{r}, \theta, \tilde{\tau})\}_{z=q+\zeta} \right\} \\ &= \int_0^\tau d\tilde{\tau} \frac{2(\cos \theta - V)}{1 - V^2} - \int_0^\tau d\tilde{\tau} \frac{2(\cos \theta + V)}{1 - V^2} \end{aligned} \quad (57)$$

Since the time variable has units of length, one can convert to integration along the  $z$ -axis. For the regions  $z < \tau \cos \beta_1$  ( $\tau = 0$ ) +  $q(\tau)$ , and  $z \geq \tau \cos \beta_2$  ( $\tau = 0$ ) -  $q(\tau)$ , only incident waves exist which contribute nothing to the momentum change. Adjusting the limits of integration accordingly, the integrals become:

$$\begin{aligned} & \int_0^\tau d\tilde{\tau} \left\{ \{\hat{\mathbf{z}} \cdot \kappa(\mathbf{r}, \theta, \tilde{\tau})\}_{z=q-\zeta} - \{\hat{\mathbf{z}} \cdot \kappa(\mathbf{r}, \theta, \tilde{\tau})\}_{z=q+\zeta} \right\} \\ &= \int_{-q_1(\tau)}^{q(\tau)} d\tilde{\tau} \frac{(\cos \theta - V(\tau + \tilde{\tau}))}{1 - V^2(\tau + \tilde{\tau})} \\ &- \int_{q(\tau)}^{q_2(\tau)} d\tilde{\tau} \frac{(\cos \theta + V(\tau - \tilde{\tau}))}{1 - V^2(\tau - \tilde{\tau})} \end{aligned} \quad (58)$$

where  $\chi_1$  and  $\chi_2$  are given by:

$$\frac{d}{d\tau} \chi_1 = \max \left\{ 0, \frac{-2V + (1 + V^2) \cos \theta}{1 - 2V \cos \theta + V^2} \right\}, \quad \frac{d}{d\tau} \chi_2 = \frac{2V + (1 + V^2) \cos \theta}{1 + 2V \cos \theta + V^2} \quad (59)$$

The result for the force becomes:

$$\begin{aligned} \langle F_z \rangle &= A \frac{\hbar c}{(2\pi)^2} \left( \int_0^\pi dk R(k) k^3 \right) \\ &\times \frac{d}{d\tau} \left[ \int_0^{\pi/2} \sin \theta d\theta \left\{ \int_{-q_1(\tau)}^{q(\tau)} d\tilde{\tau} \frac{(\cos \theta - V(\tau + \tilde{\tau}))}{1 - V^2(\tau + \tilde{\tau})} - \int_{q(\tau)}^{q_2(\tau)} d\tilde{\tau} \frac{(\cos \theta + V(\tau - \tilde{\tau}))}{1 - V^2(\tau - \tilde{\tau})} \right\} \right] \end{aligned} \quad (60)$$

If the velocity is constant, the force is zero. Let  $V = \bar{V} = \text{const}$  then:

$$\chi_1 = \max \left\{ 0, \frac{-2\bar{V} + (1 + \bar{V}^2) \cos \theta}{1 - 2\bar{V} \cos \theta + \bar{V}^2} \right\} \tau, \quad \chi_2 = \frac{2\bar{V} + (1 + \bar{V}^2) \cos \theta}{1 + 2\bar{V} \cos \theta + \bar{V}^2} \tau \quad (61 \text{ a, b})$$

and the integrals in the above force expression become:

$$\begin{aligned} & \int_{-q_1(\tau)}^{q(\tau)} d\tilde{\tau} \frac{(\cos \theta - V(\tau + \tilde{\tau}))}{1 - V^2(\tau + \tilde{\tau})} - \int_{q(\tau)}^{q_2(\tau)} d\tilde{\tau} \frac{(\cos \theta + V(\tau - \tilde{\tau}))}{1 - V^2(\tau - \tilde{\tau})} \\ &= \left( \frac{\cos \theta - \bar{V}}{1 - \bar{V}^2} \right) \left( \bar{V} + \frac{(1 + \bar{V}^2) \cos \theta - 2\bar{V}}{1 - 2\bar{V} \cos \theta + \bar{V}^2} \right) - \left( \frac{\cos \theta + \bar{V}}{1 - \bar{V}^2} \right) \left( -\bar{V} + \frac{(1 + \bar{V}^2) \cos \theta + 2\bar{V}}{1 + 2\bar{V} \cos \theta + \bar{V}^2} \right) \\ &= \left( \frac{\cos \theta - \bar{V}}{1 - \bar{V}^2} \right) \left( \frac{(1 - \bar{V}^2)(\cos \theta - \bar{V})}{1 - 2\bar{V} \cos \theta + \bar{V}^2} \right) - \left( \frac{\cos \theta + \bar{V}}{1 - \bar{V}^2} \right) \left( \frac{(1 - \bar{V}^2)(\cos \theta + \bar{V})}{1 + 2\bar{V} \cos \theta + \bar{V}^2} \right) \\ &= \left( \frac{(\cos \theta - \bar{V})^2}{1 - 2\bar{V} \cos \theta + \bar{V}^2} \right) - \left( \frac{(\cos \theta + \bar{V})^2}{1 + 2\bar{V} \cos \theta + \bar{V}^2} \right) \end{aligned} \quad (62)$$

In the integral of the first term, the sign of the cosine can be reversed. Therefore the integral of the first term is equal and opposite in sign to that of the second term and the force vanishes.

## APPROXIMATION FOR HIGH- AND LOW-SPEED SCANS

Since the epitaxial device is intended to both increase the amplitude, and the speed of the reflective surface motion it is well to consider the case where  $V$  is a significant fraction of unity. Let  $V = 1 - \nu$ , and  $\nu \ll 1$ . Then the relations for the reflection angles yield:

$$\cos \beta_1 = 1 + O(\nu^2), \quad \cos \beta_2 = 1 + O(\nu^2) \quad (63 \text{ a, b})$$

Secondly, note that  $-\frac{(\cos \theta - V)}{1 - V^2} \geq -\frac{\cos \theta}{1 + V}$ , and  $\frac{(\cos \theta + V)}{1 - V^2} \geq \frac{\cos \theta}{1 - V}$ .

Using these inequalities and the above approximations for the reflection angle cosines, one obtains an upper bound for the spatial integral:

$$\begin{aligned} & \int_{-z_1(\tau)}^{q(\tau)} d\tilde{\tau} \frac{(\cos \theta - V(\tau + \tilde{\tau}))}{1 - V^2(\tau + \tilde{\tau})} - \int_{q(\tau)}^{z_2(\tau)} d\tilde{\tau} \frac{(\cos \theta + V(\tau - \tilde{\tau}))}{1 - V^2(\tau - \tilde{\tau})} \\ & \leq \cos \theta \left[ \int_{-\tau}^{q(\tau)} dz \frac{1}{1 + V(\tau + \tilde{\tau})} - \int_{q(\tau)}^{\tau} dz \frac{1}{1 - V(\tau - \tilde{\tau})} \right] + O(v^2) \end{aligned} \quad (64)$$

Substituting this into the force expression, and performing the integration over  $\theta$  yields:

$$\begin{aligned} & \langle F_z \rangle / A \geq \left| \langle \hat{F}_z \rangle / A + O(v^2) \right| \\ & \left| \langle \hat{F}_z \rangle / A \right| = \frac{\hbar c}{8\pi^2} \left( \int_0^{\bar{k}} dk R(k) k^3 \right) \bar{Z} \left| \frac{d}{d\tau} \hat{\Lambda}(\tau) \right| \\ & \hat{\Lambda}(\tau) = \frac{1}{\bar{Z}} \left\{ \int_{-\tau}^{q(\tau)} d\tilde{\tau} \frac{1}{1 + V(\tau + \tilde{\tau})} - \int_{q(\tau)}^{\tau} d\tilde{\tau} \frac{1}{1 - V(\tau - \tilde{\tau})} \right\} \end{aligned} \quad (65 \text{ a, b, c})$$

The expression in the bracket obviously vanishes when  $V$  is constant. This lower bound is identical to the magnitude of the one-dimensional approximation.

On the other hand, assuming  $V \ll 1$ , an upper bound can be discerned:

$$\begin{aligned} & \int_{-z_1(\tau)}^{q(\tau)} d\tilde{\tau} \frac{(\cos \theta - V(\tau + \tilde{\tau}))}{1 - V^2(\tau + \tilde{\tau})} - \int_{q(\tau)}^{z_2(\tau)} d\tilde{\tau} \frac{(\cos \theta + V(\tau - \tilde{\tau}))}{1 - V^2(\tau - \tilde{\tau})} \\ & \cong \int_{-\tau \cos \theta}^{q(\tau)} d\tilde{\tau} \frac{(\cos \theta - V(\tau + \tilde{\tau}))}{1 - V^2(\tau + \tilde{\tau})} - \int_{q(\tau)}^{\tau \cos \theta} d\tilde{\tau} \frac{(\cos \theta + V(\tau - \tilde{\tau}))}{1 - V^2(\tau - \tilde{\tau})} \\ & \leq \int_{-\tau \cos \theta}^{q(\tau)} d\tilde{\tau} \frac{1}{1 + V(\tau + \tilde{\tau})} - \int_{q(\tau)}^{\tau \cos \theta} d\tilde{\tau} \frac{1}{1 - V(\tau - \tilde{\tau})} \end{aligned} \quad (66)$$

The force expression then yields:

$$\begin{aligned} & \langle F_z \rangle / A = \left| \langle \hat{F}_z \rangle / A \right| + O(V) \\ & \left| \langle \hat{F}_z \rangle / A \right| \leq \frac{2\hbar c}{8\pi^2} \left( \int_0^{\bar{k}} dk R(k) k^3 \right) \bar{Z} \left| \frac{d}{d\tau} \tilde{\Lambda}(\tau) \right| \\ & \tilde{\Lambda}(\tau) = \frac{1}{\bar{Z}} \left\{ \int_{-\tau}^{q(\tau)} d\tilde{\tau} \frac{1}{1 + V(\tau + \tilde{\tau})} - \int_{q(\tau)}^{\tau} d\tilde{\tau} \frac{1}{1 - V(\tau - \tilde{\tau})} \right\} \end{aligned} \quad (67 \text{ a, b, c})$$

## AVERAGE FORCE IN THE CASE OF PERIODIC SCANS

One could create a periodic disturbance by repeating the surface displacement waveform. However, if the motion is immediately repeated at the end of a cycle, there will be interaction between the newly created waves and the reverberant wave still crossing the segment  $z \in [0, \bar{Z}]$ . Such interaction ceases if one waits for time  $\bar{Z}/c$  to begin the new cycle. The momentum increment will then be the same for each cycle. The following analysis adopts the one-dimensional approximation for the Casimir force, (65). Fig. 5-a shows, schematically, the cyclic surface position waveform so produced. By momentum conservation, the force on the mirror device is the negative derivative of the momentum change, which is proportional to  $\Lambda(\tau = T)$ . This is illustrated in Fig. 5-b. Note the negative direction of the force.

Using Equation (65), and setting the total duration of the cycle equal to  $(T + \bar{Z})/c$  one concludes:

$$\begin{aligned} & \langle \langle F_z \rangle / A \rangle_t = \frac{\hbar c}{8\pi^2} \left( \int_0^{\infty} dk R(k) k^3 \right) \frac{\bar{Z}}{T + \bar{Z}} \Lambda(T) \\ & \Lambda(T) = \frac{1}{\bar{Z}} \left\{ \int_{-T}^{\bar{Z}} d\tilde{\tau} \frac{1}{1 + V(\tau + \tilde{\tau})} - \int_{\bar{Z}}^T d\tilde{\tau} \frac{1}{1 - V(\tau - \tilde{\tau})} \right\} \end{aligned} \quad (68 \text{ a, b})$$

At this point it is well to examine the effect of various parameters on the force produced, and perhaps reformulate their definitions. At the outset, it was assumed that the reflection coefficient was unity (perfect reflection) up to some wave number cutoff beyond which it is zero (perfect transparency). A somewhat more realistic, albeit still crude, model is that:

$$R(k) = \begin{cases} 1, & k \in [k_L, k_U] \\ 0, & \text{otherwise} \end{cases} \quad (69)$$

where  $k_U > k_L$ . With this expression, the wave number integral can be seen to be:

$$\begin{aligned} & \left( \int_0^{\infty} dk R(k) k^3 \right) = \bar{k}^3 \Delta \bar{k} \\ & \bar{k} = \left[ \frac{1}{2} (k_U^2 + k_L^2) \cdot \frac{1}{2} (k_U + k_L) \right]^{1/3} \\ & \Delta \bar{k} = k_U - k_L \end{aligned} \quad (70)$$

$\bar{k}$  represents the approximate middle (weighted heavily at

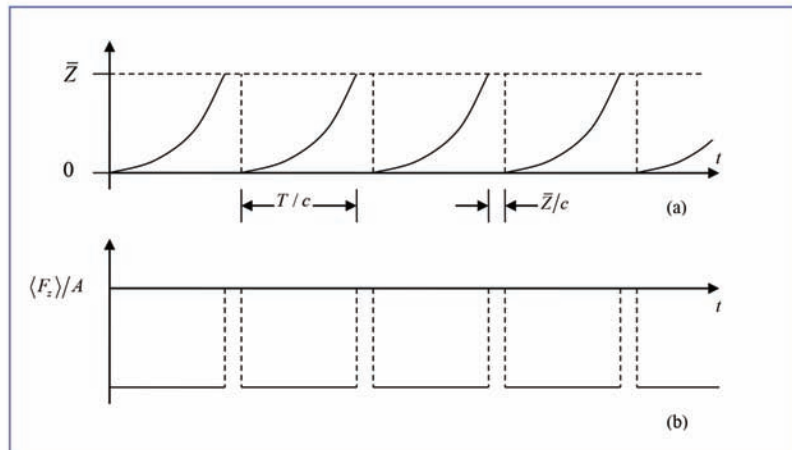


Fig. 5: (a) Cyclic waveform of the reflective surface position; (b) Force on the epitaxial device.



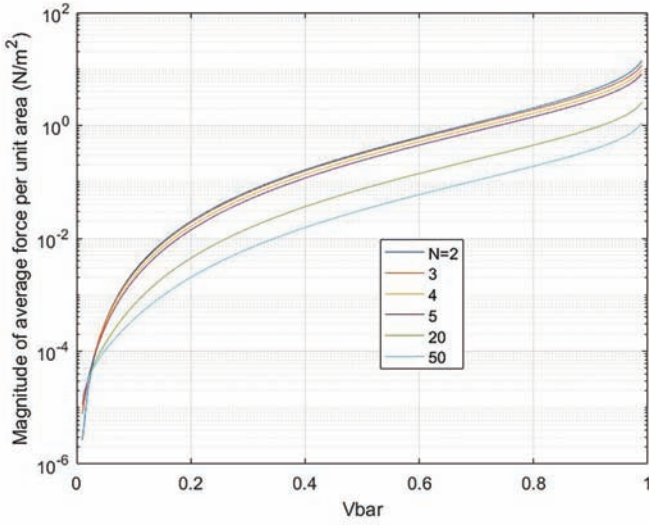


Fig. 6: Force per unit area as a function of the maximum waveform velocity, integer powers.

the upper end) of the useful band wherein reflectivity/transparency can be switched on and off, and  $\Delta\bar{k}$  is the width of this band.

Another parameter of interest is  $\bar{\beta} = 2\bar{Z}/(T + \bar{Z}) \in [0, 1]$ . This is the average speed, relative to  $c$ , that the activated laminae sweep through the total period of the waveform. Finally,  $\Lambda(T)$  is dimensionless, depends only on the normalized velocity profile, and is of order unity unless  $V$  is nearly unity. To summarize:

$$\begin{aligned} \langle \langle F_z \rangle / A \rangle_t &= \frac{\hbar c}{(4\pi)^2} \bar{k}^3 \Delta\bar{k} \bar{\beta} \Lambda(T) \\ \Lambda(T) &= \frac{1}{\bar{Z}} \left\{ \int_{-T}^{\bar{Z}} d\tilde{\tau} \frac{1}{1+V(\tau+\tilde{\tau})} - \int_{\bar{Z}}^T d\tilde{\tau} \frac{1}{1-V(\tau-\tilde{\tau})} \right\} \\ \bar{k} &= \left[ \frac{1}{2} (k_U^2 + k_L^2) \cdot \frac{1}{2} (k_U + k_L) \right]^{1/3} \\ \Delta\bar{k} &= k_U - k_L \\ \bar{\beta} &= 2\bar{Z}/(T + \bar{Z}) \in [0, 1] \end{aligned} \quad (71)$$

## CONCLUDING REMARKS

This paper re-examines the dynamic Casimir effect as a possible mechanism for propulsion. Previous investigations assumed mechanical motion of a mirror to generate thrust. In this case, because of the finite strength of materials and the high frequencies necessary, the amplitudes of motion must be restricted to the nanometer range. Here, an epitaxial stack of transparent semiconductor laminae is proposed, where voltage is rapidly switched to successive laminae, thereby creating continuous motion of a front of charge carrier density. The result is the creation of a reflective surface in rapid, large amplitude motion without the use of mechanical contrivances. Since previous analysis of the propulsive effect was restricted to motions much smaller than the wavelengths of importance, it was nec-

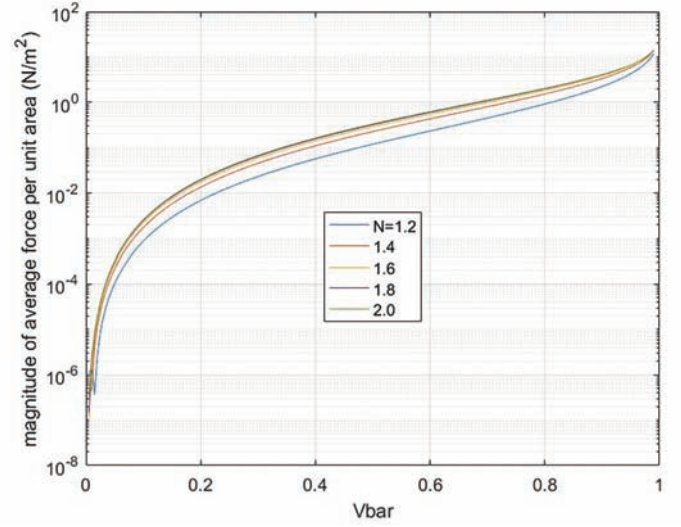


Fig. 7: Force per unit area as a function of the maximum waveform velocity, fractional powers.

## EXAMPLE: PERIODIC MOTION WITH POWER LAW WAVEFORMS

Here some numerical examples are shown, involving the waveforms proportional to an integer power of time, treated earlier, with  $\bar{V}$  denoting the maximum velocity of the reflective surface. To appreciate the magnitude of the force per unit area, assign plausible values to the various parameters. Suppose the plasma frequency is in the range  $10^{14}$  Hz to  $10^{16}$  Hz. Specifically, let us fix  $k_U = 2 \times 10^7$  ( $\lambda \cong 0.3 \mu\text{m}$ ) and set  $k_L = 4 \times 10^6$  ( $\lambda = 1.5 \mu\text{m}$ ). Note that since  $T = N\bar{Z}/\bar{V}$ , it follows that  $\bar{\beta} = 2\bar{V}/(\bar{V} + N)$ . Hence the average force depends only on the maximum speed and the power law exponent.

Fig. 6 shows the variation of the force with maximum speed for integers powers,  $N = 1$  to 7. Similar results are shown in Fig. 7 for fractional powers between 1.1 and 2. It appears that for any given maximum speed (below  $c$ ), an approximately quadratic velocity yields the maximum force per unit area.

essary to derive correct relativistic expressions appropriate for large amplitude motion. This was accomplished for the general motion case and examined in detail for a variety of possible motions. All calculations assumed an initial zero temperature state. Another restriction is that detailed dielectric function models were not used; rather the reflectivity was based on a simple wave number cut-off model. Moreover, as for previous workers, the treatment is semi-quantum in that the epitaxial stack is modeled as a set of prescribed boundary conditions on the field operators. Despite these restrictions, if reasonable charge carrier volumetric densities are assumed, the propulsive forces may be quite significant. The assumption of finite temperature and surface velocities that are a significant fraction of the light speed may possibly increase the magnitude of the present estimates.

## APPENDIX A

The finite response time of a semiconductor lamina allows us to create a continuously moving “front” at which the cumulative areal density of charge carriers suffices to produce a desired level of reflectance. Thus, although the laminae are discrete, their sequential stimulus at the proper rate yields the effect of a continuously moving mirror.

As an illustration, suppose that the conductivity,  $h(t)$ , in response to a voltage pulse has a simple linear rise and fall, as in:

$$h(t) = \rho_{\max} \begin{cases} t/\tau_R, & t \leq \tau_R \\ 2 - t/\tau_R, & 2\tau_R \geq t \geq \tau_R \\ 0, & t > 2\tau_R \end{cases} \quad (\text{A-1})$$

where  $\tau_R$  is the finite rise time and  $h(t)$  is the impulse response of the lamina conductivity. Suppose each successive lamina is stimulated at a sub-multiple of the rise time after its immediate predecessor, such that each rise in the reflectance is a small fraction of complete reflectivity. Fig. A-1 illustrates the resulting motion of the conductivity profile. An incoming plane wave suffers a cumulative reflection in proportion to the total charge carrier population per unit area along its path. In the example of the figure, the total areal population

corresponding to some reflection coefficient,  $|R(k)|$ , is suggested by the gray-shaded areas. In general, the position of the “front” along which the total reflectance reaches some value is seen to move continuously in the direction of, and with the approximate speed of, the conductivity profile (illustrated by the blue-shaded boundary in the Figure). Even if the charge carrier profile has the staircase form as shown in the Figure, the Courant-Friedrichs-Lewy condition can be satisfied so that the effective conductivity profile approximates a continuously increasing distribution. This permits the device to approximate the reflective properties of a mechanical mirror, including the relativistic Doppler effects. Moreover, remaining discretization effects can be mitigated by designing a suitable charge carrier gradient for each lamina. Because of length limitations, detailed proofs of the foregoing results must be deferred to a later manuscript.

To assess the achievable front speeds, consider the example of Fig. A-1 where the time between inputs to successive laminae is a third of the rise time. Then the average speed of the reflective surface is  $\sim 3\delta/\tau_R$  where  $\delta$  is the lamina thickness. Taking a typical rise time of  $10^{-9}$  s and a lamina thickness of a millimeter, obtains a reflective surface speed of  $\sim 3 \times 10^{-3}$  m/s, i.e.,  $\beta \cong 0.1$ . This could be significantly improved by advanced high-speed switching technology.

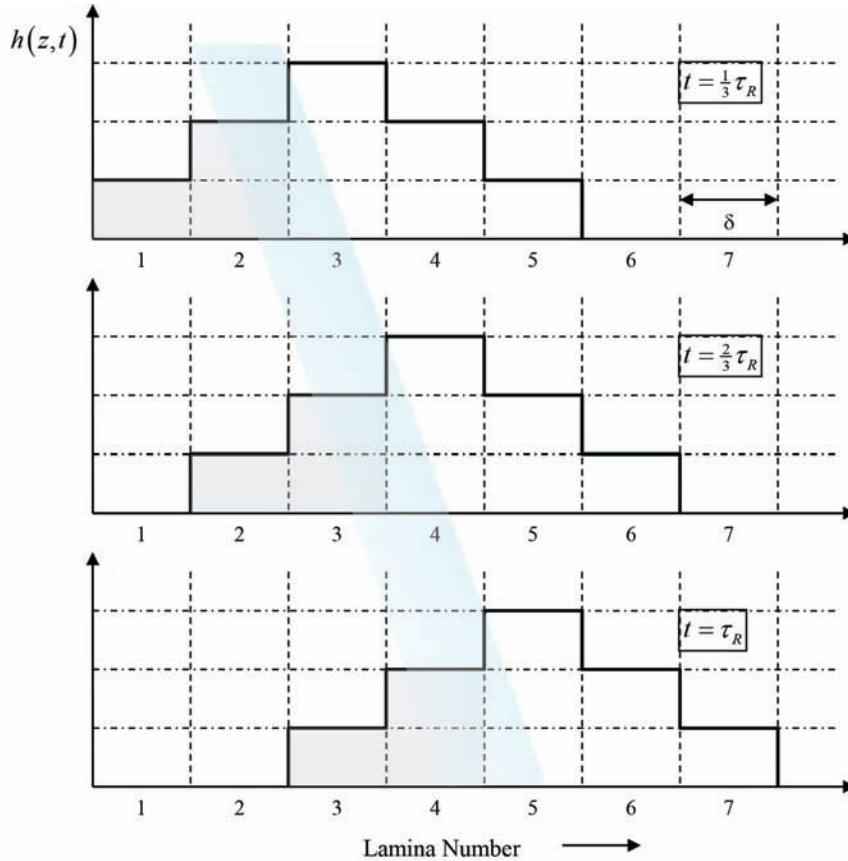


Fig. A-1: Temporal progression of conductivity as the laminae are successively pulsed. The blue-shaded boundary indicates the continuous motion of the front having a particular value of reflectance.

## APPENDIX B

$$\begin{aligned}
\sum_{\alpha=-1}^{+1} \int_{-\infty}^{\infty} \text{Im} \left[ \Phi_{\alpha k}(z, \tau) \frac{\partial}{\partial z} \Phi_{\alpha k}^*(z, \tau) \right] dz = & \\
& \int_{-\tau}^{q(\tau)} dz \text{Im} \left\{ \left[ \exp(ik(z-\tau)) - \exp(ikS_+(z-\tau)) \right] \left[ -ik \exp(-ik(z-\tau)) + ik \frac{\partial S_+(-z-\tau)}{\partial z} \exp(-ikS_+(-z-\tau)) \right] \right\} \\
& + \int_{q(\tau)}^{\tau} dz \text{Im} \left\{ \left[ \exp(ik(-z-\tau)) - \exp(ikS_-(z-\tau)) \right] \left[ ik \exp(-ik(-z-\tau)) + ik \frac{\partial S_-(z-\tau)}{\partial z} \exp(-ikS_-(z-\tau)) \right] \right\} \\
= & \int_{-\tau}^{q(\tau)} dz \text{Im} \left\{ -ik + ik \frac{\partial S_+(-z-\tau)}{\partial z} \exp(ik(z-\tau-S_+(-z-\tau))) + ik \exp(-ik(z-\tau-S_+(-z-\tau))) - ik \frac{\partial S_+(-z-\tau)}{\partial z} \right\} \\
& + \int_{q(\tau)}^{\tau} dz \text{Im} \left\{ ik + ik \frac{\partial S_-(z-\tau)}{\partial z} \exp(ik(-z-\tau-S_-(z-\tau))) - ik \exp(-ik(-z-\tau-S_-(z-\tau))) - ik \frac{\partial S_-(z-\tau)}{\partial z} \right\} \\
= & k \int_{-\tau}^{q(\tau)} dz \left\{ -1 + \frac{\partial S_+(-z-\tau)}{\partial z} \cos(k(z-\tau-S_+(-z-\tau))) + \cos(k(z-\tau-S_+(-z-\tau))) - \frac{\partial S_+(-z-\tau)}{\partial z} \right\} \\
& + k \int_{q(\tau)}^{\tau} dz \left\{ 1 + \frac{\partial S_-(z-\tau)}{\partial z} \cos(k(z+\tau-S_-(z-\tau))) - \cos(k(z+\tau-S_-(z-\tau))) - \frac{\partial S_-(z-\tau)}{\partial z} \right\} \\
= & k \int_{-\tau}^{q(\tau)} dz \left[ 1 - \cos(k(z-\tau-S_+(-z-\tau))) \right] \left[ \frac{\partial S_+(-z-\tau)}{\partial(-z)} - 1 \right] \\
& - k \int_{q(\tau)}^{\tau} dz \left[ 1 - \cos(k(z+\tau-S_-(z-\tau))) \right] \left[ \frac{\partial S_-(z-\tau)}{\partial z} - 1 \right]
\end{aligned} \tag{B-1}$$

$$\text{Let: } \chi_+ = -z - \tau, \quad \chi_- = z - \tau \tag{B-2}$$

Then we have:

$$\begin{aligned}
\sum_{\alpha=-1}^{+1} \int_{-\infty}^{\infty} \text{Im} \left[ \Phi_{\alpha k}(z, \tau) \frac{\partial}{\partial z} \Phi_{\alpha k}^*(z, \tau) \right] dz & \\
= & k \int_{-\tau}^{q(\tau)} dz \left[ 1 - \cos(k(z-\tau-S_+(-z-\tau))) \right] \left[ \frac{\partial S_+(-z-\tau)}{\partial(-z)} - 1 \right] \\
& - k \int_{q(\tau)}^{\tau} dz \left[ 1 - \cos(k(z+\tau-S_-(z-\tau))) \right] \left[ \frac{\partial S_-(z-\tau)}{\partial z} - 1 \right] \\
= & -k \int_0^{-q(\tau)-\tau} d\chi_+ \left[ 1 - \cos(k(\chi_+ - 2\tau - S_+(\chi_+))) \right] \left[ \frac{\partial S_+(\chi_+)}{\partial \chi_+} - 1 \right] \\
& + k \int_{q(\tau)-\tau}^0 d\chi_- \left[ 1 - \cos(k(\chi_- + 2\tau - S_-(\chi_-))) \right] \left[ \frac{\partial S_-(\chi_-)}{\partial \chi_-} - 1 \right]
\end{aligned} \tag{B-3}$$

## REFERENCES

1. H. B. G. Casimir, Proc. Kon. Nederl. Akad. Wet. 51, 793, 1948.
2. H. B. G. Casimir, D. Polder, Phys. Rev. 73, 360, 1948.
3. G. Plunien, B. Muller, W. Greiner, Phys. Rep. 134, 87, 1986.
4. V. M. Mostepanenko, N. N. Trunov, Sov. Phys. —Usp.(USA) 31, 985, 1988.
5. V. M. Mostepanenko, N. N. Trunov, *The Casimir Effect and its Applications*, Clarendon Press, Oxford, 1997.
6. M. Bordag, U. Mohideen and V. M. Mostepanenko. "New developments in the Casimir effect". *Physics Reports* 353 (2001) 1–205, December 2000.
7. P. Neto, "Vacuum Radiation Pressure on Moving Mirrors", *J. Phys. A : Math. Gen.* 27, 2167, 1994.
8. G. J. Maclay and R. L. Forward, "A Gedanken Spacecraft that Operates Using the Quantum Vacuum (Dynamic Casimir Effect)", *Foundations of Physics*, Vol. 34 No. 3, March 2004
9. Minami and Tadatsugu. "Transparent conducting oxide semiconductors for transparent electrodes". *Semiconductor Science and Technology* 20 (4): S35, 2005.
10. P. P. Edwards, A. Porch, M. O. Jones, D. V. Morgan and R. M. Perks. "Basic materials physics of transparent conducting oxides". *Dalton Transactions* (19): 2995–3002, 2004.
11. L. Hu, D. S. Hecht and G. Grüner. "Infrared transparent carbon nanotube thin films". *Applied Physics Letters* 94 (8): 081103, 2009.
12. J. Ouyang, C. W. Chu, F.-C. Chen, Q. Xu and Y. Yang. "High-Conductivity Poly (3,4-ethylenedioxythiophene):Poly(styrene sulfonate) Film and Its Application in Polymer Optoelectronic Devices". *Advanced Functional Materials* 15 (2): 203, 2005
13. S. H. Lee, H. Park, S. Kim, W. Son, I. W. Cheong and Jung Hyun Kim. "Transparent and flexible organic semiconductor nanofilms with enhanced thermoelectric efficiency". *J. Mater. Chem. A*, 2, 7288-7294, 2014
14. T. Kamiya, and H. Hosono. "Material characteristics and applications of transparent amorphous oxide semiconductors". *NPG Asia Materials* (2010) 2, 15–22 2010.5. 17, 2010.
15. P.J. Burke, I. B. Spielman, J. P. Eisenstein, L. N. Pfeiffer, and K. W. West. "High frequency conductivity of the high-mobility two-dimensional electron gas". *Appl. Phys. Lett.* 76 (6). 745-747. 2000.
16. A. Sommerfeld and H. Bethe. *Elektrontheorie der Metalle*. H. Geiger and K. Seel, Eds. *Handbuch der Physik*, Vol. 24, Part 2, 333-622. Springer 1933. Also: *Elektrontheorie der Metalle*. Springer, 1967.
17. M. Dressel, and M. Scheffler. "Verifying the Drude response". *Ann. Phys.* 15 (7-8), 535-544. 2006.
18. L. Mandel and E. Wolf, *Optical Coherence and Quantum Optics*, Cambridge University Press. 1995.
19. S. S. Schweber, *An Introduction to Relativistic Quantum Field Theory*, Harper and Row, New York. Chap. 7.
20. A. Einstein, "Zur Elektrodynamik Bewegter Körper." *Ann. Phys.* (Leipzig) 17, 891-921, 1905; reprinted in *Einstein's Miraculous Year: Five papers that changed the face of physics*, edited by John Stachel, Princeton University Press, Princeton, 1998.
21. A. Gjurchinovski, "Reflection of light from a uniformly moving mirror," *Am. J. Phys.* 72, 1316-1324 (2004).

Received 18 December, 2017 Accepted 22 February 2017



# DYNAMICAL CASIMIR EFFECT AND THE POSSIBILITY OF LASER-LIKE GENERATION OF GRAVITATIONAL RADIATION

R.Y. CHIAO, J.S. SHARPING, L.A. MARTINEZ, B.S. KANG, A. CASTELLI, N. INAN, and J.J. THOMPSON, Dept. of physics, University of California at Merced. 5200 Lake Rd, Merced, CA 95340, USA

Email: rchiao@ucmerced.edu, jsharping@ucmerced.edu

In this paper, we address the question as to whether or not measurable sources for gravitational waves could possibly be made in the laboratory. Based on an analogy of the dynamical Casimir effect with the stimulated emission of radiation in the laser, our answer to this question is in the affirmative, provided that superconducting radio-frequency cavities in fact possess high quality factors for both electromagnetic and gravitational microwave radiation, as one would expect due to a quantum-mechanical gravitational Meissner-like effect. In order to characterize the response of matter to *tensor* gravitational fields, we introduce a prefactor to the source term of the gravitational wave equation, which we call the “relative gravitational permeativity” analogous to the “relative electric permittivity” and “relative magnetic permeability” that characterize the *vector* response of matter to applied fields in electromagnetism. This allows for a possibly large quantum mechanical enhancement of the response of a superconductor to an incident tensor gravitational wave field. Finally, we describe our experimental work with high-superconducting radio-frequency cavities, and propose a design for a coupled-cavity system with a flexible superconducting membrane in its middle as its amplifying element. This will then allow us to test for a Meissner-like expulsion, and therefore reflection, of incident tensor gravitational wave fields, and, above a certain threshold, to generate coherent gravitational radiation via the Dynamical Casimir Effect.

**Keywords:** Laser-like generation of gravitational radiation, Reflection of gravitational waves on superconductor, Triple cavity parametric amplifier

## INTRODUCTION

The 2017 Nobel prize in physics was awarded for observations of gravitational waves arising from the inspiral of black hole pairs [1] [2]. Recently, the emission of gravitational waves was also observed due to the inspiral of a pair of neutron stars, along with the simultaneous observations of gamma ray and optical detections of the same event from the same source [3].

The question naturally arises: Is it possible to generate gravitational radiation in the laboratory? A common response to this question is the one given by Misner, Thorne, and Wheeler (MTW), in their classic text [4]:

*“The construction of a laboratory generator of gravitational radiation is a non-attractive enterprise in the absence of new engineering or a new idea or both.”*

This response was a result of Einstein's investigation of the power emitted in gravitational radiation  $P_{\text{Einstein}}$  by a rotating steel beam, based on his quadrupole formula [4][5][6]:

$$P_{\text{Einstein}} = \frac{G}{45c^5} \langle \ddot{Q}_{ij}^2 \rangle \quad (1)$$

where  $G$  is Newton's constant,  $c$  is the speed of light, and where [5]:

$$Q_{ij} = \int \rho (3x_i x_j - \delta_{ij} x^k x_k) dV \quad (2)$$

is the mass quadrupole tensor (Einstein's summation convention is being used here, with Latin indices denoting spatial dimensions).

MTW [4] calculated the gravitational radiation emitted from a massive steel beam with a length of 20 meters and a radius of 1 meter, whose mass is  $4.9 \times 10^5$  kilograms, rotating end-over-end around its midpoint at its maximum possible angular velocity near its breaking point, which is determined by the tensile strength of steel,  $3 \times 10^6 \text{ J m}^{-2}$ . Then the maximum possible angular velocity of the steel beam due to its tensile strength is 28 radians per second, and the gravitational radiation power predicted by the quadrupole formula (1) turns out to be:

$$P_{\text{Einstein}} \simeq 2.2 \times 10^{-29} \text{ Watts} \quad (3)$$

which is a miniscule amount of power. The basic reason for this arises from the fact that the prefactor

$$G/c^5 \sim 10^{-53} (\text{Watts})^{-1} \quad (4)$$

in Einstein's quadrupole formula (1), is an extremely small number. This is a consequence of the fact that Newton's constant  $G$ , which is a tiny number to begin with, is combined with the inverse quintic power of the speed of light  $c$ , which is yet a much tinier number.

Put differently, there arises a characteristic power  $P_{\text{GR}}$  in general relativity which is given by the fundamental constants  $G$  and  $c$  in the combination:

$$P_{\text{GR}} \equiv \frac{c^5}{G} = 3.6 \times 10^{52} \text{ Watts} \quad (5)$$

As pointed out by MTW in the beginning of their classic text [4], the only place where such enormous powers could occur

naturally is in astrophysical sources, such as supernova explosions. In fact, the first direct observation of gravitational waves by LIGO [2], was in the merger of a pair of massive black holes orbiting each other at relativistic speeds – an extreme case of an astrophysical source. Thus it would seem impossible, for all practical purposes, for gravitational radiation power ever to be produced in laboratory sources.

However, note that Planck's constant  $\hbar$  is absent from Einstein's quadrupole formula (1) for the emission of gravitational radiation. Could the “new engineering or a new idea or both” as suggested in the above quotation from MTW, be “quantum engineering,” in which  $\hbar$  somehow replaces  $G$  and  $c$ , so that the necessity for the use of astrophysical sources for the generation of gravitational waves could somehow be avoided? Here we propose a possibly affirmative answer to this question that involves the laser-like generation of gravitational radiation via the process of the Dynamical Casimir Effect [7].

The starting point for this new “quantum engineering” approach to the generation of gravitational waves is the assumption that the Uncertainty Principle:

$$\Delta E \Delta t \geq \frac{\hbar}{2} \quad (6)$$

leads to the existence of zero-point fluctuations with the zero-point energy:

$$E_0 = \frac{1}{2} \hbar \omega \quad (7)$$

for any kind of wave which oscillates with a frequency  $\omega$ . In particular, this zero-point energy should apply to gravitational waves, as well as to electromagnetic waves. In the case of gravitational waves, note that the size of the zero-point energy (7) is independent of Newton's constant  $G$  and of the speed of light  $c$ . Rather, it depends solely on Planck's constant  $\hbar$  and the frequency  $\omega$ . Although  $\hbar$  is a tiny number, its tininess can be compensated for by the exponential growth of the gravitational wave arising from the process of stimulated emission of radiation, just as in the case of the laser.

Stimulated emission of gravitational-wave quanta, i.e., of gravitons, follows from a quantum treatment of the radiation oscillators [8] that result from a *linearization* of the theory of general relativity [9], in which the metric tensor  $g_{\mu\nu}$  is decomposed into the Minkowski metric tensor components  $\eta_{\mu\nu} = \text{diag}(-1; +1; +1; +1)$ , which are large, and the metric deviation tensor components  $h_{\mu\nu}$ , which are small, viz.,

$$g_{\mu\nu} = \eta_{\mu\nu} + h_{\mu\nu} \quad (8)$$

The small, simple harmonic motion of the linearized gravitational radiation oscillators can be quantized by means of the standard quantization condition:

$$[a_G, a_G^\dagger] = 1 \quad (9)$$

where  $a_G$  is the annihilation operator for a given gravitational radiation oscillator, and  $a_G^\dagger$  is the creation operator for the same radiation oscillator (all other commutators for nonidentical radiation oscillators being set equal to zero). It follows from the canonical commutator (9) that:

$$a_G^\dagger |n_G\rangle = \sqrt{n_G + 1} |n_G + 1\rangle \quad (10)$$

where  $|n_G\rangle$  is the number state containing  $n_G$  gravitons in a giv-

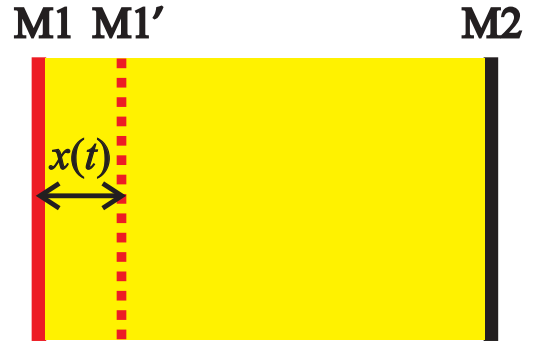


**Fig. 1: Sketch of the Dynamical Casimir Effect (“DCE”).** A Fabry-Perot cavity consists of two parallel mirrors M1 and M2. Mirror M1 is moving back and forth sinusoidally with a time-dependent displacement  $x(t)$  relative to mirror M2, which is a stationary mirror. The piston-like pumping action of M1 upon the vacuum fluctuations contained inside the Fabry-Perot cavity amplifies them parametrically so that they will become macroscopically observable radiation (indicated in yellow) that fills up this resonator.

en mode of the radiation field (i.e., an excitation of a given radiation oscillator with  $n_G$  quanta), and  $|n_G + 1\rangle$  is the number state containing  $\sqrt{n_G + 1}$  gravitons. As Feynman has pointed out in [10], the creation of an extra radiation quantum with the probability amplitude of  $\sqrt{n_G + 1}$  in the recursion relationship (10) leads to the process of stimulated emission of radiation. Hence the recursion relationship (10) implies the possibility of the laser-like generation of gravitational radiation.

Fig. 1 is an illustration of the Dynamical Casimir Effect (“DCE”), in which a moving mirror M1 (red) of an initially empty Fabry-Perot interferometer moves sinusoidally with a displacement  $x(t)$  relative to a fixed mirror M2 [11] [12]. The back-and-forth motion of mirror M1 is like the back-and-forth motion of a piston that can do work on the vacuum fluctuations which are contained within the two mirrors of the Fabry-Perot cavity, thus amplifying them into laser-like light (yellow) via the process of stimulated emission of radiation. However, unlike in an ordinary laser, there is no need here for the introduction of a medium consisting of two-level atoms with inverted populations in between the two mirrors of the Fabry-Perot, since the push-and-pull mechanical pumping motions of the mirror M1, in conjunction with the vacuum fluctuations in EM or GR radiation fields as “seed radiation,” are sufficient for the laser-like, coherent generation of both EM and GR kinds of radiations.

In other words, even if the Fabry-Perot resonator in Fig.1 were to be initially totally empty except for vacuum fluctuations, the pumping action of the mechanically moving mirror upon these fluctuations will cause the resonator to fill up with radiation (indicated by the yellow region in between M1 and M2 in Fig. 1), seemingly “out of nothing,” just as coherent light is seemingly generated “out of nothing” in a laser above its threshold. This is because the action of the moving mirror is like the action of a moving piston which pushes and pulls on a gas of photons or gravitons contained within the resonator. Thus the piston can impart energy into this gas. As a result, the action of the piston can parametrically amplify the radiation contained inside the resonator [13], so that it can become, via an exponential growth mechanism [7], a macroscopically observable beam of coherent radiation, just as in a laser.

Nation et al [14] have pointed out that the quantum amplifi-

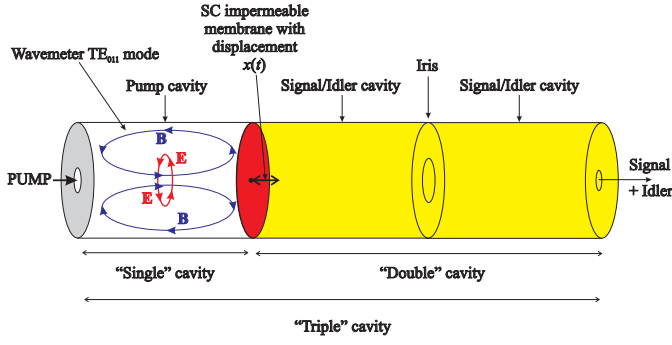


Fig. 2: “Triple” cavity parametric amplifier (paramp) is divided into three adjacent superconducting (SC) cylindrical chambers.

The first chamber (i.e., the pump cavity) is separated from the second and third chambers (i.e., the signal and idler cavities) by an impermeable SC membrane (red), which is the active element of the paramp that can be driven into motion with a displacement of  $x(t)$  by radiation pressure from a pump wave of the “single” cavity. The initially empty SC “double cavity” on its right side then fills up with radiation (yellow) that grows exponentially out of vacuum fluctuations in the DCE.

cation process in the Dynamical Casimir Effect (DCE) is equivalent to the amplification process in a parametric amplifier (paramp), such as the one in the “triple” cavity paramp configuration illustrated in Fig. 2, in which a membrane is pumped into mechanical motion by the radiation pressure from pump microwaves in the leftmost “single” cavity. This membrane moves like the moving mirror M1 in Fig. 1 with a sinusoidal displacement  $x(t)$  that amplifies the signal and idler waves inside the “double” cavity on the right side of the membrane [15].

For this and similar paramps, Nation et al [14] give the following threshold:

$$v_{\max} \geq \frac{c}{Q} \quad (11)$$

where  $v_{\max}$  is the threshold speed of the moving mirror in Fig. 1, or of the moving membrane in Figure 2, where  $c$  is the vacuum speed of light, and where  $Q$  is the quality factor of the cavity for producing the DCE. The maximum velocity amplitude of the moving membrane at threshold is given by:

$$v_{\max} = \Omega \varepsilon_{\max} \quad (12)$$

where  $\Omega$  is the angular frequency of the sinusoidal mechanical motion of the moving mirror (i.e., of mirror M1 in Figure 1, or of the moving membrane in Figure 2), and where  $\varepsilon_{\max}$  is the maximum displacement in the sinusoidal motion of this mirror at threshold.

For superconducting radio frequency (“SRF”) cavities with  $Q$  in the order of  $10^{10}$  [16], we see the  $v_{\max}$  will be in the order of centimeters per second, which is clearly a non-relativistic velocity scale that is readily achievable under laboratory conditions. Therefore, although the generation of radiation is a relativistic effect, the motion of the mirror that generates the DCE at its threshold is non-relativistic due to the high quality factors of SRF cavities. One can understand the non-relativistic threshold condition (11) as arising from a multiple-imaging effect, along with its cumulative Doppler shifts, that occurs repetitively between the moving mirror M1 and the fixed mirror M2 of the Fabry-Perot cavity in Fig. 1 [17].

Converting (11) into an expression for the kinetic energy in the motion of a mirror with a mass  $m$ , we find:

$$U_{\text{kin}} = \frac{1}{2} m v_{\max}^2 \geq \frac{1}{2} \frac{m c^2}{Q^2} \quad (13)$$

If the mirror M1 in Fig.1 were to be driven on its left side by radiation pressure from a pump wave stored inside a separate high- $Q$  pump cavity on the left side of M1 (not shown in Fig. 1, but shown in Fig. 2), then by energy conservation, we find that the required amount of pump power that needs to be injected into the pump cavity for the DCE at threshold, would be:

$$P_{\text{thres}} \geq \frac{U_{\text{kin}}}{\tau_p} = \omega_p \frac{U_{\text{kin}}}{Q_p} \quad (14)$$

where  $\tau_p$  is the “cavity ring-down time” for the energy stored inside the pump cavity. The last equality follows from the fact that the pump-cavity quality factor  $Q_p$  is related to the pump cavity ring-down time  $\tau_p$  by  $Q_p = \omega_p \tau_p$  where  $\omega_p$  is the angular frequency of the pump wave.

For the “triple-cavity” paramp pictured in Fig. 2 whose membrane (red) is being pumped from the left by a radiation pressure force, the frequency of the mechanical motion of this moving membrane will be at the *second harmonic*  $2\omega_p$  of the pump frequency. The meaning of the equality in (14) is that in steady-state equilibrium, the amount of pump power being injected into the “single” pump cavity through the left porthole of this cavity must be balanced by the amount of mechanical power leaking away from the system due to the fact that pump waves which are driving the motion of the membrane will also be escaping from the “single” pump cavity through the same porthole, or will be lost into heat.

Now if we set  $Q_p = Q$  (i.e., that the pump and the DCE cavities to the left and to the right of the moving membrane in Fig. 2, will have comparable  $Q$  values), then it follows from (13) and (14) that the injected pump power for achieving threshold for the DCE should be:

$$P_{\text{thres}} \geq \frac{1}{2} \frac{m \omega_p c^2}{Q^3} \quad (15)$$

where  $m$  is the mass of the moving mirror,  $\omega_p$  is the pump frequency, and  $Q$  is the quality factor of cavities. Note that this DCE threshold power scales inversely as the *cube* of the  $Q$  value of the pump and the DCE cavities. This points out the importance of utilizing cavities with the highest possible  $Q$  values in order to be able to achieve the DCE with reasonable pump powers. Therefore, SRF cavities with  $Q \sim 10^{10}$  [16] would be good candidates for this purpose.

A more detailed derivation of the threshold power (15) is given in [7], and yields the following result:

$$P_{\text{thres}} \geq \frac{m \omega_p \omega_s \omega_i L^2}{4 Q_p Q_s Q_i} \quad (16)$$

where  $m$  is the mass of the moving membrane, where  $\omega_p$ ,  $\omega_s$ , and  $\omega_i$  are respectively, the pump, signal, and idler frequencies of the “triple” cavity depicted in Fig. 2, where  $L$  is the length of the “double” cavity in Fig. 2, and where  $Q_p$ ,  $Q_s$ , and  $Q_i$  are respectively, the pump, signal, and idler quality factors of the three tandem SRF cavities that constitute the “triple” paramp cavity.



Numerically, if we assume that:

$$m = 3 \text{ milligrams} \quad (17)$$

$$\omega_p \approx \omega_i \approx \omega_s \approx 2\pi \times 10 \text{ GHz} \quad (18)$$

$$L \approx \lambda_i \approx \lambda_s \approx 3 \text{ cm} \quad (19)$$

$$Q_p \approx Q_i \approx Q_s \approx 10^{10} \quad (20)$$

then we conclude that for observing the DCE, and thus the generation of gravitational microwave radiation, the threshold pump power at a frequency of 10 GHz to be injected through the left hole of the “triple” paramp cavity of Fig. 2, needs to be at least:

$$P_{\text{thres}} \approx 0.17 \text{ microwatts} \quad (21)$$

which is easily achievable experimentally.

A crucial question now arises: How can we construct a high-Q cavity for gravitational radiation when we know that all known ordinary (that is, nonastrophysical) material, are essentially completely transparent to this kind of radiation? To answer this question, consider a (x) polarized GR plane wave incident upon a square piece of SC (yellow square), as pictured in Fig. 3(a).

The strain fields  $h_{\mu\nu}$  of the incident GR wave will interact with the stress-energy tensor  $T^{\mu\nu}$  of the SC via the interaction Hamiltonian density [19]:

$$H'_{\text{interaction}} = \frac{1}{2} h_{\mu\nu} T^{\mu\nu} \quad (22)$$

In particular, the instantaneous spatial components of the transverse-traceless metric deviation tensor  $h_{ij}^{(\times)}$  for a (x) polarized plane wave, described in Cartesian  $(x, y)$  coordinates in a plane  $z = \text{constant}$  perpendicular to the  $+z$  propagation direction of the wave, are given by the following matrix [4]:

$$\begin{pmatrix} h_{ij}^{(\times)} \end{pmatrix} = \begin{pmatrix} h_{xx} & h_{xy} \\ h_{yx} & h_{yy} \end{pmatrix} = h_0(z - ct) \begin{pmatrix} +\frac{1}{2}(x^2 - y^2) & xy \\ xy & -\frac{1}{2}(x^2 - y^2) \end{pmatrix} \quad (23)$$

where  $(i, j) = (x, y)$  and where  $h_0(z - ct)$  is the dimensionless strain of space due to the passage of the plane wave. A snapshot of the tidal “force” fields that are produced by the metric deviation tensor  $= h_{ij}^{(\times)}(x, y, z, t)$  in (23) is represented by the hyperbolae (blue curves) in Fig. 3(a). One can easily verify by direct substitution that the Ansatz given in (23) is a transverse-traceless vacuum solution to the wave equation that follows from linearized general relativity, viz.,

$$\nabla_{\perp}^2 h_{ij}^{(\times)} + \frac{\partial^2 h_{ij}^{(\times)}}{\partial z^2} - \frac{1}{c^2} \frac{\partial^2 h_{ij}^{(\times)}}{\partial t^2} = 0 \quad (24)$$

where  $\nabla^2$  is the transverse Laplacian in a Cartesian  $(x, y)$  coordinate system, where  $+z$  is the direction of propagation of the plane wave  $h_{ij}^{(\times)}(x, y, z, t)$  (23) into the page that is depicted in Figure 3(a), and where  $c$  is the speed of light.

The highly unusual quantum response of the SC square (yellow) to this wave, which we called the “Heisenberg-Coulomb” effect in [18], is illustrated in Fig. 3(b). Quantum mechanics on a macroscopic length scale inside the SC takes effect below the SC transition temperature, due to the fact that Cooper pairs are bosons that will all undergo Bose-Einstein condensation

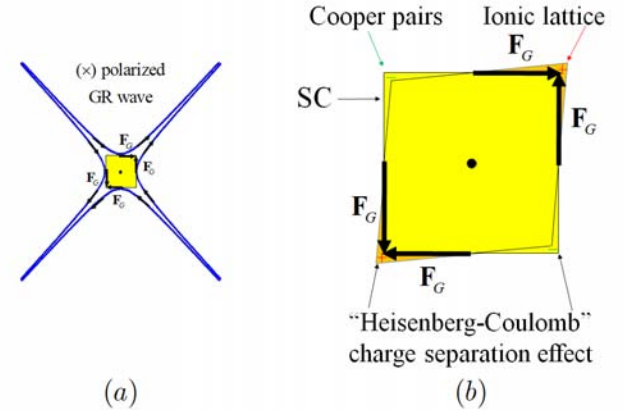


**Fig. 3:** (a) A quadrupolar pattern (blue) of an incident (x) polarized GR plane wave propagating into the page, impinges upon a square piece of superconductor (yellow). Tidal “forces”  $F_G$  acting upon the square due to this wave exert a shear stress. (b) The strain of the ionic lattice of the square superconductor (SC) due to this stress causes a slight extrusion of positive (+) charge into corners of a rhombus (orange) produced by the wave, but the Cooper pairs (yellow) of the SC will not respond, since they are all Bose-condensed in a nonlocalizable, zero-momentum eigenstate. There results an extrusion of negative (–) charge into corners of an undistorted square (yellow), in a “Heisenberg-Coulomb” charge separation effect [18]. The Coulomb attraction of the (+) and (–) charges opposes the tidal “forces”  $F_G$ , leading to a huge GR-EM coupling.

into the lowest possible energy state of the system, namely the unique ground state in which all the bosons occupy the same single-particle zero-momentum eigenstate relative to the center of mass of the SC (which is represented by the large black dot at the center of the yellow square in Figure 3(b)). Because their momenta will all be exactly known in the zero-momentum eigenstate (their momenta will all certainly be exactly zero), it follows from the Heisenberg Uncertainty relations for momentum and position that the locations of the Cooper pairs inside the SC square will be completely uncertain. Thus the Cooper pairs are all completely non-localizable within the SC square in Fig. 3.

It therefore follows from Heisenberg's Uncertainty Principle that the Cooper pairs cannot respond at all to the passage of the gravitational plane wave, in contrast to the response to this wave of the ions inside the ionic lattice, which are all completely localizable, since they will be located at the lattice sites of the ionic lattice inside the SC material. Since the microwave frequencies of the incident gravitational plane wave in Fig. 3 are typically orders of magnitude higher than the typical acoustical frequencies of the ionic lattice, it follows that the ions will move essentially as freely falling masses along the geodesics of general relativity in their response to the passage of the plane wave. By contrast, the Cooper pairs are completely nonlocalizable due to the uncertainty principle, and therefore it is forbidden in quantum mechanics for them to follow any classical trajectory, including the geodesics of general relativity. This difference in response of the Cooper pairs and lattice ions has been demonstrated quantitatively in [20][21].

One can arrive at this same conclusion from another point of view. The quantum adiabatic theorem tells us that for any SC sample, the BCS ground state, which is separated from all possible excited states by the BCS energy gap,  $E_{\text{BCS}}$ , cannot respond to any slowly varying external perturbation whose characteristic frequency lies well below the BCS gap frequen-

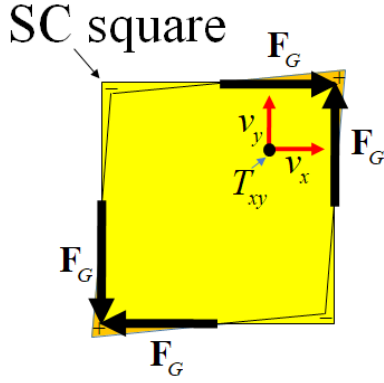


**Fig. 4:** Gravitational Meissner-like effect inside a SC square (yellow) subjected to tidal “forces”  $F_G$  from the  $(\times)$  polarized gravitational plane wave depicted in Fig. 3. The stress-energy tensor  $T_{xy}$  at a point along the main diagonal of the rhombus (orange) produced in response to the tidal “forces”  $F_G$ , is a tensor product of the two supercurrent vector components  $v_x$  and  $v_y$ , both of which decay into the interior on the scale of the London penetration depth.

cy of  $f_{\text{BCS}} = E_{\text{BCS}}/2\pi\hbar$ . For the case of niobium,  $E_{\text{BCS}}$  is around 3 meV, corresponding to a BCS gap frequency  $f_{\text{BCS}} \approx 730$  GHz. Therefore any perturbations arising from an incident GR wave whose typical frequency lies in the microwave range of around 10 GHz, which is much less than 730 GHz, cannot cause any transitions out of the BCS ground state. Hence the Cooper pairs inside the SC (niobium) square of Fig. 3 will remain rigidly in the BCS ground state, and cannot respond to the incident GR microwaves at 10 GHz that we are using in our experiments.

However, the ions of the ionic lattice of the SC will undergo free fall in response to the Newtonian tidal “forces”  $F_G$  (i.e., the blue hyperbolae in Fig.3(a)). Thus the ionic lattice will undergo a shear strain that distorts the SC square (yellow) into a rhombus (orange), as shown in Figs. 3 and 4. This rhomboidal distortion leads to an extrusion of positive ionic charges into the acute corners of the rhombus (orange corners labeled by (+) signs). The overall charge of the SC, however, must remain neutral. Hence the corners of the original square (yellow) (labeled by (−) signs) adjacent to obtuse corners of the rhombus must have compensating extrusions of negative charges arising from the negative charges of the Cooper pairs that remain in these corners during the rhomboidal distortion of the ionic lattice because of the fact that these pairs must remain adiabatically in their zero-momentum ground state everywhere.

There results a “charge-separation effect” (or “Heisenberg-Coulomb effect”; see below) [18] [20] [22], in which positive charges appear near the acute corners of the rhombus of Figs. 3 and 4, but negative charges appear near the obtuse corners of this rhombus. This leads to a huge Coulomb force of attraction between the separated positive and negative charges that strongly opposes the Newtonian tidal “forces”  $F_G$  of the incoming gravitational wave that produced this charge separation in the first place. There arises an enormously stiff effective Hooke’s law, i.e., a strong restoring force inside the SC material, in that there will arise an enormous Coulomb-strength back-action that strongly resists the tidal action of the incoming gravitational plane wave, so much so that this wave is *expelled*, and therefore *reflected*, from the SC square, in what we shall call a “gravitational Meissner effect.” Since this effect re-

sults from a combination of the Heisenberg Uncertainty Principle with the huge Coulomb force of attraction that arises from the resulting separation of the ions from the Cooper pairs, we have dubbed this the “Heisenberg-Coulomb effect.” Therefore this effect differs from the usual “charge-separation effect” that occurs in electrically polarized dielectrics in response to the application of an electric field firstly because it is a response to the *tensor*  $h_{ij}$  field of gravitational radiation, and not to the *vector* electric field of electromagnetism; and secondly because it is purely quantum mechanical in nature, and possesses no classical explanation.

According to [18] [22] [23], the strength of the “Heisenberg-Coulomb” effect is characterized by the ratio of the strength of the Coulomb electrical force between two electrons to the strength of their Newtonian gravitational force:

$$\left| \frac{F_{\text{Coulomb}}}{F_{\text{Newton}}} \right| = \frac{e^2}{4\pi\epsilon_0 r^2 (Gm_e^2/r^2)} = \frac{e^2}{4\pi\epsilon_0 Gm_e^2} \approx 4.2 \times 10^{42} \quad (25)$$

where  $e$  is the electron charge,  $\epsilon_0$  is the electrical permittivity of free space,  $G$  is Newton’s constant, and  $m_e$  is the mass of the electron (note that the Coulomb and Newtonian forces both obey inverse-law force laws, so that this result is independent of distance  $r$  between the two electrons). The ratio given by (25) is obviously a huge dimensionless number.

One surprising consequence of the enormous number (25) predicted in [18] is that it leads to such an enormous enhancement of the reflection process from the SC square that the SC behaves like a material with hard-wall boundary conditions with respect to the incident gravitational wave, and thus behaves like a highly reflective mirror. But for such a hard-wall reflection to occur, it is necessary that the incident gravitational wave would somehow generate sufficiently strong mass currents on the surface of the mirror such that these currents would then re-radiate a plane wave in the forwards direction that would cancel out the incident wave, and would simultaneously re-radiate a plane wave in the backwards direction that is 180 degrees out of phase with respect to the incident wave, in order to create the totally reflected wave.

Due to the enormity of the “Heisenberg-Coulomb effect” predicted in (25), there could indeed arise such enormous quantum-mechanical mass supercurrents, which are induced by the extremely tiny strains of space associated with the incident gravitational plane wave, so that even the tininess of Einstein’s coupling constant  $8\pi G/c^4$  that couples sources to fields in Einstein’s field equations, might somehow be overcome during reflection. But how could one possibly reconcile this with the Einstein field equations without somehow modifying its extremely tiny  $8\pi G/c^4$  coupling constant?

There already exists a hint as to how to handle this situation in magnetostatics, in which the field equation in the vacuum is given by Ampere’s law:

$$\nabla^2 \mathbf{A} = -\mu_0 \mathbf{j} \quad (26)$$

where  $\mathbf{A}$  is the vector potential from which the magnetic field is derived,  $\mu_0$  is the magnetic permeability of free space (i.e., the vacuum without any medium), and  $\mathbf{j}$  is the total current density, which is the source of this field equation.

However, suppose that there exists a magnetic medium with

a relative magnetic permeability  $\mu_r$ , such as some ferromagnetic material that fills all of space. It is a well known empirical fact that the insertion of a high-permeability ferromagnetic material, such as iron, into the interior of an electromagnet will greatly enhance the strength of the magnetic field generated by this electromagnet. This empirical fact provides ample justification for a modification of the field equation (26), in which one inserts a prefactor  $\mu_r$  in front of the source-to-field coupling constant  $\mu_0$ , so that this modified field equation now reads:

$$\nabla^2 \mathbf{A} = -\mu_r \mu_0 \mathbf{j} \quad (27)$$

Thus in the presence of a homogeneous and isotropic magnetic medium, there exists a dimensionless number  $\mu_r$  (i.e., the “relative permeability” of the medium), which has a sign and a magnitude that must be determined by experiment, as the prefactor of the source term in the field equation (27).

Now for most “normal” materials, it turns out that the magnitude of  $\mu_r$  is very close to unity. Both signs of the permeability for magnetic materials (i.e., diamagnetic and paramagnetic signs) exist in nature, but all of these permeabilities are quantum mechanical, and not classical, in origin [24]. In both cases of diamagnetism and paramagnetism, quantum mechanical currents are required to explain the phenomena. Moreover, in the case of ferromagnetic materials,  $|\mu_r|$  has been observed to have very large values, such as  $10^6$  in iron-nickel alloys.

Note that one must carefully distinguish here between the “relative permeability” and the “relative permittivity” of material media, because the magnetic response of a given material is fundamentally different from its electric response, since the magnetic field is fundamentally different in nature from the electric field. Likewise, the question now arises: Does one need to make similar distinctions in the case of the different possible responses of various kinds of material media to the different kinds of gravitational fields in general relativity?

We argue here that the answer to this question is yes. One reason for this affirmative answer is that we know that in general relativity, there exists the Lense-Thirring field, which is a *gravito-magnetic* field, which is fundamentally different in nature from the usual Newtonian gravitational field, which is a *gravito-electric* field. However, in addition to these two kinds of fields, there exists in general relativity a third, fundamentally different kind of field, namely, the transverse-traceless  $h_{ij}$  *gravito-tensor* field associated with gravitational radiation, which has no analog in electromagnetism. In general relativity, we know that the different components of the stress-energy tensor  $T_{\mu\nu}$  can be sources for three different possible kinds of gravitational fields, and thus in principle can lead to three different possible kinds of responses of different material media to gravitational fields, namely, a scalar, a vector, and a tensor response, which correspond to the components  $T_{00}$ ,  $T_{0i}$ , and  $T_{ij}$  of the tensor  $T_{\mu\nu}$ , respectively.

The modification of Ampere's law (27) in order to allow for the different possible responses of homogeneous and isotropic magnetic media due to an applied magnetic  $\mathbf{H}$  field arising from a solenoid, for example, justifies a similar modification of Einstein's field equations, after they have been reduced to a linearized wave equation for  $h_{ij}$ , in order to allow for the possibility of different responses of homogeneous and isotropic material media to a gravitational wave. In particular, there could arise enormous quantum-mechanical mass supercurrents induced in a superconductor due to even a tiny applied  $T_{ij}$  stress field

arising from the incident ( $\times$ ) polarized plane wave depicted in Figs. 3 and 4, which, in light of the above “Heisenberg-Coulomb” effect, would lead to internal electric fields inside the superconductor that would drive these enormous supercurrents.

Before modification, the wave equation for gravitational waves is [25]

$$\nabla^2 h_{ij} - \frac{1}{c^2} \frac{\partial^2 h_{ij}}{\partial t^2} = -2\kappa_0 T_{ij} \quad (28)$$

where the extremely tiny dimensionful constant

$$\kappa_0 = \frac{8\pi G}{c^4} \quad (29)$$

is Einstein's coupling constant for the vacuum in the absence of any medium. The dimensionful constant  $\kappa_0$  is analogous to the dimensionful constant  $\mu_0$ , the magnetic permeability of free space (i.e., for the vacuum in the absence of any magnetic medium) in Ampere's law (26).

After making the proposed modification, in which one inserts a prefactor  $\kappa_r$  in front of the source-to-field coupling constant  $\kappa_0$ , the wave equation for gravitational waves now reads as follows:

$$\nabla^2 h_{ij} - \frac{1}{c^2} \frac{\partial^2 h_{ij}}{\partial t^2} = -2\kappa_r \kappa_0 T_{ij} \quad (30)$$

where the dimensionless number  $\kappa_r$  on the right hand side of this wave equation [26] [27], is an empirically determined constant that we shall call the “relative gravitational permeativity” [28], in analogy with  $\mu_r$ , the “relative magnetic permeability” that was introduced into Ampere's law (27). Although the typical sizes of the relative permeability observed in ferromagnetic media  $|\mu_r| \sim 10^6$  may not be as large as the typical sizes of the relative gravitational permeativity  $|\kappa_r|$  that may eventually be observed in future experiments in superconducting media, both the sign and the magnitude of  $\kappa_r$  must ultimately be arrived at empirically; they cannot be ruled out on any *a priori* basis [29].

Now for most “normal” materials, the relative gravitational permeativity  $\kappa_r$  will most likely be very close to unity, so that these media will be essentially completely transparent to gravitational waves. Note, however, that the wave equation (30) is still *linear*, even after the inclusion of the prefactor  $\kappa_r$ . This *linearity* leads to the applicability of the superposition principle for the solutions of this wave equation, and also permits the resulting classical waves to be quantized using the canonical quantization procedure outlined above.

For a superconductor, however,  $\kappa_r$  may turn out to be huge. Although an estimate based on an incorrect *vector* coupling theory yields  $|\kappa_r| \sim 10^{42}$  (as in (25) based on [18] [23]), both the sign and the magnitude of this empirical constant must ultimately be determined by measurements, such as via the Fresnel reflection coefficient  $|\rho(\omega)|^2$  off of the surface of a square plate, which is given by

$$|\rho(\omega)|^2 = \left| \frac{n(\omega) - 1}{n(\omega) + 1} \right|^2 \quad (31)$$

where  $n(\omega)$  is given by a plasma-like formula for the index of refraction, as shown in Appendix B. This measurement of  $|\rho(\omega)|^2$ , however, has never been performed, since there exist at



the present time no laboratory sources for gravitational waves.

But perhaps the strongest reason for introducing the “relative gravitational permeativity”  $\kappa_r$  into the wave equation (30), would be the existence of a “gravitational Meissner-like effect.” To this end, let us consider evaluating the stress-energy tensor  $T_{xy}$  at a point along the major diagonal of the rhombus sketched in Figs. 3 and 4. Since any second-rank tensor can be written as a tensor product of two vectors, one can always express  $T_{xy}$  as the direct product

$$T_{xy} \propto v_x v_y \quad (32)$$

where  $v_x$  and  $v_y$  are the  $x$  and  $y$  components of some vector field inside the SC. But the only physically relevant vector field in the problem at hand is the quantum-mechanical supercurrent velocity vector field that is induced by the incident ( $\times$ )-polarized gravitational plane wave sketched in Fig. 3(a).

Now the supercurrent velocity field  $\mathbf{v}$  is directly proportional to the supercurrent density  $\mathbf{j}$ , which in turn is directly proportional to vector potential  $\mathbf{A}$  via London's constitutive relationship. This leads to the following proportionalities:

$$\mathbf{A} \propto \mathbf{j} \propto \mathbf{v} \quad (33)$$

But Ampere's law leads to the following equalities:

$$\nabla \times \mathbf{B} = \nabla \times \nabla \times \mathbf{A} = \mu_0 \mathbf{j} \quad (34)$$

Using the vector identity:

$$\nabla \times \nabla \times \mathbf{A} = \nabla (\nabla \cdot \mathbf{A}) - \nabla^2 \mathbf{A} \quad (35)$$

and using the London gauge  $\nabla \cdot \mathbf{A} = 0$ , one then arrives at London's equation, i.e., the following Yukawa-like equation with an empirical constant  $\kappa_L$ :

$$\nabla^2 \mathbf{A} - \kappa_L^2 \mathbf{A} = 0 \quad (36)$$

which is a linear PDE. Using London's constitutive relations (33), we also arrive at the following Yukawa-like, linear PDE for the supercurrent velocity field:

$$\nabla^2 \mathbf{v} - \kappa_L^2 \mathbf{v} = 0 \quad (37)$$

For the transverse supercurrent velocities flowing in the SC square configurations of Figs. 3 and 4, we find the following two PDEs:

$$\begin{aligned} \frac{\partial^2 v_x}{\partial z^2} - \kappa_L^2 v_x &= 0 \\ \frac{\partial^2 v_y}{\partial z^2} - \kappa_L^2 v_y &= 0 \end{aligned} \quad (38)$$

These equations possess the following exponentially decaying solutions:

$$v_x(z) = v_x(0) \exp(-\kappa_L z) = v_x(0) \exp(-z/\lambda_L) \quad (39)$$

$$v_x(z) = v_x(0) \exp(-\kappa_L z) = v_x(0) \exp(-z/\lambda_L) \quad (40)$$

where the London penetration depth  $\lambda_L$  is given by

$$\lambda_L = \frac{1}{\kappa_L} \quad (41)$$

For superconducting niobium,  $\lambda_L$  is measured to be around 40 nm.

From the tensor product relationship (32) and from the solutions for the supercurrent velocity field components (39) and (40), we conclude that the stress-energy tensor has the following  $z$  dependence

$$T_{xy}(z) \propto v_x(z) v_y(z) = (v_x(0) \exp(-z/\lambda_L)) \cdot (v_y(0) \exp(-z/\lambda_L)) \quad (42)$$

Therefore it follows that the exponential decay solution for the stress-energy tensor in the  $z$  direction is given by

$$T_{xy}(z) = T_{xy}(0) \exp(-2z/\lambda_L) \propto \exp(-2z/\lambda_L) \quad (43)$$

so that  $T_{xy}(z)$  decays twice as fast as the supercurrent velocity field into the depth of the SC. Therefore the exponential decay length scale of  $T_{xy}$ , i.e., its gravitational penetration depth, is *half* that of the electromagnetic London penetration depth (41).

Now from the linearity of the wave equation (30) and from the solution (43), we conclude that the solution for the gravitational wave field  $h_{xy}$  penetrating into the SC square must also obey the proportionality relations

$$h_{xy}(z) \propto T_{xy}(z) \propto \exp(-2z/\lambda_L) \quad (44)$$

Therefore we conclude that the gravitational wave amplitude  $h_{xy}$ , like  $T_{xy}$ , decays *twice* as fast as the supercurrent velocity field into the depth of the SC. Hence the exponential decay length scale of gravitational plane amplitude  $h_{xy}(z)$  deep inside the SC is also half that of the usual electromagnetic London penetration depth (41), i.e., around 20 nm for the case of niobium. This is a “gravitational Meissner-like effect” that will lead to the *expulsion* of the incident gravitational plane wave from the interior of the SC square in Figs. 3 and 4, and therefore will lead to a mirror-like total *reflection* of this wave.

## EXPERIMENTAL PROGRESS

Now we present a progress report concerning our experiments towards achieving the goal of observations of the DCE and of the laser-like generation of gravitational waves.

Fig. 5 overleaf shows a photograph of a silicon nitride membrane sample, which is coated with niobium on its back side. [33] This membrane will be the active amplifying element in our paramps. We are planning to place the sample shown in Fig. 5 at the center of a degenerate paramp as a vibrating membrane (red) driven by pump microwaves, as sketched in Fig 6 overleaf.

In this dual-SRF cavity setup, the pump injected into the left chamber is identical in frequency to the signal and idler frequencies that will be produced in the DCE in the right chamber (yellow in Fig. 6) above a certain threshold. Due to our prediction that the London penetration depth for GR waves will be *half* that for EM waves, the modal volume for the right

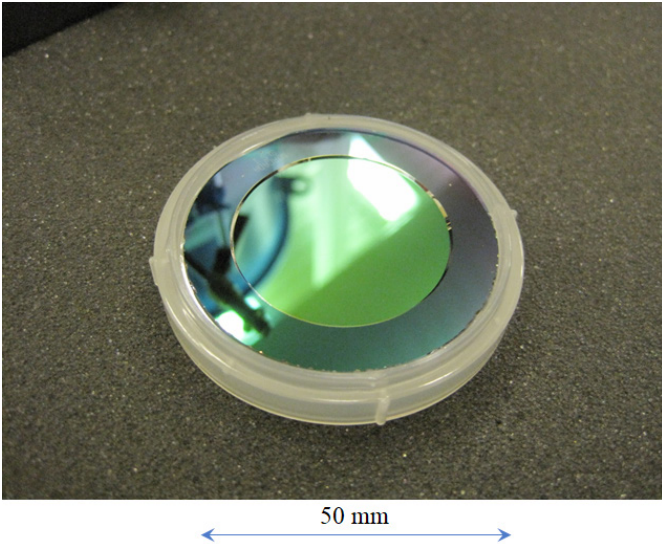


Fig. 5: A flexible silicon nitride membrane (green; 500 nm thick) is stretched over a circular window frame of an etched silicon wafer (gray; 50 mm diameter). A niobium coating (not shown) is sputtered onto the other side of the membrane.

chamber at resonance will be slightly smaller for the case of GR wave generation as compared to the case of EM wave generation. Hence, there should be a well resolved difference in the position of the tuner (green) for EM wave production relative to that for GR wave production inside the right chamber. This difference will be a convenient signature that we can use to distinguish between the two cases.

However, since the detection of GR waves will be difficult, we will first try to *indirectly* infer that these invisible waves are in fact being generated by looking for a “pump depletion effect” in which there will arise a dip in the reflected pump signal from the left chamber at the threshold for GR wave generation. This dip will arise from the “missing energy” that will be escaping in the form of these invisible waves from the right chamber. Thus we can infer from energy conservation that GR waves are in fact being generated, although they will not be directly detectable.

In a follow-up experiment, we plan to make a copy of the degenerate paramp apparatus pictured in Fig. 6 as a “receiver,”

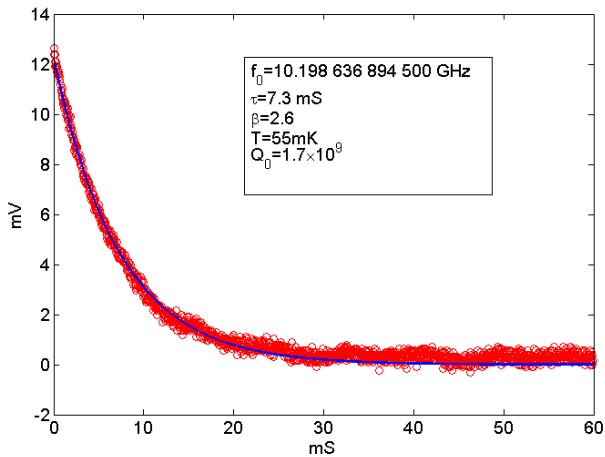


Fig. 7: Exponential decay curve of a TEM microwave mode excitation of an SRF stub cavity with a resonant frequency around 10 GHz. The exponential ring-down time is 7.3 ms, implying a  $Q$  of  $1.7 \times 10^9$  at a temperature of 55 mK.

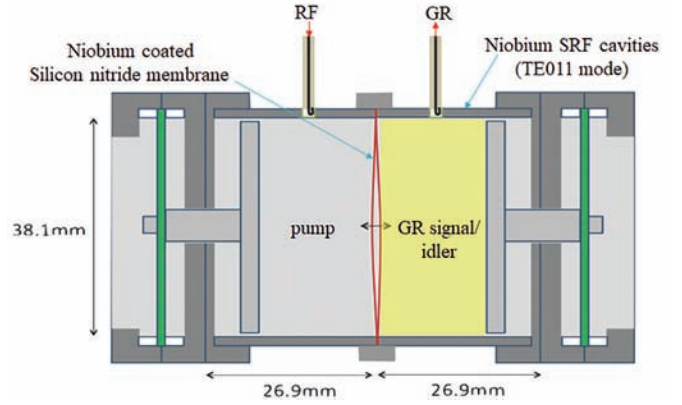


Fig. 6: Degenerate parametric amplifier/oscillator design for generating gravitational radiation (GR) in the signal/idler cavity (yellow) via the mechanical motions (double-headed black arrow) of a silicon nitride membrane coated with SC niobium (red) driven by microwaves in the pump cavity with tuner (green).

and place it side-by-side with respect to the “transmitter,” in a Hertz-like “transmitter-receiver” configuration. The amplification of GR waves in the “receiver” paramp can serve as a low-noise preamp, i.e., a first-stage amplifier, of a GR-wave detection system whose final stage could consist of a membrane-displacement measurement of a final-stage SC membrane and whose displacement arises from the radiation pressure being exerted on the membrane from the received GR waves.

In Fig. 7, we show the progress that we have been making concerning the  $Q$  problem. It turns out that gaps and other imperfections in the joints between the cylindrical body of the SRF cavities and their endcaps can degrade the  $Q$  of the cavity by orders of magnitude. However, by fabricating a seamless resonator using a coaxial stub cavity, one can evade these kinds of degradations of the  $Q$ . Fig. 7 is a plot of data from a ring-down measurement of a SC niobium stub resonator that demonstrates that we can achieve a  $Q$  in the order of a billion at the typical temperature of 55 millikelvin that we have been using in our dilution refrigerators. If we can achieve such a high  $Q$  in the dual-SRF cavity sketched in Fig. 6, we will be well on our way towards demonstrating the DCE and, possibly, the laser-like generation of gravitational waves.

It should be emphasized at this point that we are not trying to detect the received GR waves by measuring the dimensionless *strain* of space produced by these waves, which would be exceedingly tiny (see Appendix A), but rather we shall try to detect the radiation pressure, and hence the received *power*, associated with these waves.

#### APPENDIX A: The strain of space produced by one milliwatt of gravitational microwave power

Since spacetime can be thought of as an extremely stiff medium, the question naturally arises: How could one possibly produce any measurable amount of strain of space, even if one were to succeed in a laser-like scheme for generating gravitational (GR) waves? The short answer is this: One does not need to be able to directly measure the *strain* of space; one only needs to be able to directly measure the *power* in a laser-like

beam of GR waves. Nevertheless, it will be instructive to put in some numbers in order to answer this question. Suppose that one were able to generate one milliwatt of power in a laser-like beam of a GR wave. The gravitational analog of the time-averaged Poynting vector, which is the flux of energy, is given by [34] [35]

$$\langle S \rangle = \frac{\omega^2 c^3}{32\pi G} h_{\times}^2 \quad (45)$$

where  $h_{\times}$  is the strain of space for a ( $\times$ ) polarized plane wave. For one milliwatt of power in such a plane wave at 30 GHz, say, focused by a Newtonian SC telescope to a 1 cm<sup>2</sup> Gaussian beam waist, one obtains a strain of space of

$$h_{\times} \approx 0.8 \times 10^{-28} \quad (46)$$

within the focal area. Such a tiny strain of space would be exceedingly difficult to detect directly, even using advanced LIGO. However, it is unnecessary to directly measure the strain of space in order to detect the GR wave, just as it is unnecessary to directly detect the optical electric field amplitude of a laser beam in order to detect the light wave. Rather, one can directly measure the power carried by the laser-like GR beam, for example by measuring the back conversion of one milliwatt of the incident GR wave power into one milliwatt of EM wave power via a measurement of the radiation pressure exerted by the received GR wave upon a SC membrane in a time-reversed parametric process inside a replica of the dual-SRF cavity of Fig. 6. It would then be easy to detect one milliwatt of the back-converted EM microwave power.

## APPENDIX B: Plasma-like gravitational-wave refractive index of a superconductor

The modified gravitational wave equation in a medium (such as a superconductor (SC)) is

$$\nabla^2 h_{ij} - \frac{1}{c^2} \frac{\partial^2 h_{ij}}{\partial t^2} = -2\kappa T_{ij} \quad (47)$$

where we define

$$\kappa \equiv \kappa_r \kappa_0 \quad (48)$$

where  $\kappa_0 = 8\pi G = c^4$  is Einstein's coupling constant in vacuum, and where  $\kappa_r$  is the “relative gravitational permeativity” of the medium (to be determined by experiment). We shall call  $\kappa$  the “gravitational permeativity” of an SC medium, in analogy with the “magnetic permeability” of a magnetic medium

$$\mu \equiv \mu_r \mu_0 \quad (49)$$

where  $\mu_r$  is the relative magnetic permeability that appears as the prefactor of the source term for Ampere's law in a medium

$$\nabla^2 \mathbf{A} = -\mu \mathbf{j} \quad (50)$$

Let us define the constitutive relation of an SC medium as follows:

$$T_{ij} \equiv -\mu_G h_{ij} \quad (51)$$

where  $\mu_G$  is the “gravitational shear modulus” of the material to an applied  $h_{ij}$  field. Substituting this constitutive relation into the modified wave equation in a medium (47), we find

$$\nabla^2 h_{ij} - \frac{1}{c^2} \frac{\partial^2 h_{ij}}{\partial t^2} = -2\kappa \mu_G h_{ij} \quad (52)$$

Upon substitution of the monochromatic plane wave Ansatz,

$$h_{ij}(x, y, z, t) = A \exp(ikz - i\omega t) \quad (53)$$

into this equation, we obtain the implicit dispersion relation

$$k^2 - \frac{\omega^2}{c^2} = -2\kappa \mu_G \quad (54)$$

Let us now define the “gravitational plasma frequency” as

$$\omega_G \equiv \sqrt{2\kappa c^2 \mu_G} \quad (55)$$

This agrees with [20] since

$$\kappa = \kappa_r \kappa_0 \quad (56)$$

Solving for  $\kappa(\omega)$  from (54), one finds the explicit dispersion relation

$$k(\omega) = \frac{\omega}{c} \sqrt{1 - \frac{\omega_G^2}{\omega^2}} \quad (57)$$

from which we see that the meaning of the plasma frequency is that

$$k(\omega_G) = 0 \quad (58)$$

i.e., that the plasma frequency is a cutoff frequency below which a gravitational wave cannot propagate inside the SC medium because the propagation wave number  $\kappa(\omega)$  becomes a pure imaginary quantity.

Alternatively, let us introduce the index of refraction  $n(\omega)$  as follows:

$$k(\omega) = \frac{n(\omega) \omega}{c} \quad (59)$$

Comparing this with (57), we see that

$$n(\omega) = \sqrt{1 - \frac{\omega_G^2}{\omega^2}} \quad (60)$$

which is a plasma-like index of refraction. Note that for  $\omega < \omega_G$ , the refractive index becomes a pure imaginary quantity, which implies total reflection, just like the reflection from a plasma of an EM wave whose frequency is below cutoff.

Thus the Fresnel reflection formula (31) is [36]

$$|\rho(\omega)|^2 = \left| \frac{n(\omega) - 1}{n(\omega) + 1} \right|^2 \quad (61)$$

## ACKNOWLEDGEMENTS

This work was supported in part by DARPA. We thank Professors Douglas Singleton and Gerardo Muñoz for their help on the theory, and Jacob Pate for his help on the experiments.

This paper is based on a talk given on November 3, 2017 by RYC at the Aerospace Advanced Propulsion Workshop.



## REFERENCES

1. See [https://www.nobelprize.org/nobel\\_prizes/physics/](https://www.nobelprize.org/nobel_prizes/physics/). Note that LIGO is a prototype of an optomechanical experiment.
2. B. P. Abbott et al., "Observation of gravitational waves from a binary black hole merger," *Phys. Rev. Lett.* 116, 061102 (2016).
3. B. P. Abbott et al., "GW170817: Observation of gravitational waves from a binary neutron star inspiral," *Phys. Rev. Lett.* 119, 161101 (2017).
4. C.W. Misner, K.S. Thorne, J.A. Wheeler, *Gravitation* (Princeton University Press, 2017), page 979.
5. L. Landau and E. Lifshitz, *Classical Theory of Fields* (Addison-Wesley, 1951), page 331, Eq. (11-115).
6. A. Einstein, "Über Gravitationswellen," *Sitzungsberichte der Königlich-Preussischen Akademie der Wissenschaften Berlin*, part 1, 154 (1918), A. S. Eddington, "The Propagation of Gravitational Waves," *Proc. Roy. Soc.* 102 A. p. 268 (1922)
7. R. Y. Chiao, R. Haun, N. Inan, B.S. Kang, L.A. Martinez, S.J. Minter, G. Muñoz, and D. Singleton, "A Gravitational Aharonov-Bohm Effect, and its Connection to Parametric Oscillators and Gravitational Radiation," in *Quantum Theory: A Two-Time Success Story*, Yakir Aharonov Festschrift. D. Struppa, and J. Tollaksen, eds. (Springer, 2013), p. 213-246; arXiv 1301.4270. Although it was first suggested in this paper that laser-like generation of gravitational radiation via the Dynamical Casimir Effect using moving SC mirrors could occur, it should be pointed that that we made a mistake in this paper, and also in the paper [18], in that we used the DeWitt minimal coupling rule, and treated gravitational waves as if they were *vector*, and not *tensor*, waves. The DeWitt minimal coupling rule leads to an interaction Hamiltonian of the form  $\mathbf{p} \cdot \mathbf{A}$  and not of the form  $h_{\mu\nu} T^{\mu\nu}$  (22) that was used by Dyson [19] for the interaction of gravitational waves with matter. The latter form is correct, but the former incorrect.
8. J. C. Garrison and R. Y. Chiao, *Quantum Optics* (Oxford University Press, Oxford, 2008), Chapters 2 and 3.
9. R.Y. Chiao, Princeton 1961 B.A. thesis with J.A. Wheeler (unpublished).
10. R. Feynman, R. Leighton, and M. Sands, *The Feynman Lectures on Physics*, volume III.
11. G.T. Moore, "Quantum theory of the electromagnetic field in a variable length one-dimensional cavity," *J. Math. Phys. (N.Y.)* 11, 2679 (1970)
12. S.A. Fulling and P.C.W. Davies, "Radiation from a moving mirror in two dimensional spacetime: conformal anomaly," *Proc. Roy. Soc. A* 348, 393 (1976).
13. Parametric amplification arising from the pumping motion of the moving mirror is much like the result of the pumping action of a child repeatedly standing and squatting on a swing, whose center of mass moves up and down at twice the natural frequency of the swing.
14. P.D. Nation, J.R. Johansson, M.P. Blencowe, and F. Nori, "Colloquium: Stimulating uncertainty: Amplifying the quantum vacuum with superconducting circuits," *Rev. Mod. Phys.* 84, 1 (2012).
15. For the "triple-cavity" paramp depicted in Fig. 2, the pump, signal, and idler frequencies obey the relationship  $2\omega_p = \omega_s + \omega_i$ , where the "double" cavity possesses a doublet spectrum  $(\omega_s, \omega_i)$ , whose splitting frequency is determined by the size of the iris in the middle of this "double" cavity. This paramp is a phase-sensitive amplifier that obeys the phase relationships  $2\phi_p = \phi_s + \phi_i = 2$ , where the phase  $-\pi/2$  corresponds to maximum amplification, and  $+\pi/2$  corresponds to maximum deamplification [7].
16. G. Rempe, H. Walther, and N. Klein, "Observation of quantum collapse and revival in a one-atom maser," *Phys. Rev. Lett.* 58, 353 (1987).
17. R.Y. Chiao, "Method of images applied to an opto-mechanical Fabry-Perot resonator," arXiv:1303.4020.
18. S.J. Minter, K. Wegter-McNelly, and R.Y. Chiao, "Do mirrors for gravitational waves exist?," *Physica E* 42, 234 (2010); arXiv:0903.0661.
19. F.J. Dyson, "Seismic response of the earth to a gravitational wave in the 1-Hz band," *Astrophys. J.* 156, 529 (1969).
20. N.A. Inan, J.J. Thompson, and R.Y. Chiao, "Interaction of gravitational waves with superconductors," *Fortschr. Phys.* (2016) doi:10.1002/prop.201600066.
21. N.A. Inan, "A new approach to detecting gravitational waves via the coupling of gravity to the zero-point energy of the phonon modes of a superconductor," *IJMPD*, Vol. 26, No. 12 (2017) 1743031, DOI: 10.1142/S0218271817430313. (Essay received Honorable Mention in the 2017 Essay Competition of the Gravity Research Foundation.)
22. J.Q. Quach, "Gravitational Casimir effect," *Phys. Rev. Lett.* 114, 081104 (2015).
23. However, the enormous enhancement found in [18] of the reflectivity of a SC mirror by huge dimensionless ratio  $|F_{\text{Coulomb}}/F_{\text{Newton}}| \sim 10^{42}$  was derived on the basis of the incorrect *vector* interaction Hamiltonian of the form  $\mathbf{p} \cdot \mathbf{A}$  between the Cooper pairs and *vector* gravitational fields, and not on the basis of the correct *tensor* interaction Hamiltonian of the form  $h_{\mu\nu} T^{\mu\nu}$  between the Cooper pairs and *tensor* gravitational fields used in [20].
24. Niels Bohr, PhD thesis: *Studier over Metallernes Elektrontheori* (Studies on the Electron Theory of Metals), May 1911.
25. S. Balbus, "Simplified derivation of the gravitational wave stress tensor from the linearized Einstein field equations," *PNAS* 113, 11662 (2016); ArXiv 1604.05974.
26. Note that the introduction of the relative gravitational permeativity  $\kappa_r$  into the source of the wave equation (30) affects solely the source of the tensor  $h_{ij}$  field associated with gravitational waves. This is not equivalent to the introduction of an effective Newton's gravitational constant  $G_{eff}$  to replace Newton's constant  $G$  in front of the source term in the full Einstein's field equations so that they would now read as follows:
$$R_{\mu\nu} - \frac{1}{2}g_{\mu\nu}R = \frac{8\pi G_{eff}}{c^4}T_{\mu\nu} \quad (62)$$
since this replacement  $G \rightarrow G_{eff}$  would affect *all* the components of  $T_{\mu\nu}$  equally. Such a replacement makes no distinction at all between the scalar, vector, or tensor sources  $T_{00}$ ,  $T_{0i}$ , or  $T_{ij}$  of the three different kinds of gravitational fields. However, the Newtonian gravitational field of the Earth, whose source is  $T_{00}$ , will not be affected by the introduction of the relative gravitational permeativity  $\kappa_r$  in (30). Hence there cannot be any "antigravity" arising from the presence of superconductors.
27. Since  $\kappa_r$  affects solely the metric deviation tensor  $h_{ij}$  field associated with gravitational waves, but not the other components of  $h_{\mu\nu}$  whose sources are the other components of the full stress-energy tensor  $T_{\mu\nu}$ , the question naturally arises as to how the introduction of a non-unity relative gravitational permeativity  $\kappa_r$  into the wave equation (30) would affect the conservation law  $T^{\mu\nu}_{;\nu} = 0$ . The same question, however, also arises in Maxwell's equations modied by the permittivity and permeability of electrical and magnetic media (for example, in the case of the large measured relative magnetic permeability  $\mu_r \sim 10^6$  for a Metglas alloy). As the ongoing Abraham-Minkowski controversy shows, the answer to this question in the case of electromagnetic fields that pervade the space inside dielectric and magnetic media, requires a careful rethinking of the physical meaning of the concept of *momentum* of these fields inside a medium, as well as a rethinking of the physical meaning of the concept of *inertia* (see [https://en.wikipedia.org/wiki/Abraham-Minkowski\\_controversy](https://en.wikipedia.org/wiki/Abraham-Minkowski_controversy)). One must also confront this same rethinking in the case of media for the various kinds of gravitational fields in general relativity. Ultimately, experiments must settle this controversy.
28. We have coined a new word "permeativity" to supplement the words "permeability" and "permittivity."
29. Note that Szekeres [30], Press [31], and Flanagan and Hughes [32] do not distinguish between values of  $\kappa_r$  for the scalar, vector, and tensor parts of Einstein's equations. However, following the analogy with electromagnetism, where  $\epsilon$  and  $\mu$  can vary independently for different kinds of macroscopic media, we consider the possibility that they may also vary independently for the scalar, vector, and tensor parts of Einstein's equation.
30. P. Szekeres, "Linearized Gravitation Theory in Macroscopic Media," *Annals of Physics*, 64, 599-630 (1971).
31. W. Press, "On Gravitational Conductors, Waveguides, and Circuits," *General Relativity and Gravitation*, 11, 105 (1979).
32. E. Flanagan and S. Hughes, "The basics of gravitational wave theory," *New J. Phys.* 7, 204 (2005).
33. The membrane shown in Fig. 5 was made for us by Norcada Inc. (<http://www.norcada.com>).
34. P.R. Saulson, "How an interferometer extracts and amplifies power from a gravitational wave," *Classical and Quantum Gravity* 14, 2435 (1997), Equation (7).
35. R.Y. Chiao, "New directions for gravitational-wave physics via 'Millikan oil drops'," in *Visions of Discovery*, edited by R.Y. Chiao, M.L. Cohen, A.J. Leggett, W.D. Phillips, and C.L. Harper, Jr. (Cambridge University Press, 2011), p. 348.
36. M. Born and E. Wolf, *Principles of Optics*, sixth edition (Pergamon Press, 1980). = 0.

Received 18 December 2017 Accepted 22 February 2018



# PREPARATIONS FOR THRUST MEASUREMENT AND ERROR DISCUSSION OF THE IMPULSE RESONANT MICROWAVE CAVITY

MICHAEL S. MCDONALD, MICHAEL W. NURNBERGER and LOGAN T. WILLIAMS, U. S. Naval Research Laboratory, Washington, D.C., 20375 USA

Email: michael.mcdonald@nrl.navy.mil

This paper reports on preparations for independent validation and verification (IV&V) of a recently proposed speculative class of spacecraft propulsion which we label an “impulse drive”. The most prominent example device, and the only one offering peer-reviewed experimental results, is the closed resonant microwave cavity of White et. al. from NASA Johnson Space Center. White reports anomalous thrust production with no conventional expulsion of reaction mass via a new and unconventional interpretation of physics. Such a device would have remarkable applications for spacecraft propulsion, but the positive experimental results to date, while suggestive, are near the limits of state of the art measurement resolution and subject to significant confounding errors due to thermal drifts and other subtle effects. Our objective is to rigorously weed out potential false positive thrust signals with null and control experiments, create an impartial baseline dataset to either validate or refute claims of anomalous thrust, and if merited form a solid foundation for further experimental and theoretical investigation. We duplicate the resonant geometry (length, diameter, taper) of White’s experimental apparatus in a replica cavity with mechanical construction and driving microwave circuit of our own design, with careful attention to maximizing driving RF power capability and cavity resonant quality factor  $Q$ . We report on the fabrication and initial thermal testing of our replica cavity and the development of a noncontact RF power interface we dub a “finger joint” to permit frictionless power transmission to a freely swinging torsional thrust stand arm. No thrust measurements have been completed to date; this paper only presents experimental methods and risk reduction test results in preparation for performance measurements on a torsional thrust stand at vacuum. Potential sources of error including thermal drift, RF effects, magnetic tearing via dipole coupling, and electrostrictive response in the cavity dielectric insert are discussed.

**Keywords:** Torsional pendulum, Force measurement, Non-contact RF power transmission, Thermal drift, Microwave cavity, Vacuum

## I INTRODUCTION

IMPULSE, for the In-Depth Measurement of Performance in Unconventional Low-thrust Spacecraft Engines, is an effort underway at the Naval Research Laboratory to independently validate or refute recent reports of anomalous force (thrust) generated from a closed microwave resonant cavity. The measured thrusting force is anomalous because there is no apparent reaction mass expelled by the device, so as advertised the device either violates the conservation of momentum or is demonstrating some form of new physics to preserve momentum conservation. In most cases this class of device is named by its investigator according to their preferred physical theory. Such names include the  $Q$ -thruster or quantum vacuum plasma thruster (QVPT) claimed by White to produce thrust by pushing off the quantum vacuum as a medium [1]; the EM-Drive, claimed by Shawyer to work via purely electromagnetic phenomena [2]; and Mach-effect thrusters, claimed by Fearn and Woodward to work by varying the inertial mass of a device in phase with a (typically piezoelectric) oscillation [3]. For the time being, the authors of this work are agnostic on the physical mechanism at play in these thrusters, if indeed any is present aside from experimental error, and we refer to the whole class as *impulse drives*.

This experimental effort focuses on the cavity point design of White et. al from NASA JSC in Ref. [1] as both the best-described and only peer-reviewed result currently available, and

reproduces their cavity geometry while re-engineering the fabrication technique and microwave (RF) power feed system into the cavity. White et. al. observed thrust levels in vacuum of approximately 90  $\mu\text{N}$  force for about 80 W input power with a cavity quality factor  $Q$  of about 8000. Our NASA-replica cavity has a  $Q$  of about 16000 and we plan to test it under vacuum on a torsional thrust stand with an approximately 5  $\mu\text{N}$  noise floor at power levels up to 100 W in the near term. Assuming that thrust scales linearly with power and at least positively with cavity  $Q$ , this leads to an expected thrust signal in the low hundreds of microNewtons assuming the phenomena can be replicated in NRL’s facilities.

The following sections discuss the overarching design drivers of our experimental approach, walk through the prospective error sources we anticipate, review our experimental equipment, and present results from basic risk reduction testing performed to date to measure thermal profiles, closed loop frequency feedback control, and the performance of our noncontacting finger joint for frictionless RF power transmission onto the thrust stand.

## II. EXPERIMENT DESIGN DRIVERS: MAXIMIZING SIGNAL, MINIMIZING NOISE, AND MITIGATING OR QUANTIFYING ERROR

Performing a high-fidelity measurement for this class of resonant microwave cavity requires accurate measurement of re-

ported forces of 10s-100s  $\mu\text{N}$  at RF powers of order 100 W at about 2 GHz at vacuum. We define “accurate” to be a measurement resolution and/or noise floor of order single microNewtons, in order to eventually permit decomposition of the 10-100  $\mu\text{N}$  total force signals into individual error sources, and/or to distinguish small changes in total signal magnitude due to changes in device under test (DUT) operating conditions such as forward RF power or resonant mode. A typical displacement sensitivity of our torsional thrust stand is of order 1 micron ( $\mu\text{m}$ ) displacement per 15-20 microNewtons ( $\mu\text{N}$ ) applied force, given our spring stiffness and 20 cm moment arm. However, at typical operating temperatures our DUT thermally expands by hundreds of microns, so thermal displacements alone could dwarf any true force signal. This makes an impulse drive test fundamentally a signal to noise problem, so improving the signal to noise ratio (SNR) by increasing the force signal and decreasing errors and noise drives our design. To maximize signal, we wish to maximize cavity RF power and achieve a good cavity quality factor  $Q$ . To minimize noise, we wish to minimize DUT heating, minimize thermal drift due to heating that does occur, isolate the stand from vibration, operate stably on resonance indefinitely, and operate at vacuum.

Maximizing RF power delivery to a thrust stand in vacuum typically forces a choice between two bad options. The first is to keep the power amplifier at atmosphere, running high power cables to the thrust stand and accepting the stiffness and thermal expansion from the hot cables corrupting the thrust measurement. Many RF-based plasma propulsion tests have used the former approach [4], [5]. The second is to send only DC power to the thrust stand and perform DC-RF power conversion and RF power amplification on the torsional arm in a self-contained system, accepting the attendant waste heat and mass; White et. al. used this technique [1]. In either case, it is not trivial to decouple thermal and propulsive effects. Shortcomings of on-the-stand amplification method are the limited selection and high cost of vacuum-compatible RF amplifiers, and the operating temperature limits of those units. These factors have prevented steady state operating tests of proposed impulse drives in vacuum testing to date.

Here we adopt a new technique to transmit RF power across a wideband noncontact joint, using capacitive coupling between interlaced “fingers” in a stripline-like configuration to transmit up to several hundred watts of power at desired frequencies between 0.7 and 2.5 GHz. This design, discussed in more detail in Section IV-E, permits the use of standard rack-mount amplifiers and other equipment and mostly decouples the RF transmission lines from affecting the cavity on the thrust stand.

To minimize DUT heating we use a high-emissivity coating to increase radiative heat transfer, while to minimize thermal drift we use resistive heaters on the cavity external surface to pre-heat the cavity to a stable temperature close to that expected from RF heating before switching over to RF power to take force measurements. While not perfect, this technique reduces the magnitude of the temperature transients associated with RF power cycling. A solid state relay mounted on the thrust stand shorts the resistive heaters during RF testing so that constant current is maintained through the heater wires crossing the torsional pivot bearing at all times, minimizing thermal drift from heater wire expansion.

Finally, to maintain the cavity on resonance we use a simple dither technique implemented in LabView to monitor and adjust the driving frequency to minimize reflected power. While

increasing cavity resonant quality factor  $Q$  has been reported to increase the anomalous force (see [2] Fig. 1), it also makes it more difficult to keep the cavity on resonance under manual control. The thermal load from Ohmic heating by RF-induced cavity wall currents drives thermal expansion in the cavity, increasing its size slightly and altering its resonant frequency. For an aluminum cavity like ours with  $Q \approx 16000$  and coefficient of thermal expansion  $23 \times 10^{-6} \text{ m/m-}^\circ\text{C}$  [6], a temperature increase of less than  $3^\circ\text{C}$  will expand the cavity by one part in  $Q$  ( $1/16000$ ) and throw a fixed frequency source off resonance.

### III PROSPECTIVE ERROR SOURCES

The section below outlines several prospective error sources in this class of measurement, including due to thermal, RF, magnetic and electrostrictive mechanisms, and where appropriate notes what means are taken to mitigate them or why they are ignored for the time being.

#### A. Thermal

For any viable thruster the thrusting force should increase with power, motivating testing at as high a power level as practical. However, resonant microwave cavities dissipate their RF power as Ohmic heating caused by induced currents in the resistive cavity walls, so higher RF power directly translates to an increased thermal load in the experimental setup. This thermal load manifests in several ways, including thermal drift and potentially outgassing. We find that thermal drift is a major source of error, while outgassing is not a likely source of concern.

#### Thermal Drift

A torsional thrust stand is a collection of mechanical assemblies and electronic components, all of which have properties that vary with temperature. The thermal load of the cavity operating at steady state is equal to the RF power (perhaps less some small fraction of the power creating the speculated thrust), and that heat will drive thermal expansion of the stand components, slightly shift the test device’s center of gravity, and change the response of electronic components like inclinometers and laser displacement sensors.

An increase from room temperature at about  $20^\circ\text{C}$  to an operating temperature near  $100^\circ\text{C}$  will expand the approximately 10in long cavity by about .020in, shifting the CG by up to .010in or  $250 \mu\text{m}$ . This is significant on a thrust stand where total displacement for 100  $\mu\text{N}$  load is less than  $10 \mu\text{m}$ . Thermal expansion in the wires crossing the torsional pivot bearing and in the arm and base of the thrust stand itself as it heats up due to the DUT thermal load can also drive thermal drift.

To reduce thermal loading and thermal drift at high RF power, we supply RF power from a source outside the vacuum chamber and use a noncontact stripline connector to transfer RF power across a vacuum gap to the resonant cavity. RF power cables for high power application are notoriously stiff and prone to heating, and the power conversion efficiency of RF sources from wall power or DC power is rarely as good as 50%. Keeping the RF source outside the vacuum chamber increases the maximum potential RF power during testing since the RF source can be cooled more easily. The noncontact connector prevents RF cabling from crossing the torsional pivot, eliminating thermal expansion of RF cabling as an error source. It will introduce new risks of RF interference, addressed later.

To further reduce thermal drift, tests are performed at ther-

mal steady state. Resistive heaters mounted to the thrust stand base platform and the DUT provide a steady AC (60Hz) heating power for several hours before testing begins, thermally soaking the experimental setup. Dual PID loops tune the heating currents to maintain the thrust stand base at 50 °C and maintain the DUT at a pre-set temperature determined by earlier RF testing at a desired RF power. Due to slight differences in the heating patterns of the resistive vs. RF heating, the temperature of a reference location on the cavity is matched instead of total heating power. Calibration takes place at elevated temperature at steady state, and the heaters are turned off immediately prior to RF testing and restored immediately after RF testing before post-test calibrations. Since the lead wires to the resistive heaters cross the torsional pivot and are also subject to thermal expansion, special care is taken to use flexible, high-strand count wire and to maintain fixed current flow through the lead wires at all times. During RF testing a solid state relay mounted on the torsional arm shorts the heaters to cut the heating power to the cavity while maintaining constant heater current and wire temperature that might affect the arm torsional stiffness.

Finally, to quantify what thermal drift remains, the resonant cavity, thrust stand torsional arm, and thrust stand base are all instrumented with thermocouples to provide some measure of what level of temperature change between AC heating and RF testing occurs.

### Outgassing

The small force magnitudes reported in the literature to date, the lack of steady state thermal testing conditions, the presence of non-vacuum rated components including a large dielectric disc inside the cavity, and the lack of reported vacuum chamber operating pressure profiles during thrust recording all raise outgassing as a potential concern. If absorbed water or other volatile species are baked off during testing at elevated temperature, any directionality in the departing species will produce a net thrust force. This would be a real force, in essence a very poor resistojet, and not a drift error, but the force would be short-lived until the volatile species baked off.

To evaluate whether an outgassing event of sufficient magnitude to create a measurable force could have escaped notice in testing to date, consider an operating pressure in the  $10^{-6}$  Torr range giving a typical visible pressure gauge resolution of  $\Delta P = 1 \times 10^{-7}$  Torr, with a pumping speed  $S = 300$  L/s comparable to the value for the turbopump used by White. We note the following conversion equations between volumetric flow rates in standard cubic centimeters per minute (sccm), atomic flow rate, and mass flow rate from Goebel (see App. B of Ref. [7]):

$$1 \text{ sccm} = 4.477962 \times 10^{17} \frac{\text{atoms}}{\text{s}} = 0.01267 \frac{\text{Torr} \cdot \text{L}}{\text{s}} = 7.43583 \times 10^{-4} M_a \frac{\text{mg}}{\text{s}}$$

where  $M_a$  is the fluid mass in atomic mass units (amu). The gas throughput  $\Delta Q$  associated with the visible increase  $\Delta P$  in the chamber pressure with pumping speed  $S$  is then

$$\Delta Q = S \Delta P = \left( 300 \frac{\text{L}}{\text{s}} \right) (1 \times 10^{-7} \text{ Torr}) = 3 \times 10^{-5} \frac{\text{Torr} \cdot \text{L}}{\text{s}}$$

which we convert to a volumetric ( $v$ -dot) and mass ( $m$ -dot) flow rate via the conversions above, assuming water with  $M_a = 18$  amu is the typical dominant outgassing species:

$$\begin{aligned} \dot{v} &= \left( 3 \times 10^{-5} \frac{\text{Torr} \cdot \text{L}}{\text{s}} \right) \left( 0.01267 \frac{\text{sccm}}{\text{Torr} \cdot \text{L} / \text{s}} \right) = 0.0024 \text{ sccm} \\ \dot{m} &= (0.0024 \text{ sccm}) / (7.43583 \times 10^{-4} (18 \text{ amu})) = 3.17 \times 10^{-5} \frac{\text{mg}}{\text{s}} \end{aligned}$$

Assuming all these particles leave at a temperature of 300 K and form a perfectly collimated beam aligned with the thrust axis with thermal velocity  $v_{th}$  gives a thrust  $T$ :

$$\begin{aligned} v_{th} &= \sqrt{\frac{kT}{m}} = \sqrt{\frac{(1.38 \times 10^{-23} \frac{\text{J}}{\text{K}})(300 \text{ K})}{(18 \text{ amu}) \left( 1.66 \times 10^{-27} \frac{\text{kg}}{\text{amu}} \right)}} = 372 \frac{\text{m}}{\text{s}} \\ \dot{m} v_{th} &= \left( 3.17 \times 10^{-5} \frac{\text{mg}}{\text{s}} \right) \left( 10^{-6} \frac{\text{kg}}{\text{mg}} \right) \left( 372 \frac{\text{m}}{\text{s}} \right) = 0.012 \mu\text{N} \end{aligned}$$

For an outgassing event with a pressure spike of  $1 \times 10^{-7}$  Torr or less, even this conservative value for thrust would be far beneath notice. The effect is linear in pressure, so observed forces of 100  $\mu\text{N}$  due to outgassing would have associated pressure spikes of order  $10^{-3}$  Torr. Neutral outgassing is therefore not a viable explanation for the observed anomalous forces.

Nevertheless, to guard against faulty assumptions above, the chamber pressure is recorded digitally and any variations above the baseline will be noted. If significant pressure spikes are observed, a residual gas analyzer will also be engaged to monitor species from 0-100 amu during all tests, and these traces are also reported.

Finally, to promote rapid evacuation of the resonant cavity at high vacuum, several vent holes are located on the endplates in the null (non-current carrying) locations of the 212 mode excited during this test. These holes double as fastener locations for securing dielectric discs at each end of the cavity. The small holes do not significantly affect the Q of the cavity, and they are far smaller than the resonant wavelength, so do not permit RF leakage.

### Convective Air Currents

Any atmospheric pressure thrust measurements requiring accuracy in the microNewton range raise concerns that convective air currents caused by DUT heating might appear as spurious thrust forces [8]. The recent test by White was at vacuum,[1] as is this reported test. We do not consider convective wind currents as a major source of error at high vacuum.

### B. RF Effects

RF power can do many worrisome things to affect thruster performance measurements, including radiate, generate electromagnetic interference, ionize particles and create plasma, and generate multipactor discharges across gaps. In lieu of a deep dive into specific error mechanisms associated with RF power on a thrust stand, in our initial IV&V we will largely rely on dummy load testing as a gross check that the RF power delivery system is not causing false thrust, and leave investigations into RF interplay with the resonant cavity for future work, if merited. Nevertheless, below we discuss plasma production and interference as a spur to discussion.

### Plasma Discharges or Ion Production

We largely dismissed a possible warm gas thruster effect during outgassing as an error source given the large gas flow rates and noticeable pressure spikes that would be required to produce  $\sim 100 \mu\text{N}$  force from directed warm neutral flow. However, might the strong fields present in the resonant RF cavity be sufficient to ionize trace gas particles, accelerating a small number of ions to high velocity? This also seems unlikely based on the low background pressures in the chamber, and at present we do not explicitly test for it.

However, assuming this mechanism were viable, one would expect to see a slow decrease in the magnitude of the thrust force as any outgassing species are baked out of the hot cavity and its surroundings. This effect should continue on subsequent test days as the chamber base pressure gradually reduces to ultimate pressure. Conversely, one would expect thrust to increase dramatically if background gas were fed into the chamber. If these symptoms occurred, one could install a Faraday cup on each side of the cavity to detect any stray ion current.

### Interference with other signals

To ensure that RF interference is not causing a spurious effect, we run RF power to a high-power dummy load placed on the torsional arm prior to any cavity testing. The RF noncontacting finger joint is oriented similarly between the dummy and cavity tests, providing an initial check that neither heating nor leakage from the finger joint produce spurious test signals.

In later testing it will be possible to run RF power to the resonant cavity in active and null orientations if merited, all level to horizontal: forward, reverse, and radially inward or outward. Due to the orientation of the finger joint, it would be difficult to aim the cavity straight up or down. In later tests, if anomalous thrust is observed we may monitor radiated RF power levels using one or a series of drooping-ground plane monopole antennas near the cavity, but during initial testing we will rely on numerical simulations in Altair FEKO that emissions from the cavity and the joint are minimal.

### C. Magnetic Tearing or Dipole Coupling

Magnetostatic effects are familiar in Hall thruster testing where “tearing” occurs when strong DC magnetic fields from the DUT couple with magnetic components in the thrust stand to produce operating condition-dependent false thrust readings. There are no applied DC magnetic fields in a resonant microwave cavity, so it is not clear how such a coupling would have occurred in literature reports of thrust in impulse drives, especially since the anomalous thrusting force is associated only with the turn-on of RF power. However, in our experiment the heating currents of several amperes running through the resistive heaters on both the cavity and the thrust stand baseplate will produce magnetic fields, and the heating current through the cavity will turn off each time the RF power turns on, and vice versa. There is a potential for magnetic effects there.

To minimize the magnetic field generated by the heaters we use alternating current (60 Hz), so dipole coupling should wash out in the  $\sim 1$  Hz time-averaged thrust displacement readings. In addition to this mitigation technique, we can also bound the maximum thrust error by measuring the swing in readings induced by running DC current of opposite polarities through the cavity heaters.

The cavity, thrust stand and immediate environment are also almost entirely constructed of nonmagnetic materials, primarily aluminum, 316 stainless steel and various plastic components. The exceptions are the small permanent magnets in the damper assembly and some magnetic steel in the large optical table supporting vibration isolation stage and thrust stand, approximately 18in below the DUT.

### D. Electrostriction

An outstanding puzzle for the whole class of proposed impulse drives is how harmonic fields are supposed to generate

a net force. Since the electromagnetic fields everywhere in the cavity are sinusoidal, they point in equal and opposite directions over each RF cycle – therefore, shouldn’t any “pushing” anywhere in the system balance out to zero?

One possible rectifying phenomenon is electrostriction. Electrostriction is the general material property that nonconductors expand when placed in an electric field, as ions in the crystal lattice respond to the applied field and induce a slight strain. The effect is rectifying because materials only undergo expansion from the rest state, so regardless of the electric field direction  $E$  the material gets longer. This effect is proportional to  $E^2$ . Most materials experience only miniscule strains, and since the phenomenon is mechanical due to physical displacement of ions in the crystal lattice, it generally is restricted to exciting frequencies  $< 100$  kHz. However, previous work at NRL has shown that electrostriction can be induced in materials by exciting frequencies in the GHz range, provided a second nearby signal produces a beat frequency in the appropriate kHz range [9]. In the work cited, this phenomena was leveraged for microwave signal detection in a fiber optic electrostrictive sensor by exciting a locally applied 1-20 GHz signal with remotely sensed microwave signals.

In our experimental configuration, one potential source for a nearby frequency source is from sidebands in the applied microwave signal to the cavity. Both the synthesizer and amplifier are in principle capable of generating low-amplitude sidebands within 100 kHz of the main driving frequency, and such sidebands have been noted in passing, though not yet specifically quantified in frequency or amplitude. Moreover, these sidebands will also resonate if they are within the resonant bandwidth of the cavity, which spans about  $\pm 50$  kHz for our cavity with  $Q \approx 16000$  at 1.86 GHz.

If this mechanism is found to be plausible after further investigation, a reasonable experimental test would be to observe whether a cylindrical resonant cavity filled almost completely with a dielectric insert, but secured only to one endcap of the cavity, still produces an anomalous force. Such a configuration ought to produce no or minimal anomalous force under any propulsive theory by symmetry arguments, so any detected force could be attributed to an electrostrictive effect. An added bonus is that a cylindrical configuration almost filled with a dielectric would be analytically tractable to a close approximation. Alternately, a fiber optic sensor like the one reported in Ref. [9] could be inserted into a proposed thruster cavity dielectric as a sensitive, nonintrusive strain gauge to directly verify an electrostrictive response.

## IV EXPERIMENTAL SETUP

### A. Vacuum Facility

All testing reported in this paper takes place in the South Chamber, a 2.3m tall by 2 m diameter upright cylindrical stainless steel chamber. The chamber is mounted vertically and suspended about 3 meters in the air, with the bottom endcap raised and lowered by a hydraulic lift. The thrust stand is fixed to the endcap and brought to ground level for experimental access.

South Chamber is brought to rough vacuum by a Leybold WH2500 blower and SV-630B roughing pump with combined pumping speed 1530 CFM, and maintained at high vacuum by a NRC 48in diffusion pump with nominal pumping speed



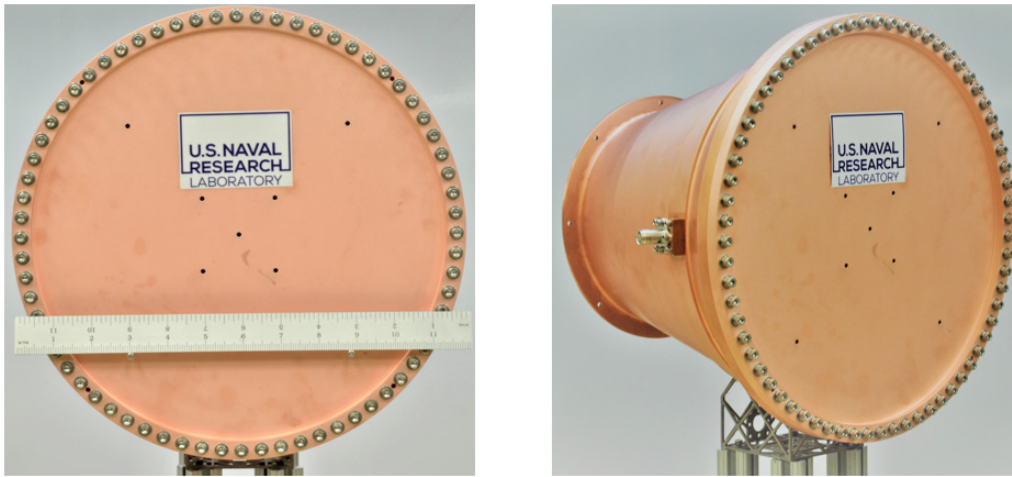


**Fig. 1: NRL's replica cavity reproduces the relevant internal resonant geometry of the NASA JSC design with independent mechanical, thermal and RF power feed design.**

100,000 L/s on air. Due to conductance losses through internal shrouds for thermal vacuum cycle testing, the effective pumping speed of the diffusion pump is reduced to an effective speed of about 20,000 L/s, giving a typical base pressure in the low to mid  $10^{-6}$  Torr range after 24 hours at high vacuum. High vacuum pressure is monitored using a Bayard-Alpert type hot ion gauge.

### B. Torsional Stand

The torsional thrust stand used for this work was manufactured by Busek Co. for NRL and is described in much greater detail by Williams [10]. The base and free-swinging arm of the stand are joined by two stainless steel Riverhawk flexural pivots. The stand and arm are each made of dip-brazed aluminum to relieve thermal stresses and have a chromate conversion coating to prevent static charging. The arm is 48 cm long with two 7.5 cm square mounting platforms at each end. The moment arm from the torsional axis through the center of the mounting platform where the device under test (DUT) is placed is 20 cm. The DUT is alone at one end of the arm, while the other end houses the balance mass to counteract the gravitational load of the DUT on the torsional pivots, the mirror for the optical displacement sensor, and one of the two metal discs used as a capacitive force generator (CFG). The entire stand is mounted to a 24in square x  $\frac{1}{2}$ in thick black anodized aluminum optical breadboard.

The optical displacement sensor (ODS) is a Philtec model D63. The sensor has an accuracy of 25 nm at a distance of approximately 1 mm from the mirror, in the so-called “far side” of the instrument response curve. A nominal spring constant for the system is of order 15-20  $\mu\text{N}/\mu\text{m}$ . Optical signals from the ODS are passed through two fiber optic cables to measurement electronics outside the vacuum chamber.

The capacitive force generator (CFG) calibrates the displacement response of the ODS to a known applied electrostatic force. Two conducting discs, one attached to the torsional arm and the other mounted to the optical breadboard, are swept through a series of gap spacings and the capacitance of the two discs is measured at each gap by a BK Precision 889B LCR meter. The force between the two plates is a known function of the plate capacitance, applied voltage, and gap distance, so by measuring the capacitance and monitoring the gap spacing the voltage can be swept to generate a range of applied forces to

calibrate the ODS response. The capacitive plates are shorted together when not in use to prevent inadvertent bias.

Oscillations induced by ambient environmental vibration and shocks are damped by inducing eddy currents in a 2in x 3in x  $\frac{1}{8}$ in copper plate suspended from the balance end of the torsional arm. Two  $\frac{3}{4}$ in square x  $\frac{1}{8}$ in thick neodymium magnets are mounted on a motorized stage oriented parallel with the torsional arm and positioned close to the copper damping plate to excite eddy currents when the plate moves back and forth in front of the permanent magnets. The separation between the magnets and the copper plate is reduced until the arm oscillation is slightly underdamped.

The 24in square black anodized aluminum optical breadboard is thermally stabilized during testing at 50 °C using a LabView software PID loop running at 1 Hz. The process temperature is read from a K-type thermocouple mounted to the thrust stand base by a Measurement Computing E-TC multichannel thermocouple reader. The PID output is used to compute a 60 Hz sine wave RMS voltage output on an Agilent 33512B waveform generator, which in turn drives the analog input of a Kepco BOP 36-12M bipolar amplifier in current control mode to produce a 60 Hz AC current through a set of sixteen parallel Minco HK5249 53  $\Omega$  polyimide Thermofoil heaters distributed across the breadboard, for an effective 3.3  $\Omega$  resistance.

To balance the stand, the DUT mass is measured to 0.1g accuracy, and an approximately equal mass of fine tungsten carbide powder in a glass jar is placed on the balance end of the arm. Tungsten carbide's high density makes it a very effective ballast mass in a small volume, and the powder form permits easy adjustment to match varied weight conditions.

### C. Resonant Cavity

#### Mechanical Design

The DUT cavity closely replicates the internal geometry (length, diameter and taper) reported by White with an independent mechanical, thermal and RF power feed design. This replica cavity (see Fig. 1 and Fig. 2) is of two-piece aluminum construction, with a .001in thick copper plating applied to improve surface conductivity. Sixty-eight 8-32 fasteners and thirty-four plate nuts uniformly clamp the lid shut. The base piece of the cavity has internal length 9in, large diameter 11in,

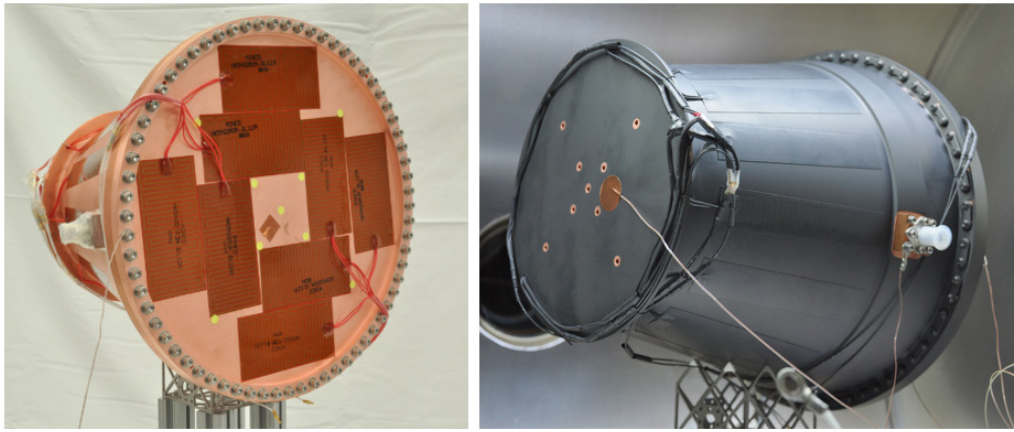


Fig. 2: Cavity with resistive heaters, before (left) and after (right) high-emissivity coating

small diameter 6.25in and an additional .093in radius fillet at the small end to improve machinability from a single piece of aluminum. The internal surface of the lid has an 11in diameter, .025in deep recess to permit focused lapping of the lid clamping surface, bringing the total cavity internal length to 9.025in. This recess has a .020in radius fillet. The total mass of the assembled cavity is approximately 3 kg.

A second, dummy resonant cavity was also fabricated to support benchtop testing. This dummy cavity is a squat aluminum cylinder used as a testbed for the resonance tuning closed loop feedback circuit. It also uses a two-piece lid-and-base construction, with internal diameter  $D = 3.688\text{in}$  and height  $H = \frac{1}{2} * D = 1.844\text{in}$ . A “candlestick” style SMA connector mounted off-center on the lid excites the cavity at a fundamental frequency of 2.45 GHz with a quality factor of approximately 5000. Twenty  $\frac{1}{4}$ -20 fasteners provide strong uniform clamping pressure to secure the lid to the base. Aside from light lapping of the interface between lid and base, no post-machining of the cavity was performed after CNC milling.

### Thermal Design

Initial tests of the bare cavity confirmed that the low emissivity of the copper plating drove excessive heating. This motivated application of a high-emissivity coating in preparation for thrust stand testing. Radiated power varies linearly with emissivity so increasing the device emissivity directly increases the maximum permissible operating power given operating temperature limits. The high emissivity coating also enables more rapid thermal equilibration, though this still takes a few hours at vacuum.

Our self-imposed requirement to test at thermal steady state and desire to decouple RF-induced effects from thermal effects also motivate the use auxiliary resistive heaters on the cavity. Several polyimide test heaters (Minco models HK5422 35  $\Omega$  and HK5334 38  $\Omega$ ) are applied to the cavity walls and lid to permit cavity heating independent of RF power. Eight parallel 35  $\Omega$  heaters on the lid are wired in series to sixteen parallel 38  $\Omega$  heaters on the cavity walls to create an effective 6.7 $\Omega$  resistor covering much of the outer cavity surface. To prevent magnetic tearing due to dipole coupling the heaters run off 60 Hz AC power in a temperature-stabilized PID mode identical to the baseplate heating discussed earlier. The acrylic adhesive on the heater sets our test temperature ceiling of 100 °C. Future testing at higher temperatures up to 200 °C and thus higher power as well would be possible with clamped heaters in place of acrylic adhesive heaters.

### Polymer Insert

An apparently crucial contribution to the anomalous force reported by White et. al. is provided by a high density polyethylene (HDPE) disc approximately 6in diameter x 2in thick inserted in the small end of the cavity. While no published data comparing force production with and without an insert is available, and the mechanism by which this disc contributes to the thrust has not yet been fully described, we replicate it in our planned test configuration as well. We plan to run initial cavity thrust stand testing without the insert before running a second set of tests with the insert installed. Assuming the cavity without the critical insert produces no or negligible anomalous thrust, this will be an additional level of control testing.

The NRL insert is cut from a rod of extruded HDPE into a disc 15.6 cm diameter x 5.4 cm thick. A (presumably) minor difference from the NASA insert is the inclusion of several thru holes .089in in diameter aligned with the vent holes on the lid and base of our replica cavity. These holes are tapped to permit attachment of the insert to either end of the replica cavity as desired using alumina ceramic bolts. Thru holes instead of tapped holes were chosen to remove the possibility of trapped gas volumes in blind holes in the insert, and to facilitate any initial volatile outgassing of the material during vacuum bakeout. One other minor difference is a 1mm chamfer on the bottom edge of the insert to allow a flush fit in the small end of the replica cavity, which has a small fillet.

### RF Design

Initial rough RF design and mode calculations were performed semi-analytically by numerically solving the Maxwell equation boundary conditions for the resonant TE and TM modes in a cavity replicating the NASA internal dimensions

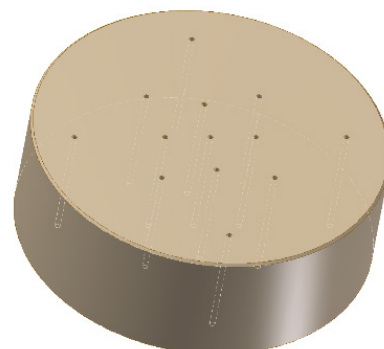


Fig. 3: Polymer insert for NRL replica cavity (CAD image)

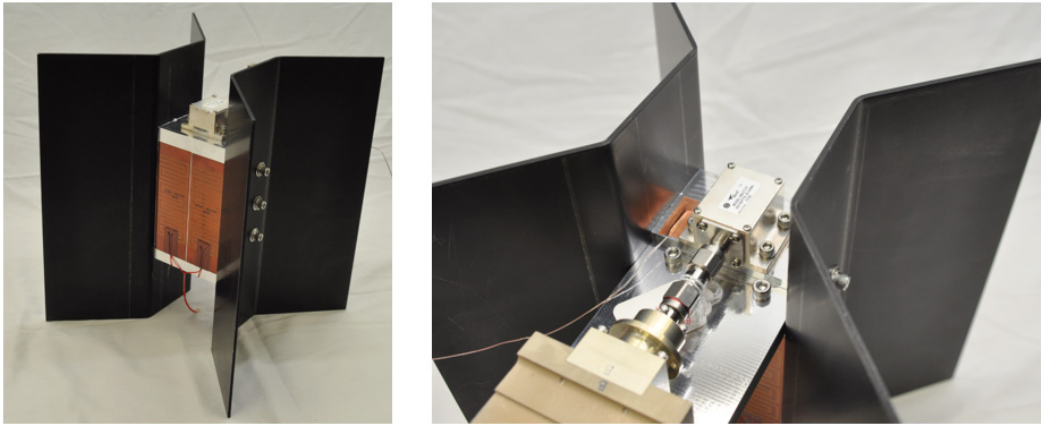


Fig. 4: RF dummy load with resistive heaters and radiator fins.

but with a spherical endcap geometry. This provided an approximate roadmap to which modes to expect at which frequencies in the flat endcap geometry of the frustum replica cavity.

Subsequent detailed RF design work, including loop antenna placement, antenna sizing and RF transmission joint design, was performed using Altair FEKO. Mode identification in FEKO was performed using slices at various axial and azimuthal locations to view electric and magnetic field strengths, and matched to the nearby predicted modes of the spherical endcap cavity.

The cavity RF feed is a TNC connector mounted 6.75in axially from the small end of the cavity. A small coupling loop protrudes into the cavity, mounted normal to the cavity wall. One lead of the loop is soldered to the center conductor of the connector while the other end is screwed into a copper adapter block mating the connector to the cavity. The connector, copper adapter and cavity are mechanically secured by 4-40 screws. The cavity is tuned by adjusting the diameter of the coupling loop; the loop is not rotated within the cavity.

#### D. Dummy Load

We use a high power RF dummy load (Bird 250-CT-FT, 50  $\Omega$ , 250 W), modified significantly to operate in a vacuum environment, mounted to an aluminum block heatsink with black anodized aluminum radiator fins. The dummy load uses similar Minco resistive heaters as the cavity and is approximately the same height so that it can use the same noncontact finger joint for RF power. The all-aluminum construction is designed to maximize conductive heat transfer, and the black anodized fins are sized to radiate approximately 100 W at 100 °C so that the load can run at approximately the same power levels and temperatures as the cavity.

#### E. RF Power Generation and Transmission

The simplest experimental knob to turn to increase the SNR is to increase driving RF power, as for any claimed thruster the thrust should increase with power. White reports thrust / power of order 1-2 microNewtons per watt ( $\mu\text{N}/\text{W}$ ) at 80 W total forward RF power. The challenge of testing at several 10s-100s W in the few GHz frequency range is minimizing the thermal load to the torsional stand. We approach this problem by performing RF signal synthesis and amplification outside the vacuum chamber and routing power approximately 15 feet

from the amplifier through a vacuum feedthrough and onto the thrust stand, using a custom non-contacting power transmission joint to cross the torsional pivot from the thrust stand base to the torsional arm.

#### Wall Power to Thrust Stand: RF Generation, Amplification and Vacuum Feedthrough

An Agilent N5171B 9 kHz – 3 GHz signal generator drives an approximately 2 GHz signal to an IFI S251 0.8 – 2.5 GHz 150 W solid state microwave power amplifier. The high power signal passes through a Narda 3022 20 dB directional coupler to a ~8ft Andrew LDF4-50A heliax coaxial cable and into the vacuum chamber through a Radiall R143.753.000 TNC hermetic bulkhead feedthrough. Inside the vacuum chamber, power continues through two flexible Micro-Coax UFB311A cables with high-power TNC connectors, the first 52in long and the second 26in long, joined through another identical Radiall bulkhead feedthrough inside the chamber. The shorter 26in cable terminates at the stationary side of the noncontact finger joint, discussed below. All cables were chosen from on-hand materials for their relatively low loss, and the use of two cables at vacuum was to permit intermediate strain relief and thermal heatsinking for the long, relatively stiff cables. The longer 52in vacuum cable uses additional heatsinking through copper straps near the cable midpoint.

At atmosphere, both the forward and reflected power outputs of the Narda directional coupler go to separate Narda 3372A-4 4-port power dividers for direct visual monitoring, telemetry, and feedback control. Forward power spectra, as well as reverse second harmonic and reverse close-in noise floor (both for multipactor detection) are visually monitored on two Agilent E4443A spectrum analyzers. The forward and reflected power telemetry are recorded from two Agilent E4418B power meters with Agilent 8481A power sensors. An analog 0-100 mV reflected power signal is produced by a HP 423B Schottky diode detector for closed loop frequency feedback control.

#### Thrust Stand to DUT: Noncontact RF Power Transmission

RF power transmission from the stationary thrust stand base to the freely swinging torsional arm is accomplished through a noncontact “finger joint”, so named for its side-on appearance of interlocking fingers. The design is based on a stripline geometry, which takes advantage of the lack of azimuthal currents in a coaxial cable or waveguide to split the shield conductor in half and flatten it to a rectangular geometry with length and width adjusted to maintain a 50-ohm impedance. In the finger





Fig. 5: Left, a cross-section of a typical round coaxial waveguide compared to the rectangular cross section of a stripline; right, a side view of a conceptual finger joint showing the splitting of the stripline pieces into overlapping fingers.



Fig. 6: Side view of finger joint showing overlapping ground and center conductor plane to allow operation over a range from 0.7-2.5 GHz.

joint the center conductor and ground planes are both split into axially overlapping sections that are nominally  $\lambda/4$  in length at the cavity operating frequency; other portions of the geometry are chosen to maximize the capacitance to significantly extend the lower frequency end of its operating range. The result is a joint that has a relatively large bandwidth about its nominal design frequency to permit testing of multiple resonant modes in the future if desired.

## V. PRELIMINARY THERMAL AND RESONANCE RESULTS

No thrust stand performance measurements have been performed on the thrust stand. However, initial tests of thermal response, frequency feedback control, temperature stabilization, and finger joint performance have been completed. These are discussed below.

### A. Bare Cavity RF Heating with Cable

Initial RF resonant heating of the bare copper cavity, shown in Fig. 1 and below in Fig. 7, demonstrated good ability to stay on resonance over several hours using the closed loop frequency feedback tuning, even during rapid temperature changes. The tests also indicated that the cavity as fabricated would get

extremely hot at relatively low input power due to its very low emissivity. This low emissivity created a near isothermal cavity, as conduction was far favored over radiation all over the cavity, and it caused very long thermal equilibration times. This motivated the high emissivity coating shown in the next section. The RF cable did not see high temperatures during this test, peaking at less than 40 °C.

### B. Black Cavity DC Heating with Cable

After coating the cavity for higher emissivity, the available operating power range expanded dramatically. We were able to operate at nearly 85 W while maintaining peak temperatures under 100 °C. This test used direct current (DC) resistive heating, and is important as a comparison with the next section using RF heating. There is an approximately 30 °C temperature difference between the center of the large end of the cavity and the center of the small end. Note that thermocouples T4 and T5 are in different locations during this test. Thermocouple T4 moved from the edge of the cavity small end to the center of the cavity small end, and T5 moved from the RF cable (not present in this test) to the solid state relay shown at bottom left in Fig. 8. The relay saw temperatures peaking at about 30 °C, with slightly higher temperatures starting at about 2 hours when it was actuated to short the cavity resistors while maintaining

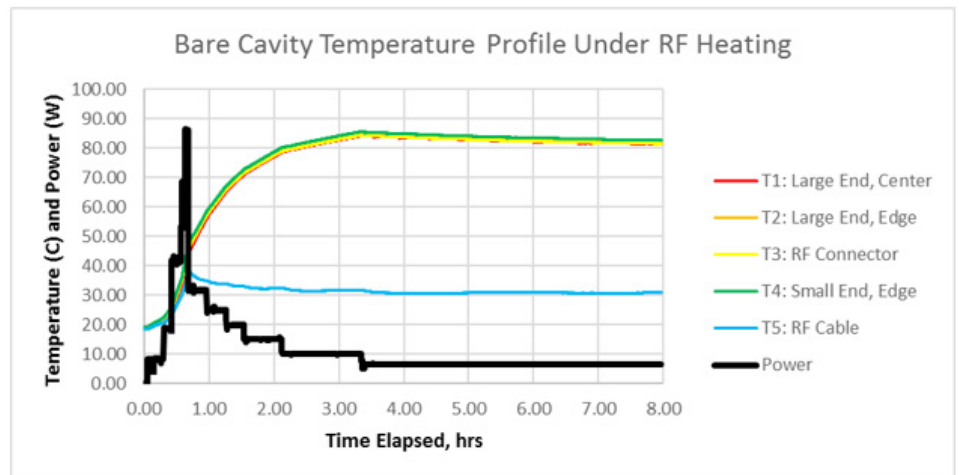
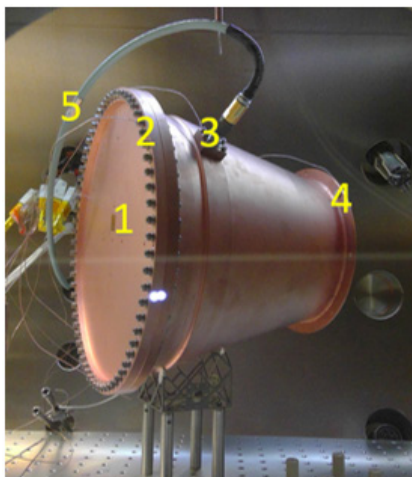


Fig. 7: Left, the bare copper cavity mounted in the PTF with thermocouple locations shown; right, the temperature profile over 8 hours to arrive at an accelerated thermal equilibrium.



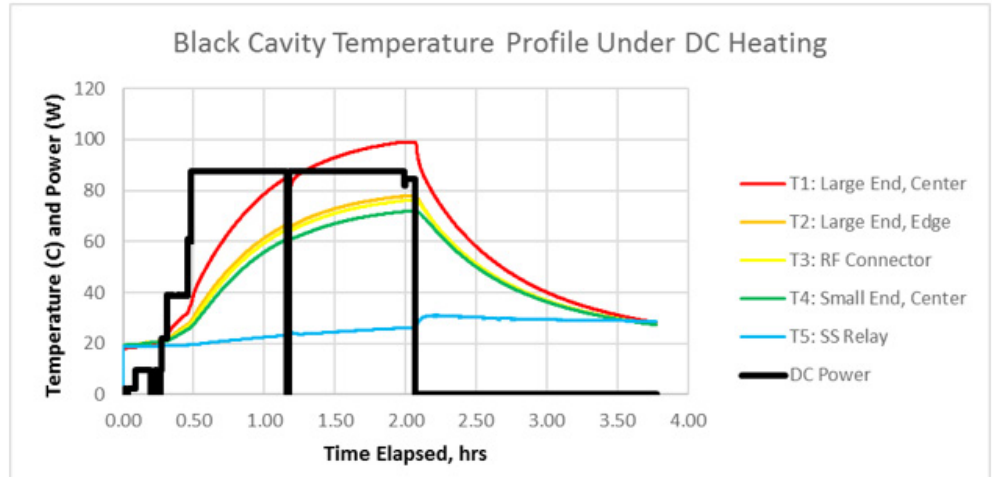
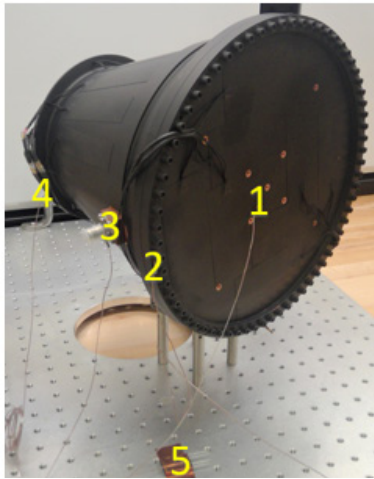


Fig. 8: Left, the black cavity with thermocouple locations shown; right, the temperature profile over 4 hours under DC heating. Note that thermocouples T4 and T5 are in new locations.

constant heating current.

### C. Black Cavity RF Heating with Cable

The RF testing of the black cavity showed a wider spread of temperatures than in the initial bare cavity case, but only about 15 °C from one end of the cavity to the other – less than produced by the resistive heating. This suggests that the eddy currents in the cavity are spread more uniformly than the resistor placement can reproduce. Fig. 9 is for approximately the same total power as Fig. 8, with a slightly lower peak temperature. Notably, at this near-full power condition, the RF cable is still only at about 65 °C.

### D. Dummy Load RF Heating with Finger Joint

The final test to date validated the feasibility of aligning the noncontact finger joint and maintaining alignment at high power in spite of thermal expansion. This test took place at 100 W power and monitored temperature of the aluminum block immediately adjacent to the dummy load, as well as on the RF cable as before. Because of this placement, the thermocouple will often register an initial spike in temperature at a new power before the heat conducts sufficiently to the radiator fins to enable a cooler steady state temperature. As a result, the profile in Fig. 10 has a rapid ramp to just over 100 °C at only 50 W applied power, then after a pause was able to accommodate a full 100 W power input with temperature under 100 °C. The total return loss throughout this test was about 23 dB, much of which is due to the dummy load itself rather than the finger joint.

## VI. CONCLUSIONS

This paper has presented the basic design drivers and experimental pitfalls for a high-fidelity impulse drive test, and outlined initial risk reduction results of a Naval Research Laboratory effort to independently validate and verify (IV&V) the anomalous thrust production reported by White et. al of NASA JSC in a resonant tapered microwave cavity. We have defined an impulse drive as any one of several recently proposed devices that claim to produce thrust without observable reaction mass, in apparent violation of the conservation of momentum. Our default assumption is that any observed thrust is most likely due to experimental error, but the above published results in a

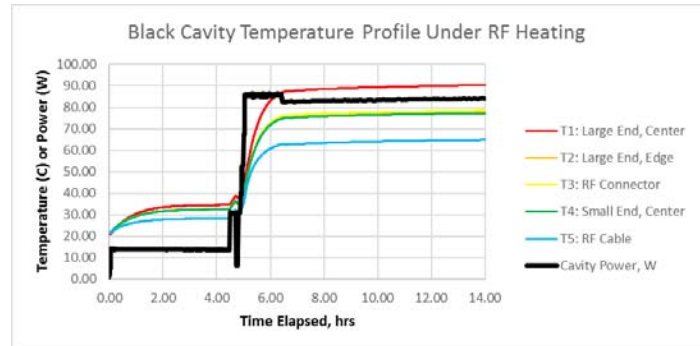


Fig. 9: Heating profile under resonant RF power for the black cavity, showing steady operation just over 90 °C at about 85 W power. 8 hours to arrive at an accelerated thermal equilibrium.

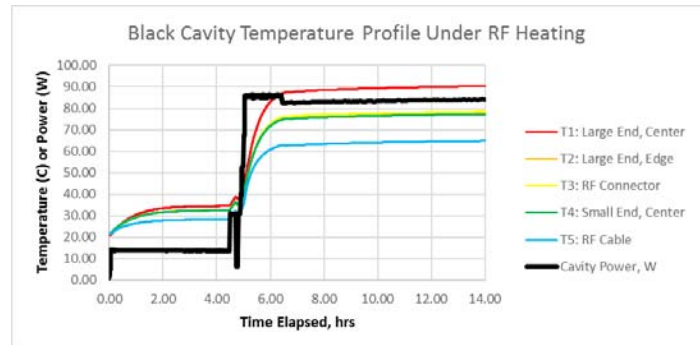


Fig. 9: Excerpt of a dummy load heating profile. The radiator fins take a while to heat up and wick heat from the load, so the load was rapidly heated to near-operating temperature at about 50% power and allowed to partially equilibrate before going to full power.

peer-reviewed venue compel us to perform IV&V as due diligence to either confirm the results or identify the error.

We have independently designed a replica cavity test article and validated its thermal response to both AC and RF heating. We have also developed a noncontact RF power transmission technique called a finger joint and demonstrated successful power deposition to a dummy load in vacuum on a stationary platform using the finger joint. After reviewing several error mechanisms that can contribute to false readings of thrust, we

identify thermal drift and potentially electrostrictive effects as the most promising error candidates.

In the near future we expect to begin vacuum thrust stand testing of the dummy load and finger joint to identify and account for spurious force readings due to thermal drift, RF effects, or both, and to prepare for cavity thrust stand testing with and without a polymer insert. We will test without the polymer insert first, anticipating this as an additional control

test which is not expected to produce any anomalous force, and follow with tests of the cavity with insert. All tests will be conducted at thermal steady state or as close to it as practical.

## ACKNOWLEDGMENTS

The authors wish to gratefully acknowledge Dr. Harold White of NASA Johnson Space Center for many helpful discussions of his test setup, methods and apparatus.

---

## REFERENCES

1. H. White et al., "Measurement of Impulsive Thrust from a Closed Radio-Frequency Cavity in Vacuum," *J. Propuls. Power*, vol. 0, no. 0, pp. 1–12, 2016.
2. R. Shawyer, "Second generation EmDrive propulsion applied to SSTO launcher and interstellar probe," *Acta Astronautica*, vol. 116, pp. 166–174, Nov. 2015.
3. H. Fearn, N. van Rossum, K. Wanser, and J. F. Woodward, "Theory of a Mach Effect Thruster II," *J. Mod. Phys.*, vol. 06, no. 13, p. 1868, Oct. 2015.
4. L. T. Williams and M. L. R. Walker, "Thrust Measurements of a Radio Frequency Plasma Source," *J. Propuls. Power*, vol. 29, no. 3, pp. 520–527, 2013.
5. A. Shabshelowitz and A. D. Gallimore, "Performance and Probe Measurements of a Radio-Frequency Plasma Thruster," *J. Propuls. Power*, vol. 29, no. 4, pp. 919–929, 2013.
6. *CRC Handbook of Chemistry and Physics*, 92nd ed. Boca Raton, FL: CRC Press, 2012.
7. D. M. Goebel and I. Katz, *Fundamentals of Electric Propulsion*. John Wiley and Sons, 2008.
8. D. Brady, H. G. White, P. March, J. T. Lawrence, and F. J. Davies, "Anomalous Thrust Production from an RF Test Device Measured on a Low-Thrust Torsion Pendulum," presented at the AIAA/ASME/SAE/ASEE Joint Propulsion Conference, 28–30 Jul. 2014, United States, 2014.
9. S. T. Vohra and L. Fabiny, "Mixing and detection of microwave signals in fibre-optic electrostrictive sensor," *Electron. Lett.*, vol. 30, no. 5, pp. 444–445, Mar. 1994.
10. L. T. Williams, M. S. McDonald, and M. F. Osborn, "Performance and Vibration Characterization of a Low-Thrust Torsional Thrust Balance," in 35th International Electric Propulsion Conference, Atlanta, GA USA, 2017.

Received 18 December 2017 Accepted 22 February 2018

## FORTHCOMING LECTURES & MEETINGS OF THE BIS

### ORBITAL ACCESS TO SPACE FROM THE UK?

**17 May 2018, 7pm**

**VENUE:** BIS, 27-29 South Lambeth Road, London SW8 1SZ

Project Leader Robin Brand will present the results of the two-year BIS Technical Project examining the commercial opportunities and challenges involved in establishing a national space launch facility.

### NEIL ARMSTRONG: FIRST MAN ON THE MOON

**23 May 2018, 7pm**

**VENUE:** BIS, 27-29 South Lambeth Road, London SW8 1SZ

Film director Chris Riley talks about his BBC biopic on Neil Armstrong, and how the film was made with the full support of Armstrong's family and friends in the weeks after his untimely death in the autumn of 2012.

### RUSSIAN/SINO FORUM

**2 and 3 June 2018, 9.30pm-5.30pm**

**VENUE:** BIS, 27-29 South Lambeth Road, London SW8 1SZ

One of the most popular and longest-running events in the Society's history. Papers are invited for the 38th Forum and registration is now open.

### BLOCKBUSTERS FROM SPACE?

**7 June 2018, 7pm**

**VENUE:** BIS, 27-29 South Lambeth Road, London SW8 1SZ

Earth-i launched its first prototype satellite in January this year. Mr. Xu Teo, Client Services at Earth-I, will be touching on Earth-i's exciting plans to launch further satellites, again built by Surrey Satellite Technology, into the Vivid-i Constellation – the world's first satellite constellation that will deliver near real-time Ultra High Definition, full colour video and still images from space. This is in addition to the 3 other satellite constellations with which Earth-i is already working.

### THE SPACE AGE: A GLOBAL REVOLUTION

**19 June 2018, all day**

**VENUE:** The Exhibition Centre, Liverpool

As the age of commercial space travel dawns, leaders and innovators from across the global space industry are gathering at the International Business Festival 2018 to discuss the sectors emerging challenges and opportunities. The BIS is in partnership with the Northern Space Consortium to present a specially invited panel of key organisations and individuals.

### 73<sup>RD</sup> ANNUAL GENERAL MEETING

**28 July 2018, 1 pm**

**VENUE:** Royal Gunpowder Mills, Beaulieu Drive, Waltham Abbey, Essex, EN9 1JY

Admission to the AGM is open to Fellows only but all Members are welcome to join the discussion after the formalities conclude around 1.15 pm. Please advise in advance if you wish to attend (attendance to this part of the afternoon is free).

The AGM will be followed by the BIS Summer Get-together at the same venue; tickets are £20 and are on sale now on our website.

Council nomination forms are obtainable from the Executive Secretary or from the the BIS website. These must be completed and returned not later than 12 noon on 4 May 2017. If the number of nominations exceeds the number of vacancies, election will be by postal ballot. Voting papers will then be prepared and circulated to all Corporate Members.

### EXOMARS TALKS

**13 September 2018, 7pm**

**VENUE:** BIS, 27/29 South Lambeth Road, London SW8 1SZ

The joint European-Russian ExoMars Rover is due for launch in 2020 following its assembly by Airbus in Stevenage. Paul Meacham, Lead Systems Engineer at Airbus presents the current status of the ExoMars mission.

# JBIS

Journal of the British Interplanetary Society



[jbis.org.uk](http://jbis.org.uk)